Highly Constrained Dithienylethenes

D I S S E R T A T I O N

zur Erlangung des akademischen Grades

d o c t o r r e r u m n a t u r a l i u m

(Dr. rer. Nat.)

im Fach Chemie

eingereicht an der

Mathematisch-Naturwissenschaftlichen Fakultät

der Humboldt-Universität zu Berlin

von

Dipl.-Chem. Michael Kleinwächter

Präsidentin der Humboldt-Universität zu Berlin

Prof. Dr. Sabine Kunst

Dekan der Mathematisch-Naturwissenschaftlichen Fakultät

Prof. Dr. Elmar Kulke

Gutachter: 1. Prof. Stefan Hecht, Ph.D. (HU Berlin)

2. Prof. Dr. Karola Rück-Braun (TU Berlin)

3. Prof. Dr. Werner Abraham (HU Berlin)

Tag der mündlichen Prüfung: 13.02.2018

Für Anke und Charlotte

A scientist in his laboratory is not only a technician:
he is also a child placed before natural phenomena
which impress him like a fairy tale.

Marie Curie

Danksagung

Mein erster Dank gilt Prof. Stefan Hecht, der durch das Schaffen hervorragender Arbeitsbedingungen und viele fachliche Diskussionen die vorliegende Arbeit überhaupt erst ermöglicht hat.

Obwohl diese Doktorarbeit nur von einer Person geschrieben wurde, ist sie dennoch ein Werk, das allein nicht zu bewältigen gewesen wäre. Ich möchte deshalb den Menschen danken, die mir während der Promotion zur Seite gestanden haben.
Dies ist zunächst der gesamte Arbeitskreis Hecht. Ein besonderer Dank sei jedoch speziell an Martin, Björn, Yves und Andreas gerichtet, da sie stets für eine gute Diskussion zu haben waren und hierbei viele gute Ideen entstanden sind. Gleichermaßen habe ich von euch viel über Photochemie und andere Techniken gelernt. Ebenso wichtig wie die intellektuelle Unterstützung war auch die praktische Hilfe, wofür ich insbesondere Ellen und Jutta, aber auch vielen Studenten danken möchte. Ohne euch hätte ich etliche Stunden mehr vor dem Abzug stehen müssen.
Viele der speziellen Analysen wurden von Kollegen durchgeführt. Ich danke Herrn Grubert für die zahlreichen elektrochemischen Messungen, Bernd für die Vielzahl an schnell gelösten Kristallstrukturen, Björn für seine Unterstützung bei HPLC- und UPLC-Belangen, Sergey für die Messung der Kurzzeitspektroskopie und dem NMR-Team für seine Arbeit. Für die Korrektur dieses Werkes danke ich besonders Martin, Dennis, Yves und Kristin.

Zusätzlich zum fachlichen Austausch war unter meinen Kollegen auch stets ein Gesprächspartner für Privates und zum moralischen Wiederaufbau zu finden. Danke für die sozialen Kaffeepausen und geteilten Schokokekse, gemeinsamen Mittagessen, und für diverse Grill- und Skatrunden zum Feierabend, die aus der Doktorarbeit mehr als eine Arbeit gemacht haben. Darüber hinaus haben auch meine über die Zeit zahlreichen Laborkollegen mit (meist) guter Musik, Scherzen und Diskussionen jeder Art stark zur guten Arbeitsatmosphäre und Motivation beigetragen.

Als Letztes bleibt mir noch, meinen Freunden, meiner Familie und insbesondere Anke zu danken, dass sie diesen Weg zusammen mit mir gegangen sind. Ohne eure Hilfe und euren Zuspruch wäre es, wenn nicht gar unmöglich, so doch gewiss wesentlich anstrengender gewesen, dieses Ziel zu erreichen.

Kurzzusammenfassung

Diarylethene sind molekulare Schalter, welche sich unter Einwirkung von Licht in einer pericyclischen Reaktion in ein konjugiertes Isomer umwandeln. Dieser Vorgang kann durch Bestrahlung mit längerwelligem Licht umgekehrt werden. Die Effizienz dieser beiden Photoreaktionen ist von verschiedenen Parametern abhängig, welche bisher nur unzureichend verstanden sind. Ein entscheidender Faktor für die Hinreaktion ist das Verhältnis zwischen zwei Konformeren, da nur eine der beiden Formen photochemisch aktiv ist. Bisherige Ansätze, das thermische Gleichgewicht zugunsten der aktiven Spezies zu verschieben, nutzen hauptsächlich sterische und intramolekulare Wechselwirkungen

In der vorliegenden Arbeit wird eine neue Klasse von Diarylethenen beschrieben, in welcher die aktive Konformation durch kovalente Verbrückungen unterschiedlicher Länge stabilisiert wird. Durch den gleichzeitigen Verzicht auf das Einbinden der zentralen Doppelbindung in eine Ringstruktur eröffnet sich ein zusätzlicher photochemischer Reaktionspfad in Form einer Doppelbindungsisomerisierung. Es stellte sich heraus, dass bei geeigneter Verbrückungslänge das zyklisierte Isomer mit ungewöhnlich hoher Effizienz gebildet wird, während die Effizienz der Ringöffnungsreaktion nicht beeinflusst wird. Der Mechanismus und die Dynamik der Photoreaktion wurden anhand ausgewählter Vertreter durch Ultrakurzzeitspektroskopie untersucht. Weiterhin konnte gezeigt werden, dass alternativ zur photochemischen Zyklisierung ein Ringschluss auch durch elektrochemische Oxidation oder Reduktion erfolgen kann. Die vorgestellten annelierten Systeme agieren bei direkter photochemischer Anregung wie herkömmliche Diarylethene nur im Ringschluss/Ringöffnungsregime. Gleichzeitig kann durch Tripletsensibilisierung eine selektive *Z*→*E*-Isomerisierung erzielt werden, was diese Diarylethenklasse zu reversiblen 3-Zustandssystemen erweitert.

In einer Erweiterung des Projektes wurde die Struktur des Diarylethens noch stärker fixiert, um die Effizienz der Ringschlussreaktion weiter zu steigern. Nach vielseitigen Syntheseversuchen konnten zwei Vertreter dieser Klasse erhalten und photochemisch untersucht werden. Für eine der beiden Verbindungen wurde ein Umsatz zu etwa 60% zyklisiertem Isomer bei der Bestrahlung mit UV-Licht gefunden.

Zusammengefasst stellt die kovalente Verbrückung der Diarylethenstruktur eine erfolgreiche Strategie dar, um sowohl die Effizienz der Ringschlussreaktion zu steigern als auch photochrome Verbindungen mit drei Schaltzuständen zu kreieren.

Abstract

Diarylethenes are molecular switches that convert reversibly to a conjugated closed isomer in a photon-induced pericyclic reaction. This process can be reverted by irradiation with light of longer wavelengths. The efficiency of both photochemical reactions depends on several parameters, which, so far, are only insufficiently understood. One important factor influencing the efficiency of the cyclization reaction is the presence of two conformations of the open isomer. According to the Woodward-Hoffmann rules, only one of these two conformers is photochemically active. Few approaches have been undertaken to bias the thermal equilibrium towards the active form, and in most cases steric or intramolecular interactions have been used to achieve this goal.

In the current work, a new class of diarylethenes is presented, in which the active conformation is covalently stabilized by alkyl chains of different lengths. Since the central double bond is not fixated by incorporation into a cyclic moiety, the double bond isomerization emerges as an additional photochemical pathway in these annulated diarylethenes. It was found that in dependence of the chosen ring size both open isomers convert with increased efficiency to the closed isomer upon irradiation with UV-light, whereas the efficiency of the cycloreversion process remains unaffected. The mechanism and dynamic of the photoreaction were investigated for selected compounds using transient absorption spectroscopy. Furthermore, electrochemical studies revealed that both the *E*- and the *Z*-isomer cyclize rapidly upon anodic oxidation or cathodic reduction.
In general, the photochemical reactivity of annulated diarylethenes parallels that of normal diarylethenes and takes place exclusively in the cyclization/cycloreversion regime if irradiated directly. However, it was demonstrated that a selective $Z \rightarrow E$ double bond isomerization is possible by indirect methods such as triplet sensitization, thus implementing a 3-state photoswitchable system.

In an extension of the project, the structure of diarylethenes was further stiffened in order to increase the efficiency of the photochemical cyclization. Using diverse synthetic approaches, two members of this class could be obtained. Photochemical investigation showed a conversion to the closed isomer of 60% upon irradiation with UV-light.

In brief, the covalent fixation of diarylethenes represents an attractive strategy to increase the efficiency of the photochemical cyclization and extent the scope of diarylethenes to 3-state photochromic systems.

Die vorliegende Arbeit entstand in der Zeit von Januar 2013 bis Dezember 2017 unter der Betreuung von Herrn Prof. Stefan Hecht, Ph.D. am Institut für Chemie der Humboldt-Universität zu Berlin.

Contents

Danksagung ..... **v**

Kurzzusammenfassung ..... **vii**

Abstract ..... **ix**

Contents ..... **xi**

1. Introduction **1**

1.1 Preliminary remarks 1

1.2 Theoretical background 3

1.2.1 Photochromic compounds 3

1.2.2 Stilbenes 6

1.2.3 Diarylethenes 10

1.2.4 Dual mode photochromism in diarylethenes 15

2. The (photo)chemistry of aDTEs **19**

2.1 Aim of the project 19

2.2 Synthesis of aDTEs 23

2.2.1 General synthetic strategies for aDTEs 23

2.2.2 Synthesis of simple aDTEs 25

2.2.3 Synthesis of functionalized aDTEs 36

2.2.4 Synthesis of half-stiff aDTEs and reference compounds 44

2.2.5 Synthesis of unconstrained reference compounds 45

2.2.6 Summary 46

2.3 Steady-state spectroscopy of aDTEs 49

2.3.1 General considerations 49

2.3.2 Determination of the molar extinction coefficients 50

2.3.3 The course of the photoreaction 54

2.3.4 Quantum yields of the photoreactions 63

2.3.5 Photochemical fatigue 67

2.3.6 Switching in the solid state 68

2.3.7 Towards $Z \rightarrow E$ isomerization 69

2.3.8 Summary 73

2.4 (Spectro)electrochemistry of aDTEs 77

2.4.1 Motivation 77

2.4.2 The electrochemistry of $aDTE_{66}$-Me 78

2.4.3 Substitution and ring size effects 82

2.4.4 Summary 86

2.5 Transient absorption spectroscopy of aDTEs 89

2.5.1 Motivation 89
2.5.2 Transient absorption spectroscopy of unconstrained DTEs 90
2.5.3 Transient absorption spectroscopy of $aDTE_{66}$-Me 94
2.5.4 Transient absorption spectroscopy of $aDTE_{66}$-PhCN 97
2.5.5 Summary 100

3. The (photo)chemistry of pcDTEs 103

3.1 Aim of the project 103
3.2 Synthesis of pcDTEs 105
3.2.1 General synthetic strategies for pcDTEs 105
3.2.2 Synthesis by direct C2-bridging 106
3.2.3 Synthesis by heteroatomic bridging 111
3.2.4 Synthesis by dimerization of a Michael system 113
3.3 Photochemistry of pcDTEs 123
3.4 Conclusion 127

4. Experimental section 131

4.1 General methods 131
4.2 Photochemistry 133
4.3 (Spectro)electrochemistry 134
4.4 Transient absorption spectroscopy 134
4.5 Synthetic procedures 134
4.5.1 Synthesis of the simple building blocks 136
4.5.2 Synthesis of the functionalizable building blocks 145
4.5.3 Reductive couplings of the building blocks 152
4.5.4 Functionalization of aDTEs 159
4.5.5 Synthesis of pcDTE 166
4.6 Selected ^{1}H and ^{13}C-NMR spectra 182
4.7 Crystal structures 184

5. References 197

6. Appendix 209

6.1 Abbreviations 209
6.2 Index of compounds 212
6.3 Index of figures 216
6.4 Index of schemes 216
6.5 Index of tables 223
6.6 Emission spectra of additional light sources 225

1. Introduction

1.1 Preliminary remarks

Since the rise of the first cultures, chemical processes were used to transform raw materials to products of higher value for humankind, such as metals and alloys from ores, leather and parchment from animal skin or dyestuff from organic and inorganic sources. With an increased comprehension of the underlying chemical transformations, the foundation for modern chemistry was laid, and today's analytical possibilities continuously improve our understanding of the interrelationship between structure and reactivity. Consequently, chemical research today is not only about understanding existing systems, but more and more about creating increasingly specific characteristics by precise tailoring of the molecular structure.
Once synthesized, the properties of a molecule are usually considered unalterable. In contrast, molecular switches display the fascinating possibility to change their intrinsic properties dynamically and reversibly by applying an external stimulus. As such, light offers the unrivalled possibility of contactless interaction with specific molecules with a high spatial and temporal resolution, as unequivocally evidenced by the photoreaction in the human eye allowing the reader to see this text.

Artificial molecular ensembles still are far from the complexity discovered in nature. However, chemists today are not only able to combine several functional units, but also to condense the desired functionality into small systems and optimize their behavior.
In the following study, such an optimization of the photochemical efficiency of a molecular switch is achieved in parallel to the investigation of an additional, up until now unexploited reaction pathway. For this, the molecular framework of diarylethenes is simplified to its basic structure and reshaped to both stabilize the molecule in a reactive geometry and allow double bond isomerization as an alternative pathway to the governing electrocyclization reaction.

So far, several approaches have been reported to optimize diarylethenes systems towards higher efficiency of the photoreactions. However, the basic structure implemented in the late 1980's has not been varied a lot. It is hoped that the current work can extend the understanding of diarylethene systems and broaden their scope of possible applications.

1.2 Theoretical background

1.2.1 Photochromic compounds

Reversible interconversion between two or more different states of a molecule can be achieved by various stimuli. Among the most prominent are changes induced by acid or base (acidochromism, e.g. in pH-indicators as phenolphthalein), heat (thermochromism, e.g. in spiropyrans), reduction or oxidation (electrochromism, e.g. in methylviologen) or light (photochromism), which will be discussed in more detail. The term is defined as "a reversible transformation of a chemical species induced in one or both directions by absorption of electromagnetic radiation between two forms, A and B, having different absorption spectra" (Scheme 1.2-1).[1]

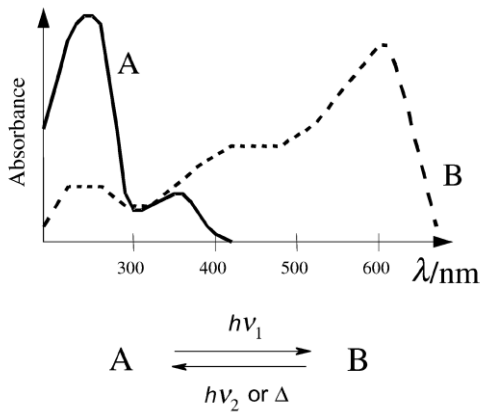

Scheme 1.2-1 Exemplary photochemical equilibrium between two chemical species A and B. Both species differ in their absorption spectrum and can be interconverted by light or heat.[1a]

The process of this transformation is termed a photoreaction, and the molecule undergoing this reversible change a photochromic compound, or in short, a photoswitch. Several reaction types are commonly used in photochromic compounds (Scheme 1.2-2):

- *Double bond isomerizations,* e.g. in stilbenes, carotenoids, azo compounds, imines, hydrazones and (thio)indigoids
- *Pericyclic reactions*, e.g. 6π-electrocyclizations in diarylethenes, chromenes, spiropyrans and the cyclophanediene/dihydropyrene system
- *Intramolecular hydrogen transfer*, e.g. in anils, salicylates, triazoles
- *Heterolytic/homolytic dissociation processes*, e.g. in triarylmethanes and hexaarylbiimidazoles

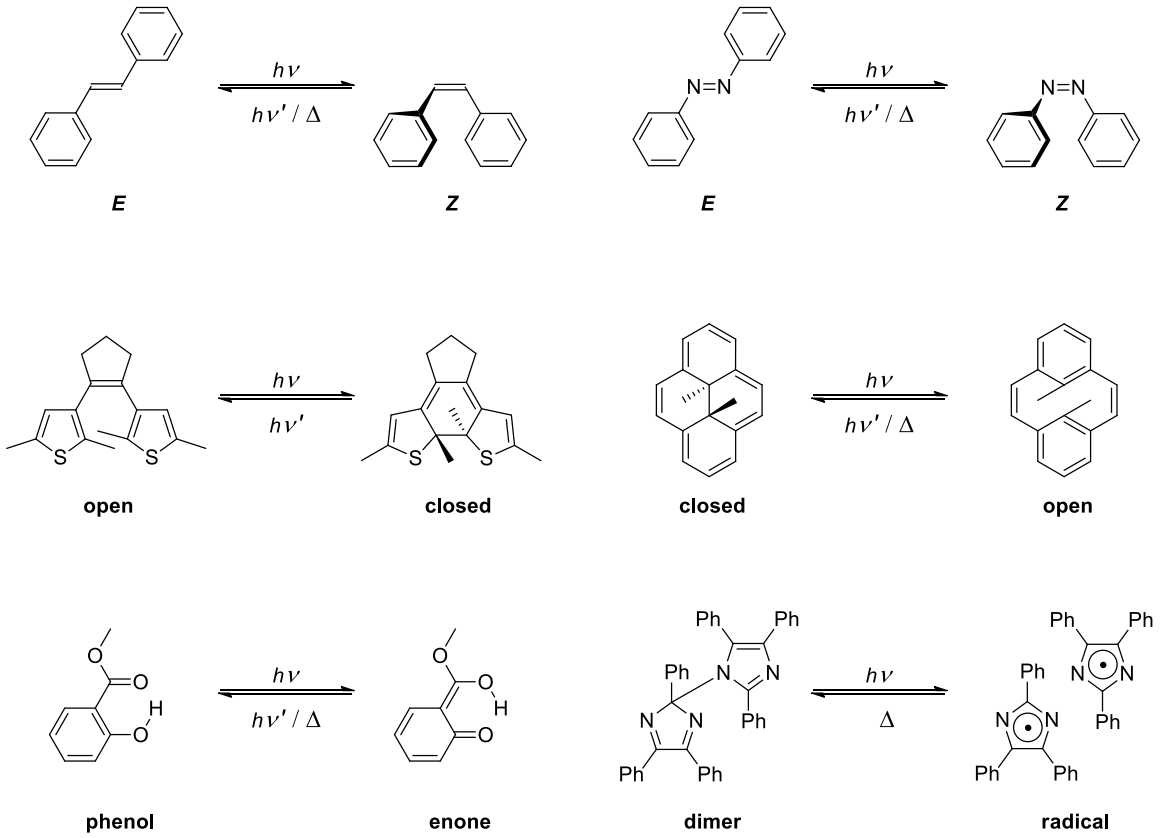

Scheme 1.2-2 Examples for photochromic systems with different photochemical reaction types. Only the major reaction pathway is considered. **Top:** Double bond isomerizations in stilbene and azobenzenes. **Middle:** Pericyclic reactions in diarylethenes and dihydropyrenes. **Bottom left:** Intramolecular hydrogen transfer in salicylates. **Bottom right:** Homolytic bond dissociation in hexaarylbiimidazoles.

Within the family of photochromic compounds, a further differentiation is made between compounds that interconvert between the two states by light exclusively (P-type photochromism) and such that convert in one direction through thermal equilibration (T-type photochromism). As the color is in general only one of several properties that will change during the photoreaction of a respective photochromic compound, the potential applications are manifold. As such, the color change itself can be used to store data or change the transmittance of a material. However, the change in color is a mere symptom of the alteration of electrochemical properties of a molecule which for example can be used to trap charges in an organic transistor or quench excited states in one of the switching states but not in the other. Geometric changes in a single molecule can alter the macromolecular shape or change the reactivity of a system by inducing or preventing proximity of functional units.

As for ground state chemical reactions, there are several parameters to describe a photoreaction. Corresponding to the yield of a chemical reaction, for photochemical

reactions the photostationary state (PSS) composition is given as a measure for the conversion of a photoactive molecule A to a respective product B when the photochemical equilibrium is reached.

$$PSS = \frac{number\ of\ isomerized\ molecules}{total\ number\ of\ molecules} \cdot 100\% \quad (1)$$

In order to achieve maximum effects by the switching process a high PSS is desired for both directions of the photochemical isomerization reaction, which is possible by separation of the absorption bands of A and B allowing for their selective excitation. However, in many photochromic compounds this is difficult to achieve at least for one of the switching directions.

Another important parameter equivalent to the reaction rate in ground state reactions is the photochemical efficiency, named quantum yield $\Phi_{A\rightarrow B}$. It is given as a ratio of photons absorbed and the photons leading to the desired photoproduct.

$$\Phi_{A\rightarrow B} = \frac{amount\ of\ B\ formed}{amount\ of\ photons\ absorbed} \quad (2)$$

The ability to tune the quantum yields of the forward and back reactions by understanding the underlying structure-property relationships is essential for designing efficient photoswitches with properties tailored to the desired use.

For T-type photochromic systems, also the thermal back reaction needs to be considered. As this is mostly a (pseudo-) first order reaction, it is in general expressed with the thermal half-life $t_{1/2}$ of the thermally labile product. For different photochromic systems, the thermal half-lifes range from tens of nanoseconds (e.g. bridged hexaarylbiimidazoles) over minutes and hours (e.g. azobenzenes and spiropyrans) up to materials that are practically P-type photochromic at room temperature (e.g. diarylethenes).

Though not often discussed in the context of academic research, a challenge to be met for practical use is the occurrence of unwanted side reactions, undermining the desired photoreaction. This “fatigue” becomes especially important for uses of the photochromic system over multiple cycles. The possibilities to circumvent unwanted reactivity and favor specific photochemical paths will be discussed for the two systems related to the current study, stilbenes, and diarylethenes.

1.2.2 Stilbenes[1]

Though its photochromic behavior was not described[5] until 1934, stilbene is one of the oldest and most thoroughly investigated photochromic compounds. Naturally occurring mostly in the planar *E*-isomer,[2] stilbene exists in two other isomers. The twisted *Z*-isomer[6] can form from *E*-stilbene by photochemical double bond isomerization, whereas the dihydrophenanthrene (DHP) is the product of a 6π-electrocyclization from *Z*-stilbene (Scheme 1.2-3).

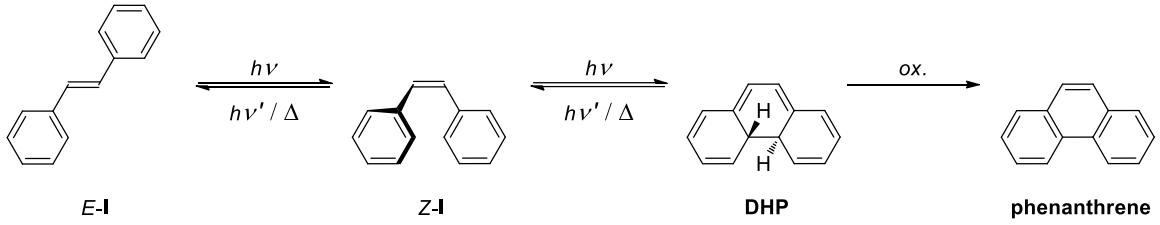

Scheme 1.2-3 Photochromism of stilbene. Upon irradiation with UV light, *E*-stilbene converts into *Z*-stilbene, which can cyclize subsequently to form the dihydrophenanthrene (DHP). The cyclization can be reversed thermally or by light, whereas the *Z*→*E* double bond isomerization has a high activation energy and favors the *Z*-isomer upon irradiation. The DHP is prone to oxidation to form phenanthrene.

The former of the two photoreactions can be reversed by light to a certain extent (*vide infra*), and with the *E*-isomer being the thermally stable form additionally by thermal equilibration (Figure 1.2-1).[2] However, due to the high activation energy of the process, the thermal reaction becomes not efficient below temperatures of 300 °C[8] unless mediators as acid or base,[9] palladium,[10] selenium[9,11] or iodine[12] are applied.

In contrast, the second photoreaction is easily reversed thermally, which was observed by the disappearance of the DHP's yellow color (λ_{max} = 450 nm) within 2-3 hours.[13] However, also photochemical conversion is possible by irradiation with visible light.
Despite its thermal lability, the DHP isomer can easily be oxidized in the presence of oxygen or other agents such as iodine and consequently be removed permanently from the photochemical equilibrium. Though undesirable in the context of photochromism, this

[1] Reviews about stilbene's occurrence in biological molecules,[2] the *Z*→*E* isomerization[3] and excited state behavior[4] have been published.

[2] The prerequisites and mechanistic considerations for bidirectional and monodirectional thermal double bond isomerization as well as thermally stable systems are discussed in Eltsovs „Organic photochromes".[7]

has been used successfully for the preparation of substituted phenanthrenes[14] and heteroaromatic analogues.[15]

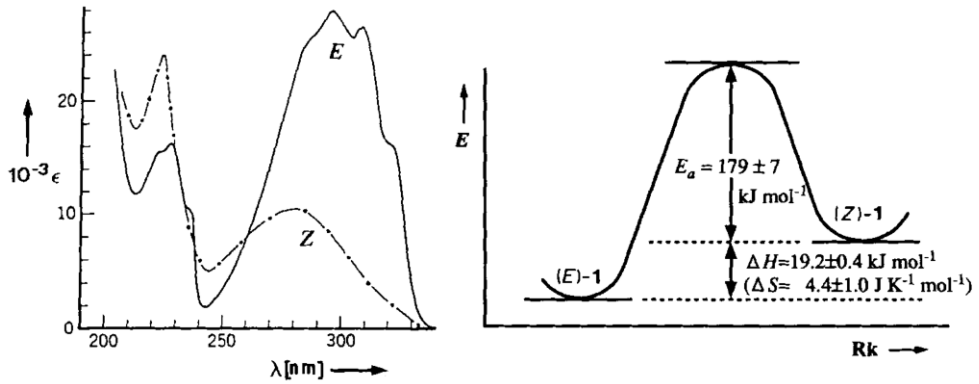

Figure 1.2-1 Double bond isomerization of stilbene.[5] **Left:** Absorptivities of *E*- and *Z*-stilbene. **Right**: Thermal barrier for isomerization in the ground state (Rk = reaction coordinate).

The mechanism of the photochemical double bond isomerization was heavily investigated[4] and is still under discussion.[16] It is assumed to progress through a common perpendicular singlet state *P*, from which relaxation to the respective ground states takes place through a conical intersection (Figure 1.2-2).[17]

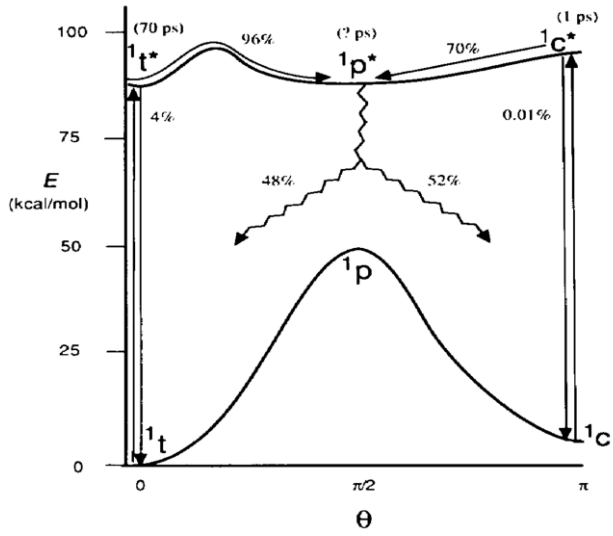

Figure 1.2-2 Potential energy curves for twisting about the central double bond of stilbene.[17a] Both the *E*-isomer ("t") and the *Z*-isomer ("c") convert to an excited perpendicular state ("p*") in the singlet manifold.

Another de-activation pathway is the fluorescence, being more important for the flat *E*-isomer ($\Phi_{F(E)} = 0.04$) than for propeller-shaped *Z*-isomer ($\Phi_{F(Z)} = 0.001$); intersystem crossing is negligible for both isomers as verified by quenching experiments. However,

for the *Z*-isomer the most important parallel reaction is the conrotatory 6π-electrocyclization according to the Woodward-Hoffman selection rules.

The quantum yields for the competing photochemical processes in stilbene are dependent on several parameters, with the temperature having a major influence (Figure 1.2-3). Especially $\Phi_{E\rightarrow Z}$ (313 nm) decreases strongly with decreasing temperature, accompanied by proportional increase of the fluorescence quantum yield ($\Phi_{F(E)}$ = 0.90 at 77 K).[5] Also the cyclization quantum yield $\Phi_{Z\rightarrow DHP}$ decreases at lower temperatures. At the same time, the back reaction quantum yield $\Phi_{Z\rightarrow E}$ does not change much over a wide range of temperatures (Figure 1.2-3 top).

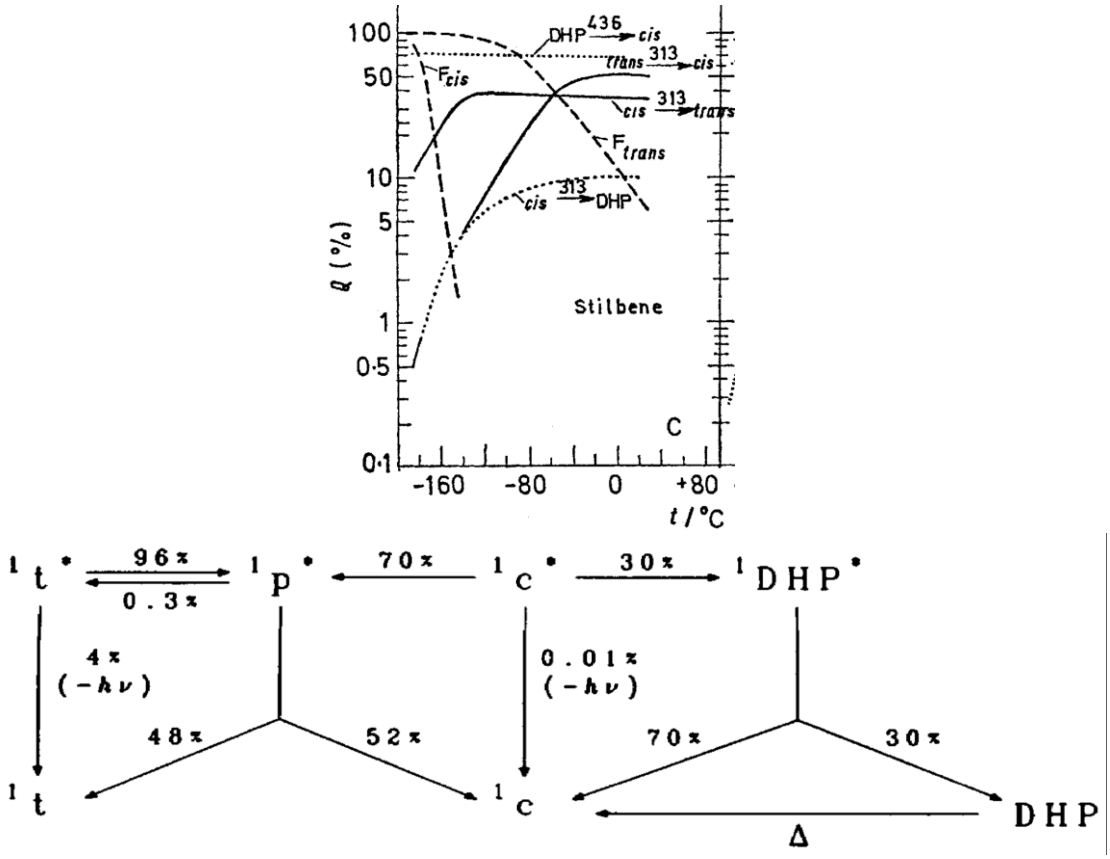

Figure 1.2-3 Interconversion of the three switching states for stilbene. **Top:** Temperature dependence of stilbene isomerization quantum yields ("Q").[18] **Bottom:** Fate of the excited states of stilbene isomers, indicated by branching rates.[17a]

For example, at room temperature in hydrocarbons the quantum yields are $\Phi_{E\rightarrow Z}$ = 0.50, $\Phi_{Z\rightarrow E}$ = 0.35 and $\Phi_{Z\rightarrow DHP}$ = 0.10 for irradiation with 313 nm, leading to a ratio of 7% *E*-isomer in the PSS due to its higher absorptivity at the irradiation wavelength.[18-19] The cycloreversion reaction quantum yield $\Phi_{DHP\rightarrow Z}$ is almost temperature independent.

Furthermore, the quantum yields, and especially $\Phi_{E\rightarrow Z}$ change with the substituents on the

stilbene in a complex manner, depending for example on the solvents polarity, viscosity and, again in particular, the temperature.[19]

During the long history of stilbenes, several changes to the basic structure were proposed to understand and influence its photochromic behavior.

As such, the activation energy for thermal *Z*→*E* isomerization can be lowered from 42.8 kcal/mol for stilbene to 32.0 kcal/mol in 1,1'-di(^{t}butyl)stilbene **II** by introduction of bulky groups in the vicinity of the double bond (Scheme 1.2-4).[20] Additional annulation of the phenyl rings to prevent out of plane torsion reduces the barrier further to 21 kcal/mol in **IIIa** (Scheme 1.2-4).[21] In this stiff stilbene system proposed by Gano *et al.*, efficient *Z*→*E* isomerization of the PSS mixture takes place within 1 h at room temperature.[22]

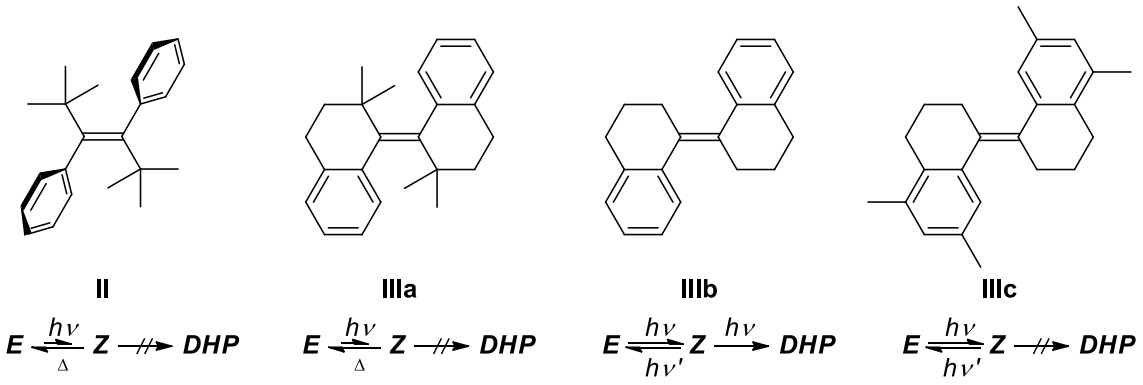

Scheme 1.2-4 Influencing the thermal equilibrium of stilbene by introduction of bulky groups. In the sterically encumbered 1,1'-di(^{t}butyl)stilbene **II**, the phenyl groups twist out of the double bond plane and are cofacial. No DHP formation is observed.[23] In the stiff stilbenes **III**, this single bond rotation is suppressed. For both methylated derivatives **IIIa**[21] and **IIIc**, the respective DHP is not detected, whereas the unsubstituted compound **IIIb** cyclizes readily.[22]

The effect of this bias can be visualized by comparing it to the unsubstituted stiff 6-membered ring analogue **IIIb** that was prepared in a comprehensive study on the effect of different annulation ring sizes.[22,24] While in methylated derivative **IIIa** no cyclization to the DHP analogue could be detected even at low temperatures, the parent stiff stilbene **IIIb** was reported to have a favorable geometry for electrocyclization.

For the other alkyl ring sizes, no cyclization was observed. Instead, the *E/Z* ratio was altered, with a PSS preferably consisting of the *E*-isomer. In general, the portion of *E*-isomer herein increased with increasing ring size from 55% for the 4-membered ring derivative to 77% for the 7-membered ring compound, with the PSS of 5-membered ring derivative being strongly wavelength-dependent.

In order to suppress the undesired oxidation of the DHP to phenanthrene, Fischer and co-workers[25] proposed the introduction of methyl groups at aromatic unit, yielding not only a cyclized product that is stable towards oxidation but also shows increased thermal stability.

Combination of the two structural changes in **IIIc**, however, lead to an unexpected finding: Introduction of methyl substituents at the *m,m*-positions of the phenyl rings completely suppressed electrocyclization due to steric effects, as already observed for **IIIa** (Scheme 1.2-4).[22] The thermal stability has not been examined.

1.2.3 Diarylethenes[3]

Though stilbene and its derivatives obviously belong to the group of diarylethenes (DAE), the term is especially used for derivatives that were designed to operate in the cyclization/cycloreversion regime.

In parallel to the stabilization against oxidation (vide supra), several modifications were made to redirect the photochemistry of stilbene from a double bond isomerization to the 6π-electrocyclization/cycloreversion regime. Common to the new design principle is the fixation of the double bond in a *Z*-geometry (Figure 1.2-4).

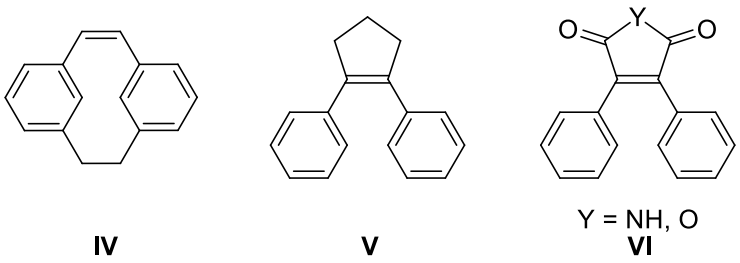

IV **V** **VI**

Figure 1.2-4 Stilbenes locked in the *Z*-configuration. [25,28]

These compounds show a decent cyclization and cycloreversion quantum yields of up to 0.6 and 0.4, respectively, for both **IV** and **V**[25b] that are not strongly temperature dependent. Though the problem of oxidation could be overcome by introduction of methyl groups[28a,29] to the reactive carbon, the problem of thermal lability persisted. Kellogg and co-workers discovered an increased stability of the cyclization product when bis-heteroaromatic ethenes were used instead of stilbenes.[15a] However, this finding was

[3] General reviews about diarylethene synthesis[26] and photochemistry[27] have been published by the groups of Krayushkin and Irie, respectively.

not exploited until the late 1980's when Irie and co-workers combined the knowledge to create the first modern DAEs (Figure 1.2-5).[30] The common design implemented for the next decades comprises a double bond that is fixated within a 5-membered ring structure (i.e. "bridge", e.g. hexafluoro/hexahydrocylopentene, maleimide or maleic anhydride) that is substituted with two heteroaromatic units (e.g. thiophene, thiazole, furan and benzylated derivatives thereof) and varying substituents on these aromats. Depending on the orientation of the non-symmetric heteroaromatic rings, a differentiation between *normal* and *inverse* DAE is possible.[31] In the following, only the more common *normal* DAE will be described.

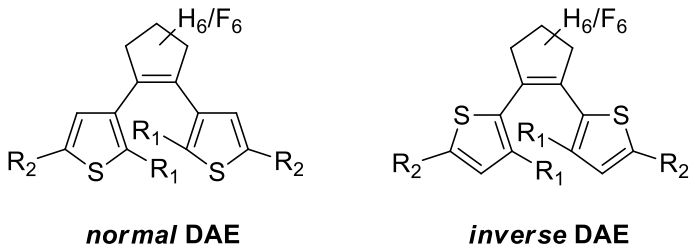

Figure 1.2-5 Exemplary structure of normal and inverse DAE. Other bridge moieties include maleimides and maleic anhydrides; aromatic systems reported additional to thiophene are thiazole or furan or benzylated derivatives thereof. The inner substituent R_1 is a methyl group in most cases, but bigger alkyls, alkoxides or aromatic systems are reported. The peripheral substituent R_2 is varied easily.

The photochemical mechanism for DAE is a 6π-electrocyclization, converting a bis-aromatic system to an extended conjugated double bond system with red-shifted absorption.

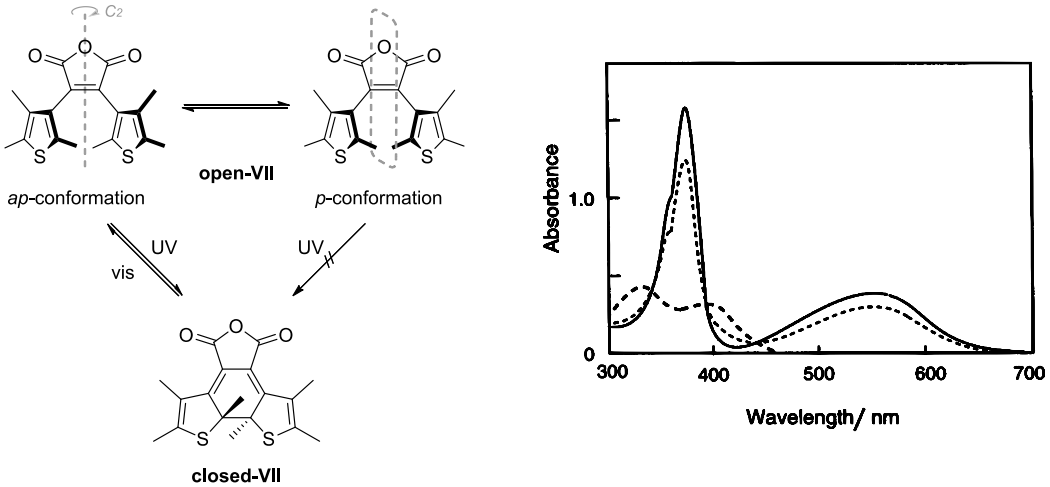

Scheme 1.2-5 Photochemistry of DAE. **Left:** The open isomer (top) exists in a photoactive antiparallel (*ap*-) conformation and an inactive parallel (*p*-) conformation that cannot cyclize. **Right:** The cyclized isomer (bottom) has a bathochromic absorption (straight line) compared to the open isomer (dashed). The PSS is indicated by the dotted line. Spectra taken from reference.[27a]

In general, both isomers are thermally stable. The quantum yields for this process normally range between $\Phi_{O\rightarrow C} = 0.1 - 0.6$,[27a,32] which is unexpected as the undesired double bond rotation as alternative relaxation path is inhibited. The common explanation for this observation, however, is the existence of two conformers (parallel *p* and anti-parallel *ap*) of the open isomer (Scheme 1.2-5). According to orbital symmetry and the resulting Woodward-Hoffman selection rules,[33] a productive electrocyclization is only possible from the *ap*-conformer. Supposing similar ground state energies for both conformers, the cyclization quantum yield is limited to about 0.5. Nevertheless, as the two conformers are in a thermal equilibrium, high PSS conversions of >90% can be achieved since the quantum yield for the back reaction $\Phi_{C\rightarrow O}$ is normally is at least an order of magnitude smaller than $\Phi_{O\rightarrow C}$. Though several examples of diarylethenes with an increased cyclization quantum yield are reported, the reasons for this behavior could not be generalized, as the basic structure was identical. With the goal of biasing the conformational equilibrium towards the active *ap*-form independently of the substituents in the periphery, several approaches to modify the common design were studied.

It could be shown by NMR spectroscopical studies that indeed the proportion of *ap*-conformer can be increased by intramolecular non-covalent interactions (Figure 1.2-6). In system **VIII**, [34] an increase of the *ap/p* ratio by increased steric bulk on the reactive carbons correlated with an increased $\Phi_{O\rightarrow C}$ (*ap/p* ratio for R_1 = Me 65:35, R_1 = ^{i}Pr 94:6).

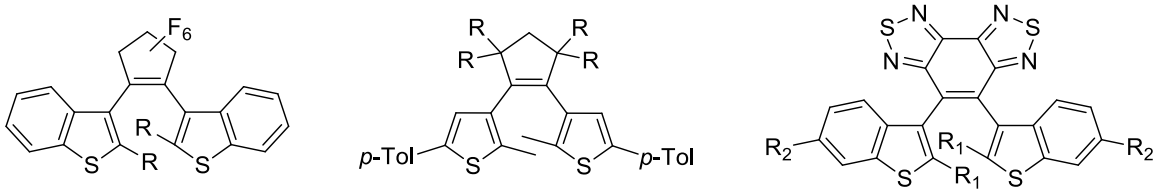

VIII

R = Me	Φ (^{n}Hex) 0.35
R = ^{i}Pr	Φ (^{n}Hex) 0.52

IX

R = H	Φ (MeCN) 0.50
R = Me	Φ (MeCN) 0.83

X

R_1 = Me	R_2 = H	Φ (THF) 0.73
R_1 = Bu	R_2 = H	Φ (THF) 0.67

Figure 1.2-6 Biasing the population of the photoactive *ap*-conformer by steric bulk. Modifications are made at the reactive carbons[34], the bridge moiety[35] or at both[36] positions.

Also an increased steric demand on the bridge moiety[35] in **IX** leads to an increased quantum yield of up to 0.83 by energetically disfavoring the *p*-conformer (*ap/p* 81:19). In the bulky system **X**,[36] the two conformers are frozen and can be separated by

chromatographic methods.[4] It was ultimately demonstrated that the *ap*-conformer has a cyclization quantum yield of up to 0.73 (0.91 with $R_1 = Me$ $R_2 = NO_2$), whereas the *p*-conformer showed no coloration under identical conditions. Given the high amount of *ap*-conformer in the three systems, it thus can be concluded that other de-activation paths are still possible in these structures.

In order not to rely on arbitrary steric interactions and restrict the structure further, intramolecular dative linkages were studied (Figure 1.2-7). Thus, by adjusting the molecular geometry, a cyclization quantum yield >0.5 was established in apolar hexane for **XI** and **XII**.[38] However, the intramolecular interactions are weak in polar solvents and the quantum yield decreased accordingly.

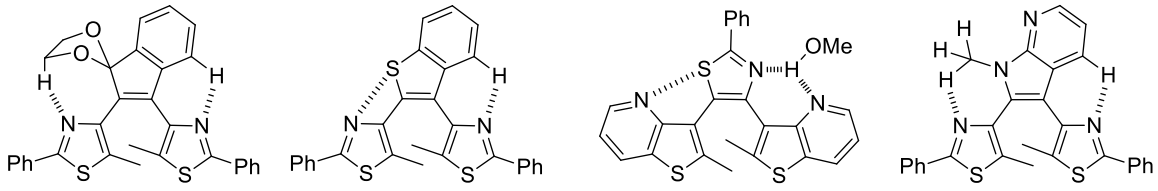

Figure 1.2-7 Biasing the population of the photoactive *ap*-conformer by intramolecular interactions. The cyclization quantum yields are determined in MeOH or EtOH.

An intriguing approach to overcome this problem was to use to the properties of the solvent and establish a host-guest interaction between the photochromic system **XIII** and methanol.[39] As such, the solvent dependency was inversed and the quantum yield increased to 0.88 in methanol, but decreased in hexane. Finally, the geometry could be adjusted in **XIV** as such that both in polar and apolar media a high quantum yield could be achieved.[40]

Another methodology to tailor the geometry of a DAE is the covalent fixation of a conformation (Figure 1.2-8). Probably due to a more complex synthesis, only few systems are reported.[5]

Although the data are scarce, it can be concluded that a poorly chosen geometry will not

[4] A similar system with isolatable atropisomers was already published earlier, but no quantum yields were reported.[37]

[5] For inverse DAEs, a study with different bridge sizes was conducted.[41]

only not increase the switching performance but even prevent successful photocyclization as in **XVI**.

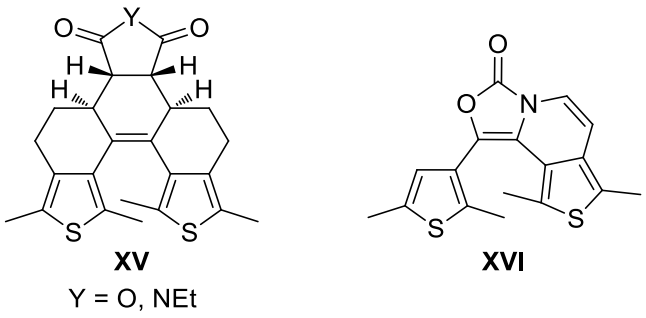

Figure 1.2-8 Fixating the conformation of DAE by covalent bonds. **Left:** The helically locked derivatives are photoactive to some extent.[42] **Right:** The half-stiff derivatives only showed photochromism after reduction of the peripheral double bond.[43] No PSS composition or quantum yield is reported for either of the compounds.

Though already reported earlier for *Z*-stilbenes,[44] Irie and co-workers discovered that efficient cyclization is also possible in single crystals of DAE and accompanied by macroscopic changes in the crystals.[27b] By comparison of a multitude of compounds, a critical maximum distance of 0.42 Å between the two reactive carbons was found to enable photocyclization in the solid state.[45] However, cases known where no coloration was observed, for example in structure **X** (Figure 1.2-6) despite its matching distance.[36]

Some DAEs are reported to be very fatigue resistant, with negligible amount of side reactions in up to several thousand switching cycles.[27a,46] However, most DAE show formation of a characteristic second photoproduct, resulting from further irradiation of the closed isomer with UV light, first characterized[47] by Irie and co-workers (Scheme 1.2-6).

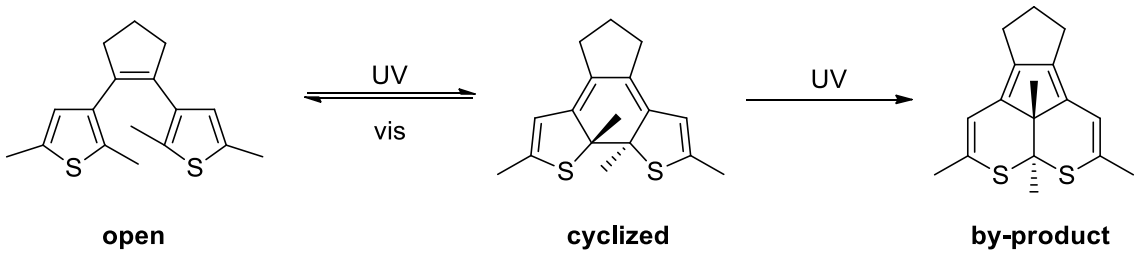

Scheme 1.2-6 Formation of the by-product results from further irradiation of the cyclized isomer with UV light. Due to their similar π-system structure, the by-product and cyclized isomer have similar absorptivities.[47b]

Though its formation mechanism is still under discussion, a comprehensive study from Herder *et al.* could show that the quantum yield for this secondary photoreaction can be

lowered drastically by introduction of electron withdrawing groups as the commercial bis(trifluoromethyl)phenyl unit.[48] In particular, the investigation showed that appropriate functionalization of one hemisphere of the DAE is sufficient to achieve a convenient reduction of the by-product formation, while the second substituent can be freely chosen.

1.2.4 Dual mode photochromism in diarylethenes

Dual mode switching refers to the capability of a photochromic system to undergo two different photoreactions. It needs to be differentiated from dyads, which contain more than one photoactive unit that can switch more or less independently. In the following section, literature-known examples of 6π-systems with an unfixed double bond able to undergo both electrocyclization and double bond isomerization are presented.[6]

Already in 1967, Kellogg and co-workers used the irreversible photochemical conversion of *E*-bis-heteroaromatic compounds to phenanthrene analogues under oxidative conditions, with the *Z*-isomer as probable intermediate.[15a]
In the initial reports about modern DAE systems by Irie and co-workers including 1,2-dicyano-1,2-bis(2,4,5-trimethyl-3-thienyl)ethene (**XVII**) (Figure 1.2-9), a negligible *Z*→*E* double bond isomerization at 405 nm and a 60% conversion to the closed isomer was described.[30a] Yet, a design to prevent double bond isomerization by fixation of the double bond was established and reproduced for a variety of systems in the following decades.
A reinvestigation[50] of the system by Erko *et al.* analyzed the rates of formation of each respective isomer and showed that irradiation with 365 nm preferably stimulates the double bond isomerization, whereas irradiation with 405 nm light induces both double bond isomerization and electrocyclization with a high amount of closed isomer in the PSS. Exact numbers for the final composition at the photochemical equilibrium cannot be given as it was not reached in either experiment. Yet, the maximum amount of *E*-isomer formed upon irradiation of *Z*-**XVII** was 30% and 20%, respectively.

In 2010, Luo *et al.* published functionalized derivatives[51] of Irie's system and the photochemical conversion of both *E*- and *Z*- **XVIII** to the closed isomer upon irradiation

[6] Double bond isomerization and electrocyclization switching in the same photochromic unit are known in other molecule classes as for example fulgimides[49]. For stilbene, methodologies to achieve efficient *Z*-*E* isomerization are reported using mediators (see Section 2.3.7); however, few reports about a dual mode photochromism in modern dithienylethenes exist.

with 365 nm light (Figure 1.2-9). Cycloreversion to the *Z*-isomer was achieved by visible light irradiation. Due to similar ground state energies of both open isomers determined by computational methods, a possible *Z*→*E* conversion was suspected. Yet, no conclusive experimental proof was given.

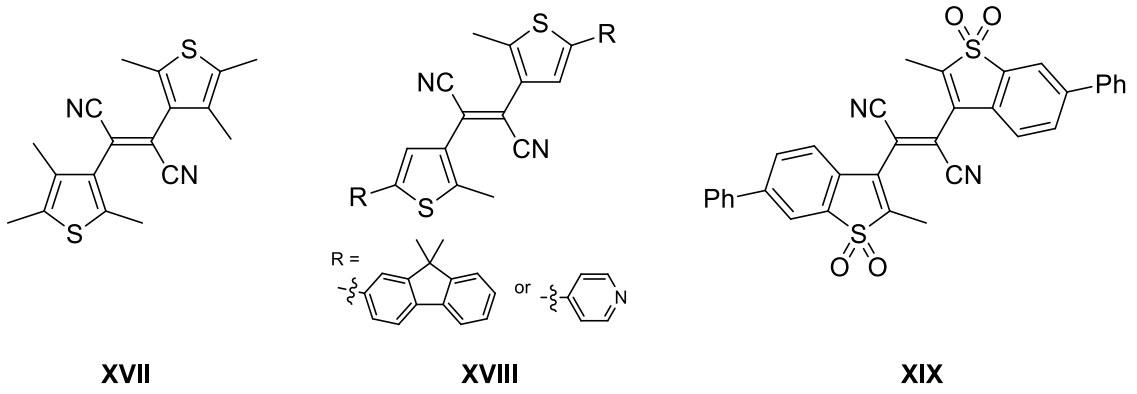

XVII **XVIII** **XIX**

Figure 1.2-9 Bis-heteroaromatic DAE with an isomarizable double bond. 1,2-dicyano-1,2-bis(2,4,5-trimethyl-3-thienyl)ethene (**XVII**)[30a,50] and its functionalized derivatives **XVIII**[51] and **XIX**[52] were found to undergo both double bond isomerization and cyclization, yielding the closed isomer as major photoproduct in the PSS.

Finally, Sumi and co-workers investigated a functionalized and oxidized derivative with increased fluorescence of the closed isomer.[52] As for the unoxidized derivatives, they found very similar absorption spectra for both open isomers, and irradiation with 313 nm light finally yielded the closed isomer in high yield from both open isomers. However, due to the comparable quantum yields for the processes involved ($\Phi_{E\rightarrow Z} = 0.34$, $\Phi_{Z\rightarrow C} = 0.28$ and $\Phi_{Z\rightarrow E} = 0.55$), no quantitative conversion to either isomer was possible. However, the closed isomer can selectively be opened by irradiation with 405 nm.

In 2015, Katz and co-workers investigated an inverse analogue of the systems mentioned above (Scheme 1.2-7).[53]

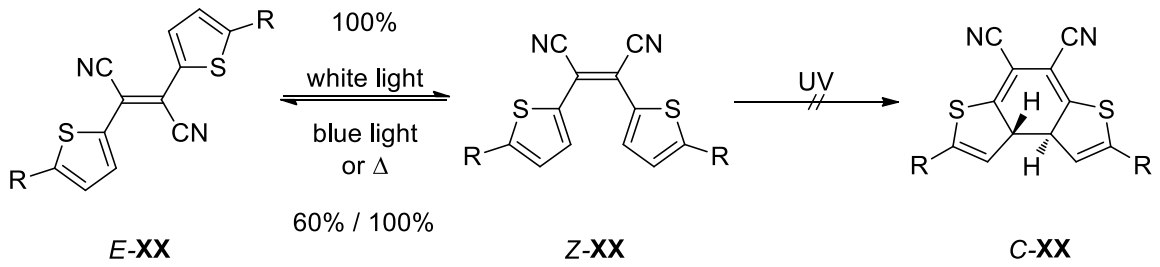

E-**XX** *Z*-**XX** *C*-**XX**

Scheme 1.2-7 Example of a bis-heteroaromatic DAE that only operates in the double bond isomerization regime.[53]

Despite its equal theoretical ability to undergo both double bond isomerization and cyclization, it solely operates in the former mode. The conversion from the *E*→*Z*-isomer is reported to be quantitative with visible light. A cyclization of the *Z*-isomer was not observed, as already described by Kellogg *et al.*[15a] and Takeshita *et al.*[54] for simpler derivatives.

Though photochemical *Z*→*E* conversion only yields 60% *E*-isomer, full conversion can be achieved by thermal isomerization of the electron-poor double bond at 80 °C. In an accompanying transient absorption study, it was suggested that *E*→*Z* isomerization operates in the singlet regime, whereas the reverse reaction undergoes fast intersystem crossing to the triplet manifold.

2. The (photo)chemistry of aDTEs

2.1 Aim of the project

Diarylethenes are known to possess characteristics such as high conversions to both switching states, high thermal stability of both isomers, and low fatigue during the switching process.[27a] However, the photochemical efficiency of the switching process is a matter of optimization, as especially prolonged irradiation with light of short wavelengths can induce unwanted side reactions. For normal DAEs, the most important secondary photoreaction is an irreversible rearrangement of the closed isomer to a by-product with similar spectral properties upon irradiation (Scheme 1.2-6). As the bathochromic cyclization product normally absorbs also at the short wavelengths used to induce the forward reaction, a high cyclization quantum yield is desirable to suppress this secondary process. This aim is challenged by the fact that normal DAEs exist in a conformational equilibrium between a photochemically active and inactive species (Scheme 1.2-5), limiting the cyclization quantum yield $\Phi_{O\rightarrow C} = 0.1\text{-}0.6$. [27a,32] Few examples to overcome this threshold of the quantum yield through biasing this equilibrium towards the active conformation are reported (see Section 1.2.3). Alternatively, by-product formation can be inhibited by electronic means as introduction of electron-withdrawing substituents[48,55] or structural modification.[27a]

In a preceding study, the synthesis of two derivatives of a new class of dithienylethenes (DTEs) with a covalently stiffened ground state geometry and enabled double bond isomerization was described (Figure 2.1-1).[56] To differentiate these dual mode photochromic systems[7] from DAEs with the classic design implemented by Irie and co-workers (compare Figure 1.2-5), the term *annulated* dithienylethenes (aDTEs) is used.

Though the study of their photochemistry had only qualitative character, it was demonstrated that both compounds display desirable behavior as high conversion to the closed isomer from both double bond isomers and a reversible electrocyclization over several switching cycles.

[7] For a definition of dual mode switching and examples, compare Section 1.2.4.

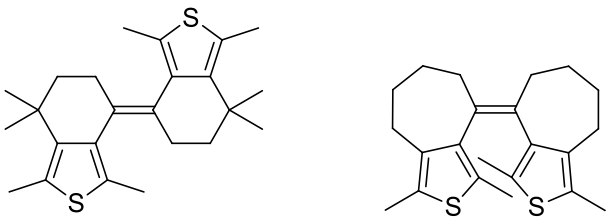

E-**aDTE$_{66}$(Me$_2$)-Me** *Z*-**aDTE$_{77}$-Me**

Figure 2.1-1 Structure of the two annulated dithienylethenes (aDTE) synthesized in an earlier study.[56]

In the current study, the understanding of these systems is deepened through a detailed analysis of their photochemical behavior, including parameters as switching efficiency and fatigue, electrochemical behavior and switching dynamics. Furthermore, the scope of this new class of photochromic systems is extended by the creation of functionalizable derivatives (*vide infra*). In addition, a new subclass, the 5-membered ring derivatives aDTE$_{55}$, are presented and both unconstrained reference compounds and a hybrid system are compared to the aDTE systems for a conceptual understanding of the covalent stiffening of diarylethenes. Finally yet importantly, methodologies to establish accessibility of all three switching states are investigated.

Introduction of a functional group on the aDTE core permits to fine tune and improve the photochemical properties of the aDTE systems as well as their covalent incorporation into larger molecules or polymers. The two positions most attractive for functionalization in aDTEs are the two α-positions of the thiophene, both having different characteristics in each respective switching state (Scheme 2.1-1).

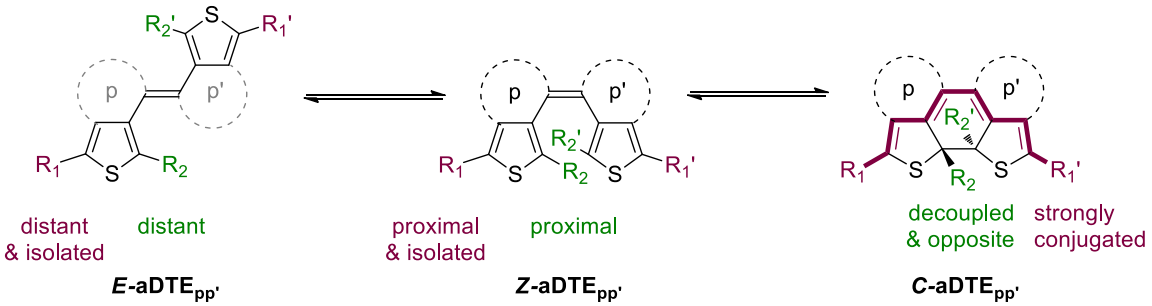

Scheme 2.1-1 Characteristics of functionalizable sides in the three aDTE isomers. While double bond isomerization changes the distance between each pair of substituents R_1 and R_2, electrocyclization induces conjugation between the peripheral substituents R_1 and a decoupling of R_2 from conjugation chain.

If functionalized in the peripheral α-positions R_1, especially the spectrum of the closed form will be influenced due to conjugation of two auxochromes. Other characteristics as

fatigue resistance and cyclization/cycloreversion quantum yields should likewise be affected.[48,55] In contrast, functionalization of the central α-positions R_2 with substituents of different steric demand may affect the thermal double bond isomerization,[57] the cyclization[34] and cycloreversion[58] quantum yields, and even enable thermal cycloreversion.[58a,59] Between all three switching states, the orientation of the substituents relative to each other changes greatly. In addition to varied distances, the inner substituents R_2 are almost in plane in the *Z*-isomer, whereas they point in opposite direction in the *C*-isomer.[60]

2.2 Synthesis of aDTEs

This section provides detailed information about the synthesis of annulated dithienylethenes (aDTEs). General considerations on possible synthetic routes are presented with a retrosynthetic analysis. The synthesis of methyl-substituted "simple aDTEs" and "functionalized aDTEs" is described according to their respective ring sizes. Herein, the identification of the configurational identity by spectroscopic methods as well as distinct structural properties are explained. Finally, the synthesis of a half-stiffened hybrid between aDTE and normal DAE is presented, together with the synthesis of two unconstrained DTEs as reference materials for transient absorption spectroscopy.

2.2.1 General synthetic strategies for aDTEs

The structure of aDTEs consists of two heterophane hemispheres with variable ring sizes *p* and *p′* of the respective aliphatic bridges, which are interconnected at the benzylic position by a double bond (Scheme 2.2-1).

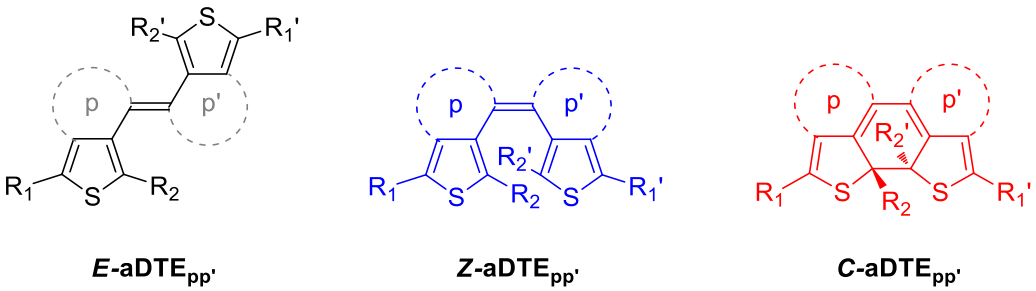

***E*-aDTE$_{pp'}$** ***Z*-aDTE$_{pp'}$** ***C*-aDTE$_{pp'}$**

Scheme 2.2-1 General structure of aDTEs. While *E*- and *Z*-isomers are available by synthesis, the closed isomer (*C*-aDTE) is only obtained by photochemical electrocyclization. For convenient recognition of ring sizes (p, p′) and substituents, the nomenclature R_1-aDTE$_{pp'}$-R_1' is used (R_2/R_2' = Me). For symmetrically substituted derivatives ($R_1 = R_1'$), it is shortened to aDTE$_{pp'}$-R_1.

Even though the steric demand of R_2 is expected to influence the double bond isomerization chemistry of aDTE, in the current studies R_2/R_2' = Me is chosen for comparability. The nomenclature used to visualize quickly ring size and the variable substituent R_1/R_1' is explained in Scheme 2.1-1.

As known for stiff stilbenes (Section 1.5), the ring size p has a fundamental influence on the photochemistry of such constrained compounds. For a detailed examination of its influence in symmetric (p = p′) and non-symmetric (p ≠ p′) aDTEs, it would be desirable

to establish a divergent synthetic sequence that allows for the easy variation of p and p′ in the final steps. However, this approach is unfavorable, as it would require either a two-fold (symmetrical aDTE) or even a selective modification (non-symmetrical aDTE) of alkyl chains on a preformed DTE building block. Alternatively, a retrosynthetic disconnection of the central double bond enables rapid construction of aDTEs with identical or variable ring sizes in both hemispheres by utilizing common heterophane building blocks with predefined ring sizes (Scheme 2.2-2). As such, the central double bond is advantageously synthesized by a McMurry coupling or a Barton-Kellogg reaction of the corresponding ketone building blocks.

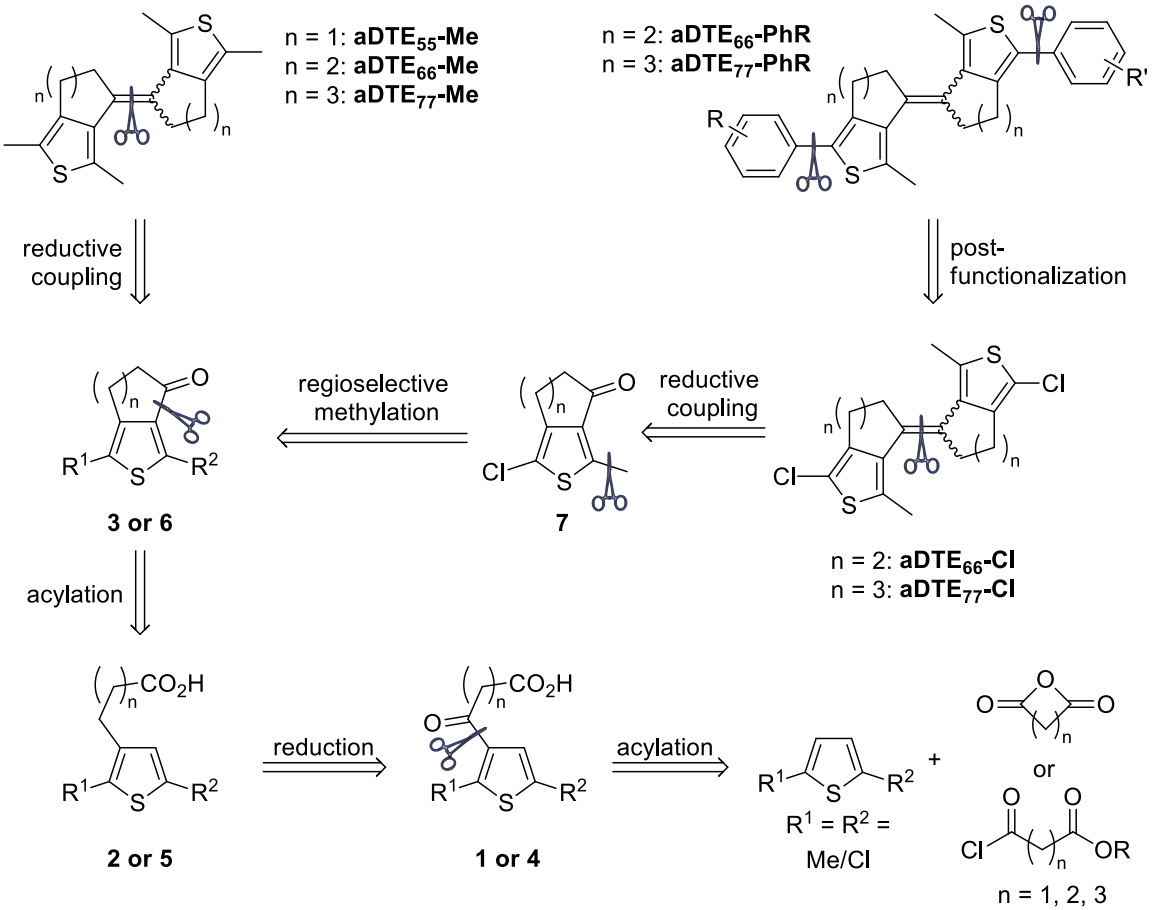

Scheme 2.2-2 Retrosynthesis of simple and functionalized aDTEs. For functionalized aDTEs, the peripheral substituents are introduced in the last step. In both the simple and functionalized systems, the central double bond is formed in a reductive coupling from identical or different cyclic ketone building blocks **3** or **7**, respectively. The ketones itself are obtained from symmetric 2,5-disubstituted thiophenes in an acylation-reduction-condensation sequence. Regioselective substitution of one chlorine substituent is achieved with the cyclic ketone **6**.

The respective cyclic ketone belongs to the rather uncommon group of [*c*]-annulated thiophenes. While several strategies are known[61] to yield benzo[*c*]thiophenes, the saturated variants are not readily available. As an earlier approach to these compounds[62]

could not be reproduced, a classical methodology[63] to [*b*]-annulated thiophenes using an acylation-reduction-condensation sequence was used instead. In order to apply this synthetic strategy in the synthesis of [*c*]-annulated thiophenes, the more reactive α-positions need to be blocked by the final substituents R_1/R_2 or other stable handles that allow for later functionalization, e.g. Cl. For these, both 2,5-disubstituted thiophenes are cheap starting materials and known to undergo the required Friedel-Crafts acylation.[64] The dicarbonyl synthon in this sequence can be either a diacid anhydride or a mono acid chloride monoester, which in general is more expensive but more reactive.

Chlorine atoms in the R_1-position offer the possibility for a late-stage functionalization of the central aDTE core (Scheme 2.2-2, top right). Thus, electronically variable substituents can be introduced easily in order to tune the photochemical properties or the aDTE can be covalently attached to larger molecules or materials. However, in order to install chlorine atoms into the structure, the synthetic sequence has to commence from the symmetrical 2,5-dichlorothiophene, as for example acylation of 2-chloro-5-methylthiophene would give the undesired regiochemistry.[8] Regioselective substitution of the chlorine atom in the R_2-position by a methyl group is preferably done on the stage of the ketone **6** as the electron withdrawing character of the carbonyl group allows for the discrimination between the two alpha positions of the thiophene.[66] In addition, this late stage substitution allows varying the inner substituent conveniently if desired.

2.2.2 Synthesis of simple aDTEs

Methyl-substituted $aDTE_{pp'}$-Me (*"simple aDTE"*) are the easiest aDTE systems imaginable. Due to their shorter synthesis, they offer quick access to evaluate the key characteristics for each ring size, as it was shown earlier.[56] Avoiding two rather arduous palladium catalyzed cross couplings facilitates the production of larger amounts of the desired target structures.

2.2.2.1 Synthesis of 6-membered ring derivatives ($aDTE_{66}$)

The 6-membered ring derivative **$aDTE_{66}$-Me** was synthesized starting from 2,5-dimethylthiophene and succinic anhydride as cheap starting materials (Scheme 2.2-3).

[8] Compare synthesis strategy for 1,2 dithienyl cyclopentenes[65] proposed by Feringa and coworkers, starting from 2-chloro-5-methylthiophene.

The targeted structure of ketone **3a** has already been published;[64a] however, the publication fails to specify the yield as well as any synthetic or analytical details. Furthermore, the approach presented in this study offers the advantage of avoiding the need of column chromatography, since ketoacid **1a** can be readily purified by acid-base extraction. Subsequent carbonyl reduction according to a modified Clemmensen reduction protocol[67] yielded the respective acid **2a** in almost quantitative yield[9] and high purity without further purification by column chromatography.

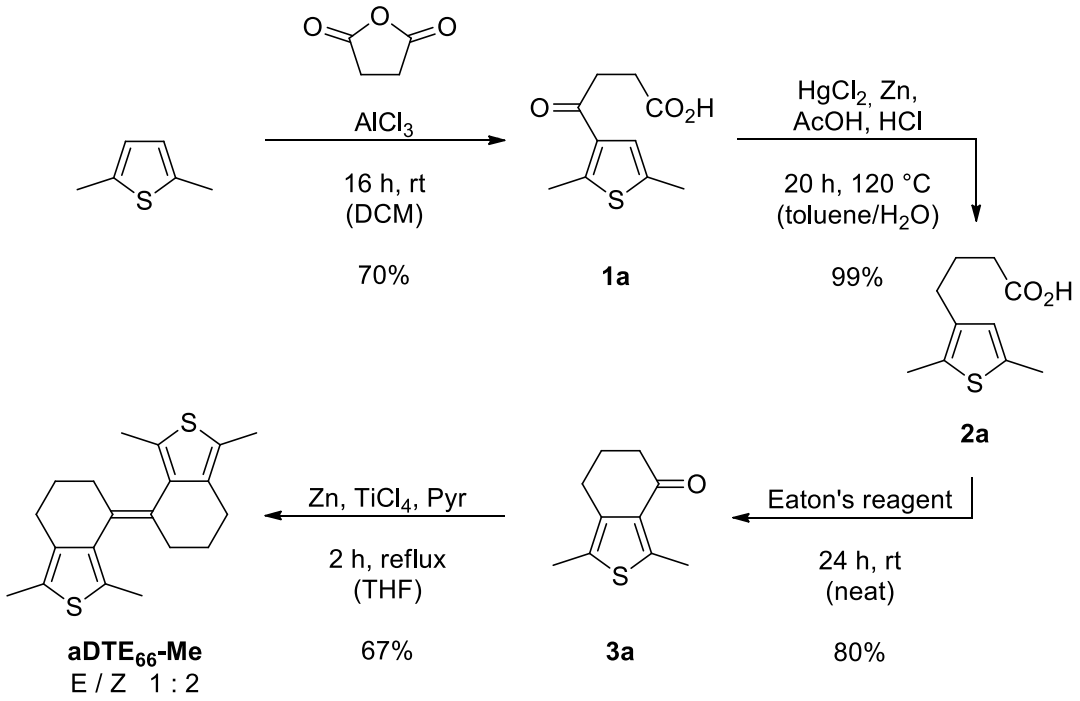

Scheme 2.2-3 Synthesis of **aDTE$_{66}$-Me.** The reaction sequence necessitates no purification by column chromatography except for the final step. Separation of both isomers of **aDTE$_{66}$-Me** can be achieved by normal phase column chromatography or prep. GPC.

Condensation of the open chain acid **2a** was carried out in neat Eatons reagent,[68] a proper replacement for the commonly used but inconvenient polyphosphoric acid (PPA)[10] Addition of DCM as inert solvent is possible to ensure homogeneity of the reaction, but slows down the reaction rate considerably. Again, purification from unreacted starting

[9] Earlier attempts to reduce similar 1,4-dicarbonyl compounds using a Wolff-Kishner protocol were unsuccessful. On the contrary, the protocol used for the dichlorothiophene ketoester **4a** (*vide infra*) yielded the corresponding dimethylthiophene acid derivative **2a** from the dimethyl ketoester **1a-Me** (not shown; obtained by esterification of ketoacid **1a** with MeOH for testing purposes) in >90% yield over two steps. Details can be found in the experimental section.

[10] In contrast to Eaton's reagent, PPA is a very viscous reagent, which can only be stirred at elevated temperatures (> 50 °C). Often, heating is also required for the reaction to take place at all. Furthermore, aqueous workup of PPA is quite tedious due to emulsion formation. The yields of condensations using Eaton's reagent are usually equal or higher than with PPA.

material and other side products bearing an acid function is possible by acid-base extraction, yielding a product pure by NMR analysis. If desired, further purification can be achieved by sublimation at high vacuum.
Finally, ketone **3a** was dimerized reductively in a McMurry coupling reaction according to a protocol inspired by the "instant method" of Fürstner and co-workers[69] and Mukaiyama and co-workers,[70] yielding the *E*- and *Z*-isomer in a 1:2 ratio (determined by ^{1}H-NMR spectroscopy) in 67% combined yield. The distribution of isomers was rather surprising, as in an earlier study[56] the reductive coupling of the related 6-ring ketone **3d** bearing additional methyl groups in the benzylic position gave exclusively *E*-**aDTE$_{66}$(Me$_2$)-Me**. Separation of the isomers was possible by careful column chromatography or preparative GPC.

First hints for the configurational assignment of the two isomers of **aDTE$_{66}$-Me** can already be drawn from the UV/vis trace of the UPLC. As shown for similar compounds,[56] and in contrast to *E*-isomers, *Z*-isomers already tend to photochemically cyclize due to the light of the measurement beam in the diode array detector. This causes a weak absorption in the otherwise empty 400-500 nm region of the spectrum, typical for the ring-closed isomer.

A stronger proof for the identity of the isomers can be derived from the chemical shifts in their ^{1}H-NMR spectra, as already proposed by Curtin et. al. for di(2-thienyl)ethenes[71] and by others for stilbenes[72] (Figure 2.2-1). Located above the aromatic thienyl groups, the methyl groups on the inner α-position are strongly shifted to higher fields in the *Z*-isomer. Since this orientation towards the anisotropic cone is not possible for geometric reasons, the methyl groups in the *E*-isomer are not influenced.
In addition to the identification of both isomers, the chemical shift furthermore gives information on the equilibrium geometry in solution. Though every DAE with the common design is *Z*-configurated, this distinct upfield shift is usually not observed in either simple[30a,65b] or functionalized[48,55,65b] derivatives, showing that their ring-open isomers in solution exist in a conformational equilibrium between different switchable and non-switchable antiparallel and parallel isomers (compare Section 1.3). Consequently, this upfield shift indicates the successful fixation of the DTE structure in the switchable, antiparallel conformation, as expected from the design concept. A similar

effect was found by Kawai and co-workers for DAE that are stabilized in the antiparallel conformation by intramolecular interactions.[38b,40]

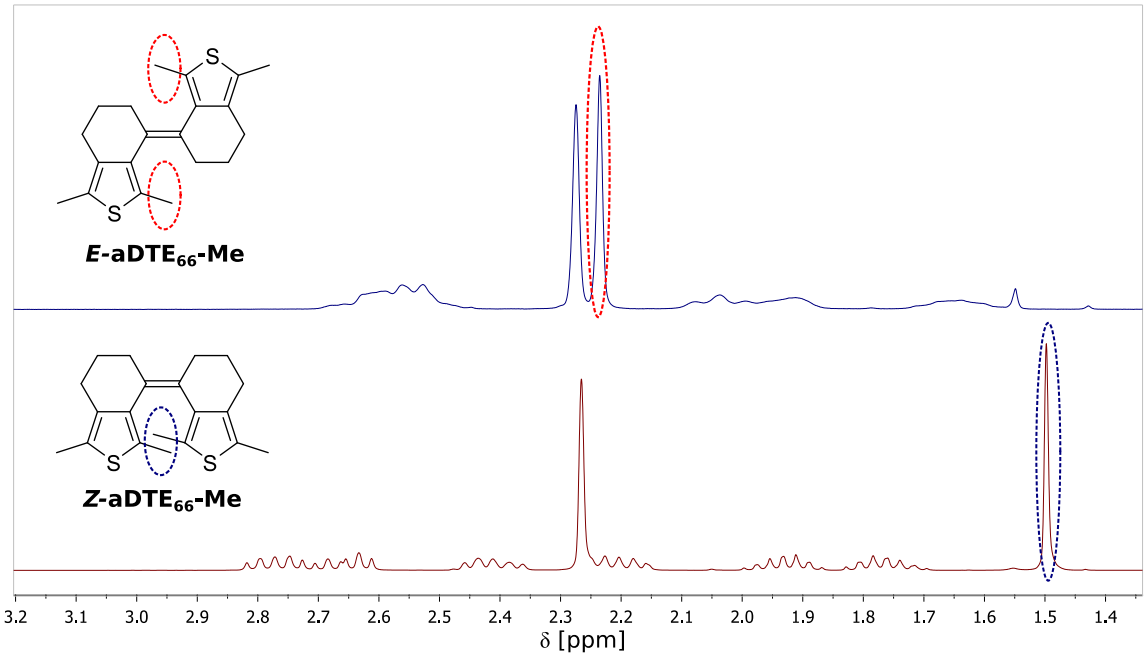

Figure 2.2-1 Configurational assignment of *E*- and *Z*-isomer by ^{1}H-NMR spectroscopy. The inner methyl group in the *Z*-isomer is shifted to higher field (0.7 ppm) due to placement within the anisotropic cone of the other thiophene. Furthermore, especially for *E*-**aDTE$_{66}$-Me** an equilibration between conformers of the 6-membered ring is indicated by the broad signals for the CH_2-groups.

Finally, the configuration of both isomers was ultimately proven by single crystal x-ray analysis[11] (Figure 2.2-2). For the characterization of stilbenoid compounds, three values are commonly considered (Scheme 2.2-4): The bond length of the central double bond r_1, the torsion around the double bond Θ, and the dihedral angle θ between the plane of the double bond and the aromatic system.[12] For DAEs, the distance between the two carbons reacting in the electrocyclization r_2 is an important value (*vide infra*).

[11] All single crystal x-ray structures shown were measured and refined by Dr. Bernd M. Schmidt.

[12] This dihedral angle is also referred to as ϕ, which was not used to prevent confusion with the photochemical quantum yield.

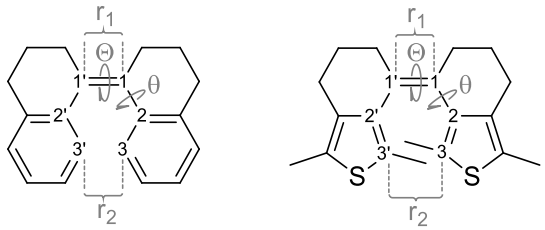

Scheme 2.2-4 Definition of key characteristics of stilbenoid compounds. The dihedral angles Θ (C2-C1-C1′-C2) and θ (C3-C2-C1-C1′) define the torsion around the double and single bond, r_1 and r_2 the double bond length (C1-C1′) and distance between the two reactive carbons in the electrocyclization reaction (C3-C3′), respectively.

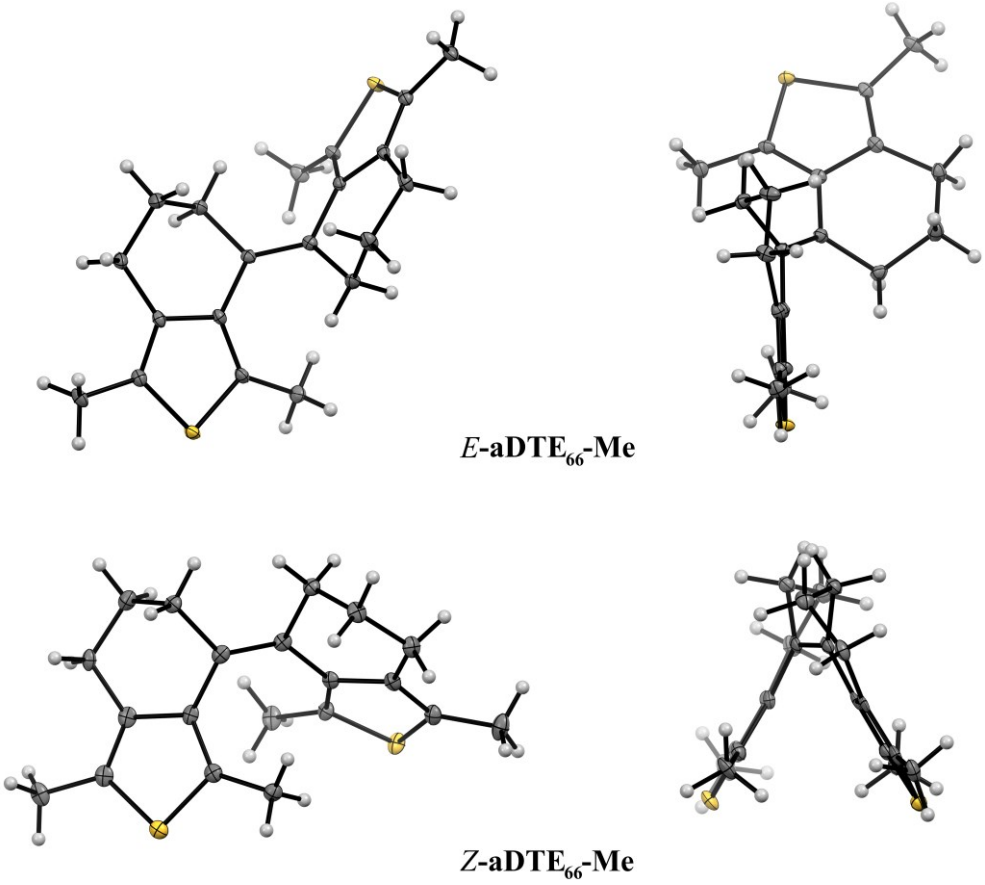

Figure 2.2-2 ORTEP plot (50% probability thermal ellipsoids) of the crystal structures of **aDTE$_{66}$-Me**. **Left:** View perpendicular to one thiophene unit. **Right:** View along the plane of one thiophene after 90° rotation.

In general, the crystal structures of *E*- and *Z*-**aDTE$_{66}$-Me** resemble their stiff stilbene counterparts.[22,73] The cyclohexenylidene motive is in a conformation best described as envelope conformation, which is typical for these structures. Most striking feature is the almost perpendicular orientation the two thiophene planes in the *E*-isomer, which stands

in strong contrast to the flat unconstrained stilbene,[13] but is similar to the analogous stiff stilbene ***E*-stilbene$_{66}$-H** and ***E*-stilbene$_{66}$-Me** (Table 2.2-1).

The double bond is almost not twisted in the *E*-isomer, even though both thiophene planes are standing practically perpendicular to each other. A similar geometry was already observed in the crystal structure of a stiff ***E*-stilbene$_{66}$-H**[22] and for a stiff ***E*-stilbene$_{55}$**[76] (Table 2.2-2), in which the introduction of a methyl substituent at the inner positions of the aromatic system twisted the otherwise flat structure. Nevertheless, the double bonds in both isomers of **aDTE$_{66}$-Me** have the same length, which is slightly longer than in the stilbene equivalent.

Table 2.2-1 Structural parameters of **aDTE$_{66}$-Me** and reference compounds in the single crystal. A separate value is given for θ for each hemisphere (compare Scheme 2.2-4). For consistency, the values for reported compounds are determined from the crystallographic data file.

Compound	Θ [°] (C=C)	θ [°] (Ar-C)	r_1 [Å] (C=C)	r_2 [Å] (C···C)	Structure
***E*-aDTE$_{66}$-Me**	178	-47 / -47	1.36	5.36	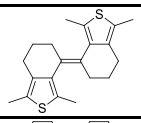
***Z*-aDTE$_{66}$-Me**	17	40 / 36	1.36	3.41	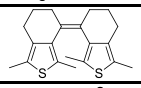
***E*-aDTE$_{66}$(Me$_2$)-Me**[14]	179	-45 / -45	1.36	5.32	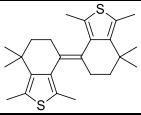
***E*-stilbene$_{66}$-H**[22]	-180	48 / 44	1.35	5.26	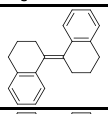
***Z*-stilbene$_{66}$-H**[22]	-11	-39 / -42	1.35	3.14	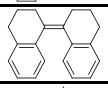
***E*-stilbene$_{66}$-Me**[22]	-166	40 / 40	1.36	4.97	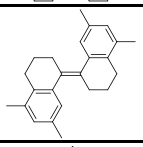
DAE-Cl[77]	-6	-43 / -49	1.35	3.51	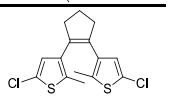

In the *Z*-isomer, this case is inverted. The double bond deviates from the unstrained planar conformation by 17°, but the thiophene planes are well aligned, with a distance of 3.41 Å between the two carbons reacting in the electrocyclization reaction. This distance is

[13] This holds true in the solid state. Gas phase electron diffraction of ***E*-stilbene**[74] revealed deviation from the planar structure, while the gas phase structure of ***Z*-stilbene**[75] is more comparable to its crystal structure.

[14] The asymmetric unit contains two molecules. The dihedral angles are similar in their absolute value but differ by their sign.

shorter than in the normal DAE **DAE-Cl**,[77] and well below the threshold for switching of normal DAEs in solid state (4.2 Å)[45] found by Irie and co-workers. In consequence, switching in the solid state should be possible for *Z*-**aDTE$_{66}$-Me**.

2.2.2.2 Synthesis of 7-membered ring derivatives (aDTE$_{77}$)

The synthesis of the 7-membered ring derivatives using glutaric acid chloride mono ester (Scheme 2.2-5, route B) was already described earlier,[56] but was repeated on a bigger scale for further investigations. The yields are similar to the ones already reported.
In parallel to the synthesis of 6-membered ring derivative **aDTE$_{66}$-Me** (Scheme 2.2-3), the utilization of inexpensive anhydride starting materials was also attempted for the synthesis of the 7-membered analogue, but gave lower yields (route A).

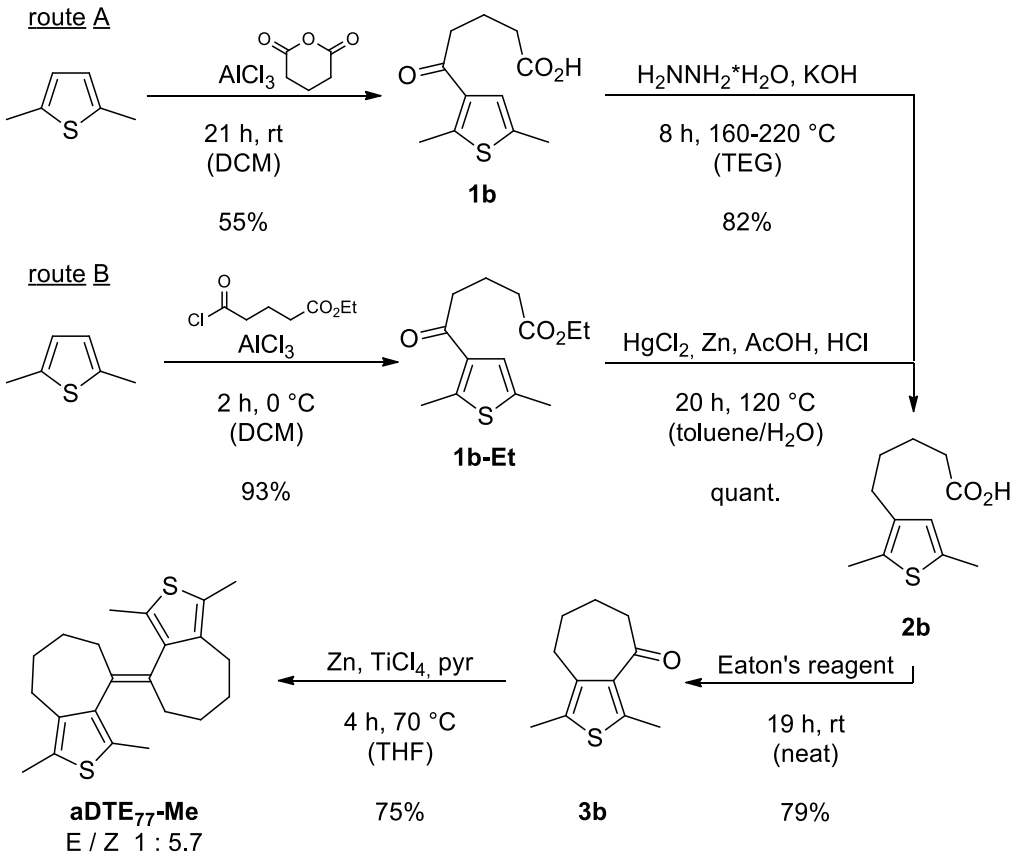

Scheme 2.2-5 Synthesis of **aDTE$_{77}$-Me**. Two pathways to acid **2b** are presented. A new synthesis from glutaric anhydride as for **aDTE$_{66}$-Me** was attempted but low yielding. Scale-up of the published synthesis (route B) was higher yielding. Again, no column chromatography is necessary except in the last step.

A possible reason for the low yield of the first acylation step may be low solubility of glutaric anhydride or low reactivity in Friedel-Crafts reactions in DCM.[15] Furthermore, the increased hydrophobicity due to increased chain length leads to more difficult phase separation during the acid-base extraction. However, no further attempt to increase the yield of this reaction was undertaken.
Compared to the published Wolff-Kishner protocol in route A, the yield of the ketone reduction to yield acid **2b** could be increased by changing to a Clemmensen-type reduction. The reduction worked equally well for both the ketoester **1b-Et** and the ketoacid **1b**, so the overall yield turned out to be higher following route B.

The subsequent condensation of acid **2b** in neat Eaton's reagent yielded ketone **3b** in comparable yield to the 6-membered ring equivalent **3a**. Reductive coupling of the larger ring was possible under standard conditions and lead to an unexpected low amount of *E*-**aDTE$_{77}$-Me** formed (*E*/*Z*-ratio 15:85 vs. 34:66 in **aDTE$_{66}$-Me**). For stiff stilbenes, McMurry couplings yielding a 70:30 and 80:20 *E/Z*-ratio for unsubstituted 7- and 6-membered rings, respectively, were reported.[22] This is in contrast to the trend described for reductive couplings of non-annulated aryl alkyl ketones by Leimner and Weyerstahl.[78] In those open-chain phenyl-alkyl ketones, enhanced steric demand in the series Me < Et < ^{n}Pr < ^{i}Pr < ^{t}Bu increased the amount of *E*-isomer formed. On the contrary, Oelgemöller *et al.* showed for a pair of stiff 6-membered ring stilbenes that a methyl substitution on the benzene ring even remote from the ketone increases the amount of *Z*-isomer formed compared to the non-methylated derivative. This presumably originates from the steric interaction between the methyl groups and the aliphatic ring on the opposing hemisphere and could be more pronounced in case of the sterically more demanding 7-membered ring derivative.
By normal phase column chromatography, only the *Z*-isomer could be obtained purely.[56] Full separation was achieved by prep. GPC. NMR studies of the isomers show again a strong upfield shift of the signal for the inner methyl groups (2.28 and 1.62 ppm in *E*- and *Z*-**aDTE$_{77}$-Me**, respectively), which proofs the desired conformation of the isomers and allows for their configurational assignment.

[15] As in the cases of acylations of less reactive 2,5-dichlorothiophene, a change to the more polar $MeNO_2$ may lead to better results.

2.2.2.3 Synthesis of 5-membered ring derivatives ($aDTE_{55}$)

In contrast to the two derivatives mentioned above, for **$aDTE_{55}$-Me** a different approach was necessary for the initial acylation-reduction steps in order to obtain acid **2c** since malonic anhydride is not readily available and reaction with its mono acid chloride mono ester[79] was sluggish with thiophenes. Alternative routes include the direct coupling of a C3-building block to dimethylthiophene (Scheme 2.2-6, route A), malonester synthesis from the corresponding aldehyde (route B) or addition of an ester group to acetylated dimethylthiophene (route C). While all routes consist of an elongation and a reduction step, route A was dismissed since the direct Heck couplings (i.e. couplings to Ar-H) are mostly reported for the more reactive α-positions of thiophenes and even in these cases, the yields are only mediocre and the optimization of conditions often tedious. Route B was reported for the synthesis of 6-amino derivatives[80] of ketone **3c**, but may also be suitable for a unsubstituted benzylic 6-position as well. Unfortunately, the aldehyde starting material was not affordable in the quantities needed, the synthesis is low yielding (*vide infra*), and the compound itself very prone to degradation.

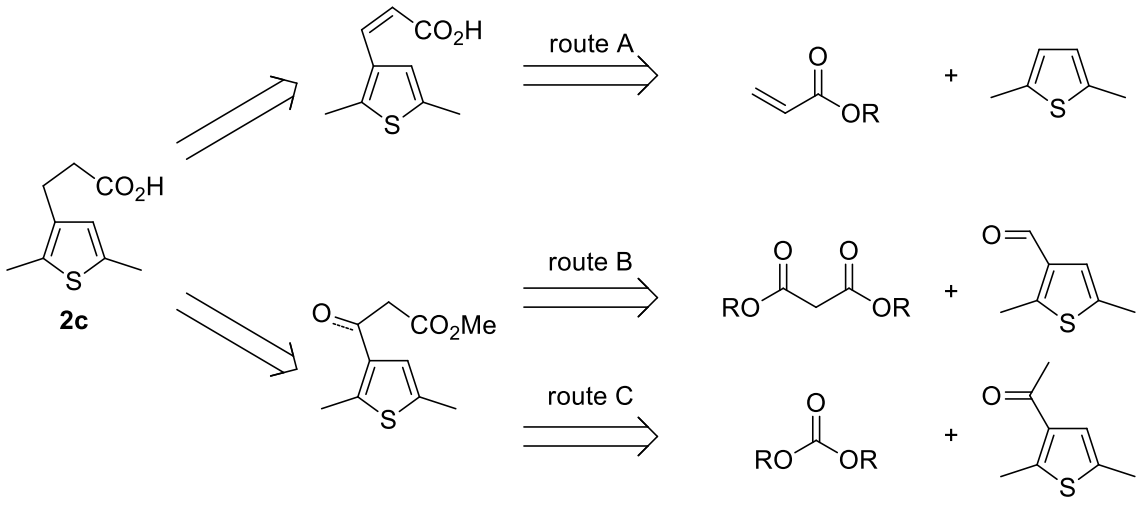

Scheme 2.2-6 Alternative routes to acid **2c**. Alternatives to Friedel-Crafts acylation of dimethylthiophene with malonic acid chloride comprise direct Heck coupling (route A), malonester synthesis (route B), or addition of an ester group (route C).

In contrast to two other methods, route C starts from the stable, commercial 3-acetyl-2,5-dimethyl-thiophene, and the elongation step and several robust carbonyl reduction methods were already successfully employed on similar compounds. The carboxylation

of the acetyl group with dimethyl carbonate and sodium hydride[81] in toluene[16] easily yielded the desired ketoester **1c-Me** and its corresponding enolester tautomer in high yield (Scheme 2.2-7). Despite unsuccessful attempts to reduce the ketone with $TiCl_4/Et_3SiH$[83] (low conversion), TFA/Et_3SiH[84] (low conversion), $H_2/Pd(C)$ in AcOH/cat. H_2SO_4[85] (decarboxylation) or AcOH only[86] (no conversion), reduction following a Clemmensen protocol[87] proceeded readily and in good yield. Reaction control by UPLC showed partial formation of the unsaturated ester that was not further reduced even by prolonged reaction times. Under the acidic conditions, the ester group was partially hydrolyzed. Subsequent basic saponification of the crude led to a uniform product, which enabled purification by acid-base extraction. Crude acid **2c** was then treated with Eaton's reagent. For solubility reasons, an equal amount of DCM was added, which slowed down the reaction considerably compared to a neat test reaction. Even though the conversion of both acids was quantitative according to TLC, basic workup and the need for column chromatography in order to separate the two products lowered the yield of the desired ketone **3c** considerably.

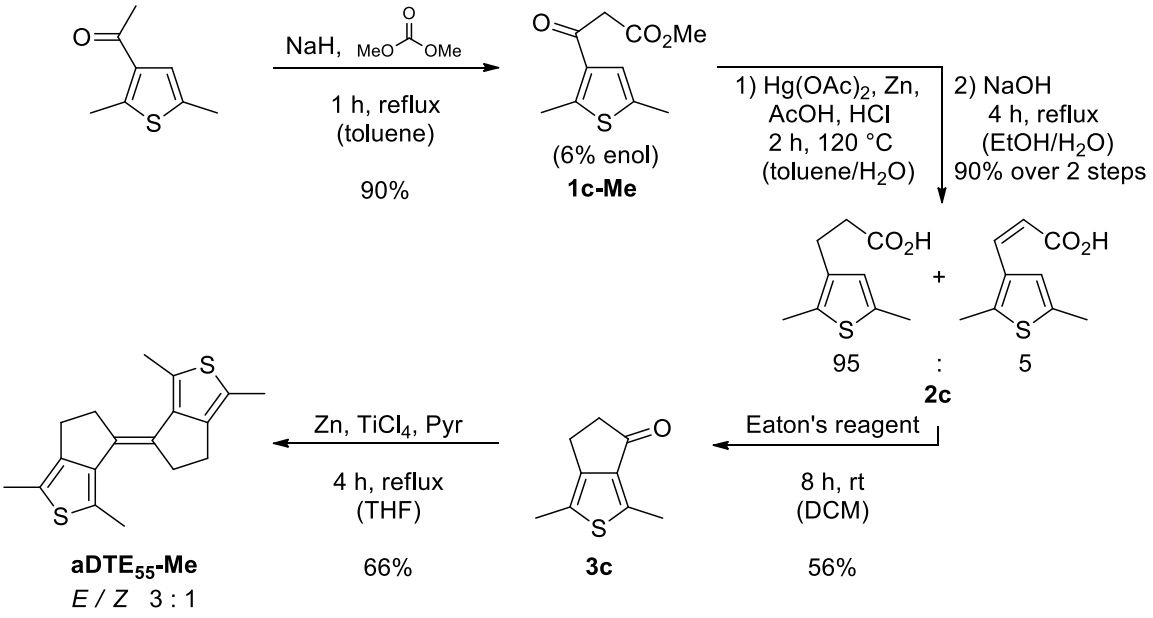

Scheme 2.2-7 Synthesis of **aDTE$_{55}$-Me**. Some unsaturated acid **2c** formed during the reduction of ketoester **1c-Me**. Saponification prior to reduction may suppress this side reaction and enable acid-base extraction workup.

[16] For the dichlorothiophene compound, the reaction was reported in neat dimethylcarbonate[82] with lower yield (67%), but without the need of column chromatography.

For future work, a change of the reaction order, i.e. saponification of the crude ketoester **1c-Me** prior to ketone reduction may be advantageous, as it will suppress the formation of the unsaturated by-product that is probably derived from the enol form of **1c-Me**. At the same time, acid-base extraction would be possible from the first step on and hence increase the yield and ease of purification. Furthermore, TFA anhydride[88] was proposed as a condensation reagent superior to PPA for 5-membered rings.

McMurry coupling of ketone **3c** was achieved under standard conditions and yielded the two isomers of **aDTE$_{55}$-Me** in a 3:1 ratio. After flushing through a pad of silica, the major isomer was obtained by preparative GPC, while the minor isomer could not be isolated in its pure form due to the low quantity. Identification of the isomer by NMR or UV/vis absorption turned out to be challenging, since the second isomer was not available for comparison and no cyclization was observed. Finally, identification of the major product as *E*-isomer was done by crystallographic analysis and investigation of its photochemical behavior (Section 2.3.3.4).

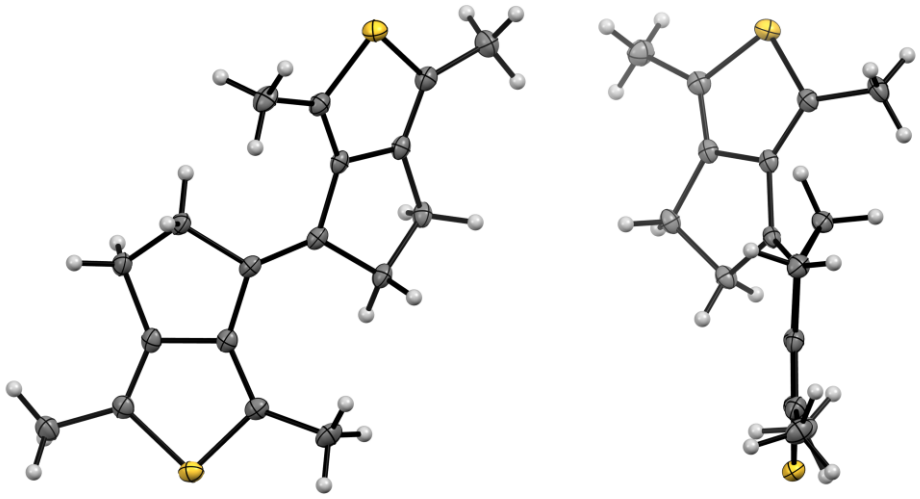

Figure 2.2-3 ORTEP plot (50% probability thermal ellipsoids) of the crystal structure of *E*-**aDTE$_{55}$-Me**. **Left:** View perpendicular to one thiophene unit. **Right:** View along the plane of one thiophene after 90° rotation. As observed for the 6-membered ring derivative **aDTE$_{66}$-Me**, both thiophene planes are almost perpendicular to each other.

The single crystal x-ray structure of *E*-**aDTE$_{55}$-Me** (Figure 2.2-3) closely resembles that of the stilbene analogue *E*-**stilbene$_{55}$-Me** and structural parameters are very similar (Table 2.2-2). Similar to their 6-membered ring analogues, they show a twisted geometry regarding the thiophene ring planes, which is in stark contrast to the non-methylated

stilbene *E*-**stilbene$_{55}$-H** being a flat molecule. This demonstrates that the steric interaction of the methyl groups with the neighboring aliphatic ring is responsible for the twisting of the structure.

Table 2.2-2 Structural parameters of **aDTE$_{55}$-Me** and reference compounds in the single crystal. For detailed definition of the parameters, see Scheme 2.2-4. Literature values are determined from the crystallographic data file.

Compound	Θ [°] (C=C)	θ [°] (Ar-C)	r_1 [Å] (C=C)	r_2 [Å] (C···C)	Structure
***E*-aDTE$_{55}$-Me**	173	32 / 33	1.34	5.84	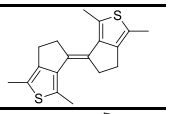
***E*-stilbene$_{55}$-H**[89]	-180	0 / 0	1.35	5.72	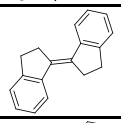
***E*-stilbene$_{55}$-Me**[90]	174	38 / 40	1.34	5.71	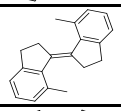
***Z*-stilbene$_{55}$-Me**[76]	13	34 / 34	1.36	3.72	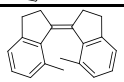

Notably, due to the more conformationally restricted 5-membered rings in *E*-**aDTE$_{55}$-Me**, the torsion around the central double bond is more pronounced as compared to *E*-**aDTE$_{66}$-Me** (Table 2.2-1), while the torsion around the neighboring single bond is smaller. Furthermore, if *Z*-**aDTE$_{55}$-Me** is structurally similar to the respective substituted *Z*-**stilbene$_{55}$-Me**, electrocyclization in the solid state should be possible.

2.2.3 Synthesis of functionalized aDTEs

The introduction of auxochromic and/or functional groups in aDTE$_{pp'}$ (*"functionalized aDTE"*) greatly enhances scope of this new molecule class and allows for photochemical tuneability.

In order to have the highest flexibility in choosing the substituents with the smallest synthetical effort, functionalization is implemented at the late steps of the divergent synthesis. By starting from a symmetrically substituted thiophene, the well-established acylation-reduction-condensation sequence can be applied again, avoiding the undesirable regiochemistry of the Friedel-Crafts acylation for unsymmetrically 2,5-substituted thiophenes.[17]

[17] For a brief discussion of this subject, see Section 2.2.1.

2.2.3.1 Synthesis of 6-membered ring derivatives

The synthesis follows the general synthetic strategy for aDTEs. Since the dichlorothiophene ketone **6a** is already reported,[64b] it was attempted to reproduce this synthesis. Starting from 2,5-dichlorothiophene, the Friedel-Crafts acylation using succinic anhydride in DCM gave rise to the respective ketoacid in 55% yield (not shown). Unfortunately, the proposed carbonyl reduction using $TiCl_4/Et_3SiH$ after in situ protection of the acid functionality with TMS-Cl did not work in our hands. Several alternative reduction methods including Clemmensen reduction or palladium-catalyzed deoxygenation proved incompatible due to partial or full dechlorination of the thiophene moiety.

Finally, reduction using the silane method[83] was successful after protection of the acid group as an ester. Since the yield for the Friedel-Crafts acylation with succinic anhydride was only mediocre and the following esterification elongates the synthesis further, the anhydride in the first step was replaced by succinic ethyl ester acid chloride, giving 73% of the respective ketoester **4a** (Scheme 2.2-8) in good purity after basic washing.

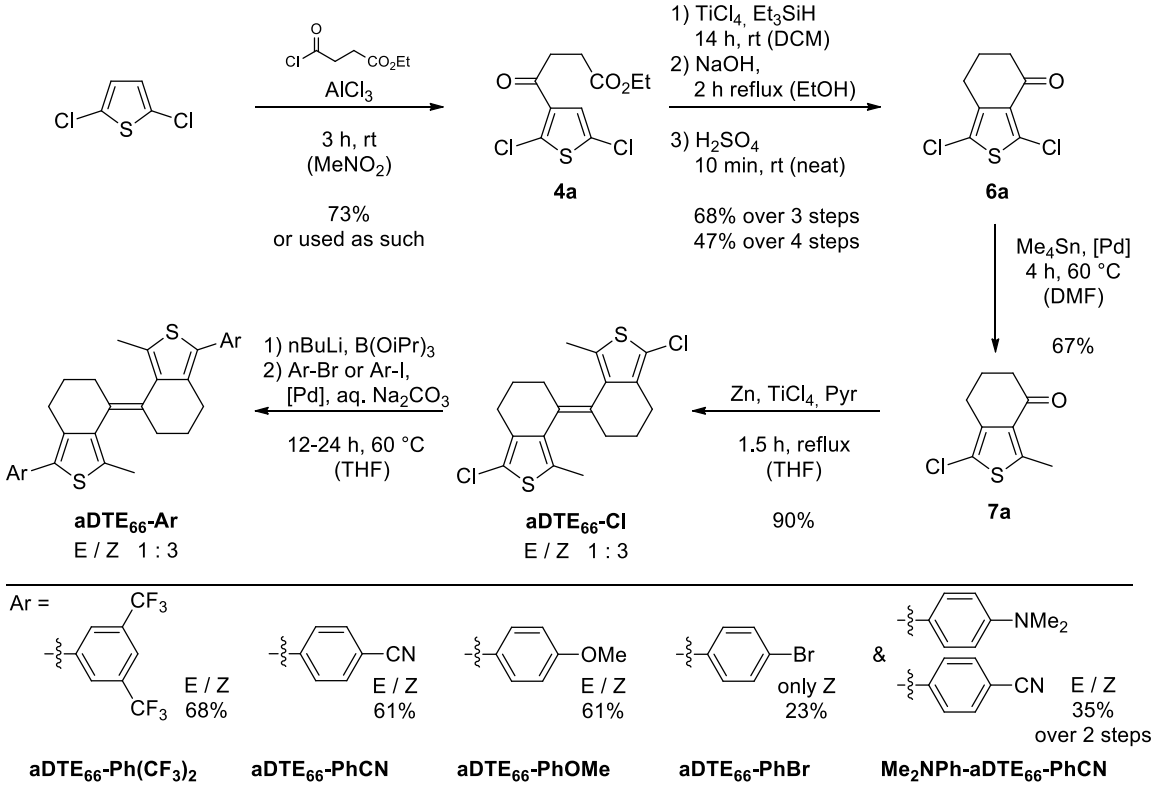

Scheme 2.2-8 Synthesis of functionalizable $aDTE_{66}$. Key step is the regiospecific functionalization of the 2,5-dichloroketone **6a**. Other substituents than a methyl group are possible but were not realized in this work. Again, no column chromatography is necessary for the first reaction steps.

Reduction of ketoester **4a** afforded a crude product contaminated with residual silane and its reaction products. Even though the separation by column chromatography is possible, their removal by means of acid-base extraction after the saponification step was preferred. In contrast to the methyl analogue **2a** (Scheme 2.2-3), condensation of acid **5a** was not possible with Eaton's reagent, but instead good yields were obtained in neat conc. H_2SO_4 as proposed by Rackelmann *et al.*[64b] Basic wash of the reaction product afforded dichloroketone **6a** in 68% yield and NMR purity from ketoester **4a**. For the sake of operational simplicity and scalability, the complete reaction sequence up to ketone **6a** was performed without resorting to column chromatography, affording 47% of a clean product after four steps.

Key step in this reaction scheme is the regiospecific functionalization of dichloroketone **6a** at the position adjacent to the ketone. Though a *preference* towards the desired regiochemistry is evident by the electron withdrawing nature of the carbonyl group, adjustment of the catalytic system allowed for *selective* formation of the desired chloromethylthiophene **7a** and tedious chromatographic separation could be avoided. Although a Suzuki-coupling with methyl boroxine gave a fair amount of the desired regioisomer, overmethylation and/or low conversion turned out to be problematic. Despite its toxicity, a Stille coupling employing Me_4Sn with $AsPh_3$ and Pd_2dba_3 in DMF was the best-suited combination. While the palladium source seems to be of minor importance on the first glance, dba is known to influence the course of Stille couplings.[91] The use of $AsPh_3$, which possesses a softer central atom than the more common homologous PPh_3, is crucial and also known to accelerate Stille reactions.[92] Removal of the highly toxic and volatile tin reaction by-products as Me_3SnCl and its dimer $Me_3Sn\text{-}SnMe_3$ is possible by precipitation with fluoride ions during the workup. Thus, the monomethylated ketone **7a** could be obtained in 67% yield.

Structural assignment of the monosubstituted product was challenging. A long-range ^{1}H-^{13}C coupling experiment (HMBC) to determine proximity of the introduced methyl group to the carbonyl group gave no conclusive results as the benzylic CH_2-group and the methyl group overlap (Figure 2.2-4, peak 1 and 4). However, comparison of the product with the signals of the already synthetized dimethyl thiophene analogue **3a** allowed to assign the structure unequivocally (Figure 2.2-5). Having almost identical spectra, for **7a** the peak 5′ of the ketone-opposing methyl group is missing while the peak 4′ of the

benzylic CH_2-group is shifted downfield due to the electron withdrawing effect of the neighboring chlorine substituent.

McMurry coupling of **7a** according to the standard protocol afforded the dichloro precursor **aDTE$_{66}$-Cl** in slightly different isomer ratio compared to the methyl derivative **aDTE$_{66}$-Me** (*E*:*Z* = 1:3 vs. 1:2). Surprisingly, in contrast to the easy separation of the latter, the isomers of **aDTE$_{66}$-Cl** could be separated neither by column chromatography nor by preparative GPC. Fortunately, due to the excess of *Z*-**aDTE$_{66}$-Cl**, it could be isolated by recrystallization from the mixture of isomers.

In order to estimate the scope of functionalizable aDTE, a variety of derivatives were synthesized by two-fold Suzuki coupling. Surprisingly, isomerically pure *Z*-**aDTE$_{66}$-Cl** did not give the expected functionalized *Z*-isomers but an isomeric mixture.[18] By consequence, the following derivatives were obtained starting from the mixture of isomers: **aDTE$_{66}$-PhOMe** (π-donor), **aDTE$_{66}$-PhCN** (π-acceptor) and **aDTE$_{66}$-Ph(CF$_3$)$_2$** (σ-acceptor), the latter known to increase fatigue resistance of DAEs.[48]

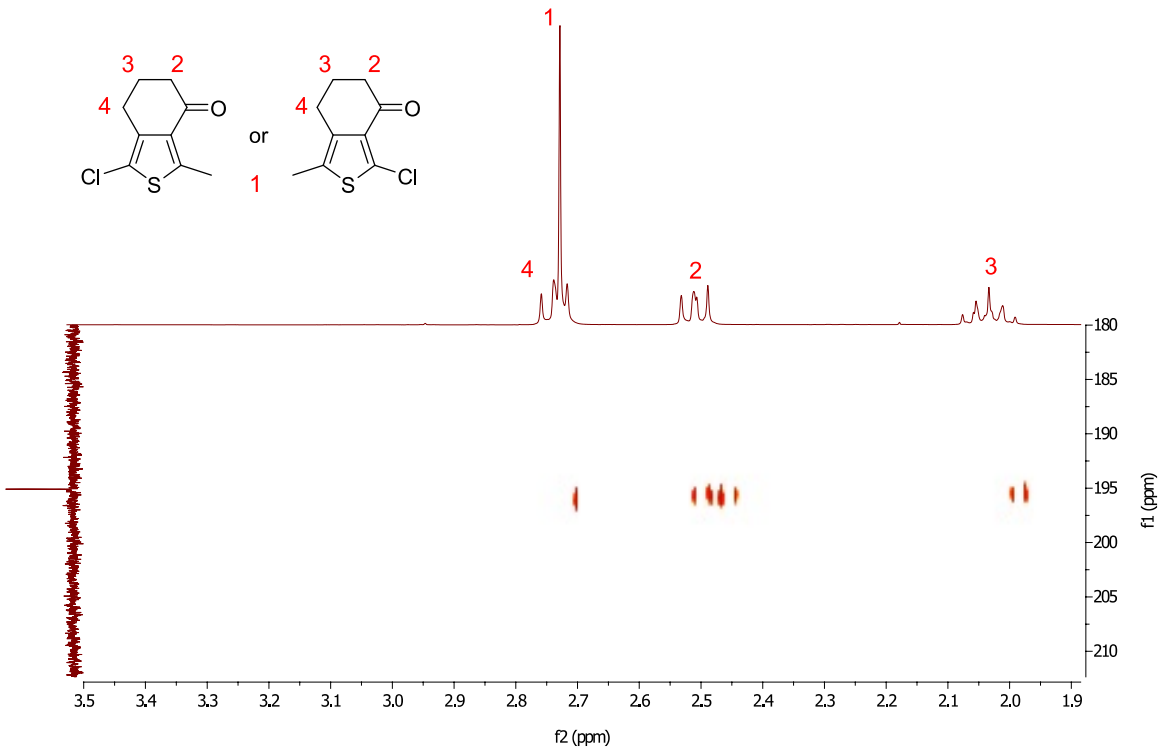

Figure 2.2-4 Attempted structural assignment of monosubstituted ketone **7a** by HMBC. Identification of the methyl group's position is not possible as the signal of the benzylic CH_2-group and of the methyl group overlap.

[18] This phenomenon will be further discussed in Section 2.3.7.2.

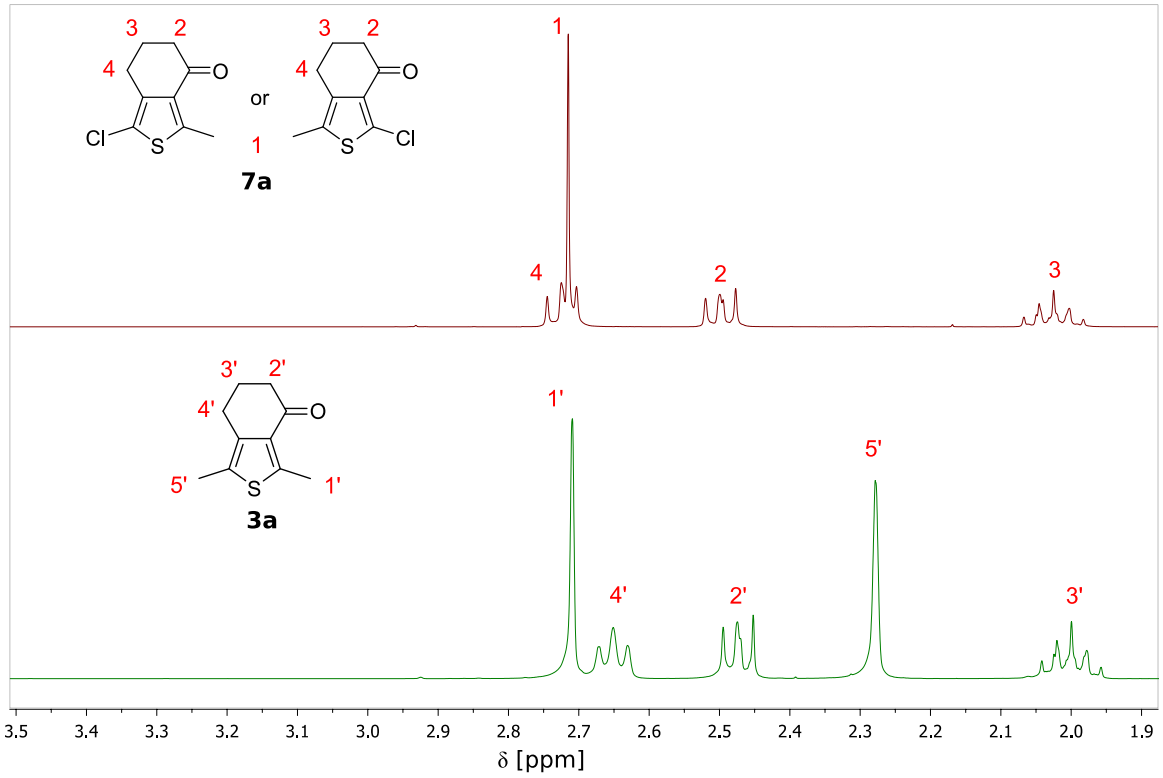

Figure 2.2-5 Structural assignment of monosubstituted ketone **7a** by comparison with dimethyl-derivative **3a**. While the spectra of both compounds are similar, the absence of signal 5′ indicates the desired constitution of **7a**.

The bromine substituted **aDTE$_{66}$-PhBr** was synthesized for the potential ease of crystallization and single-crystal structure determination. In contrast to the former compounds, the brominated derivative could only be obtained in low yield and as *Z*-isomer exclusively. A reason for both may be the low solubility of the products, leading to isolation of only the most abundant isomer. Also the unsymmetrically donor and acceptor substituted **Me$_2$NPh-aDTE$_{66}$-PhCN** was produced in a two-step sequence. Purification of all photochromic compounds was carried out by column chromatography, which however failed to separate the isomeric mixtures. Although it is to be expected that both *E*- and *Z*-isomer are photochemically converted into the closed isomer (*vide infra*), separation for analytic purposes was carried out on small scale with preparative reverse phase HPLC. Again, crystallization of the *Z*-isomer as major compound was sometimes possible by slow evaporation of a saturated MeCN/H_2O/THF mixture.

The single crystal x-ray structures could be obtained for several derivatives.[19]

[19] All single crystal x-ray structures shown were measured and refined by Dr. Bernd M. Schmidt.

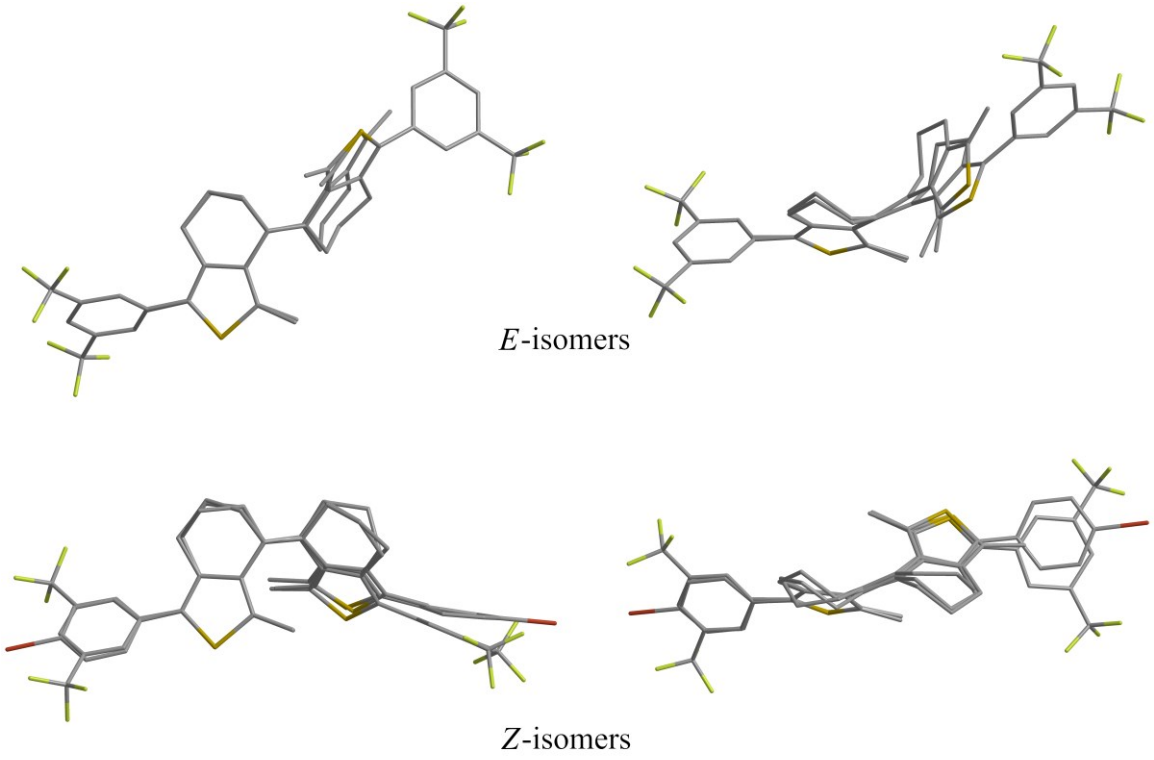

Scheme 2.2-9 Overlay of single crystal x-ray structures of simple and functionalized aDTE$_{66}$. **Top:** ***E*-aDTE$_{66}$-Me** and ***E*-aDTE$_{66}$-Ph(CF$_3$)$_2$**. **Bottom:** ***Z*-aDTE$_{66}$-Me**, ***Z*-aDTE$_{66}$-Ph(CF$_3$)$_2$** and ***Z*-aDTE$_{66}$-PhBr** using ChemBio3D (CambridgeSoft). Hydrogens and disordered fluorines omitted for clarity. The individual structures can be found in Section 4.6.

From the overlay of simple and functionalized aDTE$_{66}$, it can be derived that the basic framework is largely independent of the substituents (compare Figure 2.2-2 and Table 2.2-1).

Table 2.2-3 Structural parameters of functionalized aDTE$_{66}$ in the single crystal. The definition of the angles and distances is given in Scheme 2.2-4.

Compound	Θ [°] (C=C)	θ [°] (Ar-C)	r_1 [Å] (C=C)	r_2 [Å] (C···C)	Structure
***E*-aDTE$_{66}$-Ph(CF$_3$)$_2$**	174	-38 / -38	1.38	5.45	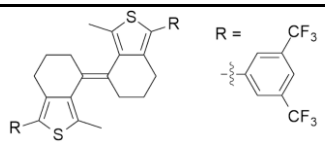
***Z*-aDTE$_{66}$-Ph(CF$_3$)$_2$**	-10	-41 / -47	1.35	3.38	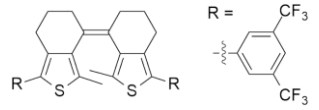
***Z*-aDTE$_{66}$-PhOMe**	-10	-41/ -47	1.35	3.26	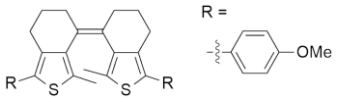
***Z*-aDTE$_{66}$-PhBr**	9	50 / 46	1.35	3.44	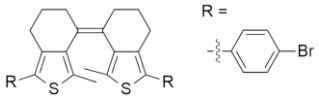

In both isomers of **aDTE$_{66}$-Ph(CF$_3$)$_2$**, some of the fluorine atoms were disordered, which may indicate only weak interaction with the neighboring molecule. Fluorine-hydrogen short contacts were found between the benzylic CH_2-positions and one fluorine atom in each hemisphere.
Additionally in the *Z*-isomer, other short contacts with the inner methyl group and other CH_2-groups are found, which may be the reason why ***Z*-aDTE$_{66}$-Ph(CF$_3$)$_2$** overlaps less with the simple aDTE$_{66}$ than the brominated derivative. Likewise, it represents a possible explanation for the stabilization of the cyclohexenylidene motives in the rather uncommon equatorial conformation.

The length of the central double bond and distance between the reactive carbons in the electrocyclization are unchanged. For the *Z*-isomer, this distance is well within the limit[45] for switching in the solid. In accordance to that, a coloration of TLC spots the products upon UV-irradiation was observed. However, due to a lack of resolution, it could not be attributed to a specific isomer.

2.2.3.2 Synthesis of 7-membered ring derivatives

The synthesis of the 7-membered ring derivatives was carried out in analogy to the 6-membered ring functionalizable derivatives (compare Scheme 2.2-8). In contrast to the reaction with succinic anhydride, acylation with glutaric anhydride yielded no uniform product, even though attempted in nitromethane, which from earlier experiments is known to improve reactions of electron poor substrates.[56]

However, acylation using the corresponding glutaric mono acid chloride was effective, although the yield of the following reduction-saponification was somewhat lower then of its homologue using the same protocol. Because of the lower reactivity of acid **5b**, the condensation protocol required modification. Conversion to the acid chloride with oxalyl chloride proceeded rapidly,[20] and the following acylation using $AlCl_3$ was performed in situ. After acid-base extraction, the product is obtained in high purity, but can be purified further by sublimation. Unexpectedly, the subsequent Stille coupling of ketone **6b** with

[20] The progress of the reaction can be checked conveniently by quenching an aliquot with a water-free alcohol and consequent TLC of the acid/ester mixture. MeOH should be used preferably since it does not form an azeotrope with water and can be obtained relatively dry from distillation.

Me_4Sn using the established protocol gave not only the desired methylated ketone **7b** but also two side-products that could be identified (Scheme 2.2-11).

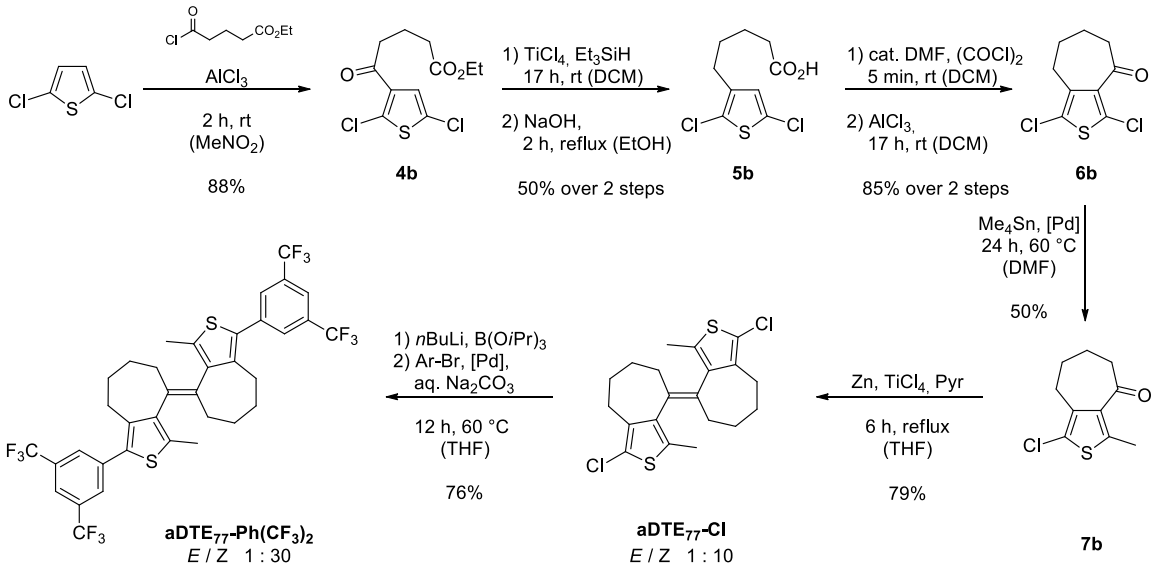

Scheme 2.2-10 Synthesis of functionalizable $aDTE_{77}$. The approach followed was adapted from the functionalized $aDTE_{66}$ (compare Scheme 2.2-8) but features a Friedel-Crafts acylation instead of acid-mediated condensation to form ketone **6b**.

It is known that homocoupling can be caused both by inter- and intramolecular exchange reactions in the palladium complex after the oxidative-addition step,[91] the latter leading to a substrate-$SnMe_3$ intermediate that can now preferably transfer the aryl-substituent and lead to diketone **8**.

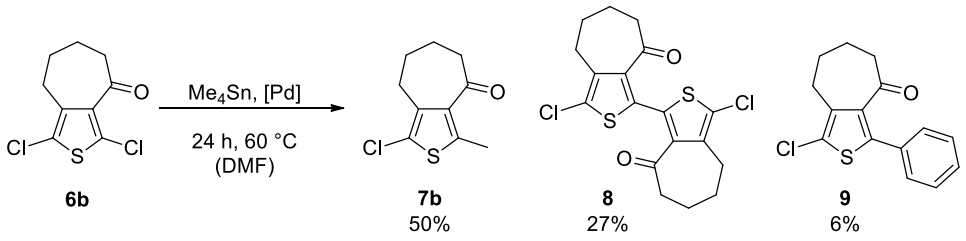

Scheme 2.2-11 Side products of Stille methylation of ketone **6b**.

With no other possible phenyl source present in the reaction mixture, the phenylated ketone **9** must derive from an exchange reaction with the $AsPh_3$ ligand. Indeed, this phenomenon has already been observed as a side reaction in Stille couplings with the PPh_3 ligand[93] and is known to be faster with $AsPh_3$ in case of electron-rich substrates.[94] With only weak long range couplings between the two aromatic rings, the constitution of ketone **9** was unclear at first, but finally could be doubtlessly proven by single crystal

x-ray diffractometry (Figure 4.7-9). Unfortunately, an attempted McMurry coupling of phenylketone **9** failed, possibly due to the increase steric demand around the carbonyl function.

In contrast, reductive dimerization of the methylated ketone **7b** gave the respective aDTE in high yield, and almost exclusively as *Z*-isomer. Exemplary functionalization with bis(trifluoromethyl)-phenyl gave pure ***Z*-aDTE$_{77}$-Ph(CF$_3$)$_2$** after crystallization.

2.2.4 Synthesis of half-stiff aDTEs and reference compounds

Earlier studies in our group by Herder *et al.* have shown that the introduction of one functionalized hemisphere is enough to maintain most of the photochemical performance of normal DAE switches and thus gives the freedom to implement other functionalities.[48,55] In order to extend the versatility of the present system accordingly, it was tested how non-symmetric, half-stiff derivatives behave. For this purpose, the functionalizable building block **7a** was coupled with 1-bromo-3,5-bis(trifluoromethyl)benzene in quantitative yield, yet, separation of the coupling partner was tedious and lowered the yield considerably. Reverse-phase chromatography may give higher yield than recrystallization. Ketone **10** was coupled with commercial 3-acetyl-2,5-dimethylthiophene as a dummy ketone in an non-symmetric McMurry coupling (*E/Z*-ratio 1:3) to obtain **(F$_3$C)$_2$Ph-aDTE$_{6Me}$-Me** almost exclusively as *Z*-isomer (Scheme 2.2-12).

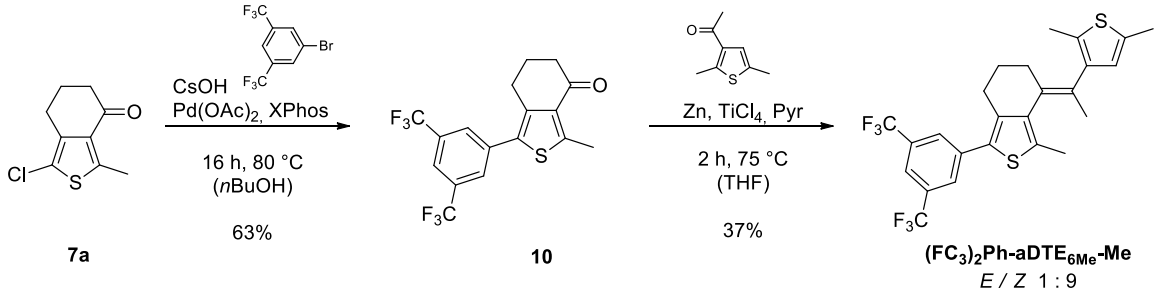

Scheme 2.2-12 Synthesis of the hybrid half-stiff **(F$_3$C)$_2$Ph-aDTE$_{6Me}$-Me**. 3-acetyl-2,5-dimethylthiophene was used exemplary and can be substituted by other aromatic ketones.

After the failure of normal phase chromatography, the undesired homocoupled products (mainly symmetrical **13**) could easily be removed by prep. GPC. Separation of both product isomers was neither possible under these conditions nor by crystallization due to its oily nature.

2.2.5 Synthesis of unconstrained reference compounds

Furthermore, two unconstrained DTE derivatives were synthesized for reference purposes in transient absorption spectroscopy. The plain dithienylethene **12** has not been described before, whereas the 1,1′dimethylated analogue *Z*-**13** has been already synthesized[30a] and was target of theoretical studies.[30b]

Unconstrained **12** was synthesized in a two-step sequence from 2,5-dimethylthiophene (Scheme 2.2-13). The formylation according to Rieche[95] with $TiCl_4$ was found to be more convenient in purification than the Vilsmeier formylation protocol, while both procedures display similar yields.

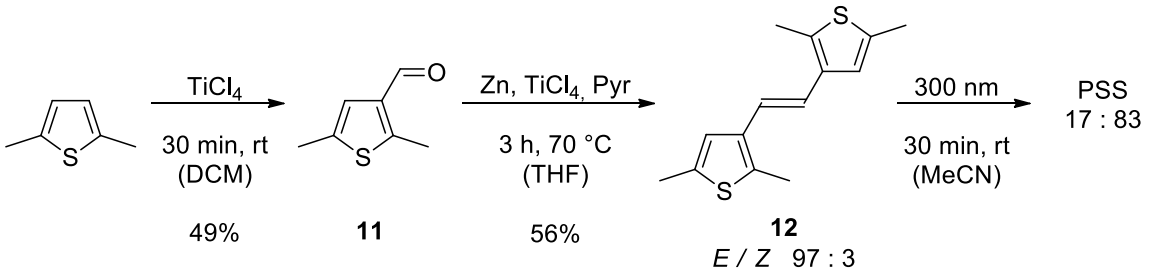

Scheme 2.2-13 Synthesis of unconstrained **12** in a two-step sequence. The *Z*-isomer was enriched by preparative irradiation at 300 nm and separated by column chromatography.

Importantly, as aldehyde **11** is prone to degradation, the yield of the reductive coupling is lowered and the reference compound **12** could be isolated in only 56% yield. As the synthesis was rather selective for the *E*-isomer, the *Z*-isomer was obtained by preparative irradiation with 300 nm light, yielding a 17:83 *E/Z* ratio in the PSS. The two isomers were separated by normal phase chromatography and identified by their NMR spectra[71-72] and their melting points. While the signals of both methyl groups in the *E*-isomer fall together, they are shifted upfield unequally for the *Z*-isomer, indicating different influence of the anisotropic effect of the thienyl group. Also, the aromatic and double bond protons are shifted upfield in the *Z*-isomer.[72c]

The second unconstrained reference compound can be synthesized from commercial 3-acetyl-2,5-dimethylthiophene in a McMurry coupling, yielding an 1:4 mixture of *E*- and *Z*-isomer, which could be separated by prep. HPLC or prep. GPC (Scheme 2.2-14).

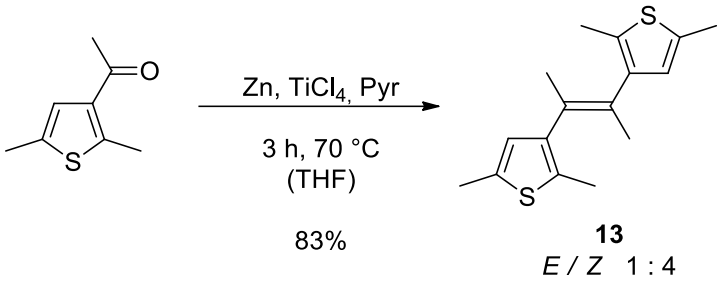

Scheme 2.2-14 Synthesis of unconstrained **13** from commercial starting material.

The isomer identity was assigned by a NOESY-experiment, in which for the *E*-isomer a coupling between the double bond methyl groups and the inner methyl group on the opposite thiophene was observed. While the aromatic protons are again shifted upfield in *Z*-**13** compared to *E*-**13**, the methyl groups on the double bond are shifted downfield by 0.3 ppm. Interestingly, the upfield shift of the inner methyl groups in the *Z*-isomer compared to the respective *E*-isomer is stronger in **13** (0.5 ppm) than in **12** (0.2 ppm) and almost comparable to that in **aDTE$_{66}$-Me** (0.7 ppm).

2.2.6 Summary

The synthesis for all aDTE derivatives proposed in this work is based on a simple reaction sequence using readily available and inexpensive starting materials (Scheme 2.2-15). Throughout the whole reaction sequence, moderate to quantitative yields were obtained, and due to easy purification procedures avoiding column chromatography in the first reaction steps, the synthesis is suitable for multi-gram scale assays. Even though some intermediates in the reaction scheme have already been published,[64] not all desired target molecules can be derived. In addition, synthetic details have not been given or key reactions carried out as published did not work in our hands.

The first and ring size-determining step in the preparation of simple aDTE derivatives is the Friedel-Crafts acylation commercial 2,5-dimethylthiophene (or carboxyalkylation from its acylated derivative for 5-membered ring systems) to yield a ketoester or ketoacid **1**. Subsequently, the ketone group in these compounds is reduced (and saponified, in case of ketoesters) to yield acid **2,** which is then converted into cyclic ketone **3** in a condensation reaction. Finally, two equivalents of the respective ketone are coupled reductively in a McMurry coupling to yield the simple aDTEs **aDTE$_{55}$-Me**,

aDTE$_{66}$-Me, and **aDTE$_{77}$-Me** in varying ratios of *E*- and *Z*-isomer, which were identified by their characteristic shift of the inner methyl groups in the ^{1}H-NMR.

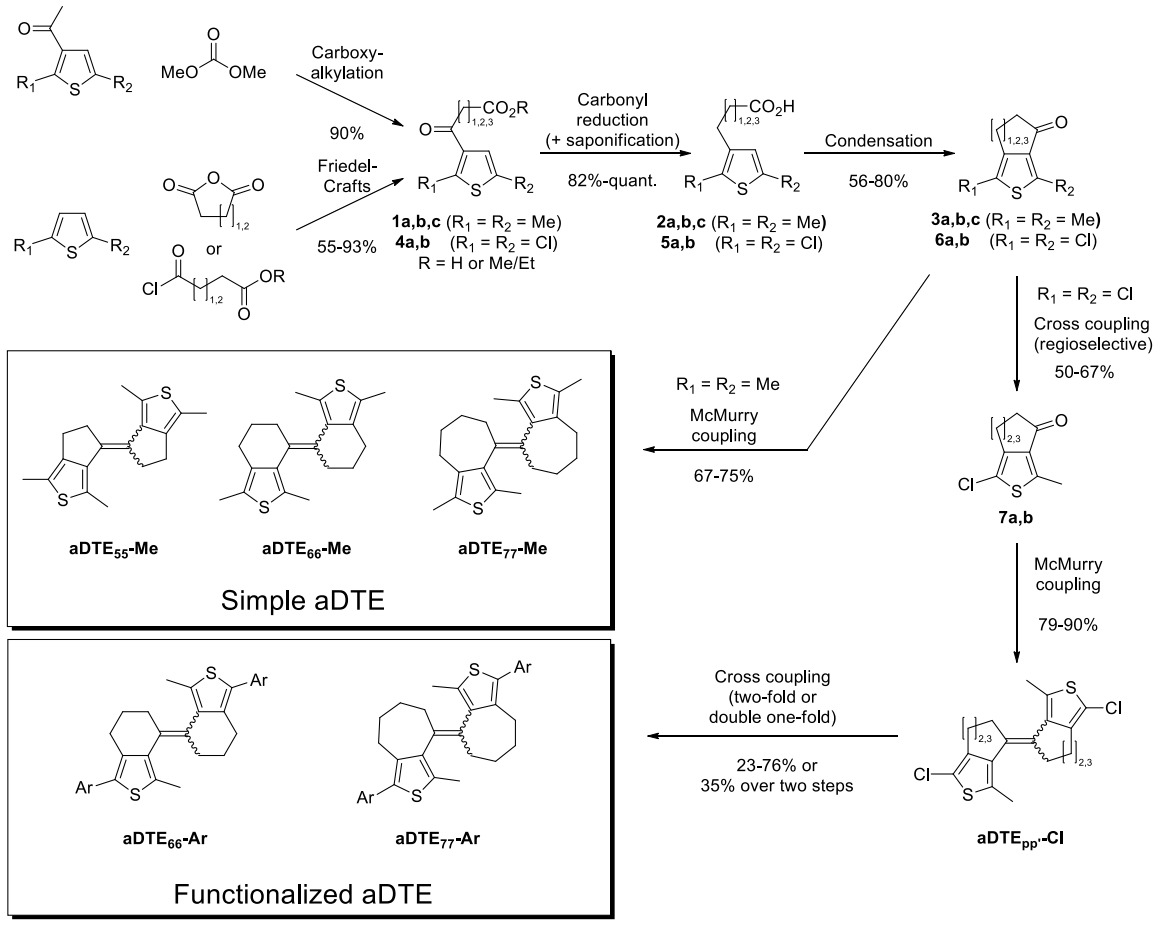

Scheme 2.2-15 General synthesis of simple and functionalized aDTE.

In order to improve the photochemical stability of the photochromes, fine-tune their properties and enable implementation of aDTEs into bigger molecules as a functional unit, functionalized aDTE bearing a functionalizable group at the periphery of the molecule were synthesized in a similar fashion from the symmetric 2,5-dichlorothiophene. The reaction sequence includes an additional regioselective monofunctionalization of the ketone building block **6**, in the present case with a methyl group, prior to McMurry coupling. The introduction of the desired functional group is carried out in the last reaction step, allowing the synthesis of several products from only one precursor for each ring size. As such, a variety of derivatives was synthesized: **aDTE$_{66}$-PhOMe** (π-donor), **aDTE$_{66}$-PhCN** (π-acceptor), **aDTE$_{66}$-Ph(CF$_3$)$_2$** (σ-acceptor). Furthermore, the bromine substituted **aDTE$_{66}$-PhBr** and the unsymmetrically substituted **Me$_2$NPh-aDTE$_{66}$-PhCN** (donor & acceptor) could be obtained. For the 7-membered ring

derivatives, **aDTE$_{77}$-Ph(CF$_3$)$_2$** was synthesized as a model compound. The major *Z*-isomer can be obtained by crystallization from the mixture; the minor *E*-isomer could be obtained by prep. HPLC. Separation by prep. GPC was, in contrast to the simple aDTE, not successful for functionalized aDTEs.

In order to widen the scope of aDTEs, the hybrid, half-stiff **(F$_3$C)$_2$Ph-aDTE$_{6Me}$-Me** was prepared to investigate whether the photochromic behavior of the parent compounds can be reproduced (Scheme 2.2-16). For a better understanding of the ultrafast dynamics of aDTEs, two unconstrained reference compounds **12** and **13** were synthesized.

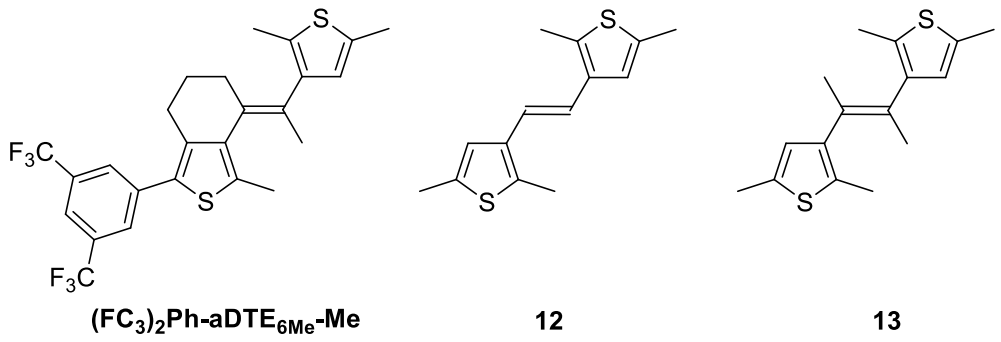

(FC$_3$)$_2$Ph-aDTE$_{6Me}$-Me **12** **13**

Scheme 2.2-16 Synthesized example of a half-stiff hybrid aDTE and two unconstrained reference compounds **12** and **13**.

The synthetic route established in this work has thus provided a robust way to prepare both the intermediate ketones and the final photochromic compounds in a simple reaction sequence. In contrast to similar procedures, pure compounds were obtained without the necessity of purification by column chromatography during the first reaction steps, thus ensuring scalability of these reactions. In addition to the proposed fine-tuning of photochromic properties, the late-stage substitution on the aDTE core in functionalizable aDTEs enables convenient modification of key elements for future studies. As such, replacement of the inner methyl groups by bulky substituents may influence the thermal stability of the open isomers with respect to the double bond isomerization. Also the introduction of other functionalities as alkoxy, cyano or CF_3-groups at this position may be interesting in order to influence the thermal stability of the closed isomer,[58a,59b,59c] the cycloreversion quantum yield[96] or the electrochemical behavior[97] of aDTEs, respectively.

2.3 Steady-state spectroscopy of aDTEs

This section presents the steady-state photochemistry of the synthesized aDTE photochromes as it was conducted in the Hecht group. The switching mechanism of aDTEs with respect to their ring sizes was further elucidated, including the prior unknown 5-membered ring derivative and the functionalized aDTEs. The analytical procedure is shown exemplary; major photochemical characteristics as the quantum yields for cyclization and cycloreversion reactions as well as photochemical and thermal stability, switching in the solid state, and the potential of triggers for double bond isomerization including triplet sensitization are discussed. A brief description on the procedures is given in this section; more details about instruments and procedures can be found in Section 4.2.

2.3.1 General considerations

The switching behavior of two simple aDTEs, namely *E*-**aDTE$_{66}$(Me$_2$)-Me** (Scheme 2.3-1) and *Z*-**aDTE$_{77}$-Me**, has been examined earlier.[56] Due to the fact that only one isomer of each compound could be isolated, the study of their photochemistry was only preliminary, advanced analysis such as determination of the quantum yields or photochemical stability was not performed. However, it was found that these compounds exhibit an apparent one-way isomerization by UV light, converting the *E*-isomer into the respective closed isomer *C* (Scheme 2.3-1), which was easily identified by its batho-chromically shifted absorption band in the UV/vis spectrum, typical for closed ring isomers of DAEs.

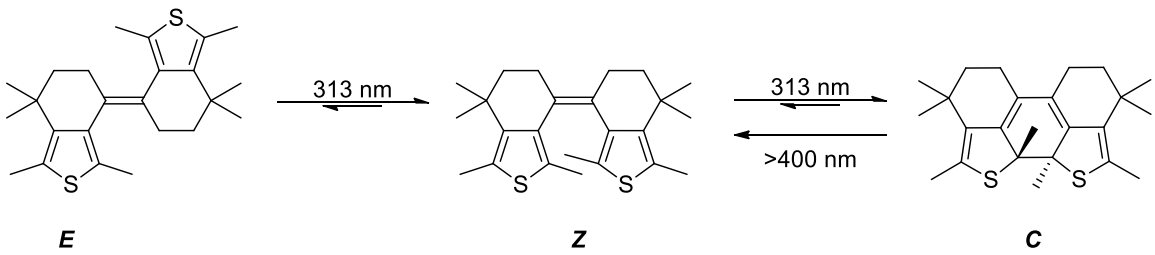

Scheme 2.3-1 Switching behavior of **aDTE$_{66}$(Me$_2$)-Me** as observed earlier.[56] Irradiation of initial *E*-isomer with UV-light ultimately yielded the closed isomer *C*, while irradiation with visible light induced cycloreversion to the *Z*-isomer exclusively.

This bathochromic band could be bleached by irradiation with visible light, however without restoration of the initial spectrum, which indicated the formation of the *Z*-isomer. Its exclusive formation could also be proven by UPLC/MS analysis of the irradiated solutions. Upon further UV- and visible light irradiation, the closed isomer and *Z*-isomer, respectively, could be regenerated in a second switching cycle.

From this observation, the following conclusions can be drawn. Firstly, since all isomers absorb to a certain extent at $\lambda_{irrad} = 313$ nm, while the final compound upon UV-irradiation is the closed isomer, the photochemical equilibrium could have a form as

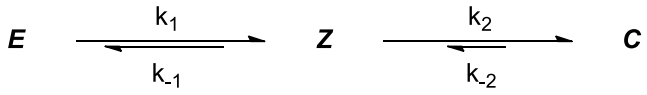

Scheme 2.3-2 General switching behavior for the aDTE photosystem upon irradiation with UV-light.

with $k_2 > k_{-2}$, as typical for *normal* DAEs, and $k_1 \approx k_{-1}$ or even $k_1 \geq k_{-1}$, which is characteristic for stilbene-type systems. These rate constants are in direct relation to photochemical quantum yields according to equation (3) with ϕ_{AB} signifying the quantum yield for the conversion of compound A into B and $I'_{abs(A)}$ the light absorbed by compound A at the irradiation wavelength. According to Lambert-Beers law, this fraction of light depends on the total absorbance at the irradiation wavelength Abs', the concentration [A] and respective molar absorptivity ε'_A. The path length of the light beam l' is 1 cm in all experiments.

$$k_i = \phi_{A\rightarrow B} I'_{abs(A)} = \phi_{A\rightarrow B} I_0 \left(1 - 10^{-Abs'}\right) \frac{[A]\varepsilon'_A l}{Abs(t)'} \tag{3}$$

2.3.2 Determination of the molar extinction coefficients

The molar absorptivities of the open isomers were determined directly from the isolated compounds and calculated according to equation (4), where *Abs* signifies absorbance, c_0 concentration of the sample and *l* the path length of the measure beam.

$$\varepsilon = \frac{Abs}{c_0 \cdot l} \tag{4}$$

The spectra of each pair of open isomers of a specific aDTE do not differ much in their band shape, though the intensities *E*- or *Z*-isomers normally are different (Figure 2.3-1). Which of the two shows a more hyperchromic absorbance depends on the specific

compound. The intensities of the most bathochromic band are similar to those observed for unsubstituted stiff stilbenes.[22] Also in aDTEs, only the spectrum of the 5-membered ring derivative *E*-**aDTE$_{55}$-Me** shows a vibronic structure. This indicates[98] that the deviation from planarity found in the crystal structures leading to a loss of the vibronic fine structure for aDTEs with higher ring sizes is also present in solution. Additionally, the spectrum is almost identical to that of the unconstrained reference compound *E*-**12** (Section 2.3.3.5). Also comparable to stiff stilbenes, the simple 7-membered ring compound **aDTE$_{77}$-Me** shows only very weak absorption around the band around 300 nm.[21] This may be attributed to torsion of the thiophenes out of the double bond plane.[99]

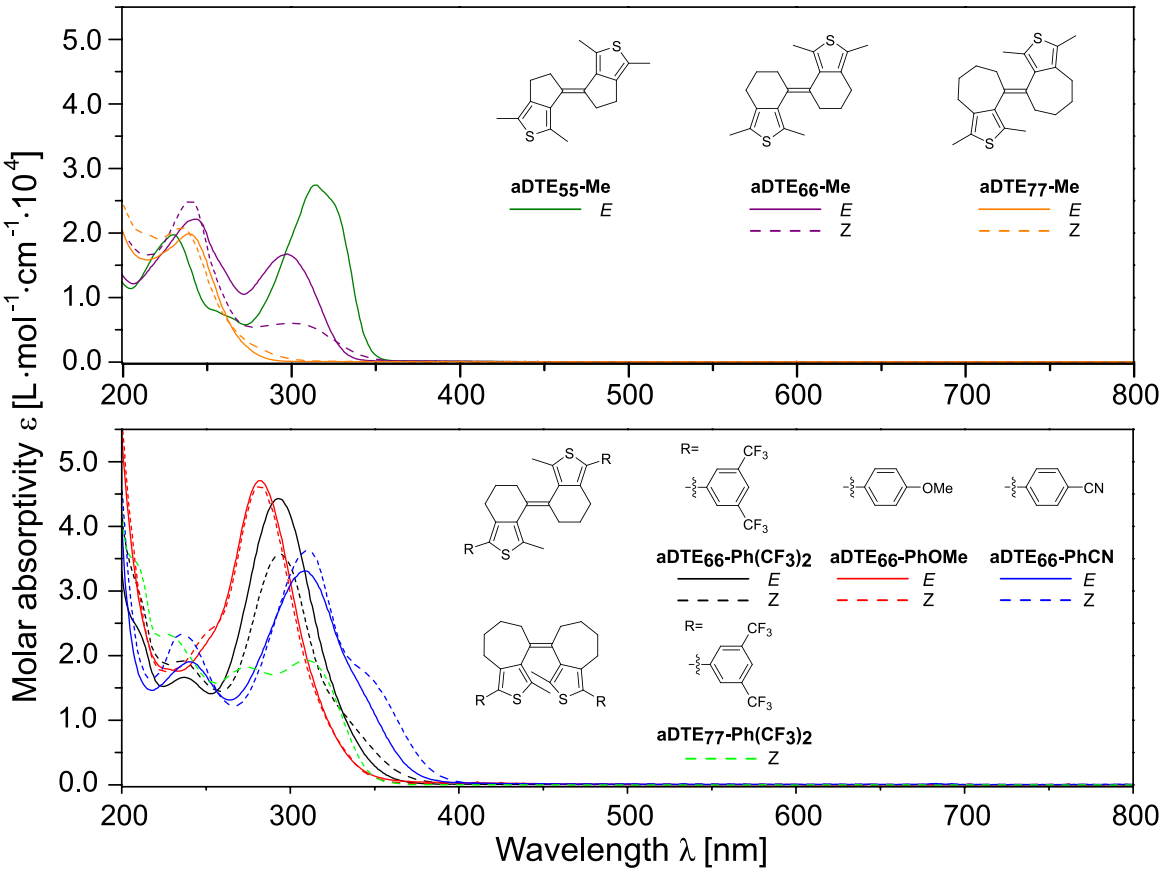

Figure 2.3-1 Extinction coefficients for *E*- and *Z*-aDTE in MeCN. **Top:** Simple aDTEs. **Bottom:** Functionalized aDTEs.

As known for DAEs, attachment of aromatic groups on the peripheral positions enhances the absorptivity compared to the simple derivatives. This also holds true for aDTEs. Interestingly, even the 7-membered ring derivative *Z*-**aDTE$_{77}$-Ph(CF$_3$)$_2$** shows an intense

[21] Compare to the unconstrained derivate **13** in Section 2.3.3.5.

transition in the near UV region, though still weaker than in the differently functionalized *Z*-aDTE$_{66}$.

The maximum of aDTE$_{66}$ shifts with different substituents, allowing a fine-tuning of the spectrum. All open isomers absorb in the near UV and are transparent in the visible region.

Secondly, the molar absorptivities of the ring-closed isomers *C* are compared (Figure 2.3-2). Here, both aromatic substituents are conjugated and contribute to the photochromic system. In order to obtain the spectra without the necessity of isolating the pure closed isomer, an indirect method was chosen that has been used in our group before and proven to yield good fitting results.[55]

A solution of a *Z*-aDTE was irradiated stepwise with UV light until the PSS was reached. During this conversion to the closed isomer, at least five UPLC samples were taken after a sufficient mixing time, and the corresponding UV/vis spectrum registered.

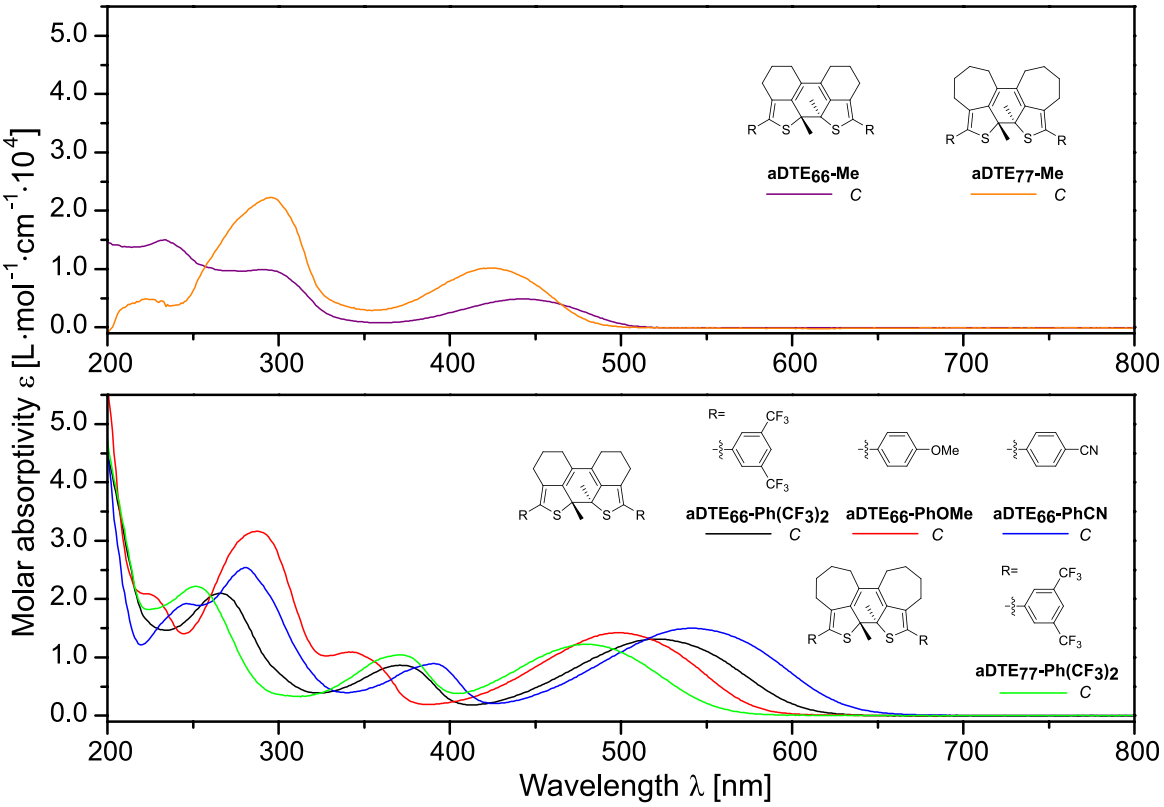

Figure 2.3-2 Extinction coefficients of the pure cyclized aDTEs isomers in MeCN. The spectra are calculated from irradiated isomeric mixtures using UPLC data for linear regression. **Top:** Simple aDTEs. 5-membered ring derivative **aDTE$_{55}$-Me** showed insufficient cyclization to extrapolate the closed isomer. **Bottom:** Functionalized *C*-aDTEs.

The isomer ratios are determined by integration of the respective peaks in the chromatogram's diode array trace at the most bathochromic isosbestic point.[22] The spectrum of the closed form was calculated either by linear extrapolation to 100% closed isomer or by subtraction of the portion of *Z*-isomer in each single spectrum and normalization of the residual spectrum to 100%. The latter of both methods offers the advantage of easy control of quality of each single fit. It furthermore showed that spectra with less than 10-20% closed isomer gave unsatisfactory results and thus were excluded from the average. The bad quality of these fits results mostly from the high scaling factor, which in turn magnifies uncertainties, e.g. in the isomer ratios, extinction coefficients and concentration determination.

All closed isomers are colored as they absorb in the visible region (Figure 2.3-2). The peak maximum of the bathochromic band can be adjusted in a range of 440-540 nm for the chosen substituents. As for the open isomers, not only the presence and the electronic properties of the phenyl substituent but also the ring size have a considerable contribution to the spectral appearance. This can be observed for both the simple aDTEs *C*-**aDTE$_{66}$-Me** and *C*-**aDTE$_{77}$-Me** ($\Delta\lambda_{max}$ = 18 nm) as well as for the functionalized derivatives *C*-**aDTE$_{66}$-Ph(CF$_3$)$_2$** and *C*-**aDTE$_{77}$-Ph(CF$_3$)$_2$** ($\Delta\lambda_{max}$ = 40 nm) bearing the same substituent. The reason for this observation may lay in a bended chromophore due to ring strain, leading to a lower conjugation in the closed isomers of aDTE$_{77}$. This also reflects in their electrochemical behavior (compare Figure 2.4-6). For the functionalized derivatives, an additional increased twisting of the phenyl unit induced by steric interaction with the bulkier alkyl ring structure is possible. The spectrum of the *C*-**aDTE$_{55}$-Me** could not be obtained (see Section 2.3.3.3).

Lastly, the difference between aDTEs and normal DAEs bearing the same substituents is shown exemplary for one pair of compounds (Figure 2.3-3). The normal **DAE-Ph(CF$_3$)$_2$** was synthesized earlier[48,55] in our group. The positions of the absorption bands for the ring open isomers only differ slightly, while a more emphasized splitting of the two transitions in case of the normal DTE leads to a small hypochromic shift. While the impact of additional alkyl chains itself on the absorptivity is expected to be small, it can

[22] The most bathochromic isosbestic point was chosen since the influence of impurities normally can be neglected for the band in the visible.

be concluded that the conjugated system of the open aDTE, compared to the non-fixated analogue, is not disturbed by the alkyl linkers.

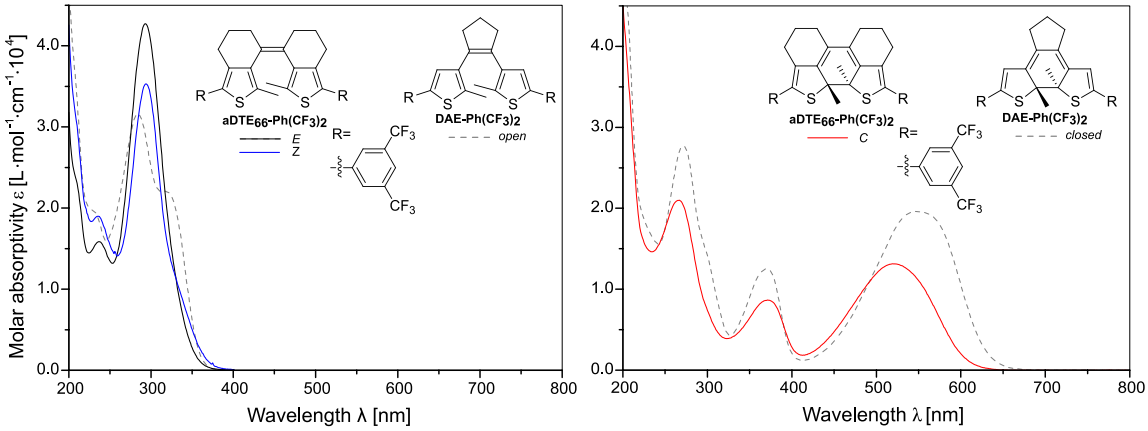

Figure 2.3-3 Comparison of UV/vis spectra of aDTEs and normal DAEs[48,55] bearing the same substituent. In MeCN. **Left:** The open aDTE isomers are bathochromically and hyperchromically shifted compared to the normal DAEs. **Right:** The cyclized isomer is more hypsochromic and hypochromic.

Surprisingly, in the ring-closed state (Figure 2.3-3 right) there are more pronounced differences between the aDTE and the normal DTE: the overall absorptivity of the cyclized form is not increased but even reduced compared to unconstrained normal DAEs. The hypsochromic and hypochromic shift in the cyclized aDTE is assigned to an increased torsion of the phenyl substituent in the closed isomer. This effect has already been observed for normal DTEs[48] and is expected to be more prominent with a rather stiff and bulky ring structure adjacent to the phenyl ring.

2.3.3 The course of the photoreaction

For the sake of convenient comparison of photoreactions starting from either of the isolated isomers of an aDTE, the spectra in this section will be normalized to the initial sample concentration. This concentration was determined according to equation (4) with the molar absorptivity at the peak maximum around 300 nm.

2.3.3.1 The course of the photoreaction of $aDTE_{66}$

The steady-state photochemistry will be described on the example of **$aDTE_{66}$-Ph(CF_3)$_2$**. The solutions were obtained from samples that were pure by UPLC, and normally degassed individually in the cuvette before irradiation. The initial concentration of each experiment was determined after degassing through the absorbance at the peak maximum.

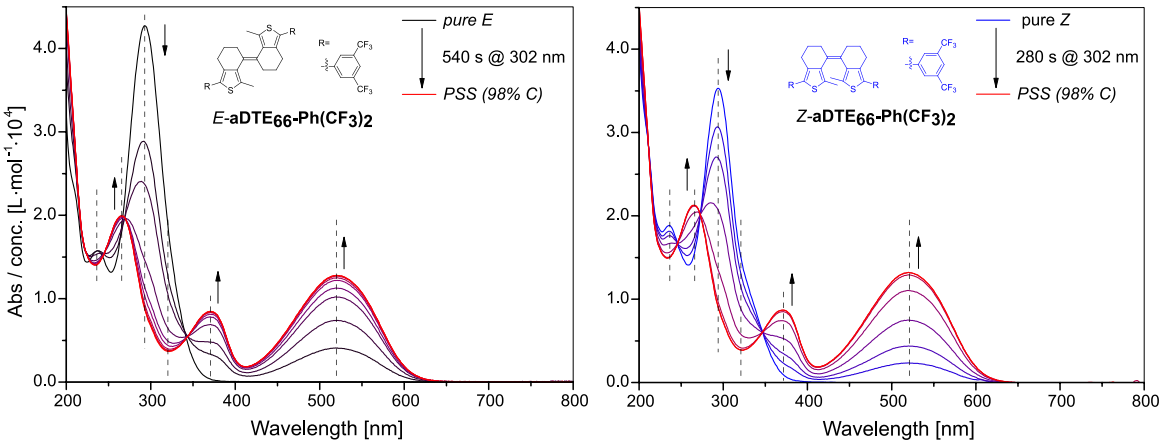

Figure 2.3-4 Spectral development during irradiation of **aDTE$_{66}$-Ph(CF$_3$)$_2$** in MeCN (c = 10^{-5} M) with 302 nm light. Dashed lines indicate wavelengths displayed in ΔAbs-diagram (Figure 2.3-5). **Left:** Starting form *E*-**aDTE$_{66}$-Ph(CF$_3$)$_2$**. **Right:** Starting from *Z*-**aDTE$_{66}$-Ph(CF$_3$)$_2$**. After different irradiation times, both experiments yield the same PSS composition of 98% cyclized isomer.

When irradiated with 302 nm UV-light, a decrease in the peak maximum around 290 nm can be observed for both open ring isomers (Figure 2.3-4). Though the irradiation time (at same light intensity) differs almost by a factor of two, both experiments reach the same photostationary state (PSS) composition of 98% closed isomer.

While the reaction of the *Z*-isomer produces clearly three isosbestic points, the evaluation for the *E*-isomer is not as unambiguous. To render the interpretation less prone to subjective interpretation, H. Mauser introduced a mathematical method to determine the number of linearly independent reactions[100] (also called rank *s*) in a photosystem. When the change in absorbance at peak maxima during irradiation with UV-light are plotted against another, the rank can be derived from the curve shape (Figure 2.3-5).

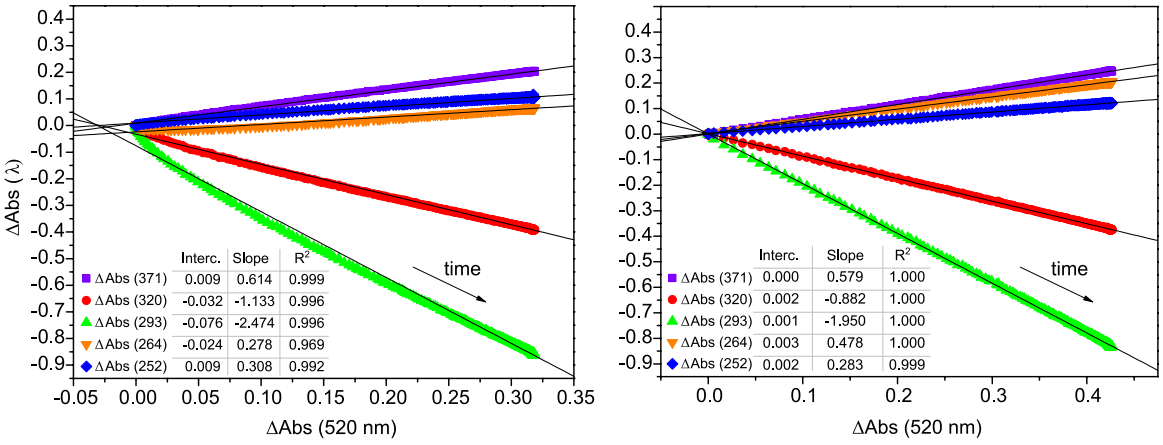

Figure 2.3-5 ΔAbs-diagram according to Mauser[100b] for **aDTE$_{66}$-Ph(CF$_3$)$_2$**. **Left:** The photoreaction of *E*-**aDTE$_{66}$-Ph(CF$_3$)$_2$** has a rank s ≥ 2. **Right:** *Z*-**aDTE$_{66}$-Ph(CF$_3$)$_2$** undergoes a uniform photocyclization.

The high linearity for the *Z*-isomer at all wavelengths indicates a simple, uniform photoreaction (s = 1). The deviation from linearity for the *E*-isomer, in particular for the absorbance at 293 nm where the biggest difference in the molar absorptivities of the *E*- and the *Z*-isomers exists, indicates a complex photoreaction with $s \geq 2$. Methods for photoreactions of higher rank using quotients of ΔAbs failed to give definite results. However, this finding is conclusive when related to the results of transient absorption spectroscopy (Section 2.5).

The assumed mechanism was investigated further using chromatographic analysis of the switching process by UPLC. Samples of both *E*- and *Z*-**aDTE$_{66}$-Ph(CF$_3$)$_2$** were irradiated with UV-light until the PSS was reached. Meanwhile, samples were taken for UPLC analysis as described for the determination of the ring-closed isomer spectrum (Figure 2.3-6).

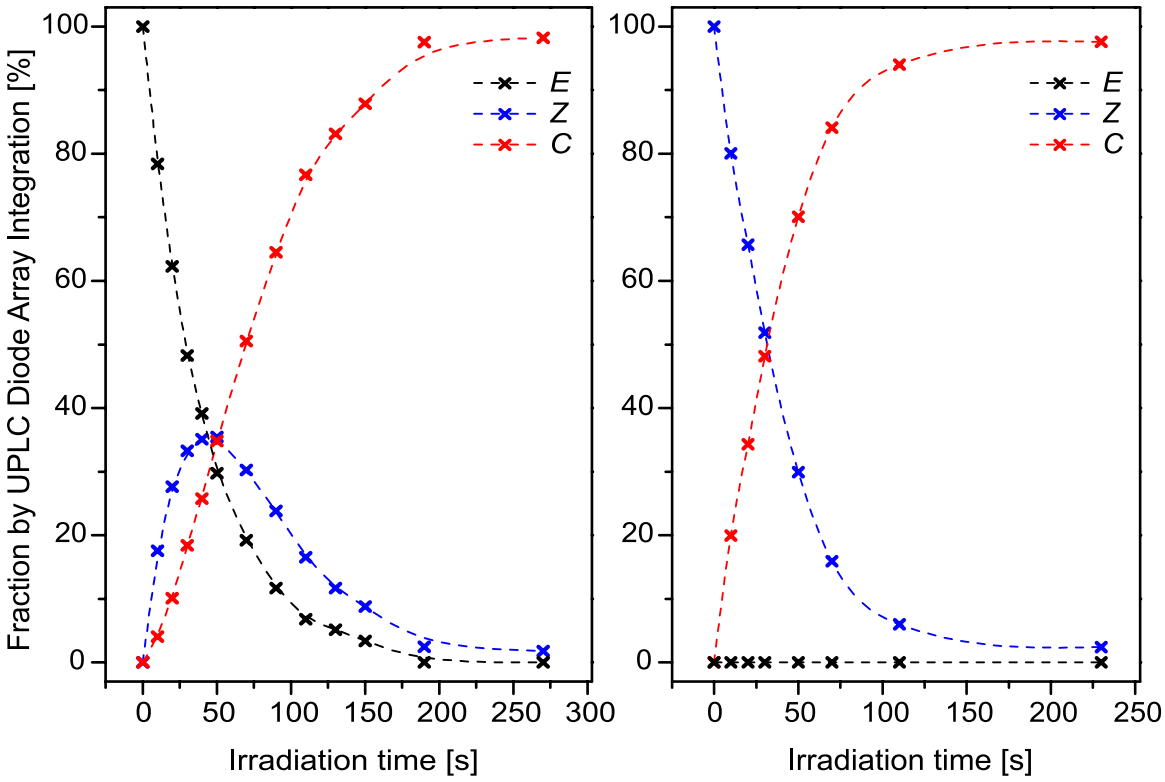

Figure 2.3-6 UPLC analysis of **aDTE$_{66}$-Ph(CF$_3$)$_2$** in MeCN ($c = 10^{-5}$ M) after distinct irradiation times with UV-light. **Left:** When starting from the *E*-**aDTE$_{66}$-Ph(CF$_3$)$_2$**, the *Z*-isomer is a detectable intermediate. **Right:** The isomerization from the *Z*-isomer yields only *C*-**aDTE$_{66}$-Ph(CF$_3$)$_2$**.

It can be seen that the course of the reaction for the *Z*-isomer does not involve any detectable formation of the *E*-isomer, but only direct conversion to the closed isomer, so $k_2 >> k_{-1}$ (see Scheme 2.3-2). This is in good agreement with the qualitative analysis

above, and enables further treatment of this photoreaction as a simple 2-state photosystem.

In contrast, for the *E*-isomer up to 35% *Z*-isomer is formed before the closed isomer evolves and the system approaches the final PSS, proving that in a first step the *E*-isomer undergoes *E*/*Z* isomerization before ring-closure. Thereby, the efficiency of both steps must be on the same order of magnitude.

As known for DAEs, the newly formed bathochromic band enables selective irradiation of the closed isomer with visible light. This can be done either with monochromatic light, or for the sake of increased intensity, with "white" light using a cut off optical filter for all wavelengths with open isomer absorbance. The decrease of the bathochromic band and increase of the 290 nm band indicates conversion to a second PSS (Figure 2.3-7). As obviously shown by the comparison with the absorptivity of the open isomers, this PSS consists of *Z*-isomer only. This was further confirmed by UPLC analysis.

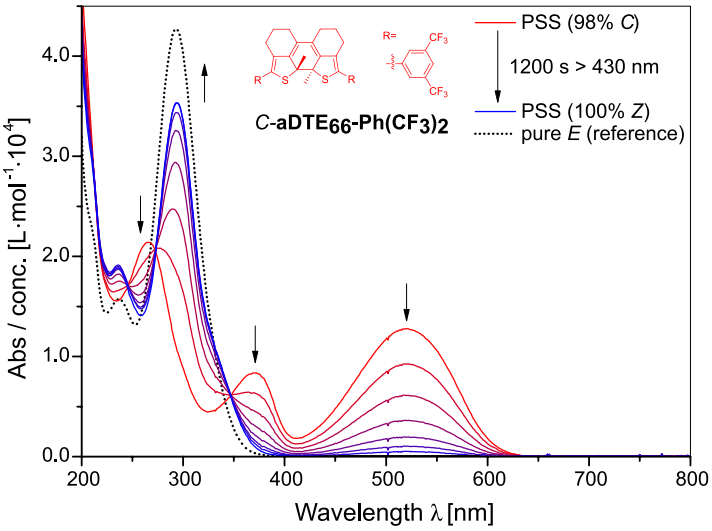

Figure 2.3-7 Cycloreversion of *C*-**aDTE$_{66}$-Ph(CF$_3$)$_2$** in MeCN (c = 10^{-5} M) with white light, starting from PSS mixture.

Finally, the thermal stability of all three isomers was investigated. To this end, a spectroscopic solution of the *E*-isomer in MeCN was irradiated until it contained all three isomers in an equal amount. This mixture was subsequently heated to 70 °C overnight while spectral changes were being monitored. As no change was detected, it can be concluded that all isomers are stable under these conditions.

The photochemical reactions are therefore connected as

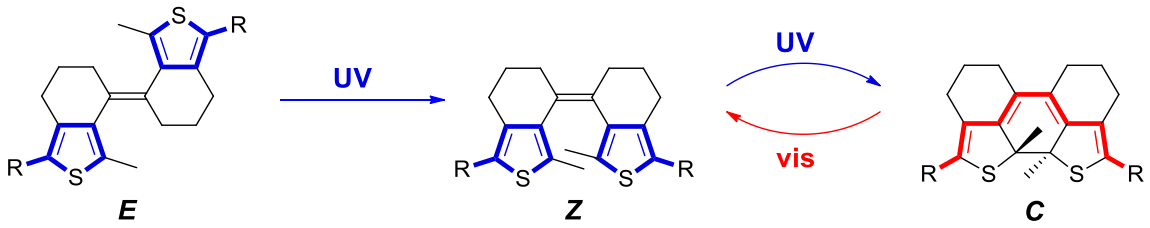

Scheme 2.3-3 General photochemical behavior of aDTE$_{66}$ upon direct excitation. The *E*-isomer converts via the *Z*-isomer to the closed isomer *C* when irradiated with near UV-light. The closed isomer undergoes cycloreversion to the *Z*-isomer when irradiated with visible light.

This general reaction scheme (Scheme 2.3-3) has been proven for all functionalized aDTE$_{66}$ derivatives. An initial *E*-isomer is converted via the *Z*-isomer to the ring-closed isomer by irradiation with UV-light; the ring-closed isomer undergoes cycloreversion exclusively to the *Z*-isomer by irradiation with visible light. A similar mechanism was already observed[22] for stiff stilbenes, with the difference of thermal instability of the ring-closed dihydrophenanthrene. Though the overall reaction mechanism is the same for **aDTE$_{66}$-Me**, a minor amount (< 5%) of *E*-isomer could be detected in photoreactions starting from the respective *Z*-isomer.

2.3.3.2 The course of the photoreaction of aDTE$_{77}$

The study was expanded towards the 7-membered ring derivatives aDTE$_{77}$. As the study of aDTE$_{66}$ indicated, the course of the photoreaction is not dependent on the substituents, so for this class only **aDTE$_{77}$-Me** and the most promising derivative **aDTE$_{77}$-Ph(CF$_3$)$_2$** were synthesized and tested. In contrast to the 6-membered ring derivatives, the *E*-**aDTE$_{77}$-Me** formed only in minor amounts during synthesis and could be obtained in spectroscopic purity in a large scale synthesis.

The *Z*-isomer of **aDTE$_{77}$-Ph(CF$_3$)$_2$** behaves similar to the 6-membered ring homologue and cyclizes readily upon irradiation with UV-light (Figure 2.3-8 left). The PSS mixture only contains the closed isomer, as evidenced by UPLC analysis. In addition, the analysis of the reaction by correlation of spectral changes proves uniformity of the reaction (Figure 2.3-8 right). Ring opening proceeds smoothly by irradiation with white light, converting the closed isomer to the initial *Z*-isomer.

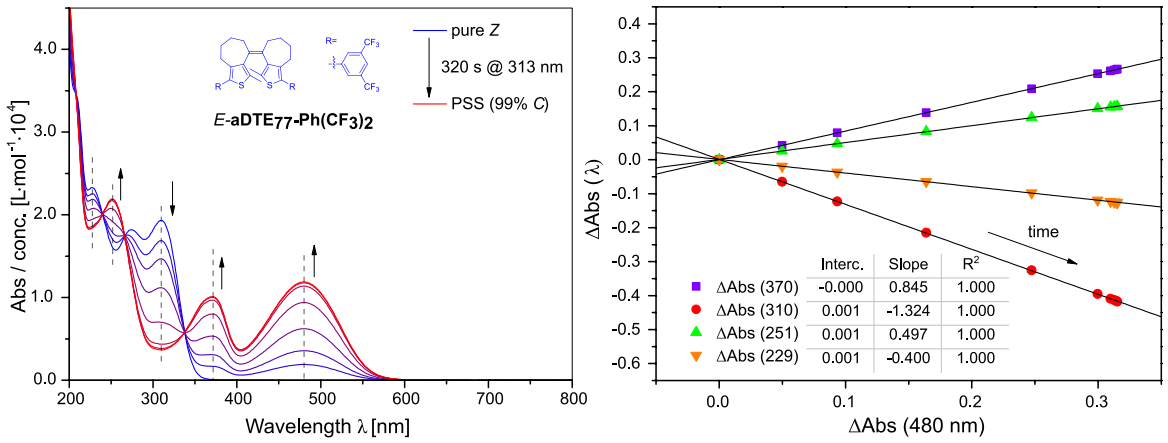

Figure 2.3-8 Irradiation of *Z*-**aDTE$_{77}$-Ph(CF$_3$)$_2$** in MeCN (c = 10^{-5} M) with 313 nm light. **Left:** The PSS is quantitatively in favor of the closed isomer. **Right:** ΔAbs-diagram according to Mauser[100b] shows a uniform cyclization reaction.

A qualitative study of the photochemistry of *Z*-**aDTE$_{77}$-Me** has already been discussed earlier.[56] Even though irradiation at longer wavelength (280 nm) is possible, the photocyclization is slow compared to the 6-membered ring derivative **aDTE$_{66}$-Me** and proceeds at acceptable rates only with shorter wavelength. In contrast to the *Z*-isomer, the newly isolated *E*-**aDTE$_{77}$-Me** shows only very little photochemical activity. The formation of *Z*-**aDTE$_{77}$-Me** is very slow, and almost no formation of closed isomer was observed within hours of irradiation with 254 nm light.

In conclusion, the proposed mechanism for the photochemistry of aDTE$_{66}$ (Scheme 2.3-3) is also valid at least for *Z*-aDTE$_{77}$. To elucidate the reasons for the photochemical inactivity of *E*-**aDTE$_{77}$-Me**, further investigations are necessary.

2.3.3.3 The course of the photoreaction of aDTE$_{55}$

Within the 5-membered ring class, only the simple aDTE derivative **aDTE$_{55}$-Me** was synthesized. Though the *Z*-isomer formed in small amounts during synthesis, only the *E*-isomer was isolated in pure form (Section 2.2.2.3). In contrast to the homologues with larger ring sizes, **aDTE$_{55}$-Me** shows only a very low PSS for the cyclization reaction (Figure 2.3-9 left). The course of the photoreaction is best visualized in a ΔAbs-diagram[23] (Figure 2.3-9 right) using distinct wavelengths for the cyclized isomer (452 nm), the degradation product (380 nm) and the open isomers (316 nm and 236 nm).

[23] Due to the little change of the most bathochromic band, the second most red-shifted peak was chosen as the y-axis.

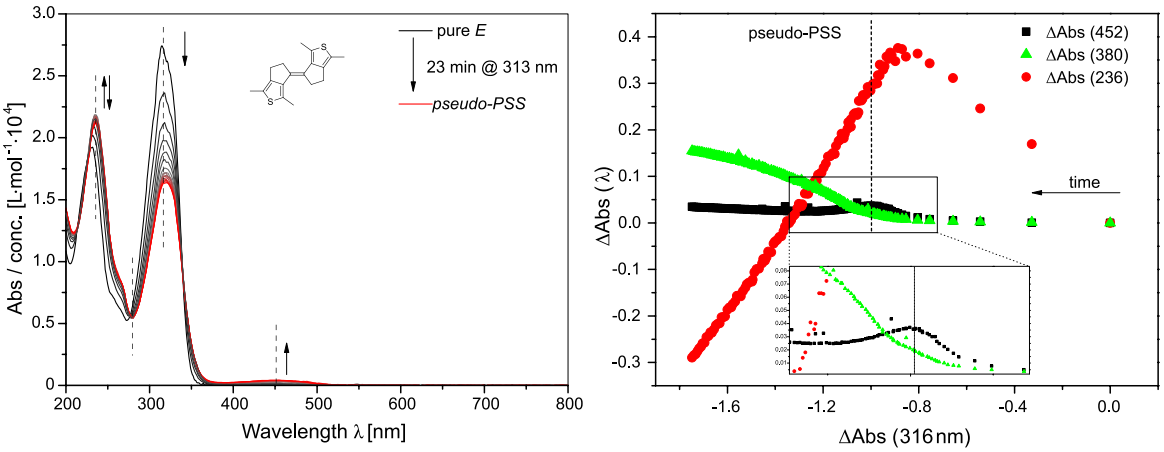

Figure 2.3-9 Photochemistry of **aDTE$_{55}$-Me** in MeCN ($c = 10^{-5}$ M) upon irradiation with 313 nm light. **Left**: Spectral changes until the pseudo-PSS. **Right**: ΔAbs-diagram for the whole photoreaction.

Initially, an open isomer with higher absorbance at 236 nm builds up. Successively, the formation of the closed isomer starts, but its concentration quickly reaches its maximum ("pseudo-PSS"). Lastly, delayed to the closed isomer build up, unidentified degradation products starts to form. The reaction scheme hence deduced is depicted in Scheme 2.3-4.

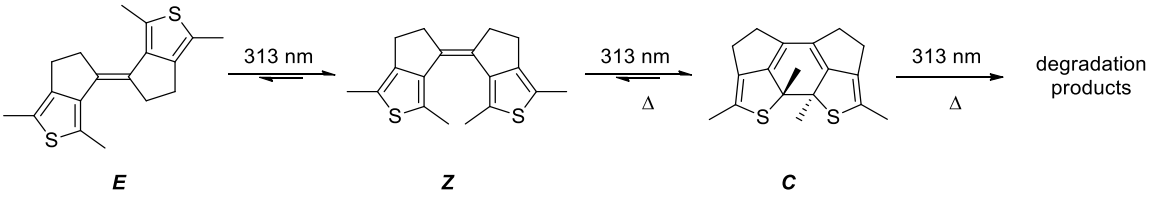

Scheme 2.3-4 Reaction scheme for the photoreaction of *E*-**aDTE$_{55}$-Me** upon irradiation with UV-light. The closed isomer *C* is thermally unstable, either due to thermal cycloreversion, degradation or a combination of both pathways.

A similar behavior was observed upon irradiation with 302 nm, though less intermediate *Z*-isomer is formed. This is conclusive as the *Z*-isomer is blue-shifted compared to the *E*-isomer, as expected from unconstrained reference compounds (Section 2.3.3.5) and stiff stilbenes.[22]

The closed isomer can be opened by irradiation with visible light. In contrast to aDTEs with larger ring sizes, the closed isomer is not stable at elevated temperatures (70 °C). Whether thermal cycloreversion or degradation is the main thermal pathway was not determined. A possible explanation for either of the possibilities is the increased strain on the newly formed σ-bond due to the rigidity of the 5-membered rings in contrast to their larger ring homologues.

2.3.3.4 The course of the photoreaction of half-stiff aDTEs

In contrast to the aDTEs described so far, due to the difficulties in isomer separation, the half-stiff **$(F_3C)_2$Ph-aDTE$_{6Me}$-Me** was investigated starting from an isomeric mixture containing 10% of the *E*-isomer.

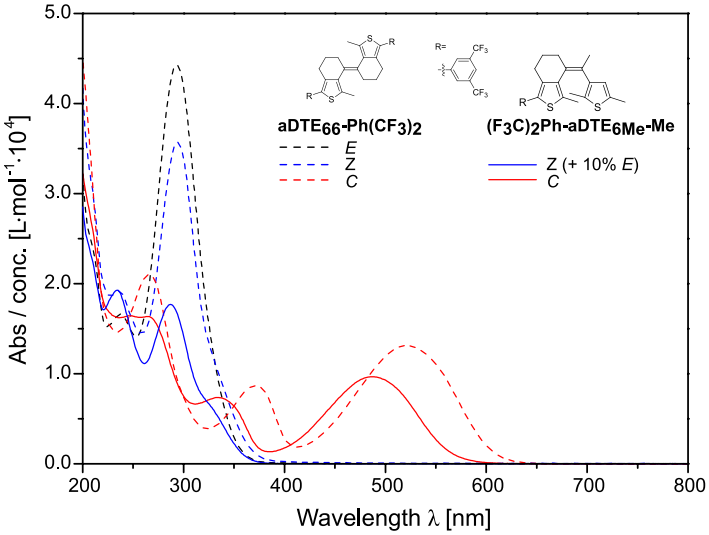

Figure 2.3-10 Comparison of normalized absorption of half-stiff **$(F_3C)_2$Ph-aDTE$_{6Me}$-Me** and its symmetrical parent compound **aDTE$_{66}$-Ph$(CF_3)_2$**.

In contrast to the symmetrical *Z*-**aDTE$_{66}$-Ph$(CF_3)_2$**, the absorption of the open isomers is hypochromic (≈ 50%) and slightly hypsochromic (287 nm vs. 293 nm), the former accounting for the reduced number of chromophores, the latter indicating a conjugation between both hemispheres in *Z*-**aDTE$_{66}$-Ph$(CF_3)_2$** to some extent. The closed isomers show a similar trend, with the difference of a more pronounced hypsochromic (478 nm vs. 520 nm) and less pronounced hypochromic shift (≈ 75%) of the broad band in the visible range.

For the quantitative analysis, the mixed spectrum was treated as pure *Z*-isomer in first approximation. During irradiation with 313 nm light, a linear decrease of both open isomers accompanied with the formation of the closed isomer was found by UPLC analysis. This is also visible in the good linearity of the ΔAbs-diagram (Figure 2.3-11). Upon irradiation with visible light, the *Z*-isomer is formed exclusively, indicating the validity of Scheme 2.3-3 also for half-stiff derivatives with the same ring size.

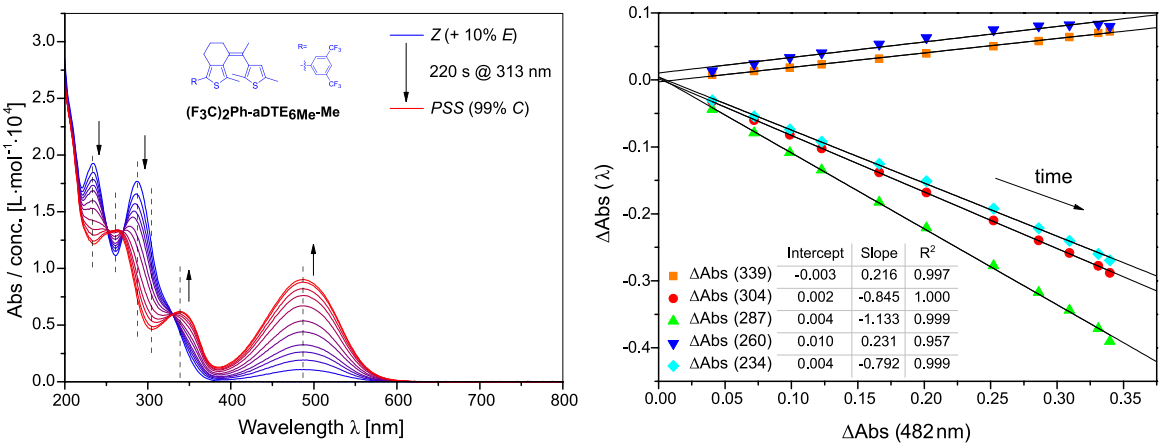

Figure 2.3-11 Photochemistry of **$(F_3C)_2$Ph-aDTE$_{6Me}$-Me** in MeCN (1:9 *E/Z* isomer mixture, c = 10^{-5} M). **Left:** Spectral evolution upon irradiation with 313 nm in MeCN. **Right:** ΔAbs-diagram for the cyclization reaction.

2.3.3.5 The course of the photoreaction of unconstrained DTEs

For reference purposes in transient absorption spectroscopy, two unconstrained DTEs, **12** and **13**, were synthesized. Comparing the UV/vis spectra of both, it can be seen that a strong hypsochromic shift occurs for the bis-methyl-substituted **13** (Figure 2.3-12). Having very similar electronic structure, this is attributed to steric interactions twisting the thiophene units out of the double bond plane. The spectral shift from **12** to **13** (81 nm / 54 nm for *E*- and *Z*-isomers, respectively) is larger than described for similar compounds without substituents on the thiophene units (51 nm / 28 nm).[101] Though weak, the vibronic structure of *E*-**12** is an indicator for a flat geometry.[98]

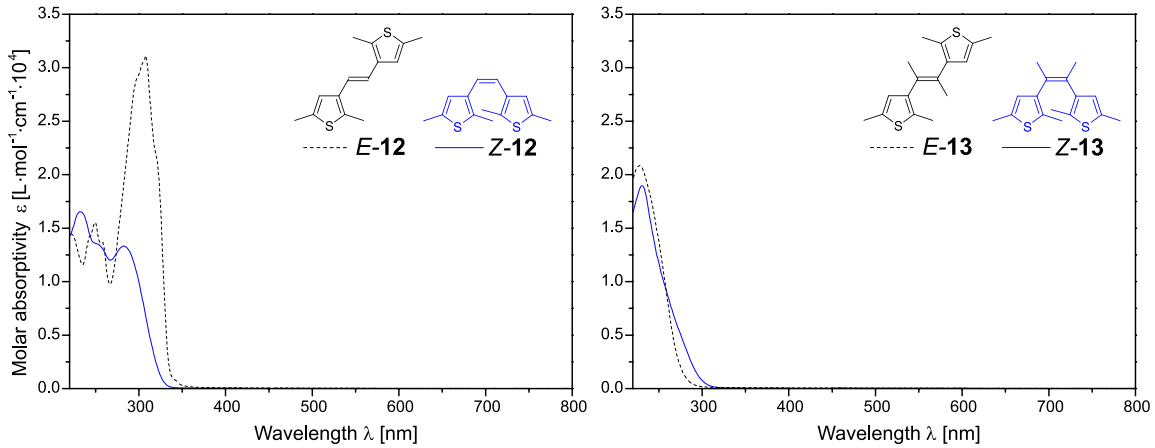

Figure 2.3-12 Molar absorptivities of unconstrained reference compounds in MeCN. **Left:** Heteroaromatic stilbene-analogue **12**. **Right:** The heteroaromatic stilbene-analogue with elongated backbone **13** displays a strong hypsochromic shift of the absorption bands.

Surprisingly, no cyclization of the new compound **12** was observed.[24] The *E*/*Z*-ratio upon irradiation with 302 nm of either isomer was found to be 21:79 *E*/*Z*.

In contrast, the photochemistry of the reported[30a] DAE **13** is rather complex. The cyclization is very slow and the contribution of the closed isomer to the PSS composition is very low. Furthermore, the photoreaction is accompanied by notable decomposition.

2.3.4 Quantum yields of the photoreactions

The quantum yields for the cyclization and cycloreversion were determined for the compounds. Knowing that all isomers investigated[25] are thermally stable under the reaction conditions and that only two isomers are involved in the isomerization of both *Z*-isomer and closed isomer, they correlate with the change in concentration via equation (5) and (6).

$$\frac{d[Z]}{dt} = 1000\, I_0\, l' \frac{\left(1-10^{-Abs'}\right)}{Abs'} \left(\varepsilon'_C \Phi_{C\rightarrow Z}[C] - \varepsilon'_Z \Phi_{Z\rightarrow C}[Z]\right) \quad (5)$$

$$\frac{d[C]}{dt} = 1000\, I_0\, l' \frac{\left(1-10^{-Abs'}\right)}{Abs'} \left(\varepsilon'_Z \Phi_{Z\rightarrow C}[Z] - \varepsilon'_C \Phi_{C\rightarrow Z}[C]\right) \quad (6)$$

with I_0 (in E s^{-1} cm^{-3}) as the number of photons[26] emitted from the lamp, $Abs'(t)$ as the time dependent absorbance at the irradiation wavelength and ε'_Z and ε'_C (in L mol^{-1} cm^{-1}) the molar absorptivities at the irradiation wavelength. [C] and [Z] (in mol L^{-1}) correspond to the concentration and l' (in cm) to the path length of the irradiation beam. With the amount of closed isomer directly derivable from the absorption in the visible region, and the amount of *Z*-isomer and closed isomer being related by mass balance, equation (6) will be used. However, for the electrocyclization this formula cannot be integrated in an analytical fashion, thus several approximations have to be employed. The *initial slope* method simplifies the calculation of the quantum yields by only considering the first 10% of the conversion and making the assumptions that:

1) The time dependent absorbance at the irradiation wavelength $Abs'(t)$ is constant during the observation, and

[24] A similar behavior has been observed for the inverse DAE analogue. Also for this system, irradiation with light of longer wavelengths leads to a PSS rich in *Z*-isomer without formation of closed isomer.[54]

[25] The quantum yield for **aDTE$_{55}$-Me** was not determined due to its low PSS.

[26] As determined by actinometry using ferrioxalate.[102] The unit Einstein (E) signifies mol of photons.

2) The photochemical back reaction is negligible.

The second premise is satisfied if $\varepsilon'_Z \, \Phi_{Z\to C} \geq \varepsilon'_C \, \Phi_{C\to Z}$, which is usually the case for DAEs and is also fulfilled for aDTEs (*vide infra*). Accordingly, the term for the backward reaction can be considered zero. Introducing the measureable variable $Abs^{obs}(t) = \varepsilon_C^{obs}[C]l^{obs}$, equation (6) simplifies and can be written as

$$\Phi_{Z\to C} = \frac{dAbs^{obs}}{dt} \frac{1}{1000\, I_0 l^{obs} \left(1 - 10^{-Abs'}\right) \varepsilon_C^{obs}} \tag{7}$$

With $dAbs^{obs}/dt$ being the slope of the absorbance at the closed isomer maximum plotted over time, accessible through a linear fit.

To verify the high cyclization quantum yield of *Z*-**aDTE$_{66}$-PhCN**, a second method was tested for this compound and *Z*-**aDTE$_{66}$-Ph(CF$_3$)$_2$** was used as reference. Thereby, the uncertainty arising from the time dependence of $Abs'(t)$ can be eliminated by performing the experiment with total absorbance at the irradiation wavelength.[103] In consequence, equation (6) can be written as

$$\Phi_{Z\to C} = -\frac{dAbs^{obs}}{dt} \frac{1}{1000\, I_0 l^{obs}\ \varepsilon_C^{obs}} \tag{8}$$

Though more exact, the problem of an increasing amount of product that absorbs at the irradiation wavelength persists, so that again only the first 10% of the conversion are considered.

For the cycloreversion, the light is actually absorbed only by the closed isomer since $\varepsilon'_Z = 0$. In this case, equation (6) simplifies to

$$\frac{d[C]}{dt} = -1000\, I_0\, l' \frac{\left(1 - 10^{-Abs'(t)}\right)}{Abs'(t)} \varepsilon'_C \Phi_{C\to Z}[C] \tag{9}$$

and can be solved analytically to

$$\frac{d[C]}{dt} = -1000\, I_0\, (1 - 10^{Abs'(t)})\, \Phi_{C\to Z} \tag{10}$$

In which the concentration can be substituted to obtain

$$\frac{dAbs'(t)}{dt} = -1000\, I_0\, l'\varepsilon'_C\, \Phi_{C\to Z}(1 - 10^{-Abs'(t)}) \tag{11}$$

Finally, integration of this formula gives

$$\Phi_{C\to Z} = \frac{d\lg(10^{-Abs'(t)} - 1)}{dt}\frac{1}{1000\, I_0\, l'\varepsilon'_C} \tag{12}$$

from which the quantum yield $\Phi_{C\to Z}$ is accessible by using a graphically determined slope.[27] The results of these evaluations are shown in Table 2.3-1.

Table 2.3-1 Photochemical efficiency and PSS composition of aDTEs in MeCN at 25 °C. Errors given describe the deviation between at least two experiments.

Compound	$\Phi_{Z\to C}$[a]	$PSS_{Z\to C}$	$\Phi_{C\to Z}$
$aDTE_{66}$-Me	0.69 ± 0.03	93%	0.257 ± 0.028[d]
$aDTE_{66}$-Ph$(CF_3)_2$	0.70 ± 0.02 0.71[b]	98%	0.004[e]
$aDTE_{66}$-PhOMe	0.63	92%	0.008[e]
$aDTE_{66}$-PhCN	0.94 ± 0.06	100%	0.002[e]
Me_2NPh-$aDTE_{66}$-PhCN	0.66	96%	0.002[f] 0.001[e]
$aDTE_{77}$-Me	0.27[c]	38%	0.131 ± 0.021[d]
$aDTE_{77}$-Ph$(CF_3)_2$	0.68 ± 0.06	99%	0.016[d] 0.011[f]
$(F_3C)_2$Ph-$aDTE_{6Me}$-Me	0.59	94%	0.042[d]

[a] λ′ = 313 nm [b] in n-hexane [c] λ′ = 254 nm [d] λ′ = 436 nm
[e] λ′ = 546 nm [f] λ′ = 492 nm

In general, the values of the cyclization quantum yield $\Phi_{Z\to C}$ range from 0.63 to 0.70 for the aDTEs examined and appear to be rather independent from the auxochrome attached. In relation to normal DAEs ($\Phi_{open\to C} \approx 50\%$), this signifies a notable elevation, which is ascribed to an increased population of the active conformation and proof of concept. The two determination methods (initial slope, see equation (7) and total absorbance, see equation (8)) gave similar quantum yields for **$aDTE_{66}$-Ph$(CF_3)_2$**. Furthermore, high PSS compositions of above 92% are obtained throughout the whole series.

Two derivatives do not follow this trend. The cyano-derivative **$aDTE_{66}$-PhCN** shows an outstanding performance with a quantum yield that is unity within the error. The larger deviation is a result of different values between the two determination methods, with the supposedly more exact full absorption method giving the higher yield of unity. This

[27] The light intensity in the visible range of the spectrum was determined with according to a procedure reported by the group of Irie using a diarylethene with known cycloreversion quantum yield[32b] as a reference.

phenomenon was further investigated with transient absorption spectroscopy and will be addressed in Section 2.5.

By contrast, **aDTE$_{77}$-Me** has a cyclization quantum yield of 0.27, which is surprisingly low.[28] As the cyclization quantum yield for **aDTE$_{77}$-Ph(CF$_3$)$_2$** falls within the range of that observed for other aDTEs, the ring size cannot solely be the explanation for this effect. Likewise, no such difference in cyclization quantum yields could be observed for 6-membered ring homologues when compared to simple and functionalized aDTEs. A striking difference for **aDTE$_{77}$-Me** as compared to the other aDTEs investigated is the short irradiation wavelength of 254 nm used, due to the strong hypsochromic shifted band. Thus, at the irradiation wavelength, other potentially unproductive de-activation pathways must be accessible, which reduce the efficiency of the electrocyclization. A profound explanation for this behavior cannot be derived from the available data though.

The cyclization quantum yield for the half-stiff **(F$_3$C)$_2$Ph-aDTE$_{6Me}$-Me** may be underestimated to a certain extent as the *E*-isomer present in the mixture most probably isomerizes in two successive steps to the closed isomer. The absolute number thus may be identical or slightly reduced compared to the parent **aDTE$_{66}$-Ph(CF$_3$)$_2$**. At the same time, the cycloreversion quantum yield is increased by an order of magnitude for the hybrid compound. Comparison with the high cycloreversion quantum yields $\Phi_{C\rightarrow Z}$ found for simple aDTEs leads to the assumption that the methyl substituted hemisphere is responsible for this effect. Yet, for a pair of mono-[104] and bis-functionalized[105] normal DAEs, almost identical quantum yields for cyclization and cycloreversion were observed. An influence of the less rigid backbone thus cannot be ruled out and should be investigated with help of a second, bis-functionalized half-stiff derivative.

As found for normal DAE systems,[106] the cycloreversion quantum yield decreases with the length of the conjugation chain in the closed isomer. As such, the simple isomers have a cycloreversion quantum yield 100 times higher than their functionalized analogues. A dependence on the ring size cannot be concluded; the simple 7-membered ring derivative **aDTE$_{77}$-Me** shows a higher cycloreversion efficiency than the simple 6-membered ring counterpart, whereas **aDTE$_{77}$-Ph(CF$_3$)$_2$** opens more efficiently than **aDTE$_{66}$-Ph(CF$_3$)$_2$** does.

[28] Taking into account that both the low cyclization quantum yield and the high cycloreversion quantum yield, the prerequesits for using the intial slope method are not strictly fullfilled and may result in an underestimated cyclization quantum yield. Nevertheless, the value is given for comparibility.

Within the series of $aDTE_{66}$, a slight decrease was observed following the order (-CN ≈ -CN + $-NMe_2$ < $(-CF_3)_2$ < -OMe) and may correlate with the auxochromes acceptor strength.

The quantum yields for the double bond isomerization $\Phi_{E\rightarrow Z}$and $\Phi_{Z\rightarrow E}$ are not directly accessible. From the roughly doubled irradiation time of *E*-**aDTE$_{66}$-Ph(CF$_3$)$_2$** compared to *Z*-**aDTE$_{66}$-Ph(CF$_3$)$_2$** to reach the PSS (Figure 2.3-6) as well as the amount of intermediate *Z*-isomer formed, the quantum yield $\Phi_{E\rightarrow Z}$ can be estimated to be of the same order of magnitude. An estimation for $\Phi_{Z\rightarrow E}$ based on the fact that

$$\sum \Phi_{A\rightarrow product} \leq 1 \qquad (13)$$

for the photoreaction of any given substance[29] shows that it must be rather small for the wavelength used. This is also in good agreement with the undetectable or low amount of *E*-isomer detected by UPLC analysis of the photocyclization for functionalized *Z*-aDTEs and for *Z*-**aDTE$_{66}$-Me**, respectively. Further information on the double bond isomerization yields can be derived from the transient absorption spectroscopy discussed in Section 2.5.

2.3.5 Photochemical fatigue

For possible uses of any photochromic compound, the endurance over prolonged irradiation with UV is an important measure. For DAEs, formation of a constitutional isomer (for an example see Section 1.2.3) from the closed form is the major pathway of photodegradation.[47b] It was shown by Herder *et al.* that the rate of formation of the rearrangement product can be reduced by attaching electron-withdrawing groups.[48,55] Without knowing the rates of formation,[48,55] the fatigue resistance can be visualized qualitatively by repeated cyclization/cycloreversion cycles and plot of the absorbance at the wavelength characteristic for the closed isomer and the degradation product (Figure 2.3-13).[30]

[29] This assumption only holds true for reactions from the same excited state.

[30] Irie introduced the benchmark of 80% residual photochrome in the mixture, after multiple cyclization irradiations to 90% of the PSS mixture.[27a] This would be reached for **aDTE$_{66}$-Ph(CF$_3$)$_2$** after 22 cycles (obtained by linear extrapolation), though irradiation was continued until no visible change in absorption occurred. With shorter irradiation times, supposedly a better value can be obtained.

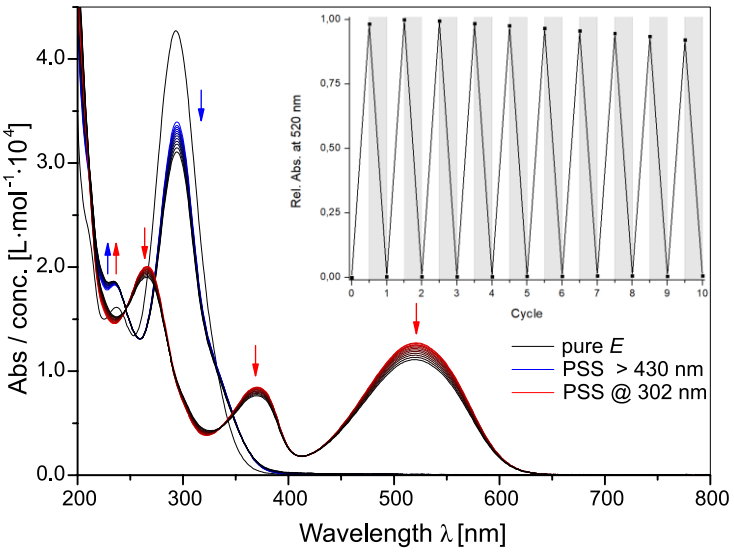

Figure 2.3-13 Spectral evolution of **aDTE$_{66}$-Ph(CF$_3$)$_2$** over multiple cyclization / cycloreversion cycles in MeCN (c = 10^{-5} M). While the amount of closed isomer formed decreases with each switching cycle, no other product absorbing in the visible part of the spectrum builds up.

While a slow decrease of the absorption maximum can be observed, the typical rise of the baseline due to the rearrangement product could not be detected after irradiation with visible light. In agreement with the fact that no specific product observed in UPLC analysis of long time irradiation samples, it can be concluded that the typical degradation mechanism is not applicable to aDTEs. The number of degradation products in combination with their elevated molecular mass (m/z = +16 or +32) indicates non-specific oxidation of the extended π-system in the closed isomer.

In conclusion, even though degradation is observed after repeated switching cycles, no colored by-product is observed and the solution remains transparent in the visible region. This may be advantageous for bulk applications or visual detection of a repeated switching process.

2.3.6 Switching in the solid state

The coloration of TLC spots upon UV-light irradiation was observed already during the synthesis of aDTEs. As discussed in Section 2.2.2.1 and 2.2.3.1, the distance between the reactive carbons in the *Z*-isomers is sufficiently small to enable electrocyclization in the solid state. In order to investigate this effect more thoroughly, a filter paper was impregnated with a DCM solution of *Z*-**aDTE$_{66}$-Ph(CF$_3$)$_2$**. After drying, it was irradiated for 30 s with a TLC hand lamp (365 nm & 254 nm) through a simple mask (Figure 2.3-14 left).

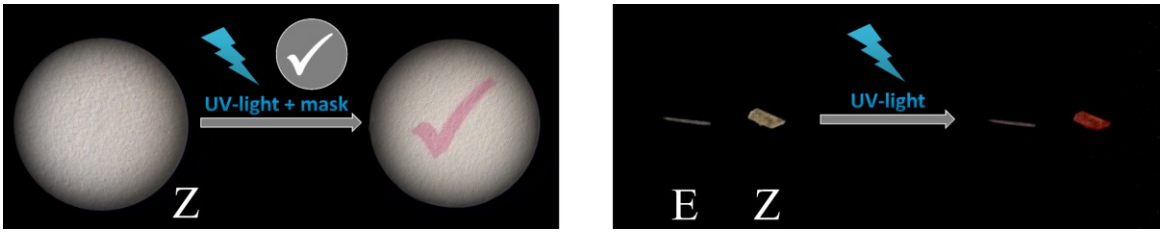

Figure 2.3-14 Switching of **aDTE$_{66}$-Ph(CF$_3$)$_2$** in the solid state. **Left**: Filter paper impregnated with DCM solution of *Z*-**aDTE$_{66}$-Ph(CF$_3$)$_2$** and before and after irradiation with UV-light (for 30 s) through a simple mask. **Right**: Single crystals of both isomers before and after irradiation with UV-light (1 min).

In contrast, no direct electrocyclization is expected for the *E*-isomers. Nevertheless, coloration of *E*-isomers would be possible by consecutive double bond isomerization and electrocyclization (Section 2.3.3). For the direct comparison of both isomers, single crystals of both *E*- and *Z*-**aDTE$_{66}$-Ph(CF$_3$)$_2$** were irradiated with UV-light (Figure 2.3-14 right). While a quick coloration was observed for the *Z*-isomer (< 1 min), the crystal of *E*-**aDTE$_{66}$-Ph(CF$_3$)$_2$** is unchanged even after 30 min of irradiation. While having comparable quantum yields for both processes in solution, the double bond isomerization is suppressed in the solid state.

2.3.7 Towards *Z*→*E* isomerization

As the photochemical *Z*→*E* conversion is not observed upon direct irradiation, the potential of orthogonal stimuli known for stilbene *Z*→*E* isomerization was investigated. Considering the long history of stilbene chemistry, this list is far from exhaustive. The isomerization of aDTEs upon electrochemical oxidation and reduction under cyclic voltammetry conditions is discussed in Section 2.4.

2.3.7.1 Thermal isomerization

The thermal stability of the open aDTE isomers in MeCN at elevated temperatures was proven during spectroscopic experiments (Section 2.3.3). The high stability of the open isomers is expected as the thermal isomerization of unsubstituted stilbene only becomes a reasonably fast process in regions of 200 °C,[107] having a large barrier of 43 kcal/mol.[8] DSC (> 200 °C) measurements of isomerically pure **aDTE$_{66}$-Me** revealed a melting point and heat flow depression over multiple heating cycles. This was assigned to isomerization in the melt, as subsequent UPLC analysis of the tempered samples confirmed the formation of the second isomer.

Motivated by these findings, it was tested whether this temperature can be lowered in solution. The thermal treatment of simple aDTEs in boiling hexane (bp = 70 °C) or in MeCN at 70 °C over several hours caused no isomerization of either isomer. Also boiling of several *Z*-isomers[31] in xylene (bp = 140 °C) for one day showed no effect.
Finally, a thermal isomerization could be observed in NMP (bp = 203 °C). The isomer ratios were detected by UPLC analysis and are summarized in Table 2.3-2.

Table 2.3-2 Thermal isomerization of distinct aDTEs in boiling NMP (bp = 203 °C). The *E*:*Z* ratios were determined by integration of the UPLC diode array at the respective peak maximum of the aDTE couple and corrected for the different absorptivities of each isomer.

Compound	Starting from *E*-		Starting from *Z*-	
	Time	*E*:*Z*	Time	*E*:*Z*
aDTE$_{55}$-Me	2 h	95:5[a]	n.d.	n.d.
aDTE$_{66}$-Me	7 h	54:46	2 h	51:49
aDTE$_{77}$-Me	7 h	100:0	7 h	0:100
aDTE$_{66}$-Ph(CF$_3$)$_2$	n.d.	n.d.	7 h	45:55
aDTE$_{66}$-PhCN	n.d.	n.d.	7 h	49:51
Me$_2$NPh-aDTE$_{66}$-PhCN	n.d.	n.d.	7 h	51:49

[a] same initial ratio

Analysis consisted of at least two measurements with appropriate delay to confirm that the thermal equilibrium is established. This was further verified for the two simple aDTEs, as both isomers could be tempered. The thermal treatment of aDTE$_{66}$ yielded roughly a 1:1 *E/Z*-mixture independently from the substitution pattern, whereas **aDTE$_{77}$-Me** did not isomerize at all under identical conditions. Heating a 95:5 *E*/*Z*-mixture of **aDTE$_{55}$-Me** brought about no change in the isomeric ratio after 2 h. Whether this sterically least demanding system had already been in equilibrium ratio or simply no isomerization occurred, cannot be determined from the experiment.

Overall, thermal *Z*→*E* isomerization is possible, however only at very high temperatures, which makes this pathway unfeasible for common applications.

[31] *Z*-**aDTE$_{66}$-Me**, *Z*-**aDTE$_{66}$-Ph(CF$_3$)$_2$**, *Z*-**aDTE$_{66}$-PhCN**, *Z*-**Me$_2$NPh-aDTE$_{66}$-PhCN** and the isomeric mixture of **aDTE$_{55}$-Me** obtained from synthesis.

2.3.7.2 (Photo-) chemical mediators

As mentioned in Section 2.2.3.1, an *E*/*Z*-isomer mixture (ca. 1:1) was obtained during mono-functionalization of *Z*-**aDTE$_{66}$-Cl** under Suzuki-conditions.[32] As the isomerization of the anion (after lithiation) was excluded[101] for similar compounds, the effect of palladium complexes on the double bond geometry was tested. On the contrary, for the 1:10 *E*/*Z*-mixture of the 7-membered ring derivative **aDTE$_{77}$-Cl** employed in synthesis of **aDTE$_{77}$-Ph(CF$_3$)$_2$**, no remarkable change in the isomer ratio was observed.
Isomerizations mediated by palladium[33] yielding a high amount of *E*-isomer were already described for *Z*-styrene derivatives with $PdCl_2 \cdot (MeCN)_2$ in DCM at room temperature [10a] and $Pd(OAc)_2$ in hot DMF.[10b] Following the protocol in DCM, isomerization of both *Z*- and *E*-isomers of **aDTE$_{66}$-Me** was observed. Yet, the isomerization stopped before a uniform final state was observed for both isomers. Since oxygen was not excluded, this may be due to oxidation of the catalyst. For more detailed investigations, careful degassing of the solution is advised.

Another pathway to induce double bond isomerization is the addition of halogen radicals as I$^{\bullet}$[109] and Br$^{\bullet}$[110] to the double bond. After free rotation of the newly formed single bond in the radical[109b] or cationic[109d] adduct, a mixture of isomers is formed after elimination.
Unfortunately, the treatment of aerated solutions in acetonitrile and ^{n}hexane of either open isomer of **aDTE$_{66}$-Ph(CF$_3$)$_2$** with iodine in the dark[12b] gave no change at room temperature or only marginal conversion when heated in ^{n}hexane. Heating in MeCN achieved isomerization, but was accompanied with notable by-product formation. The nature of the by-product was not further investigated, but the blue-shifted spectrum indicates that the central double bond may be resolved, for example by addition of iodine. The ratio of remaining substrate obtained after 5 h heating was 42:58 and 45:55 *E*/*Z* when starting from *E*- and *Z*-**aDTE$_{66}$-Ph(CF$_3$)$_2$**, respectively.

More conveniently, isomerization of *Z*-**aDTE$_{66}$-Me** could be achieved by addition of catalytic amounts of iodine and irradiation.[111] In contrast to the reported method,[109a] no isomerization was observed in ^{n}hexane upon prolonged irradiation with the wavelength

[32] 5% $Pd(PPh_3)_4$ in degassed THF at 70 °C overnight, see Section 4.5.4.1.

[33] Mechanistic considerations about double bond isomerizations and shifts have been published.[108]

corresponding to iodine absorption (530 nm). Yet, changing the solvent to acetonitrile enabled isomerization with 450 nm light[34] within a minute. Even relatively weak white room light had a noticeable effect after 5 min (for emission spectra of white light fluorescent tubes see Figure 6.6-2 and Figure 6.6-3), although the ratio of aDTE to iodine was only about 5:1.

UPLC analysis of the experiment showed the appearance of an iodine-adduct next to an increasing amount of *E*-**aDTE$_{66}$-Me**. The UV/vis absorbance of the adduct is red-shifted compared to the starting aDTE (λ_{max} = 375 nm vs. 300 nm) and has a reduced mass (m/z = 578.912, calc.: 582.949 for [**aDTE$_{66}$-Me**+2I]$^+$), indicating the formation of new double bonds by a rearrangement of the pi-system through iodination and subsequent elimination reactions.

Finally, an *E*/*Z*-ratio of 66:34 was obtained. The formation of other side-products than the iodine-adduct is marginal if carried out in degassed solution, and the occurrence of the adduct probably can be reduced with lower amounts of iodine used.

As iodine may be incompatible in some cases, another elegant method to circumvent the boundaries of direct photoexcitation was investigated. It is known for stilbenes to undergo triplet-sensitized isomerization.[3b,112] The outcome of the photoreaction is determined by the triplet energy of the sensitizers compared to the triplet energy of the two isomers. It was found that low energy sensitizers promote preferably the *Z*→*E* conversion, while excitations using high energy sensitizers tend to yield the *Z*-isomer. Conversions as high as 100% and 93% are achieved for isomerization of *Z*- and *E*-stilbene, respectively, are reported.

By contrast, for normal DAEs high energy triplet sensitizers are found to induce electrocyclization while low energy sensitizers such as methylene blue had no effect.[48,55,113] The electrocyclization using biacetyl (E_T = 236 kJ/mol)[35] occurred without the undesired by-product formation known from direct excitation (described in Section 1.2.3).

For aDTEs, indeed the behavior of stilbenes with low energy sensitizers could be reproduced. As an example, a degassed solution of *Z*-**aDTE$_{66}$-Ph(CF$_3$)$_2$** in MeCN was irradiated with a 530 nm LED in the presence of equimolar amounts of eosin Y

[34] Iodine is strongly solvatochromic.

[35] E_T = triplet energy. The values are taken from the "Handbook of Photochemistry" (3rd ed.)[114]. They are listed for polar solvents (normally EtOH).

(E_T = 177 kJ/mol)[35] (Figure 2.3-15). The increase in the 293 nm band, due to the increased absorptivity of the *E*-isomer compared to *Z*-**aDTE$_{66}$-Ph(CF$_3$)$_2$**, is accompanied by the decrease of the eosin Y band at 530 nm. A final composition of 93:7 *E*/*Z* was observed by UPLC.

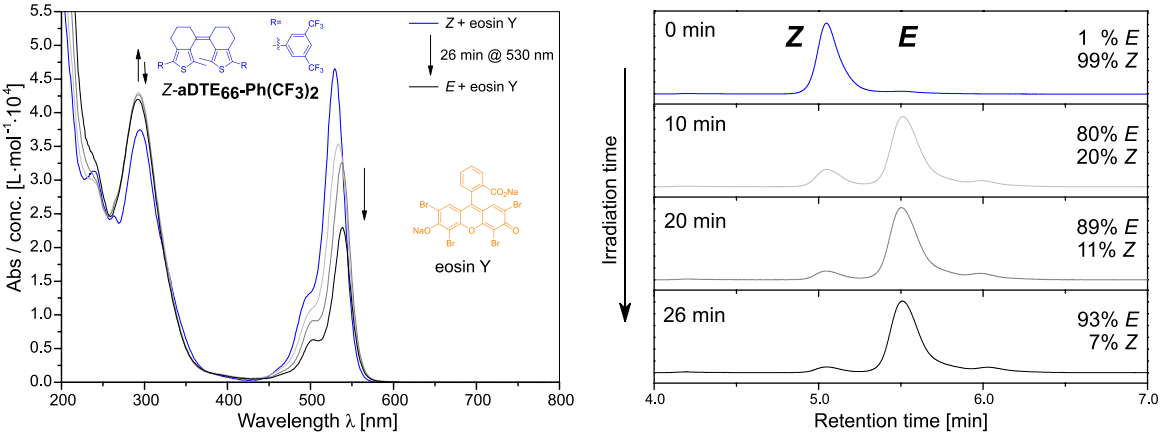

Figure 2.3-15 Conversion of Z→*E* of **aDTE$_{66}$-Ph(CF$_3$)$_2$**, mediated by eosin Y in MeCN (c = 10^{-5} M). **Left:** While the absorption band at 293 nm rises, the absorption of eosin at 530 nm decreases, probably due to degradation of the mediator. **Right:** UPLC diode array at 293 nm with isomer ratio, corrected for the respective absorptivity of each isomer.

Additionally, a control experiment without any sensitizer irradiating extensively at the respective wavelength (530 nm) as well as the fluorescence band of eosin Y (565 nm) showed no isomerization when analyzed by UPLC. This result excludes the possibility of an excitation of a low oscillator strength transition of **aDTE$_{66}$-Ph(CF$_3$)$_2$** in this region of the spectrum.

Taking into account both the high conversion and the vast amount of triplet sensitizers available, it can be concluded that triplet sensitization is a very promising pathway to achieve 3-state switching in aDTEs.

2.3.8 Summary

The photochemical behavior of several examples of simple aDTEs (i.e. methyl-substituted) and functionalized aDTEs with ring sizes ranging from 5- to 7-membered rings were analyzed. Additionally, two unconstrained bis(thienyl)ethenes and a hybrid bearing only one annulated hemisphere were examined in order to evaluate the influence of stiffening. In contrast to normal DAEs, all photochromes studied can exist in three isomeric states due to the double bond isomerization of the open isomer.

All isomers in this study are transparent in the visible region of the spectrum in both open forms. All cyclized isomers, formed upon irradiation with near UV-light, are strongly colored as known for normal DAEs. In contrast to the parent stilbene system that acts mainly as an *E*/*Z* switch and thermally reverts from the cyclized dihydropyrene to the open isomer, aDTE's photochemistry funnels very efficiently towards the thermally stable cyclization product from both open isomers.

While all $aDTE_{66}$ show similar band structures, the maximum of the bathochromic band can be shifted as a function of the substituent, allowing fine-tuning of the absorption spectrum. Compared to the corresponding 6-membered ring derivative, functionalized *Z*-**$aDTE_{77}$-Ph(CF_3)$_2$** has a lower absorptivity and more complex band structure but behaves similarly under the influence of light.
A different behavior was observed for the simple **$aDTE_{77}$-Me**. Having a very low absorption for the bathochromic band around 300 nm, irradiation was performed with 254 nm light, which brought about cyclization of the *Z*-isomer but had only limited effect By contrast, the only synthesized 5-membered ring derivative *E*-**$aDTE_{55}$-Me** proved to act mainly as double bond switch and has only very limited tendency to undergo electrocyclization. Furthermore, the cyclization product was shown to be thermally unstable.

The effect of annulation could impressively be demonstrated with the half-stiff **(F_3C)$_2$Ph-$aDTE_{6Me}$-Me**, which seems to inherit the switching mode of its parent double-annulated **$aDTE_{66}$-Ph(CF_3)$_2$**, whereas unconstrained DAEs acted almost exclusively as double bond switches. The hybrid half-stiff system may be very interesting for the practical usage of the system, as the choice of the second hemisphere is less restricted.

For all stiffened and also the hybrid half-stiff derivative, the cyclization quantum yields are enhanced compared to normal DAEs. For the benzonitrile-substituted **$aDTE_{66}$-PhCN**, even a cyclization quantum yield close to unity was observed. It was shown that for all derivatives (except **$aDTE_{55}$-Me**), it is possible to operate exclusively within the electrocyclization/-reversion regime, rendering the frozen double bond configuration used in the classical DAE design unnecessary. The photochemical fatigue during the cyclization process is comparable to normal DAEs with the same substitution pattern. In contrast to those compounds, no specific degradation product is formed and the aDTE system preserves transparency in the open form.

It could be shown that photochemical cyclization *Z*-isomer is even possible in a single crystal, as already indicated by the distance between the reactive carbons. At the same time, double bond isomerization enabling conversion of the *E*-isomer to the colored form is suppressed.

With electrocyclization as the governing reaction mechanism for aDTEs upon direct excitation, *Z*→*E* conversion was not observed for functionalized aDTEs and only in negligible amount for **aDTE$_{66}$-Me**. Similar to stilbene, it was shown that orthogonal methods such as thermal isomerization results in *Z*→*E* conversion to a 1:1 mixture that is even possible at room temperature if catalyzed by palladium complexes. The most promising methods in the preliminary investigations are isomerizations mediated by photochemically generated iodine radicals or low energy triplet sensitizers such as eosin Y. For these two processes, *E*/*Z* ratios of 66:34 and 93:7, respectively, could be achieved.

The photochemistry of aDTE$_{66}$ can thus be summarized as

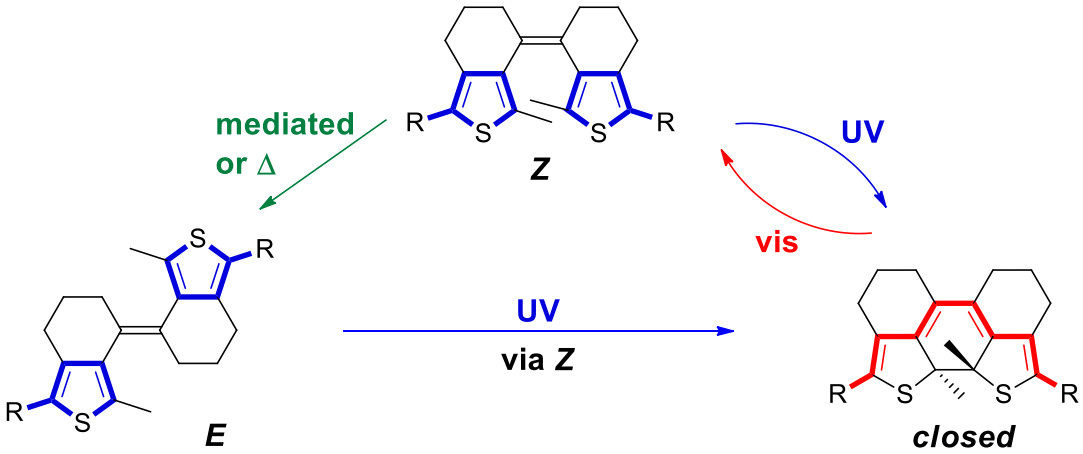

Scheme 2.3-5 Switching modes of 3-state photochrome aDTE$_{66}$. While direct excitation of both *E*- and *Z*-isomer with near UV-light causes efficient isomerization to the colored isomer *C*, cycloreversion with visible light yields the *Z*-isomer exclusively and allows operation solely in the cyclization/cycloreversion regime. The reverse double bond isomerization can be achieved thermally or mediated by iodine atoms or low energy triplet sensitizers with almost quantitative conversion.

The possibility to switch within the electrocyclization/-reversion regime with increased ring closing quantum yields shows that the design may be superior to the classic design of DAEs. The ability of *Z*→*E* isomerization by an orthogonal switching process allows using the system as a true hybrid of DAE and stilbenoid compounds, offering both the possibility to switch conjugation and geometry using a single photochromic moiety.

2.4 (Spectro)electrochemistry of aDTEs [36, 37]

This section describes the electrochemical behavior of aDTEs under oxidative and reductive conditions. For the electrochemical characteristics of open and closed isomers, cyclic voltammetry (CV) was conducted in MeCN and/or DCM. To elucidate the observed behavior further, spectro-electrochemical (SEC) analysis of distinct compounds was carried out. The behavior will be explained with the example of ***aDTE$_{66}$-Me*** *and compared to aDTEs with other ring sizes and functional groups.*

2.4.1 Motivation

For photochromic compounds, electrochemistry poses an interesting orthogonal stimulus to light[27b,115] and sometimes even enables switching pathways inaccessible by irradiation.[97,116] For normal DAEs, both electrochemical cyclization and cycloreversion have been reported.[117] While most isomerizations occur from an oxidized species, the direction of the reaction is dependent on the bridge moiety and the aromatic substituents. Even a bidirectional design could be achieved.[118]

For stilbene as the simplest DAE structure possible, three different isomers are imaginable as the double bond is not restricted to its *Z*-conformation. Indeed, upon reduction of the *Z*-isomer to its radical anion by alkali metals[119] or on an electrode[120], a fast *Z*→*E*-isomerization occurs. The radical anion of the *E*-isomer consequently can be oxidized back to the uncharged form. In contrast to heteroaromatic DAEs, no electrocyclization to dihydrophenanthrene of either stilbene isomer has been observed in reference CV measurements in our laboratory.

For 1,2-dicyano-1,2-bis(2,4,5-trimethyl-3-thienyl)ethene (**XVII**) (compare Section 1.2.4) as one of the first modern DAE systems initially presented by Irie and co-workers,[30a] SEC was used to elucidate its electrochemical behavior.[121] Yet, no concern was given about the possibilities of an electrochemical double bond isomerization in this example.

Nevertheless, indications for electrochemical double bond isomerization in heteroaromatic DAEs were found.[101,122] It has been observed that *E*- and *Z*-isomers of 1,2-(thien-2-yl)ethenes yielded identical materials when oxidatively polymerized, with

[36] Parts of this section have been published in M. Kleinwächter *et al*., *Beilstein J. Org. Chem.* **2018,** *14,* 2812–2821.

[37] The experiments in this section were carried out and the data refined by Dr. Lutz Grubert.

the *E*-isomer probably being the major product. The chemical polymerization of the corresponding anions with copper salts succeeded with retention of the double bond geometry. The possibility of anodic electrocyclization was discussed in the same context but not investigated in detail.[123]

Since both the double bond isomerization and cyclization pathway seem reasonable for aDTEs, extensive electrochemical investigations were conducted. Being the central element of both switching modes, the investigations concentrated on the *Z*-isomer and the cyclized form *C*.

2.4.2 The electrochemistry of aDTE$_{66}$-Me

The electrochemical analysis of aDTEs will be explained with the example of **aDTE$_{66}$-Me**, as it is the common core of all aDTE$_{66}$. Furthermore, both open isomers were available in sufficient amount and purity from synthesis. All cyclic voltammetry and spectro-electrochemical analyses were performed in 10^{-3} M solutions in MeCN or DCM. All potentials are given in reference to the ferrocene/ferrocenium (Fc/Fc^{+}) redox couple, which was used as an external standard.

The investigation commenced with the oxidation of the two open isomers (Figure 2.4-1 left).

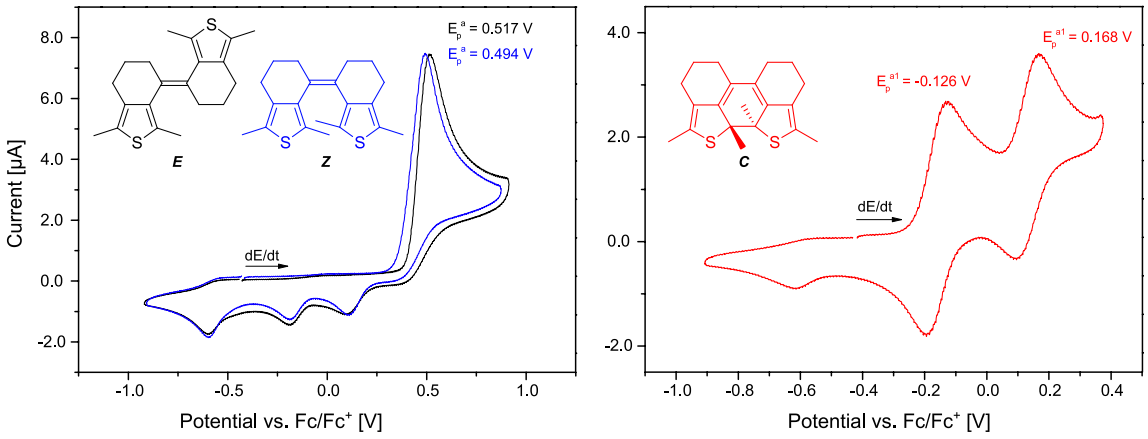

Figure 2.4-1 Cyclic voltammogram of **aDTE$_{66}$-Me**. Experiments in MeCN with 0.1 M Bu_4NPF_6, c = $1 \cdot 10^{-3}$ M, dE/dt = 1 V s^{-1}. **Left:** Both *E*- (black) and *Z*-isomer (blue) show an irreversible wave. This can be assigned to the formation of the closed isomer. **Right:** The closed isomer (red) is generated in situ from *Z*-**aDTE$_{66}$-Me** upon irradiation with 313 nm light. The first oxidation wave of the closed isomer is reversible whereas the second is quasi-reversible (*vide infra*).

A similar oxidation wave at E_p^a was observed for both open isomers, with the *Z*-isomer (blue) being slightly easier to oxidize than the *E*-isomer (black). Upon extraction of two

electrons, an irreversible reaction occurs. This behavior was already observed for *normal* DAEs[117] and was ascribed to electrochemical cyclization. Indeed, the observed two one-electron reduction waves during the back scan match exactly those of the closed isomer (red) (Figure 2.4-1 right). In a second consecutive cycle (not shown), also the two oxidation waves of the closed isomer (*vide infra*) are observed. For a detailed analysis, the closed isomer was generated photochemically within the electrochemical cell from *Z*-**aDTE$_{66}$-Me**. In contrast to the open isomers, two separate one-electron oxidation waves were observed at significantly lower potentials, reflecting the extended π-system.

To understand the course of the isomerization better, the spectral development in UV/vis during a CV cycle was measured. It was found that both *E*- and *Z*-**aDTE$_{66}$-Me** yield virtually the same oxidized state, displaying a characteristic absorption at 493 nm and 621 nm (Figure 2.4-2).

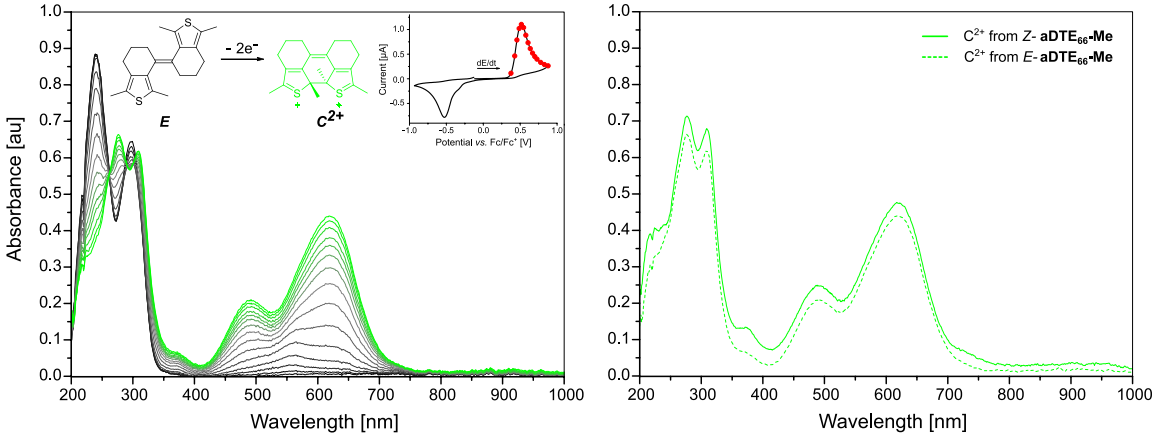

Figure 2.4-2 SEC of the open isomers of **aDTE$_{66}$-Me**. Experiments in MeCN with 0.1 M Bu_4NPF_6, c = $5 \cdot 10^{-4}$ M, dE/dt = 10 mV s^{-1}. **Left:** Exemplary SEC of *E*-**aDTE$_{66}$-Me**. A stable intermediate is formed upon oxidation. The inset shows the CV curve, red dots mark the time at which spectra were measured. **Right:** Comparison of the intermediate formed from *E*- and *Z*-**aDTE$_{66}$-Me**.

It can thus be concluded that both isomers cyclize from the same intermediate. To determine the nature of this intermediate, SEC was also carried out on the closed isomer.[38] The species initially formed upon oxidation is the cationic radical $\mathbf{C}^{+\bullet}$ (Figure 2.4-3 left). It shows the characteristic red-shifted absorption of an unpaired electron at 731 nm and 912 nm. If the potential is returned after the first oxidation wave, a fully

[38] For experiments starting from the closed isomer, it was generated by irradiation of the *Z*-isomer with 313 nm light directly within the electrochemical cell.

reversible process takes place. This is also supported by the fact that the mono-oxidized species $\mathbf{C}^{+\bullet}$ is stable even at the slow scan rates of SEC and builds up continuously.

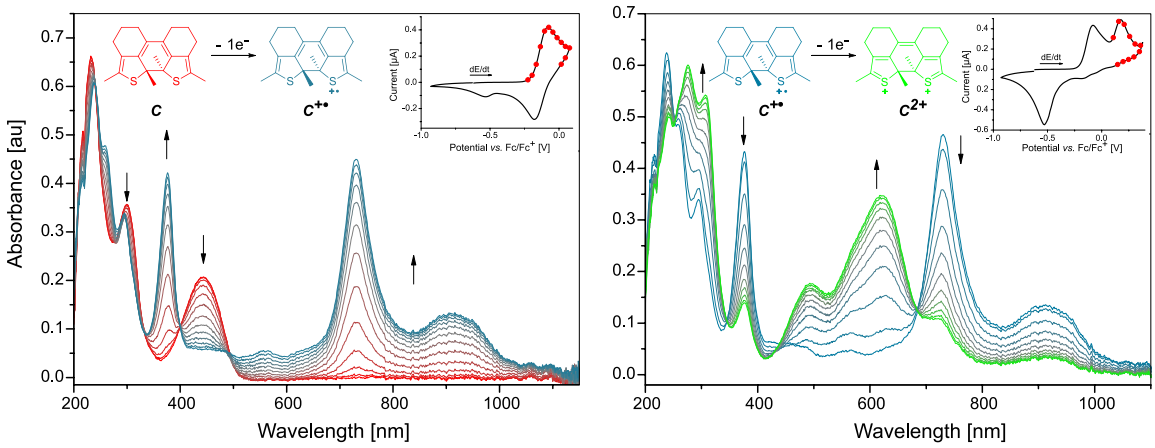

Figure 2.4-3 SEC of the closed isomer of **aDTE$_{66}$-Me**. Experiments in MeCN with 0.1 M Bu_4NPF_6, c = $5 \cdot 10^{-4}$ M, dE/dt = 10 mV s^{-1}. **Left:** Formation of the stable cationic radical species $\mathbf{C}^{+\bullet}$. The inset shows the corresponding CV curve, red dots indicate measured spectra. **Right:** Further oxidation of $\mathbf{C}^{+\bullet}$ to the dication $\mathbf{C}^{2+}$. These spectra were obtained in a separate experiment.

If the oxidation is continued instead, $\mathbf{C}^{+\bullet}$ is depleted in favor of the dication $\mathbf{C}^{2+}$ (Figure 2.4-3 right). This species shows a characteristic absorption at 493 nm and 621 nm. The hypsochromic shift indicates the absence of unpaired electrons. In contrast to the first oxidation step, this oxidation is not reversible at the slow scan rates of SEC and an irreversible reduction wave at -0.531 V is observed, leading to a species that in the following will be called by-product BP.[39] Contrarily, in the CV experiments only marginal BP formation is observed and also the second oxidation step is quasi-reversible. This kind of irreversible process from an oxidized closed isomer has already been observed[117a] for normal DAEs, but its nature was not further discussed. The little amount of this by-product formed in the one electron oxidation may be a result of disproportionation of $\mathbf{C}^{+\bullet}$.

That the by-product is different from the open isomers can clearly be seen by its absorption spectrum, which is red-shifted relative to them (Figure 2.4-4). Summarizing the information gathered, the mechanism of the cyclization from both open isomers can be understood as follows. From both open isomers upon oxidation, fast isomerization to a dicationic $\mathbf{C}^{2+}$ species takes place. The isomerization of the former double bond of the

[39] Though its nature remains unspecified in the current study, this by-product is not to be confused with the photochemical by-product known for normal diarylethenes as depicted in Scheme 1.2-6.

E-isomer as well as the cyclization reaction are always instantaneous on the timescale of the experiment. The intermediate $\mathbf{C}^{+\bullet}$ is either not formed or very short-lived, as its characteristic absorption at 731 nm is not observed (Scheme 2.4-1).

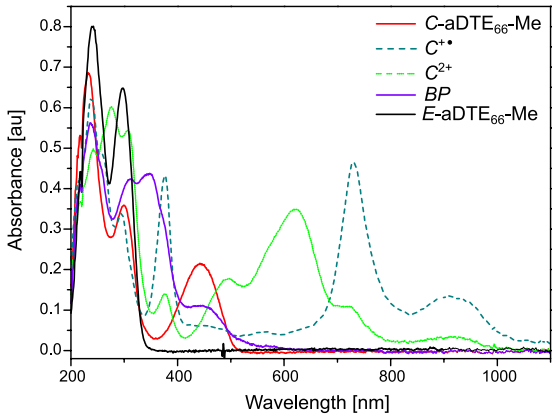

Figure 2.4-4 Comparison of the UV/vis spectra of the species observed in the SEC of **aDTE$_{66}$-Me**. Experiments in MeCN with 0.1 M Bu_4NPF_6, c = $5 \cdot 10^{-4}$ M, dE/dt = 10 mV s^{-1}. The by-product (BP) is red-shifted compared to the *E*-isomer. Due to its radical ion character, the $\mathbf{C}^{+\bullet}$ is most bathochromic.

In the literature, both the singly and doubly oxidized intermediate are discussed as the species undergoing thermal ring-closure.[115b,117,124] Previous investigations of unsymmetrical DAEs in our group showed that in these compounds cyclization occurs only from the dicationic open isomer.[97] Yet, in the current experiments, no differentiation between the two mechanisms is possible as no monocationic species could be detected.

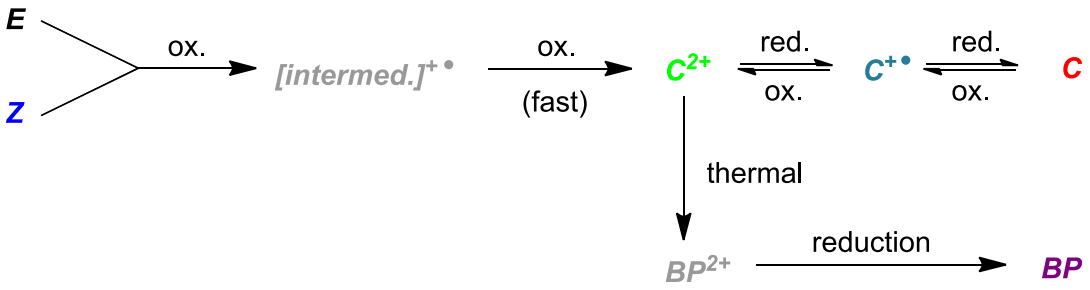

Scheme 2.4-1 Electrochemical behavior of **aDTE$_{66}$**. Upon two-fold oxidation, both open isomers isomerize to the closed isomers dication $\mathbf{C}^{2+}$. This dication can be either reduced to the closed isomer **C** or thermally converted to a by-product $\mathbf{BP}^{2+}$. As no monocationic radical intermediate could be detected, it cannot be determined whether the cyclization occurs in the first or second oxidation step.

As the by-product forms primarily from the two-fold oxidized closed isomer $\mathbf{C}^{2+}$, it is concluded that $\mathbf{C}^{2+}$ can react thermally to a follow-up product. While the nature of this by-product remains unclear, it was found that the rate of its formation is dependent on the experimental conditions as well as the structure of the aDTE and its substituents (*vide infra*). This hypothesis is strengthened by the fact that only a small amount of by-product

is formed at high scan rates in CV experiments.

As evident from the values of the cathodic reduction potential E_p^c (Table 2.4-1), the reductive *Z*→*E* isomerization pathway known for stilbenes[120] could not be investigated for **aDTE$_{66}$-Me** since the reduction potential of the open isomer is more negative than that of the electrolyte.

2.4.3 Substitution and ring size effects

The redox potentials of the synthesized aDTEs and reference compounds were determined. For the sake of comparability, the conformationally locked pcDTE (Chapter 3) are also included. The data is summarized in Table 2.4-1, and Figure 2.4-6 gives a graphical overview of the observed trends.

As the first and second oxidation wave of the open isomers in general cannot be resolved, it can be concluded that both hemispheres must be more or less electronically independent and are oxidized in a "concerted" fashion. Alternatively, fast disproportionation of the intermediate radical cation could explain the observation, as the resulting equilibrium would be shifted towards the dication due to the following thermal cyclization reaction.[97] Nevertheless, a strong divergence for the first oxidative peak potential E_p^a within the electronically similar group of simple aDTEs is found (*vide infra*). For simple aDTE, the *E*-isomer has a higher oxidation potential than the *Z*-isomer, whereas for the unconstrained derivative **12** the order is inversed (Figure 2.4-5).

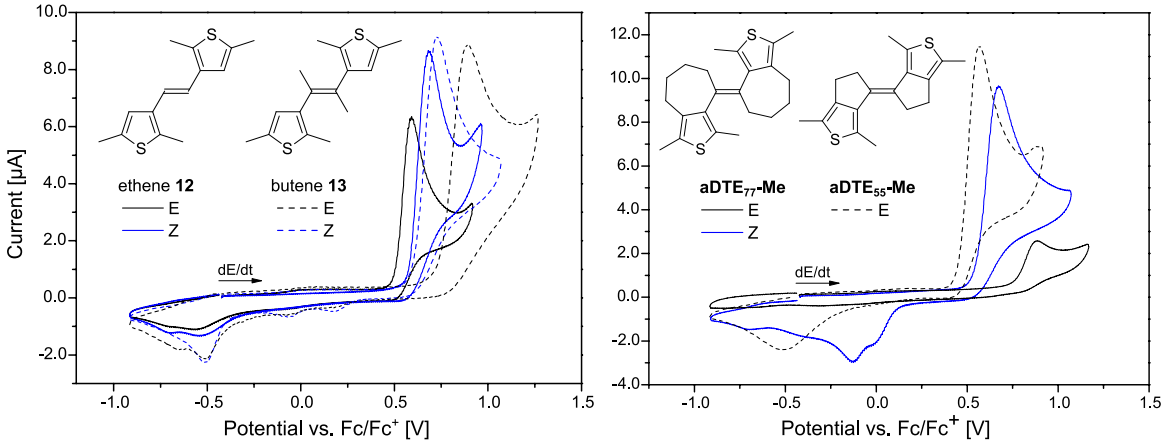

Figure 2.4-5 Cyclic voltammogram of unconstrained DTEs and simple aDTEs. Experiments in MeCN with 0.1 M Bu_4NPF_6, c = $1 \cdot 10^{-3}$ M, dE/dt = 1 V s^{-1}. **Left:** Unconstrained DTEs **12** and **13** show no or only weak reduction waves for electrochemically formed closed isomer, respectively. **Right:** While *Z*-**aDTE$_{77}$-Me** cyclized upon oxidation, *E*-**aDTE$_{77}$-Me** and *E*-**aDTE$_{55}$-Me** show no closed isomer formation in contrast to *E*-**aDTE$_{66}$-Me**.

Unexpectedly, derivatives with a higher amount of electron donating alkyl substituents can be more difficult to oxidize (**aDTE$_{66}$-Me** vs. **aDTE$_{66}$(Me$_2$)-Me**). However, *E*- and *Z*-isomers of these two compounds display no major differences in their respective oxidation potential. It can thus be deduced that the conjugation between the thiophenes and the double bond must be very similar in each pair of open isomers. In contrast, for the 7-membered ring derivative **aDTE$_{77}$-Me,** a substantial difference of $\Delta E_p^a = 0.210$ V between the two open isomers was found. Furthermore, no cyclization from *E*-**aDTE$_{77}$-Me** could be determined. This is in strong contrast to the findings for the aDTE$_{66}$ derivatives, where *E*- and *Z*-isomer behaved similarly. Both open isomers of the unconstrained ethene **12** as well as *E*-**aDTE$_{55}$-Me** failed to show cyclized product upon oxidation. For butene **13**, only faint reduction waves typical for the closed isomer were observed in the back sweep for both isomers. For all of these compounds, an irreversible oxidation wave and a re-reduction wave around $E_p^c \approx -0.5$ V was observed even at high scan rates. Whether the formation of the by-product is very fast in these system or oxidative cyclization does not occur, cannot be determined.

Since for the functionalized isomers only the *Z*-isomer was available in sufficient quantity for CV, the difference of the oxidation potentials between the *E*- and *Z*-isomer could not be determined for most compounds. The shift of the oxidation potential caused by an electronically altered substitution pattern is up to $\Delta E_p^a = 0.330$ V (**aDTE$_{66}$-PhOMe** vs. **aDTE$_{66}$-Ph(CF$_3$)$_2$**). The latter compound shows outstanding resistance towards oxidation, even in comparison to the strong π-acceptor substituted **aDTE$_{66}$-PhCN**.
Comparison of the ring sizes shows that the 6-membered ring derivatives are easier to oxidize than the 5- and 7-membered derivatives. Combination of the two characteristics leads with $E_p^a = +1.083$ V for *Z*-**aDTE$_{77}$-Ph(CF$_3$)$_2$** to the by far most resistant compound within the series. Comparison of this compound with the reported[48,55] normal **DAE-Ph(CF$_3$)$_2$** shows that a similar value is obtained, despite the increased electron density due to the additional alkyl chains. If the relation between *E*- and *Z*-isomer found in **aDTE$_{77}$-Me** is applicable to functionalized aDTEs, the so far unavailable *E*-**aDTE$_{77}$-Ph(CF$_3$)$_2$** should have an even more positive oxidation potential.

For the closed isomers, a similar overall trend following the acceptor properties of the substituent is observed for the position of the first and second oxidation potential. In

contrast to the open isomers, both the simple and functionalized aDTE$_{77}$ are not exceptionally difficult to oxidize.

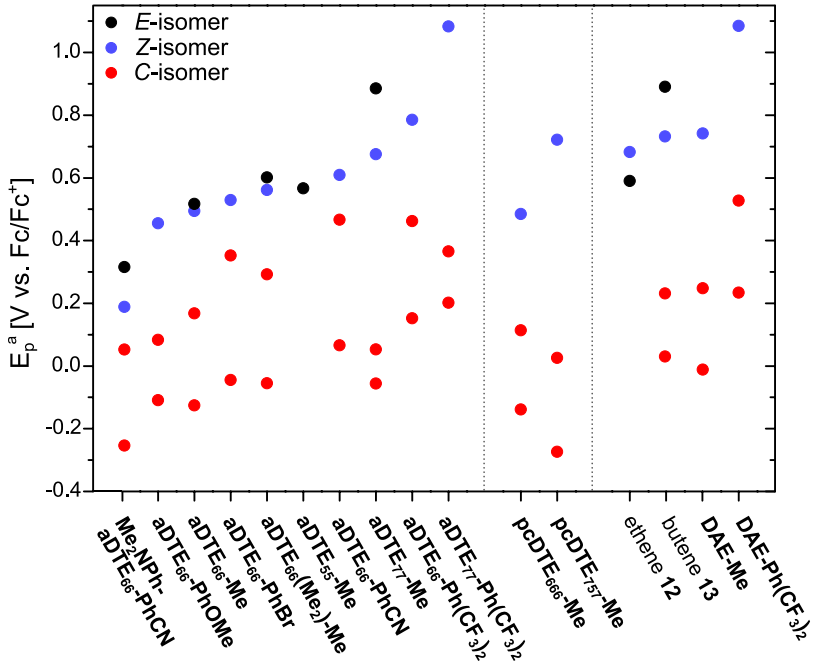

Figure 2.4-6 Graphical illustration of the peak potentials of aDTEs, pcDTEs and reference compounds in MeCN. For more details, see Table 2.4-1. **aDTE$_{55}$-Me** and ethene **12** did not form enough closed isomer to determine the corresponding oxidation potential.

Table 2.4-1 Anodic and cathodic peak potentials (E_p^a / E_p^c) of aDTEs, pcDTEs and reference compounds.

Compound	*Z* E_p^a [V]	*E* E_p^a [V]	*C* $E_p^a{}_{1/2}$ [V]		*E* or *Z* E_p^c [V]	*C* E_p^c [V]	Cycl. cond.
aDTE$_{55}$-Me	n.d.	+0.567	n.a.		n.d.	n.a.	n.a.
aDTE$_{66}$-Me	+0.494	+0.517	-0.126	+0.168	n.d.	n.d.	ox.
aDTE$_{66}$(Me$_2$)-Me	+0.561	+0.601	-0.055	+0.292	<-2.5	n.d.	ox.
aDTE$_{77}$-Me	+0.675	+0.885	-0.056	+0.053	<-3.0	n.d.	ox.
aDTE$_{66}$-Ph(CF$_3$)$_2$	+0.785	n.d.	+0.152	+0.462	<-2.5	-2.078	ox.
aDTE$_{66}$-PhOMe	+0.455	n.d.	-0.109	+0.083	<-2.5	-2.534	ox.
aDTE$_{66}$-PhBr	+0.529	n.d.	-0.045	+0.352	<-2.5	-2.190	ox.
aDTE$_{66}$-PhCN	+0.609	n.d.	+0.066	+0.466	-2.526	-1.902	ox./red.
Me$_2$NPh-aDTE$_{66}$-PhCN[a]	+0.188	+0.322	-0.248	+0.055	<-3.0	-2.249	ox.
aDTE$_{77}$-Ph(CF$_3$)$_2$	+1.083	n.d.	+0.202	+0.365	n.d.	-2.079	ox.
Ethene 12	+0.682	+0.590	n.a.		<-3.0	n.a.	n.a.
Butene 13	+0.731	+0.891	+0.030	+0.231	<-3.0	n.d.	ox.
pcDTE$_{666}$-Me[b]	+0.485 +0.714	n.a.	-0.139	+0.114	-2.567	-2.774	n.a.
pcDTE$_{757}$-Me	+0.722	n.a.	-0.274	+0.026	n.d.	n.d.	ox.
DTE-Me[c]	+0.742	n.a.	-0.012	+0.248	<-2.5	-2.750	ox.
DTE-Ph(CF$_3$)$_2$[48,55]	+1.085	n.a.	+0.234	+0.527	n.d.	-1.847	ox.
Stilbene[c]	+1.202	+1.082	n.a.		-2.954 (*Z*) -2.775 (*E*)	n.a.	n.a.
2,5-Dimethylthiophene[c]	+1.185		n.a.		-0.395		n.a.
Benzene[125]	+1.96		n.a.		n.a.		n.a.

[a] determined from *E*/*Z* mixture [b] values correspond to two different isomers [c] unpublished data

Furthermore, the differences between the first and second oxidation step of the two closed isomers are smaller than for the 6-membered ring analogues, indicating a lower conjugation between both hemispheres. This observation is consistent with their blue-shifted UV/vis absorbance spectra (Figure 2.3-1 and Figure 2.3-2).

In general, the oxidation potentials of *C*-aDTEs increase with the substituents acceptor strength. This phenomenon has already been observed for normal DAEs[48,55] and can be understood as the extraction of a second electron in an electron-poor conjugated system is more unfavorable.
For the reduction potentials of the closed isomers, no trend can be derived, but the donor substituted **aDTE$_{66}$-PhOMe** and the acceptor substituted **aDTE$_{66}$-PhCN** show the highest and lowest reduction potential, respectively.

The reduction potentials of the open isomers were mostly more negative than the reduction potential of the electrolyte and hence are only given as an upper limit. In contrast to the other aDTE systems in this study, for the electron-poor cyano derivative **aDTE$_{66}$-PhCN** the behavior of the *Z*-isomer under reductive conditions could be analyzed. During the first sweep, an irreversible reduction wave at E_p^c = -2.526 V was detected. In a second consecutive cycle, a new reduction wave at E_p^c = -1.920 V appeared, which is typical for the cyclized isomer as determined in a separate experiment. The formation of *C*-**aDTE$_{66}$-PhCN** was proven in a preparative electrolysis and subsequent UPLC analysis of the product. For quantitative conversion, four equivalents of electrons were applied.
In consequence, it is indicated that aDTEs do not undergo electrochemical *Z*→*E* isomerization upon reduction as their stilbene counterparts, but instead electrocyclize upon both oxidation and reduction. So far, the only reported examples for a reductive cyclization are pyridinium substituted dithienylhexafluoro-cyclopentenes.[118,126]

In addition, the by-product formation was analyzed with respect to the different substituents and ring sizes. While the amount of by-product is quantitative for **aDTE$_{66}$-Me** at the slow scan rates of SEC (10 mV/s), its formation is still observable at the fast scan rates of the CV (1 V/s). For functionalized aDTEs, a different speed of formation was observed. At high scan rates, a reversible oxidation was found for the derivatives **aDTE$_{66}$-PhCN**, **aDTE$_{66}$-Ph(CF$_3$)$_2$**, **aDTE$_{66}$-PhBr** and **aDTE$_{66}$-PhOMe**.

Only at slower scan rates during the SEC experiments, by-product formation was observed. The amount formed under similar conditions decreased in the order

$$Me \gg PhCN > PhBr > PhOMe$$

with **aDTE$_{66}$-PhOMe** being fully reversible. It can be seen that the spectrum of the initial closed isomer is fully recovered (Figure 2.4-7).

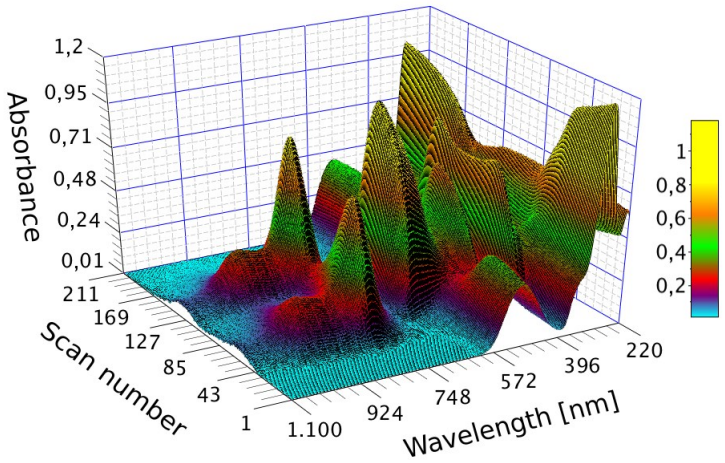

Figure 2.4-7 SEC of *C*-**aDTE$_{66}$-PhOMe.** Experiments in MeCN with 0.1 M $Bu_4NPF_{6,}$ c = $5 \cdot 10^{-4}$ M, dE/dt = 10 mV s^{-1}, return potentials at +0.32 V and -0.73 V. The formation of the hypsochromic cationic radical $\mathbf{C}^{+\bullet}$ and dicationic $\mathbf{C}^{2+}$ is fully reversible.

The dependence of the by-product formation on the ring size could not be analyzed. However, it was observed that the formation is slower in MeCN than in DCM. A similar trend was already described for other DAEs.[117b]

2.4.4 Summary

The electrochemistry of aDTEs was demonstrated with the example of **aDTE$_{66}$-Me**. It was observed that both the *E*- and the *Z*-isomer were converted equally to the closed isomer *C* upon abstraction of two electrons. The isomerization of the former double bond of the *E*-isomer as well as the cyclization reaction are always instantaneous on the timescale of the experiment.

The isomerization of the double bond as well as the cyclization are always faster than the experimental time scale, even at the high scan rates of cyclic voltammetry. To understand this behavior, spectro-electrochemical investigations on both the open and closed isomer was conducted. It was found that oxidation of the open isomers is an apparent

$2e^-$-process; an intermediate $\mathbf{E}^{+\bullet}$, $\mathbf{Z}^{+\bullet}$ or $\mathbf{C}^{+\bullet}$ could not be observed and thus is either not formed or very short-lived.

In contrast, the oxidation of the closed isomer consists of two $1e^-$-steps. The first oxidation step is reversible, but it is indicated that disproportion may take place. The second $1e^-$-oxidation is quasi-reversible, and depending on the scan rate, an irreversible wave is observed. It is concluded that the dication $\mathbf{C}^{2+}$ can react to a by-product whose nature could not yet be determined, as neither isolation for NMR nor the analysis by UPLC-MS was successful.

The amount of this by-product formed strongly depends on the substitution pattern on the aDTE and was compared for the functionalized aDTEs. Despite delocalization of the positive charges over a bigger π-system, derivatives with electron-withdrawing groups such as -CN still show a significant amount of by-product formed at slow scan rates. By contrast, electron-donating groups as -OMe completely suppress its formation.

To gain a complete picture of the influence of annulation on the electrochemistry of DTEs, aDTE derivatives with other ring sizes and two unconstrained compounds were investigated. In general, the ability to cyclize oxidatively parallels to the photochemical behavior; the derivatives with low *C*-contribution to the PSS (*E*-**aDTE$_{55}$-Me**, *E*-**aDTE$_{77}$-Me**, ethane **12,** and butane **13**) show only little or no amount of closed isomer upon oxidation.

The oxidation potentials of the functionalized derivatives follow the expected trend and relate to the acceptor strength of the substituent. The influence of ring sizes is significant (up to ΔE_p^a (*E*) = 0.37 V within the series of simple aDTEs) but objects the trend expected from an increased electron density due to an increased amount of inductively donating alkyl groups. Contrarily, the first and second oxidation potential of the closed isomers converge with increasing ring size. The reason for this finding is not yet understood, but a contribution of geometrical factors to the measured potential is conceivable.

In conclusion, *E*- and *Z*-aDTE$_{66}$ as well as *Z*-aDTE$_{77}$ are converted very efficiently from the open isomers to the cyclized form upon oxidation. Electrochemical cycloreversion was not observed. The assumed pathway to a reductive *Z*→*E* double bond isomerization as known for stilbenes could not be examined in detail, as the reduction potentials of most

Z-isomers are higher than that of the electrolyte. However, for the electron poor **aDTE$_{66}$-PhCN**, a reductive cyclization was found in addition to the oxidative pathway.

For future studies, it may be interesting to investigate aDTEs that have distinctly different redox potentials for both hemispheres. This can be achieved for example by the introduction of trifluoromethyl groups at one of the inner positions of the aDTE, leaving the substituents R available for further functionalization (Scheme 2.4-2).

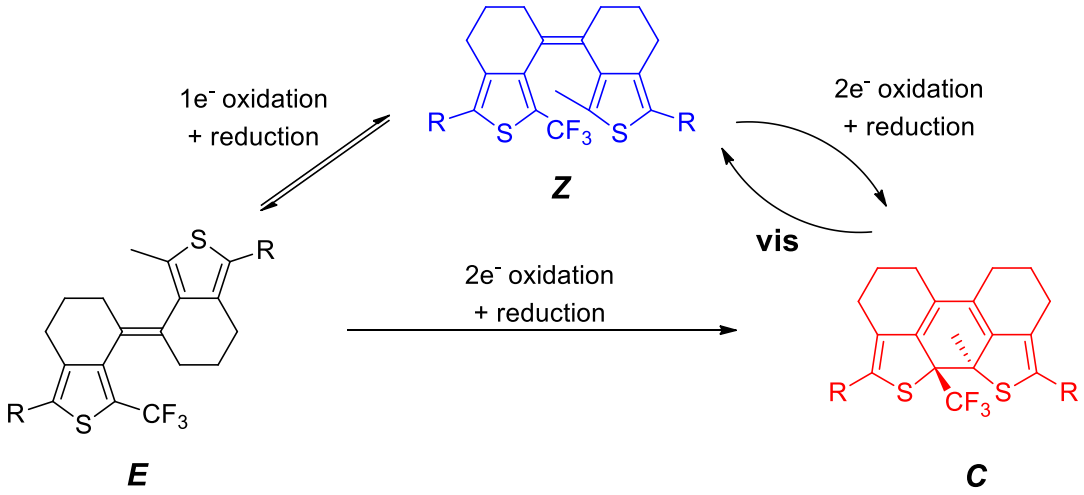

Scheme 2.4-2 Proposed modification to aDTE structures to enable a second electrochemical switching pathway. While 1e$^-$ oxidation is not sufficient to induce cyclization, the open isomers radical cation can equilibrate as the double bond is resolved. As in the present system, 2e$^-$ oxidation should induce electrocyclization.

Due to a splitting of the oxidation process into two separate oxidation steps for the open isomers, 1e$^-$ oxidation would be possible and thus allow to investigate whether the cyclization actually happens from the dicationic open isomer as proposed for similar systems.[115b] If this proves to be true, an interesting new switching methodology without the need for UV light could be applied. As the 1e$^-$ oxidation is known not to be sufficient to induce cyclization,[97] it is expected that both open isomers can equilibrate due to the removed double bond in the radical cation.[127] As shown in the present study, the closed isomer can be formed from both open isomers by 2e$^-$ oxidation followed by reduction. The closed isomer can selectively be opened to the *Z*-isomer by irradiation with visible light.

2.5 Transient absorption spectroscopy of aDTEs [40]

This section summarizes the results of the transient absorption spectroscopy experiments performed in collaboration with the group of Prof. Ernsting. For a better comparison with the already examined stilbene and stiff stilbene systems,[128] a heteroaromatic unconstrained DAE was examined as well as an example of both simple and functionalized aDTEs. The experiments were carried out in both MeCN and ^{n}hexane as examples of polar and apolar solvents to evaluate the generality of the observations. The analytical procedure and spectral evolution are explained in detail exemplarily for the unconstrained system.

2.5.1 Motivation

Both stilbenes[4] and modern diarylethenes[106b,129] have already been well investigated by transient absorption spectroscopy. The observations confirmed the theory that stilbenes double bond isomerization as the main reaction pathway proceeds via a perpendicular intermediate wherein the former double bond is twisted around 90°.[3b] Stiff stilbenes therein served as a model compound, in which the single bond rotation as an undesired de-activation pathway is suppressed.
For normal DAEs with their locked double bond geometry, 6π-electrocyclization is the only productive photochemical pathway. This photoreaction is known to proceed non-adiabatically via a conical intersection for the reactive antiparallel conformer (compare Scheme 1.2-5). The parallel conformer relaxes through a triplet pathway.[129h] As the efficiency of the back reaction was found to be temperature-dependent, the existence of a barrier in the excited state was concluded.[129i]

From the aDTE's steady-state photochemistry (Section 2.3), it is known that electrocyclization is the governing reaction pathway in these compounds. Irradiation of the *E*-isomers finally yields the closed isomer, with the *Z*-isomer as an intermediate detectable by HPLC. Starting from the respective *Z*-isomers, the closed isomer is in general the only product observed. The current investigations are performed to better understand the dynamics of these two photoreactions: Does excitation of the *Z*-isomer

[40] The experiments in this section were carried out and the data processed by Dr. Sergey Kovalenko, Michael Quick, B.Sc. and Dr. Martin Quick in the group of Prof. Nikolaus Ernsting.

only lead to the closed isomer? Is a direct conversion from the *E*- to the closed isomer possible, or are these two consecutive photoreactions? Moreover, does the double bond isomerization still proceed via a perpendicular intermediate as known for stilbenes?

Although some unsubstituted thiophene analogues of stilbene have already been investigated by transient absorption spectroscopy,[130] in general only the behavior of the *E*-isomers was examined. Furthermore, a non-negligible effect of substituents on the thiophene unit is expected due to a biased ground state structure. So far, this has not been considered in the context of double bond isomerization.
In order to separate these influences from the impact of stiffening, two unconstrained simple reference compounds with comparable substitution pattern were prepared (Section 2.2.5) for comparison with the stiffened **aDTE$_{66}$-Me**. Finally, **aDTE$_{66}$-PhCN** will be investigated as an example of functionalized aDTEs. In the steady-state absorption spectroscopy measurements, this derivative displayed an outstandingly high efficiency of almost unity for the electrocyclization reaction.

2.5.2 Transient absorption spectroscopy of unconstrained DTEs

Earlier investigations[131] in the Ernsting group revealed a significant difference in the dynamics of stilbene compared to double bond functionalized 1,1′-dimethyl and 1,1′-diethylstilbene. For a similar comparison in heteroaromatic systems, two unconstrained DTEs **12** and **13**were synthesized (Section 2.2.5) as targets for the investigation and their steady-state photochemistry examined (Section 2.3.3.5).

Unfortunately, the addition of methyl groups to the double bond did not only influence the excited state behavior but lead as well to a strong hypsochromic shift of the absorption band[41] of 81 nm and 54 nm for *E*- and *Z*-isomers in 1,1′-dimethyl-bis(2,5-dimethylthienyl)ethene (**13)**, respectively, compared to the double bond unsubstituted derivative **12** (Figure 2.3-12). In combination with the lack of distinct spectral features to differentiate both isomers, this compound was unsuitable for investigation. By consequence, only the unsubstituted bis(2,5-dimethylthienyl)ethene (**12**) will be discussed. Furthermore, as the behavior observed in apolar ^{n}hexane (Figure 2.5-1) and in

[41] In unconstrained bis(thien-2-yl)ethenes and stilbenes without substituents on the aromatic unit, the blue-shifts induced by double bond methylation are less pronounced ($\Delta\lambda_{max(E)}$ = 50 nm, $\Delta\lambda_{max(Z)}$ = 32 nm and $\Delta\lambda_{max(E)}$ = 51 nm, $\Delta\lambda_{max(Z)}$ = 28 nm, respectively).[101]

polar MeCN solutions (not shown) is very similar, only the experiment in ^{n}hexane will be described in detail.

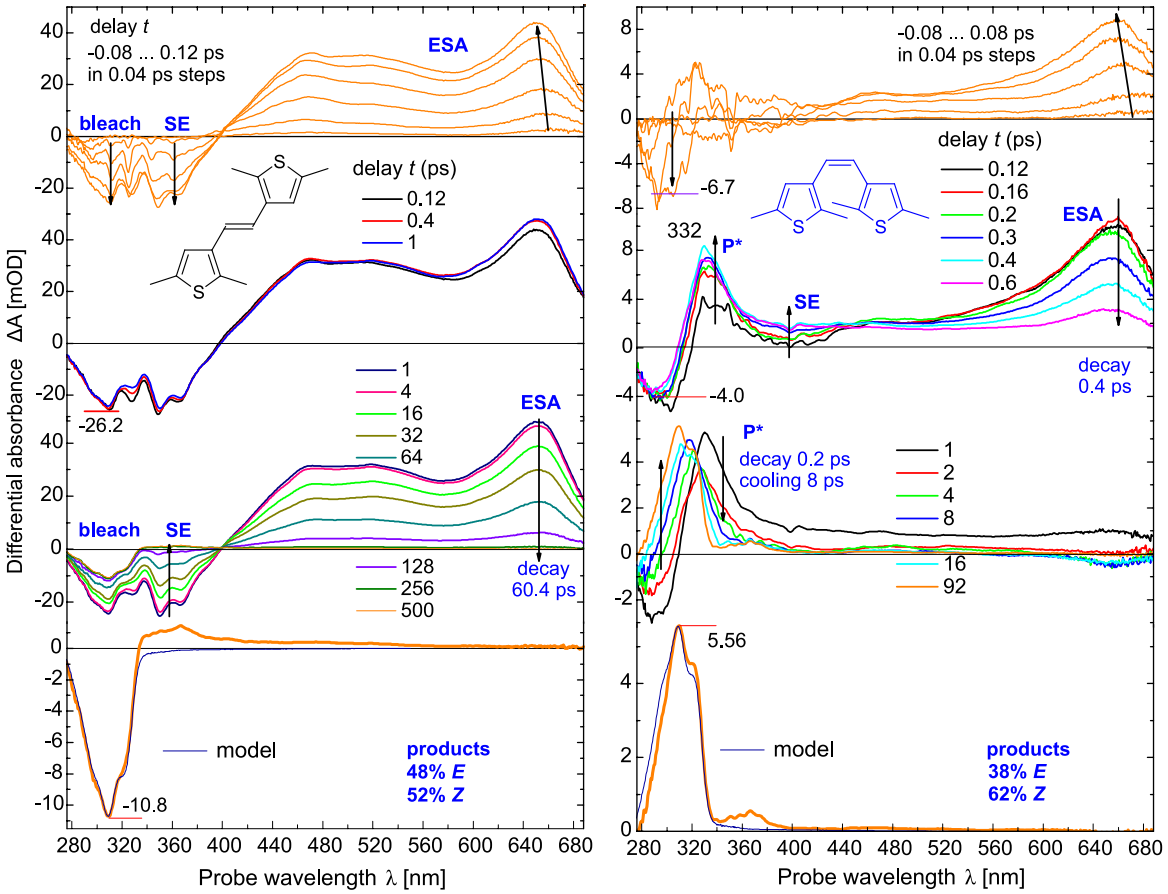

Figure 2.5-1 Transient absorption experiment of DTE **12** in ^{n}hexane. **Left:** Evolution of *E*-**12** during excitation with 324 nm laser pulses (top panel) and after Franck-Condon (FC) relaxation (second panel). The excited-state absorption (ESA) and the stimulated emission (SE) decay within the same time frame of 60.4 ps (third panel) to form a 48:52 *E*/*Z* mixture (bottom panel). **Right:** Evolution of *Z*-**12** after excitation with 319 nm. The excited molecule (top panel) isomerizes quickly (0.4 ps) to a perpendicular state P* (second panel) that decays within 0.2 ps (third panel). After vibrational cooling (8 ps), a 38:62 *E*/*Z* mixture is obtained (bottom panel).

The experiment is depicted top to bottom along the time line. The excitation of *E*-**12** with 324 nm laser pulses (top panel left) decreases the population of the ground state and increases the population of the excited state in the Franck-Condon (FC) region. This leads to a negative signal in the area of ground state absorption (bleach) and a positive signal in the 400-700 nm region (excited-state absorption, ESA). The intensity of both contributions is proportional to the number of excited molecules of the starting isomer, as no spectral shift is observed. An additional contribution is visible in the region of 340-400 nm, which results from the stimulated emission (SE) of the excited species. Within the cross-correlation time of the pump- and probe pulses, the excited molecules relax

from the Franck-Condon (FC)-region into the potential well of the S_1 state, which is seen in the slight blue-shift of the ESA. Within less than 0.4 ps, this process is finished (second panel). During the next 256 ps, the ESA and SE decrease, as the molecules return to the S_0 state and cool to the vibrational ground state (third panel). The fact that the bleach region is not fully recovered indicates a photoreaction. The isomerization yields can be derived from the composition of final spectrum (bottom panel).

The relative amount of *E*-isomer reacting to any product is given by equation (14) as a ratio of the bleach signal $A_{E(B)}$ at infinite delay time (bottom panel) and zero delay time (second panel). For normalization, both bleach signals are divided by the extinction spectrum of the *E*-isomer ε_E. However, ε_E vanishes in the calculation.

$$Y_{E\rightarrow prod.} = \frac{\left(\frac{\Delta A_{E(B)}(\infty)}{\varepsilon_E}\right)}{\left(\frac{\Delta A_{E(B)}(0)}{\varepsilon_E}\right)} = \frac{\Delta A_{E(B)}(\infty)}{\Delta A_{E(B)}(0)} \tag{14}$$

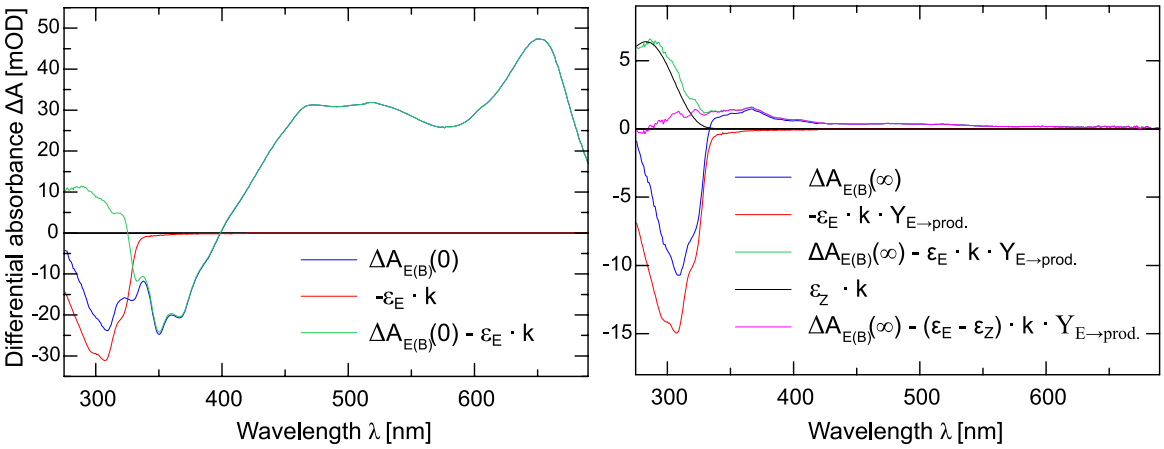

Figure 2.5-2 Modelling of population of the excited state. **Left:** Spectrum at zero time delay (blue) including bleach, SE and ESA. The bleach band contribution is proportional to the negative absorptivity ε_E by a factor k and corresponds to 100% excited state population. The difference spectrum (green), the bleach band has been removed. **Right:** Spectrum at infinite time delay (blue) containing bleach and S_0 absorption bands of all photoproducts. Additional to factor k, the isomerization yield $Y_{E\rightarrow prod.}$ (see equation (14)) is introduced to model the band shape. The residual spectrum after subtraction (green) exposes the stationary absorption spectrum of the Z-isomer as photoproduct and can be modelled using the same factors (black) to yield a spectrum where stationary contributions are removed (magenta).

As the excited *E*-isomer theoretically can react adiabatically to the *Z*-isomer and from there to the closed isomer *C*, the portion of the latter reaction $Y_{E\rightarrow C}$ is determined using equation (15). Here, the normalization factor does not vanish.

$$Y_{E\to C} = -\frac{\left(\frac{\Delta A_{E\to C}(\infty)}{\varepsilon_C}\right)}{\left(\frac{\Delta A_{E(B)}(0)}{\varepsilon_E}\right)} = -\frac{\Delta A_{E\to C}(\infty)}{\Delta A_{E(B)}(0)}\frac{\varepsilon_E}{\varepsilon_C} \tag{15}$$

Finally, a correction term *f* is introduced to correct the result for small amounts of the *Z*-isomer in the starting material.

$$f = \frac{1}{\left(1-\frac{\varepsilon_Z}{\varepsilon_E}\right)} \tag{16}$$

The yield of *E*⟶*Z* conversion $Y_{E\to Z}$ is finally given in equation (17) as a difference of equations (14) and (15), corrected by the factor *f* from equation (16):

$$Y_{E\to Z} = \left(Y_{E\to prod.} - Y_{E\to C}\right) f = \left(\frac{\Delta A_{E(B)}(\infty)}{\Delta A_{E(B)}(0)} + \frac{\Delta A_{E\to C}(\infty)}{\Delta A_{E(B)}(0)}\frac{\varepsilon_E}{\varepsilon_C}\right)\frac{1}{\left(1-\frac{\varepsilon_Z}{\varepsilon_E}\right)} \tag{17}$$

As such, a final composition of 48:52 *E*/*Z* was obtained. The small absorption band around 360 nm could not be attributed.[42] From the shape of the spectrum after infinite delay, it is concluded that no closed isomer is formed. Nevertheless, the equations are given in a form to be valid for all experiments in this section.

A different behavior was observed for *Z*-**12** (Figure 2.5-1 right). Around zero delay time, coherent artefacts dominate the UV region, while in the visible the ESA increases (top panel). Again, a blue-shift of the ESA indicates relaxation of the excited molecules away from the FC-region in the S_1-state. The fast vanish (0.4 ps) of the SE and ESA, by simultaneous constant bleach, indicates barrier-free formation of a new species in the excited state (second panel). In stilbenes, this state refers to the perpendicular conformation *P**, often referred to as phantom state. The following decay to S_0 (third panel) proceeds similarly fast but allows a sufficient amount of population to accumulate in *P** for detection. Analysis of the final spectrum analogue to equation (17) shows a 38:62 *E*/*Z* ratio. Again, a small contribution of an unknown compound around 360 nm could not be considered in the fitting. The difference in the final isomer ratios may result from the different lifetimes of the excited states or the existence of two geometrically

[42] The spectrum of the pure closed isomer could not be obtained from steady-state spectroscopy (Section 2.3.3.4). However, from comparison with the electronically similar *C*-**aDTE$_{66}$-Me** the absorption maximum is expected to be far more red-shifted (440 nm for *C*-**aDTE$_{66}$-Me**).

different perpendicular states and will be subject to further investigations. The current findings are summarized in Scheme 2.5-1.

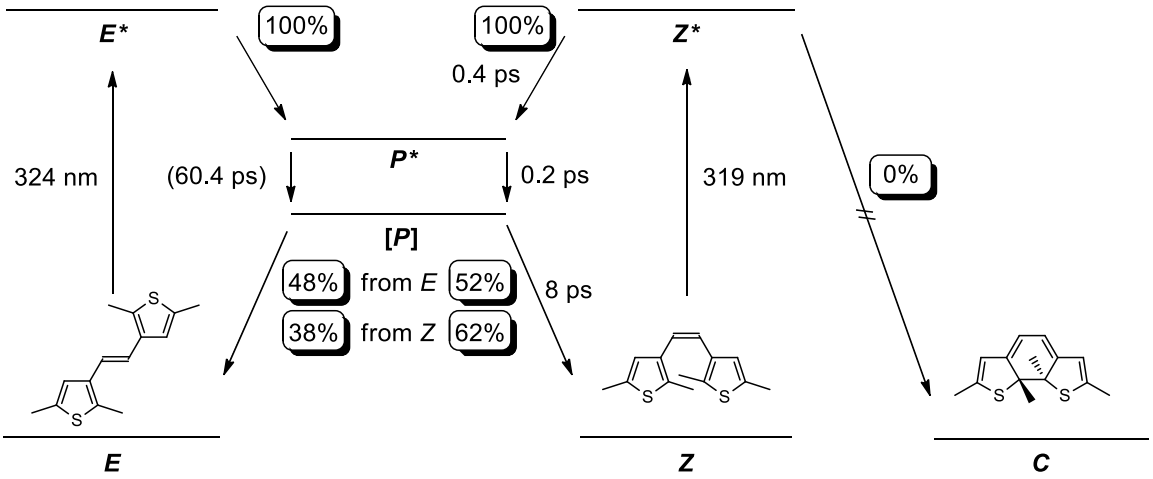

Scheme 2.5-1 Summary of the transient absorption behavior of *E*- and *Z*-**12** in n-hexane upon excitation with 324 nm. [P] signifies the hot perpendicular ground state. Starting from *E*-**12**, only one time constant was observed for all three subsequent processes, indicating that *E**→*P** is the rate determining step. The final isomer distribution differs for the two starting isomers, though no competing cyclization was detected. As a result of the stabilization of the zwitterionic perpendicular state,[132] the relaxation Z*→P* is accelerated in MeCN (0.13 ps), whereas the relaxation to [P] is slightly slower (0.3 ps).

The overall behavior is very similar to plain stilbene in the same solvent.[128] Likewise, a fast isomerization of both double bond isomers yielding similar product ratios was recorded. Also the observation of the perpendicular intermediate is more prominent for the *Z*-isomer. In contrast to unsubstituted stilbene, the amount of cyclized isomer formed is negligible for the methylated heteroaromatic compound **12**. This behavior most probably can be attributed to the methyl groups on the thiophene forcing the aromatics out of plane by steric repulsion. The double bond isomerization however is not affected by this geometry.

Unlike for stilbene and the 5-membered ring stiff stilbene, the ESA bands of both isomers are virtually identical and do not allow an interpretation of an adiabatic interconversion of the excited isomers. Using the same setup this pathway could be observed in the *E*→*Z* isomerization of the stiffened derivative but not for normal stilbene.[128]

2.5.3 Transient absorption spectroscopy of aDTE$_{66}$-Me

As a general model for annulated DTEs, the dynamics of the photoreaction of the 6-membered ring derivative **aDTE$_{66}$-Me** were investigated. In contrast to the

aforementioned **12**, in aDTE the electrocyclization is known to be the dominant photoreaction pathway for the *Z*-isomers, with almost no *E*-isomer detected in HPLC analysis of the steady-state photoreaction (Section 2.3.3.1). By consequence, also photoreactions starting from the *E*-isomer ultimately yielded the closed isomer.
An increased involvement of the cyclization pathway was already observed for the 6-membered ring stiff stilbene derivative[22] whereas only double bond isomerization was found for other ring sizes during steady-state spectroscopy.

The behavior of stiff **aDTE$_{66}$-Me** in the transient absorption experiment differs very much from unconstrained DTE **12** (*vide supra*), with the *Z*-isomer having a more complex photochemical behavior than *E*-**aDTE$_{66}$-Me** (Figure 2.5-3). Upon excitation of the *E*-isomer (top panel) with a 324 nm optical pump pulse, the population is transferred into S_1. With a 0.3 ps time-constant, the perpendicular configuration is adopted by torsion around the central double bond (second panel). In the TA spectrum of the *E*-isomer, it is apparent that *P** decays with two time constants as the *ESA of the P*-state* decays within 5 ps while the bleach remains constant.[43] The *actual decay of the P*-state* to the ground state, including vibrational cooling, follows a time constant of 11 ps and yields a final ratio of *E/Z/C* of 35:65:0. From the comparison of the final spectrum with the spectra of the pure isomers, it is concluded that the small absorption band around 480 nm (bottom panel) does not match any of the three. By consequence, it might belong to an unknown long-lived state as for example a triplet state. The preference towards the *Z*-isomer might be reasoned by a conical intersection that is located rather on the *Z*-side of the [*P*] ground-state barrier.
In contrast, the ESA of the *Z*-isomer is mostly retained and only 28% adopt the *P**-configuration with a 0.15 ps time constant (second panel). This indicates that the *Z**- and *P**-excited states must have similar energies or the conversion is hindered by a barrier, whereas the *E** is higher in energy than *P**-state and interconverts easily. Also

[43] This decay might be interpreted as the decrease of an oscillator strength and could be the consequence of a sensitive dependence on the nuclear configuration in the *P**-state. The impact of the stiffening alkyl chains during the movement on the S_1 potential energy surface is unknown and speculative at this point.

unlike the previous case this *P**-state only lives for 0.3 ps (third panel) which suggests a different perpendicular configuration when starting from the *E*-isomer.[44]

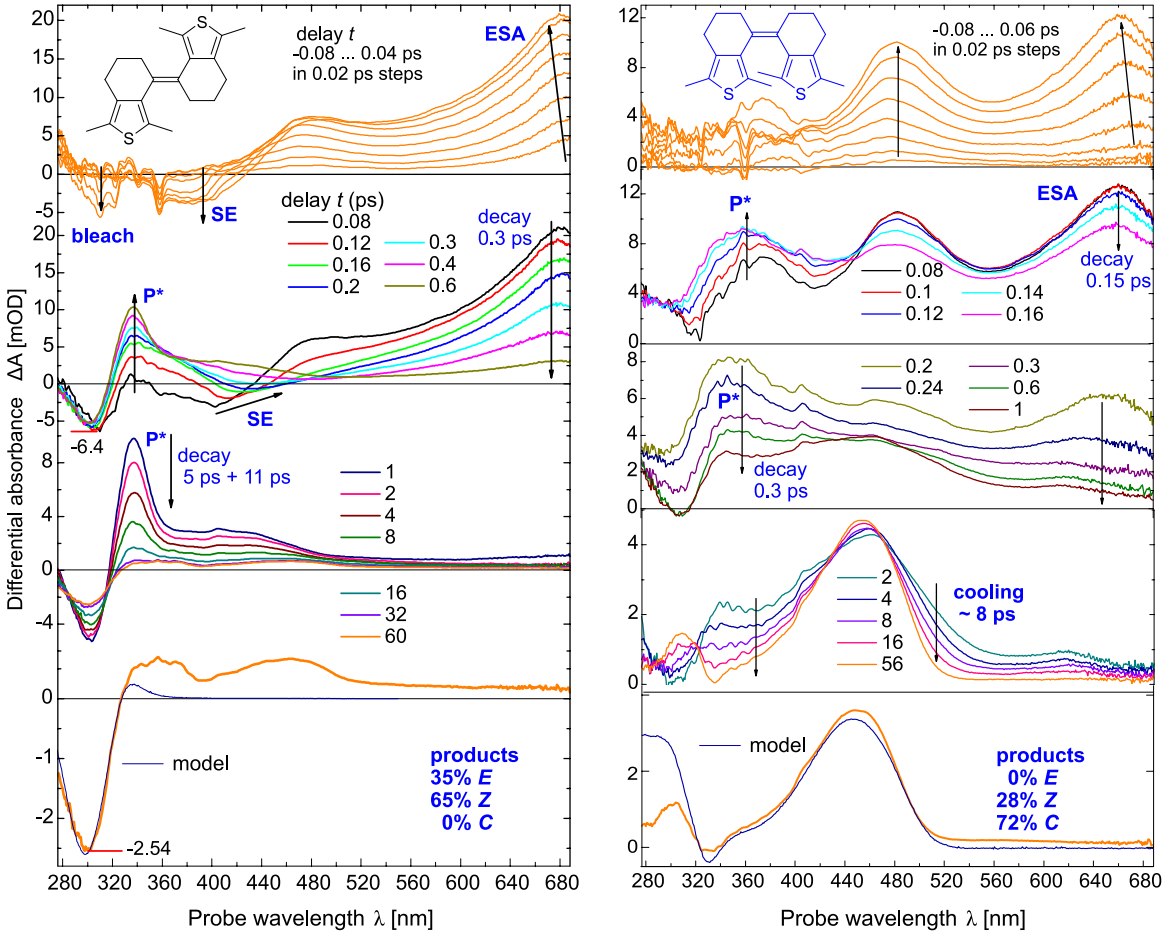

Figure 2.5-3 Transient absorption experiment of stiff **aDTE$_{66}$-Me** in ^{n}hexane. **Left:** Evolution of *E*-**aDTE$_{66}$-Me** after excitation with 324 nm laser pulses (top panel). The ESA decays completely within 0.3 ps (second panel), indicating an adiabatic conversion to *P** and a second photoproduct. Therefore, the SE shifts to longer wavelength. The perpendicular state relaxes further within the excited state for 5 ps and consequently falls to the cold ground state (third panel) within 11 ps to form a 35:65:0 *E*/*Z*/*C* mixture (bottom panel) after vibrational cooling. **Right:** Evolution of *Z*-**aDTE$_{66}$-Me** after excitation with 324 nm (top panel). The excited molecule partially isomerizes within 0.3 ps to P* (second panel). The perpendicular state and residual excited *Z*-isomer fall to the hot ground state on the same time scale (third panel). After vibrational cooling (forth panel), a 0:28:72 *E*/*Z*/*C* mixture is obtained (bottom panel).

Finally, both *P** and the residual ESA decay to yield a 0:28:72 *E*/*Z*/*C* mixture (bottom panel). The behavior after excitation with 324 nm can be summarized graphically (Scheme 2.5-2).

[44] As stated before, torsion around the double bond might be influenced by the stiff alkyl chains. In consequence, arriving the P*-state from the *Z*-configuration might lead to a faster de-activation, assisted by a potentially higher ballistic energy conserved within the molecule. As such, a different *E*/*Z* ratio starting from the *E*- or *Z*-isomer is not unlikely.

Though the isomerization yields are similar in both solvents used, it was found that the decay rates are even faster in MeCN solution. This has already been observed for the excited isomers of stilbene and the perpendicular intermediate of 1,1′-dimethyl- and 1,1′diethylstilbene[131] and is ascribed to the zwitterionic nature[132] of *P**. In **aDTE$_{66}$-Me**, all processes are faster in the polar solvent by about a factor of two.

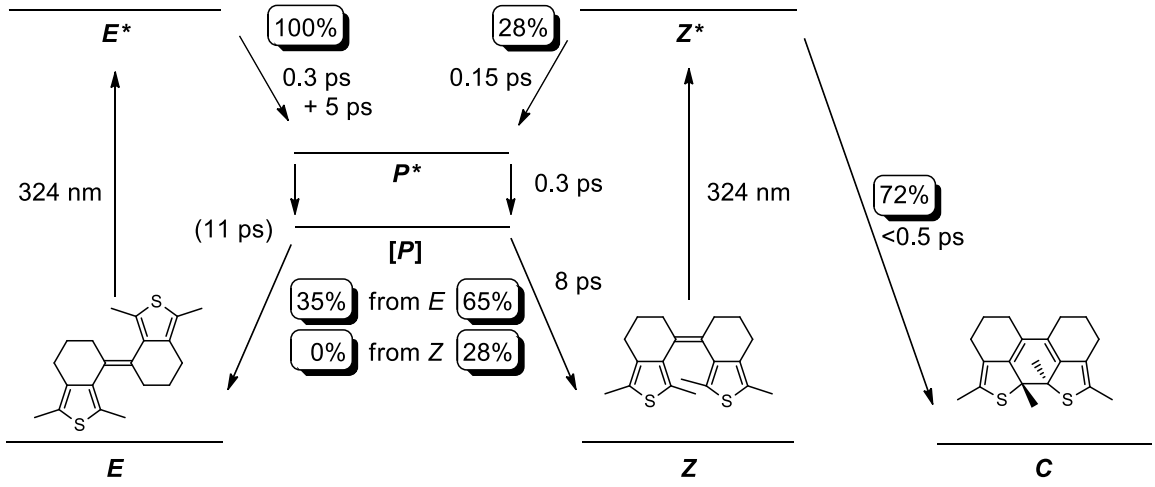

Scheme 2.5-2 Summary of the transient absorption behavior of *E*- and *Z*-**aDTE$_{66}$-Me** in ^{n}hexane upon excitation with 324 nm. Starting from *E*-**aDTE$_{66}$-Me**, two time constants are observed for the *E**→*P** relaxation (see main text). In contrast, *P** decays with only one observable time constant of 11 ps for both the change of the excited to the ground state and vibrational cooling. The final *E*/*Z* ratio again differs for the two starting isomers.

2.5.4 Transient absorption spectroscopy of aDTE$_{66}$-PhCN

Finally, the photochemical behavior of **aDTE$_{66}$-PhCN** was investigated. In steady-state spectroscopy, this derivative outperformed other derivatives with the same basic structure in terms of its cyclization quantum yield $\Phi_{Z\rightarrow C}$ of almost unity. For a better comparison, again the dynamics in ^{n}hexane solution will be explained (Figure 2.5-4).

In contrast to the unconstrained compound **12** and **aDTE$_{66}$-Me** with the same molecular frame, for **aDTE$_{66}$-PhCN** no intermediate formation of a perpendicular state was detected (second panel). Instead, the *E*-isomer decays directly to a mixture of 53:10:37 *E*/*Z*/*C* (left bottom panel), which strongly indicates an adiabatic isomerization in the excited state. For the *Z*-isomer, the closed isomer was the only product formed (right bottom panel). This is greatly in accordance with the extraordinary high cyclization quantum yield determined in steady-state photochemistry.

Interestingly, and in contrast to the *Z*-isomer, for *E*-**aDTE$_{66}$-PhCN** the decay is not accelerated by the polar solvent MeCN, but slowed down by a factor of 20 (not shown). This is accompanied by the formation of a shoulder at 350 nm, which prevented a determination of exact isomerization yields by fitting. The unexpected absorption together with the prolonged lifetime of the excited state hints towards a competing photoreaction as for example triplet formation. Nevertheless, an adiabatic *E**→*Z** pathway is indicated by the typical absorption of the closed isomer around 540 nm.

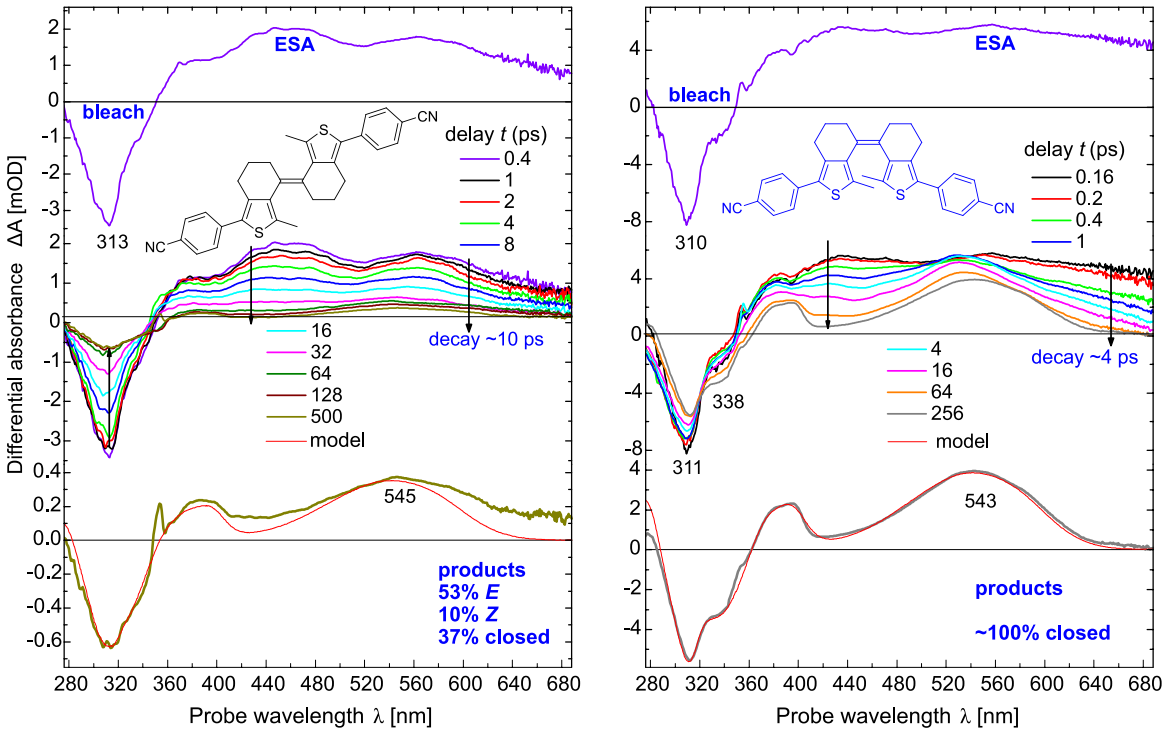

Figure 2.5-4 Transient absorption experiment of open isomers of stiff **aDTE$_{66}$-PhCN** in n-hexane. **Left:** Evolution of *E*-**aDTE$_{66}$-PhCN** after excitation with 350 nm laser pulses (top panel). No stimulated emission is observed. The ESA decays within 10 ps (second panel), showing a reduced bleach signal and spectral features of the closed isomer at 545 nm. After vibrational cooling (bottom panel), a 53:10:37 *E*/*Z*/*C* mixture is obtained. **Right:** Evolution of *Z*-**aDTE$_{66}$-PhCN** after excitation with 350 nm. The excited molecule (top panel) isomerizes within 4 ps to the closed isomer (second panel). No spectral features of either *E*- or *Z*-isomer are visible (bottom panel).

Additionally, for **aDTE$_{66}$-PhCN** the cycloreversion upon 560 nm excitation was investigated (Figure 2.5-5). Due to undesirably low solubility of the cyclized isomer in ^{n}hexane, only the experiment in MeCN allowed fitting of the final spectrum. Nevertheless, it was found that the decay of the excited species again is accelerated by the polar solvent.

Upon excitation with 560 nm, the excited state of the closed isomer *C** decays on a substantially slower timescale (30 ps and 50 ps in MeCN and ^{n}hexane) than the open isomers (< 2 ps and < 10 ps). A similar effect was already observed for normal DAEs[133], even though a wide range of relaxation times is found for the cycloreversion reactions. A given explanation is the existence of a barrier in the excited state[134] between *C** and the conical intersection, slowing down the conversion of *C** to the ground state. However, after vibrational cooling about 1% of the closed isomer was found to be converted to the *Z*-isomer. The value derived for the cycloreversion quantum yield is higher than found in steady-state photochemistry ($\Phi_{C\rightarrow Z} = 0.0017$), but may be within the error in regard to the fit quality.

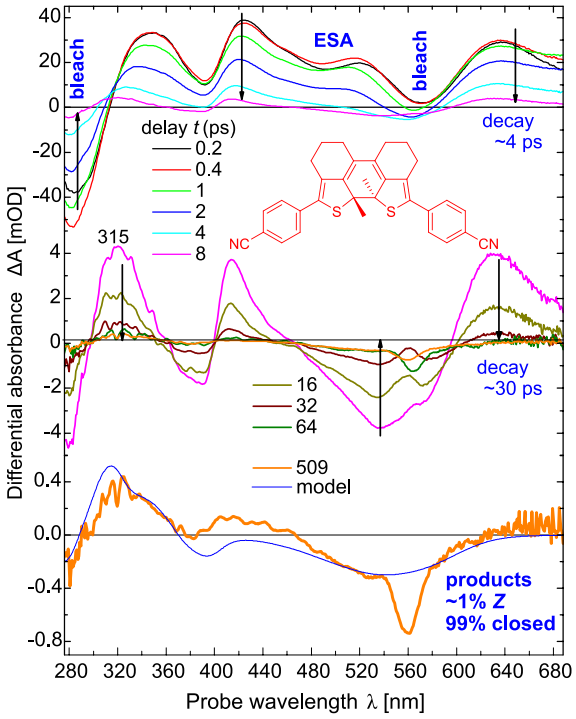

Figure 2.5-5 Transient absorption experiment of *C*-**aDTE$_{66}$-PhCN** in MeCN after excitation with 560 nm laser pulses. The excited molecules decay within 4 ps to the cool excited state (top panel). Further relaxation to the ground state within 30 ps (second panel) yields about 1% of *Z*-isomer next to 99% unchanged closed isomer (bottom panel). The spike at 560 nm is caused by scattering.

The dynamic behavior of all three isomers of **aDTE$_{66}$-PhCN** upon irradiation is summarized in Scheme 2.3-3.

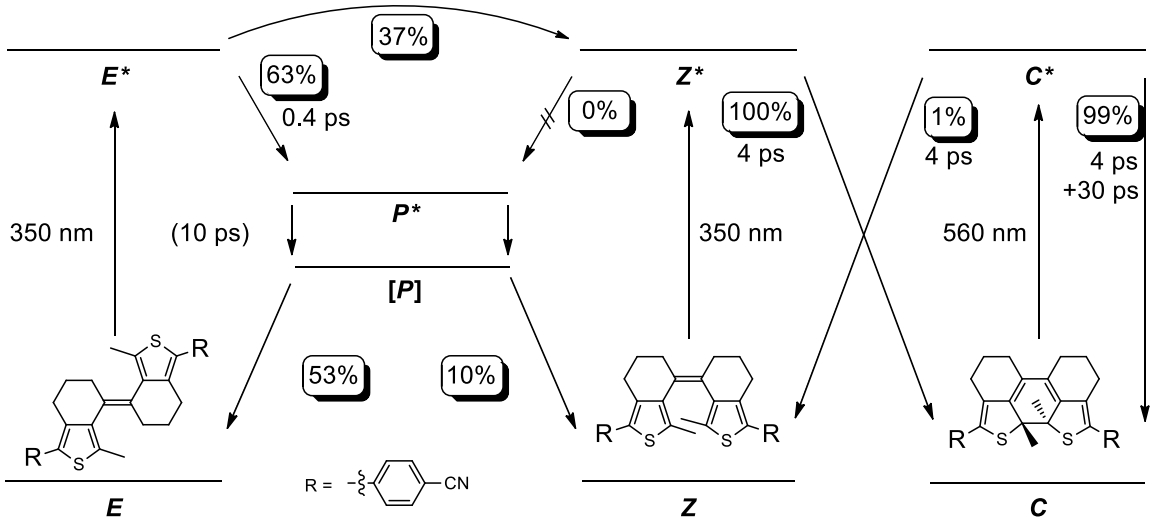

Scheme 2.5-3 Summary of the transient absorption behavior of *E*-, *Z*- and *C*-**aDTE$_{66}$-PhCN** after excitation with 350 nm and 560 nm laser pulses, respectively. The experiment was carried out in ^{n}hexane solutions for the open isomers, whereas for *C*-**aDTE$_{66}$-PhCN** MeCN had to be used for solubility reasons. In contrast to the other derivatives, an adiabatic *E**→*Z** conversion can be concluded from the formation of the cyclized product from the *E*-isomer. For the decay of *P**, only one time constant is obtained.

2.5.5 Summary

An example of an unconstrained, methyl-substituted DTE and a simple as well as a functionalized aDTE were investigated by transient absorption spectroscopy. While the first compound is solely active in the double bond isomerization regime, both aDTEs undergo double bond isomerization as well as electrocyclization. For all compounds, an accelerated decay of the excited species in polar MeCN in contrast to apolar ^{n}hexane was found. The decay times for double bond isomerization of the unconstrained photochrome **12** are comparable to those of stilbene. The overall relaxation of both stiff *E*-aDTEs is accelerated, whereas the *Z*-isomers exhibit comparable time constants to stilbene despite the altered main isomerization pathway. For the cyclization of aDTEs, similar time constants as for similar *normal DAEs* (1-3 ps)[133] are measured.

Surprisingly, *E*-**aDTE$_{66}$-PhCN** was found to undergo an adiabatic isomerization to the excited *Z*-isomer, which relaxes directly to the closed isomer in both polar and apolar solvents. As such, a 53:10:37 *E*/*Z*/*C* mixture was obtained. This pathway may also play a minor role in the methyl-substituted *E*-**aDTE$_{66}$-Me**, but could not be identified.
The efficiency of the cyclization of the *Z*-**aDTE$_{66}$-PhCN** was found to be practically unity. As expected from the steady-state spectroscopy, the cycloreversion of *C*-**aDTE$_{66}$-PhCN** was very inefficient.

It can be concluded that stiffening of the dithienylethene core not only facilitates the formation of the closed isomer greatly, but also shifts the de-activation of the perpendicular intermediate in favor of the *Z*-isomer. Further analyses of the reaction dynamics of the presented compounds are currently under way.

3. The (photo)chemistry of pcDTEs

3.1 Aim of the project

Motivated by the finding that covalent stiffening of the double bond substituents of DAE indeed fulfilled the expectation of increased quantum yield for the cyclization reaction, it was envisioned to extend this concept. Though only little to no amounts of double bond isomerization products could be detected upon irradiation of the *Z*-isomer of aDTEs, transient absorption spectroscopy proved that de-excitation still proceeds partially via the perpendicular intermediate known from stilbenes. Comparison of unconstrained DTE derivatives with the literature known cyclopentene-bridged equivalent further showed that the quantum yield for the cyclization can indeed be increased by structurally preventing this side reaction.

It is now attempted to combine both the effect of restraining single bond rotation as in aDTE and the double bond fixation known for normal DAE. First derivatives of these polycyclic dithienylethenes (pcDTE) have already been prepared.[56] The synthesis was conveniently achieved by a tandem aldol-condensation / Michael addition protocol using the ketone precursors for aDTE and formaldehyde solution under basic conditions, followed by an intramolecular McMurry coupling (Scheme 3.1-1).

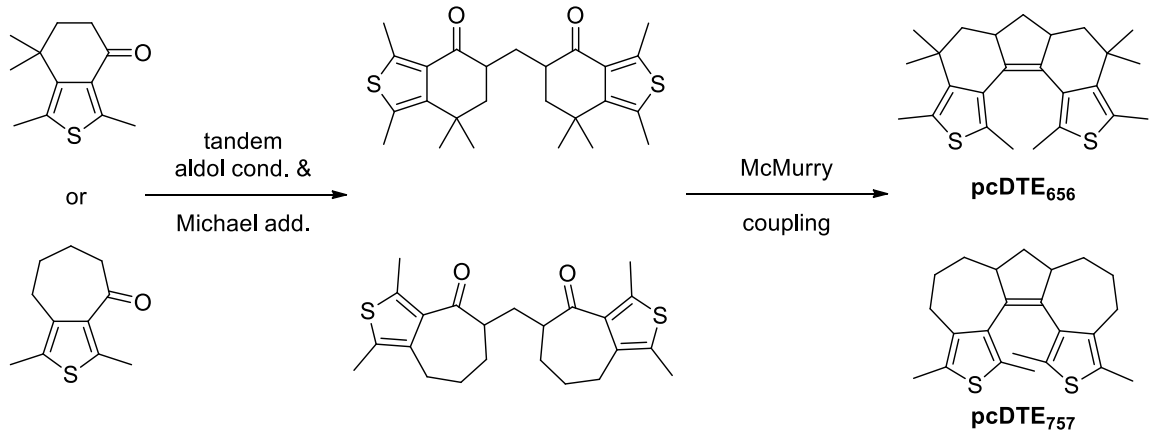

Scheme 3.1-1 Two derivatives of pcDTE have been reported earlier.[56] In analogy to the nomenclature of aDTE systems (compare Scheme 2.2-1), the digits in subscript signify the ring sizes of both peripheral and the central ring moiety.

However, the closed isomers of these derivatives proved to be unstable under irradiation. It was assumed that the reason for this is increased steric strain due to mismatching ring sizes.

Nevertheless, these two derivatives showed that even in such highly constrained pcDTEs, a photochemical cyclization is possible.
It is hoped that the photochemical performance can be greatly improved by adjusting the ground state geometry through varying of the alkyl ring sizes. According to DFT calculations[56] and supported by the results of the aDTE systems (chapter 2), the all-6-ring derivative $pcDTE_{666}$ is considered most promising (Scheme 3.1-2).

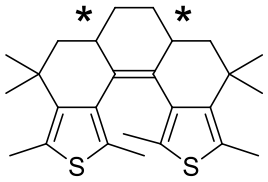

$pcDTE_{666}(Me_2)$-Me

Scheme 3.1-2 Target structure for the current pcDTE studies.

3.2 Synthesis of pcDTEs

This section demonstrates the different methodologies towards pcDTE. At first, the synthetic strategy will be explained using a retrosynthetic analysis (Section 3.2.1). As for aDTEs (Chapter 2), the synthesis of methylsubstituted derivatives was chosen as convenient possibility to evaluate main characteristics of the system. The approaches discussed are: C2-bridging of 6-membered ring ketones by direct alkylation with a biselectrophile in a concerted or stepwise fashion (Section 3.2.2), non-symmetric linkage of an enone and α-thiol derived from the ketone (Section 3.2.3) and radical linkage of two enones (Section 3.2.4).

3.2.1 General synthetic strategies for pcDTEs

In parallel to their predecessors (Scheme 3.1-1), the synthesis of pcDTE$_{666}$ will use the ketone building blocks used for aDTE synthesis. In most of this study, the ketone **3d** bearing methyl groups on the cyclohexanone moiety was used as it was already available at the beginning of the project (Scheme 3.2-1). For some experiments, also the plain 6-membered ring ketone **3a** was used. The differences in reactivity of the two compounds are discussed shortly.

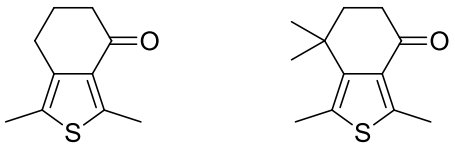

3a **3d**

Scheme 3.2-1 Precursors used for the synthesis of pcDTEs. The synthesis of ketone **3a** is described in section 2.2.2.1, ketone **3d** has been described earlier.[56]

The general synthetic strategy is reasoned by a retrosynthetic analysis (Scheme 3.2-2). As for the pcDTE derivatives already reported, disconnection at the central double bond is obvious for symmetry reasons. Though the molecule should again be disconnected symmetrically, for the second scission two possibilities are feasible.

The preferred route includes a non-symmetric scission to remove the C2-bridge moiety (path A). Resulting from the nucleophilic character of the cyclic ketone, a bis-acceptor C2-synthon needs to be introduced, which can either be achieved in a stepwise or

concerted fashion. The stepwise approach would enable the extension of the strategy to non-symmetric pcDTEs. The concerted approach however is preferred in the symmetric case, as only two reaction steps would be necessary to reach the goal (Section 3.2.2).

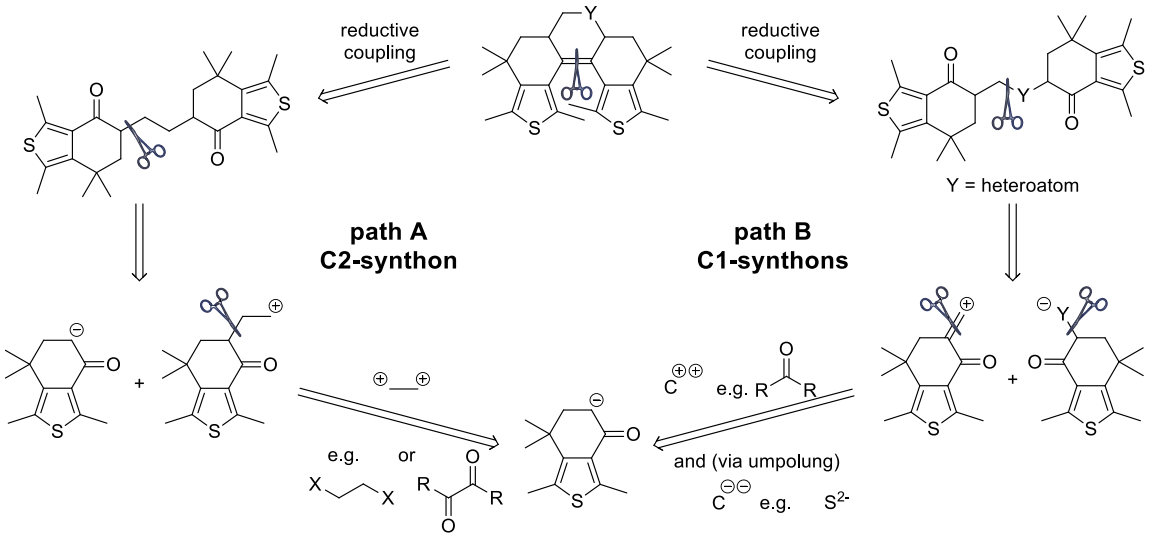

Scheme 3.2-2 Retrosynthetic considerations for the synthesis of $pcDTE_{666}$.

Alternatively, symmetric scission into two C1-functionalized ketone building blocks is imaginable. If cut heterolyticly, these two synthons necessarily possess opposite reactivity. Creation of an unsaturated ketone will easily create an acceptor at the desired position, whereas introduction of a donor-C1-synthon is only possible by changing the intrinsic nucleophilic character of the ketone. An α-halogenated ketone could be functionalized by a bis-donor synthon, which could be a heteroatom as sulfur (Section 3.2.3). Another interesting modification of path B is the homolytic bond cleavage (Section 3.2.4). Dimerization of unsaturated carbonyl-equivalents is for example known for the synthesis of adipic acid dinitrile from acrylonitrile.

3.2.2 Synthesis by direct C2-bridging

In brief, attempts to functionalize ketone **3d** or **3a** (Scheme 3.2-2 path A) in a concerted fashion were unsuccessful despite extensive efforts, whereas stepwise functionalization afforded the C2-bridged product at least in trace amounts.

For the concerted approach, numerous combinations of bis-electrophile, base and solvent/additive systems were investigated (Scheme 3.2-3) and the major findings are summarized briefly.

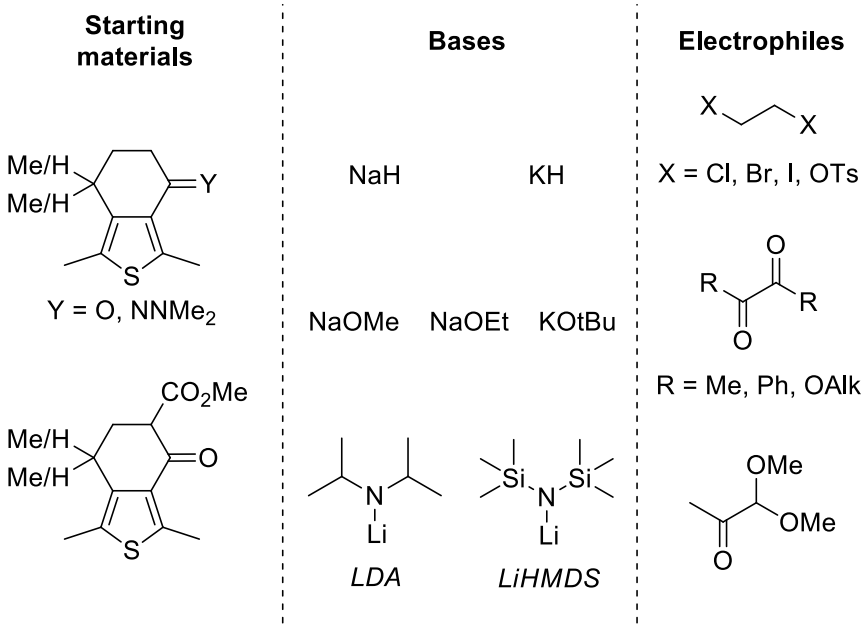

Scheme 3.2-3 Overview of attempted concerted C2-bridging starting materials, reagents and identified products.

Early attempts to bridge the sodium salt of ketone **3d** with dibromoethane[135] as well as more electrophilic analogues mostly yielded starting material only. Changing the solvent or addition of additives as *N,N'*-dimethylimidazolidinone or sodium methoxide[45] did not improve the result. Using the more nucleophilic ketoester as starting material[136], the dihaloethane acted as X^+-donor, yielding the halogenated compound itself or the corresponding alcohol after hydrolysis. This effect was already reported for sterically demanding ketones[137] and is especially strong[138] for diiodoethane.
Use of the corresponding glycol ditosylate yielded a mono-coupling product that suffered from elimination of the second leaving group.[139] Conversion of the ketone to a hydrazone of 1,1-dimethylhydrazine was successful when TMS-Cl was used as water scavenger.[140] Yet, alkylation of the hydrazone after deprotonation with lithium bases was unsuccessful.

As the conversion to any product was low in general, the reason for this behavior was investigated. Though deprotonation of the ketones was indicated by coloration of the solution, the completeness of conversion to the enolate remained questionable. To ensure that the reaction time was sufficient and the deprotonation is quantitative, an aliquot of the deprotonation reaction mixture was quenched with *p*-NO_2-benzaldehyde and analyzed

[45] In other experiments, sodium methoxide was found to be a very efficient mediator for the rather inactive sodium hydride (Scheme 3.2-7).

by UPLC (Figure 3.2-1). With this methodology, it was found that deprotonation does not proceed to completion even with strong and irreversible bases such as potassium hydride upon extended heating. Instead, the use of lithium bases at room temperature was more successful. Especially LiHMDS was able to achieve complete deprotonation within few hours at room temperature for both ketones considered. Once formed, the enolate was stable even upon prolonged stirring.

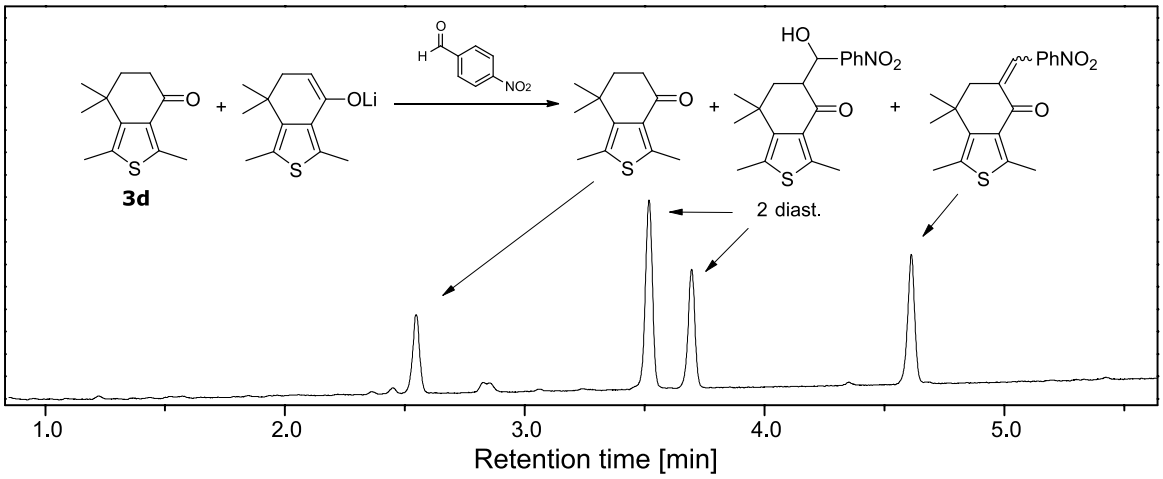

Figure 3.2-1 Qualitative deprotonation test using *p*-NO_2-benzaldehyde as trapping reagent. The figure shows the UPLC diode array trace, but conversion to the enolate can equally be checked by TLC.

With this method to ensure enolate formation, the reaction with dicarbonyl compounds was investigated. However, both biacetyl and benzil yielded only minor amounts of the mono-substituted ketone as a mixture of the ketol and the corresponding elimination product. A two-fold addition could not be forced by higher temperature or longer reaction times. Methylglyoxal acetal failed to react at all.

Diethyl oxalate, which was reported to have a high tendency for two-fold substitution,[141] showed only high conversion to the monofunctionalized product (Scheme 3.2-4).

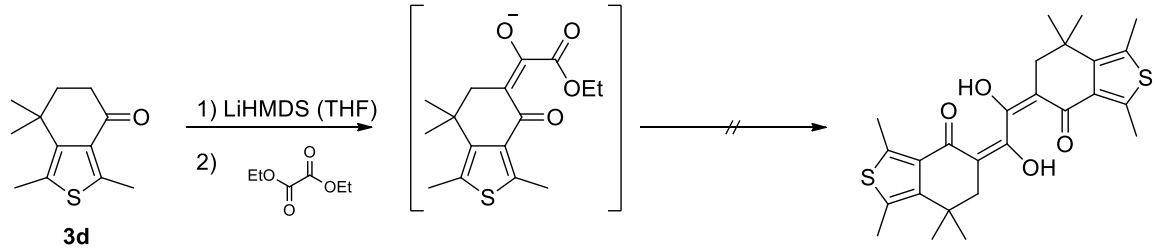

Scheme 3.2-4 Attempted C2-bridging of ketone **3d** using diethyl oxalate.

However, the product slowly decomposed upon storage and conversion to a bis-adduct was not achieved. Attempted double bond reduction in the unsaturated mono-adduct to

facilitate a second nucleophilic attack using amalgamated zinc did not afford the desired saturated γ-ketoester.

Though the final product could not be obtained, from the examples discussed here, the carboxyalkylation using dimethyl carbonate to yield the β-ketoester (not shown) and the formylation of ketone **3d** (*vide infra*), following conclusions can be drawn: The reaction of the substrate with carbonyl electrophiles seems to proceed with high conversion, if the carbonyl compound is rather small/flexible and forces the equilibrium by loss of a leaving group. Consequently, the two-fold substitution may be hindered either by the stiff structure of the mono-adduct or/and the negative charge and donating character of the enolate intermediately formed.

More promising was the alkylation in a stepwise fashion. For this, THP-protected 2-iodoethanol was chosen as a masked C2-unit, as convenient conversions of the protection group into a leaving group are reported.[142]

Using LiHMDS as base the corresponding monofunctionalized ketones were obtained in mediocre yield (Scheme 3.2-5 and Table 3.2-1). Despite variation of reaction time, temperature, and equivalents of alkylation agent used, about 50% of the starting ketone was isolated next to a varying amount of bis-functionalized product. Slow addition of the enolate agent to the alkylation had no noticeable effect.

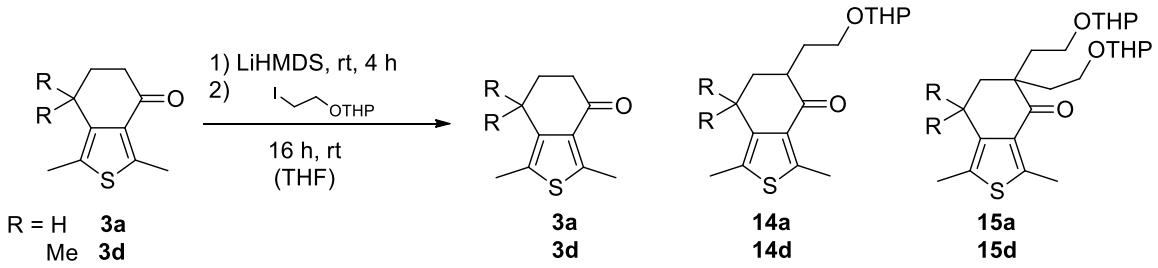

Scheme 3.2-5 Alkylation of ketones **3a** and **3d** with THP-iodoethanol. For product ratios under different reaction conditions, see Table 3.2-1.

Comparing the two ketone substrates available, it was found that during the alkylation of the derivative with benzylic methyl groups **3d** less dialkylated compound is formed than

with the plain ketone **3a**[46] Consequently, further reactions were carried out with adduct **14d**.

Table 3.2-1 Alkylation of ketones **3a** and **3d** with THP-iodoethanol and ratio of products. For molecular structures, see Scheme 3.2-5. The ratios were determined by integration of the UPLC diode array. For the deprotonation of the ketone, 1.0-1.2 eq of LiHMDS were used. The completeness of the deprotonation was checked with *p*-NO_2-benzaldehyde prior to addition of the alkylation agent (eq see table). Ratios did not change upon continued stirring.

Substrate	Eq.	T [°C]	t [h]	Ketone 3a/3d	Monoalk. 14a/14d	Dialk. 15a/15d
3a	1.0	-78 to 0	24	100	0	0
3a	1.0	0 to rt	24	44	45	11
3a	1.6	rt	72	27	54	19
3a	2.5	rt	20	44	43	11
3d	1.5	rt	22	60	40	0
3d	1.5	rt	20	42	52	6
3d	1.05	rt	16	42	52	6

Deprotection of the THP-alcohol can be achieved rapidly in dilute methanolic HCl and converted to the iodide by treatment with aq. HI solution in toluene or, more conveniently, by direct treatment of the THP-ether **14d** with aqueous hydroiodic acid (Scheme 3.2-6).

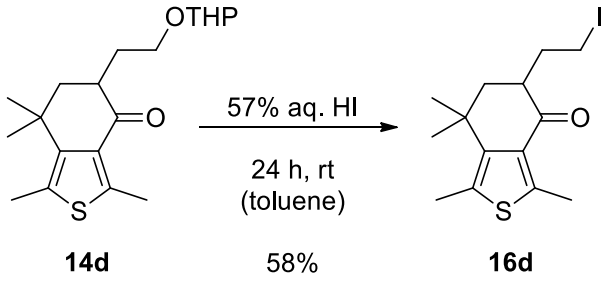

14d 58% **16d**

Scheme 3.2-6 Conversion of the THP protection group into a leaving group.

In all cases, the reaction either did not run to completion or, despite full conversion, yielded unexpectedly big amounts of the corresponding alcohol after workup. After isolation of some of the desired halogen-substituted product, it was found that even in the

[46] A similar behavior was also observed for their mono-α-bromination (Section 3.2.3, Scheme 3.2-8 and Scheme 3.2-17). Single crystal analysis of both bromo-adducts revealed that the first substituent introduced took the axial and equatorial position in brominated **3a** and **3d**, respectively. If this behavior is generally valid, the second proton in mono-alkylated **14d** could be less accessible for deprotonation. Additionally, steric interactions between the attacking electrophile and these methyl groups may hinder a second substitution further. For a comparison of both single crystal x-ray structures, see Figure 4.7-12.

pure compound the iodide is hydrolyzed at notable rate even at low temperatures. An acetalization of the ketone before conversion of the THP ether into a leaving group failed as the (lewis-) acidic conditions also triggered the deprotection.

Nevertheless, nucleophilic attack of an enolate to freshly prepared iodoethyl-ketone **16d** was attempted. Instead of the expected dimer that only occurred in trace amounts, the spiro-compound **18d** was identified as major product next to equal amounts of ketone **3d** and some alcohol derived from hydrolysis of the starting iodide (Scheme 3.2-7). It seems that proton transfer from the substituted ketone to the enolate is preferred over nucleophilic attack on the halogen moiety.

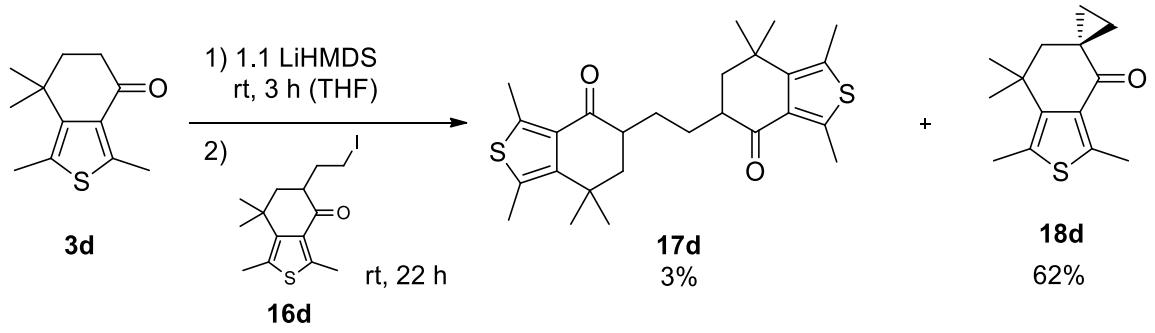

Scheme 3.2-7 Attempted bridging by nucleophilic attack of enolate **3d** on C2-iodide **16d**. The major product is spiro-derivative **18d**, the desired diketone was only obtained in traces.

In conclusion, the combination of fast hydrolysis of the leaving group at the γ-position and fast proton transfer from the substituted ketone to another enolate are sincere intrinsic problems that prevent the synthetic use of this theoretically very direct approach. As other strategies (*vide infra*) were more promising, this approach was abandoned.

3.2.3 Synthesis by heteroatomic bridging

As direct functionalization of ketone **3d** with a C2-building block proved to be challenging and a stepwise alkylation suffered from intrinsic problems of the system, a change in the synthesis strategy was necessary. As reductive couplings of sulfur-bridged 1,5-diketones to yield DAEs with a central thiacyclopentene moiety are already reported,[143] the use of sulfur as bisnucleophilic synthon was attempted.

For this, an electrophilic center at the α-carbon of ketone **3d** was formed by bromination (Scheme 3.2-8). Subsequent direct introduction of sulfur[144] by reaction with Na_2S or NaSH, however, mostly lead to dimerization to the thioether, or disulfides if an excess of

the sulfur source was used. As the sulfur bridge may allow for greater flexibility as carbon bridged pcDTE$_{656}$ reported earlier, the compound was nevertheless considered interesting.

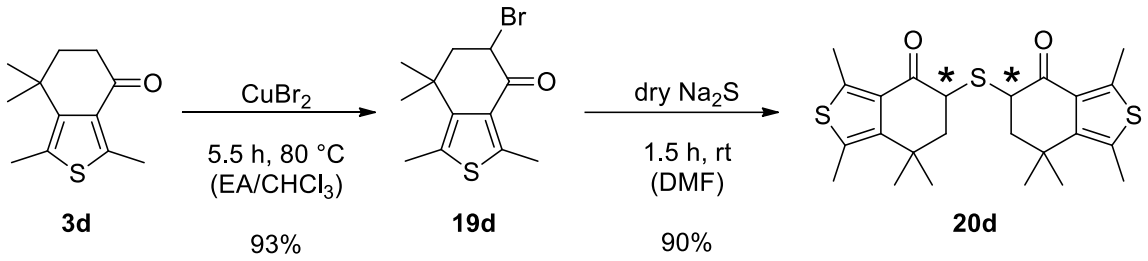

Scheme 3.2-8 Formation of 1,5-(3-thia)diketone **20d** from bromide **19d**. The use of sulfur salts under various conditions gave only minor amounts of the expected α-thiol.

As electrophilic C1-extended coupling partner, the α,β-unsaturated ketone **22d** was synthesized. Direct formation from ketone **3d**, as proposed amongst many others by Gras,[47] was unsuccessful and gave only starting material or the C1-bridged dimer as reported earlier.[56] Contrary, a two-step procedure of irreversible formylation and transaldolisation[146] yielded the desired product in almost quantitative yield (Scheme 3.2-9).

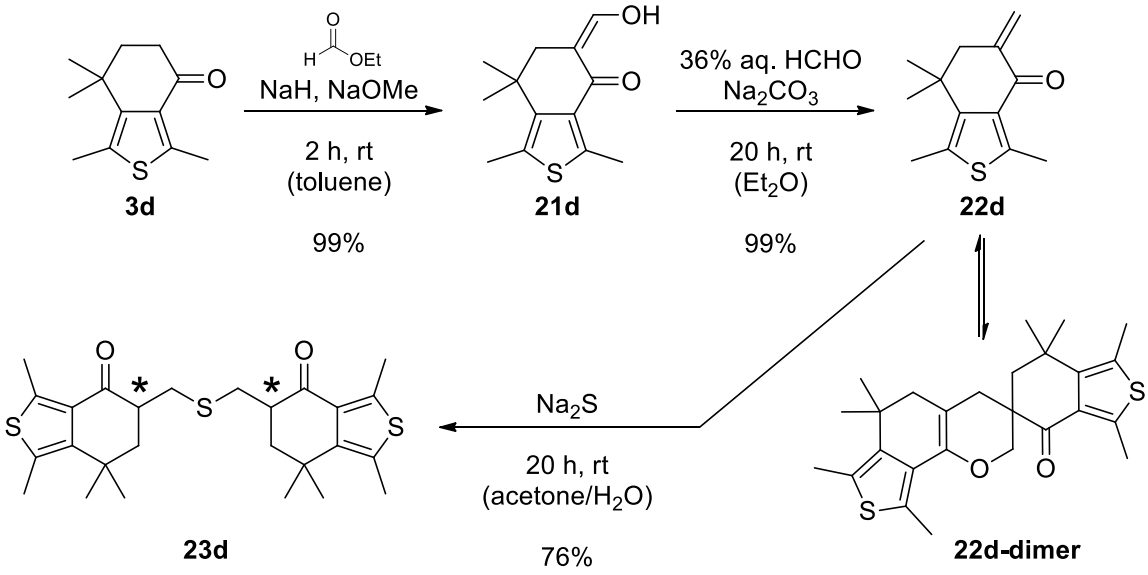

Scheme 3.2-9 Formation of the Michael-system **22d** as C1-synthon. In parallel to the 1,5-(3-thia)diketone **20d** (Scheme 3.2-8), the corresponding 1,7-(4-thia)diketone **23d** was obtained.

It was observed that even upon storage in the freezer, a small amount dimer of ketone **22d** formed. A structure for this was proposed[147] by Karmakar *et al.*. In contrast to the

[47] Fast conversion of structurally similar ketones to the corresponding enones was achieved with 1,3,5-trioxane and *N*-Methylanilinium-TFA salt as a catalyst.[145]

reported example and enone **22a** (*vide infra*), the dimer formation is not quantitative which is again ascribed to the steric hindrance caused by the benzylic methyl groups. The formation of the dimer seems to be reversible under the reaction conditions where it was used. Treatment with sulfur salts under aqueous conditions did not yield the corresponding β-thiol but the sulfur-bridged 1,7-diketone **23d** in good yield, which however can also be regarded as an interesting precursor to pcDTEs.

Finally, a selective monocoupling of sulfur was achieved with KSAc as sulfur source (Scheme 3.2-10).[148] The protected α-thiol was subsequently used in a tandem deprotection-coupling sequence[148a,149] to obtain the 1,6-diketone **25d**.

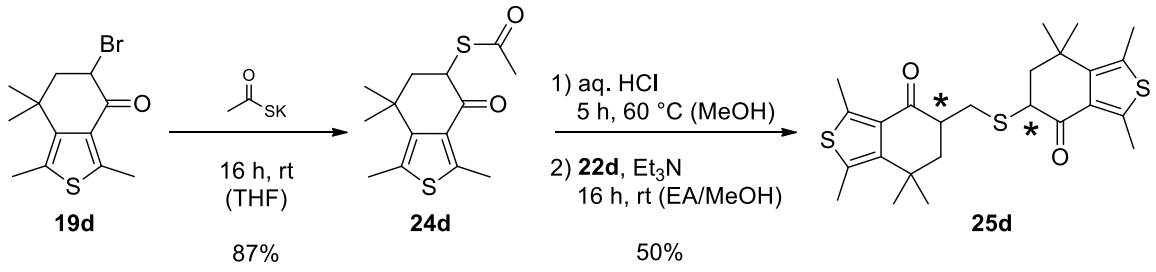

Scheme 3.2-10 Synthesis of the protected α-thiol **24d** and tandem deprotection-coupling sequence with α,β-unsaturated ketone **22d** to yield the desired 1,6-(3-thia)diketone **25d**.

Unfortunately, attempted McMurry coupling of all three sulfur-bridged diketones **20d**, **25d** and **23d** was unsuccessful and yielded complex mixtures with the corresponding thiols as the only identifiable products (Scheme 3.2-11).

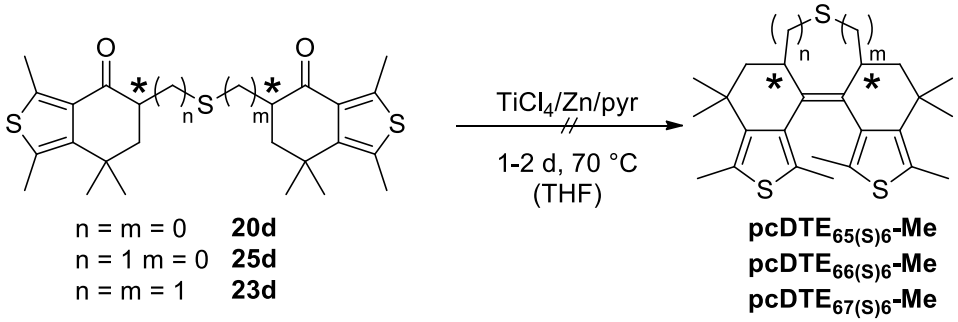

Scheme 3.2-11 Attempted McMurry coupling of the sulfur bridged diketones **20d**, **25d** and **23d**. Instead of the desired pcDTEs, complex product mixtures were obtained for all three substrates.

3.2.4 Synthesis by dimerization of a Michael system

Finally, it was envisioned to overcome the intrinsic problems of the system with direct dimerization by using the building block **22d**. As mentioned above, it is conveniently prepared in almost quantitative yield from ketone **3d** and carries a reactive C1-synthone.

Dimerization of this compound would form a stable C-C bond that should not interfere with the McMurry coupling.

Initially, dimerization was attempted using a nucleophilic approach. In-situ formation of a β-nitro ketone under acidic catalysis was expected[150] to form the unsaturated dimer (Scheme 3.2-12).

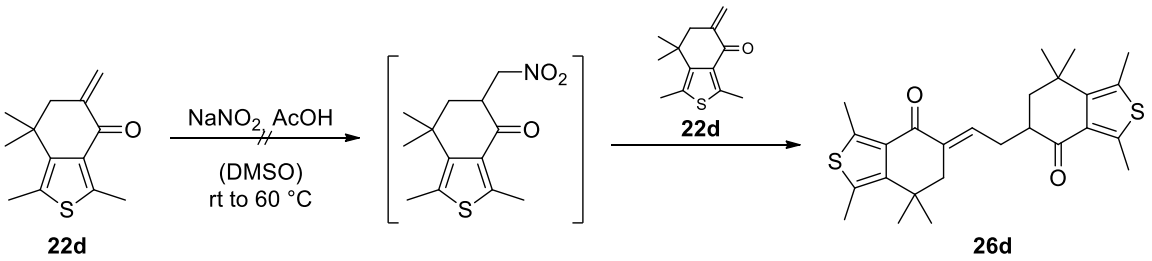

Scheme 3.2-12 Attempted dimerization of unsaturated ketone **22d** using $NaNO_2$. Neither the reported catalytic amounts nor excess of reagent could form the nitrated compound.

Unfortunately, the reaction of Michael-system **22d** with sodium nitrite in DMSO only afforded the starting material. Increasing the amount of $NaNO_2$ and temperature had no effect. In a second experiment, it could be demonstrated that already the nitration of the substrate reported for aliphatic vinyl ketones in THF[151] could not be achieved even under forcing conditions. It is assumed that steric factors in the constrained system shift the equilibrium strongly towards the starting material.

Alternatively, unsaturated ketones can be dimerized via their radical anion (Scheme 3.2-13). Various metals and conditions are proposed for the initial reduction to the radical anion, including sodium,[152] lithium,[153] magnesium,[154] and low-valent titanium.[155] In addition, preparative electrolysis has been used.[152,156]

The mechanism for this reaction has been intensively investigated by Bowers *et al.* [152] The study, carried out on aliphatic, non-enolizable enones, found that depending on the reaction conditions, either reduction of the C=C bond to form the equivalent to ketone **27d** or reductive dimerization to diketone equivalent to the target **17d** can be achieved. The report indicates that slow mixing of unsaturated ketone and reducing agent (solid or solvated sodium), the presence of proton donors as ^{t}BuOH or water and the addition at "higher" temperatures such as room temperature strongly disfavors the formation of the dimer in favor of the reduced monomer. The amount of reducing agent was reported not to influence the product ratio, but at least 1.0 eq was used in all cases.

Most striking is the speed of the reaction: the radical reaction to either product is finished within 10 s even at -78 °C.

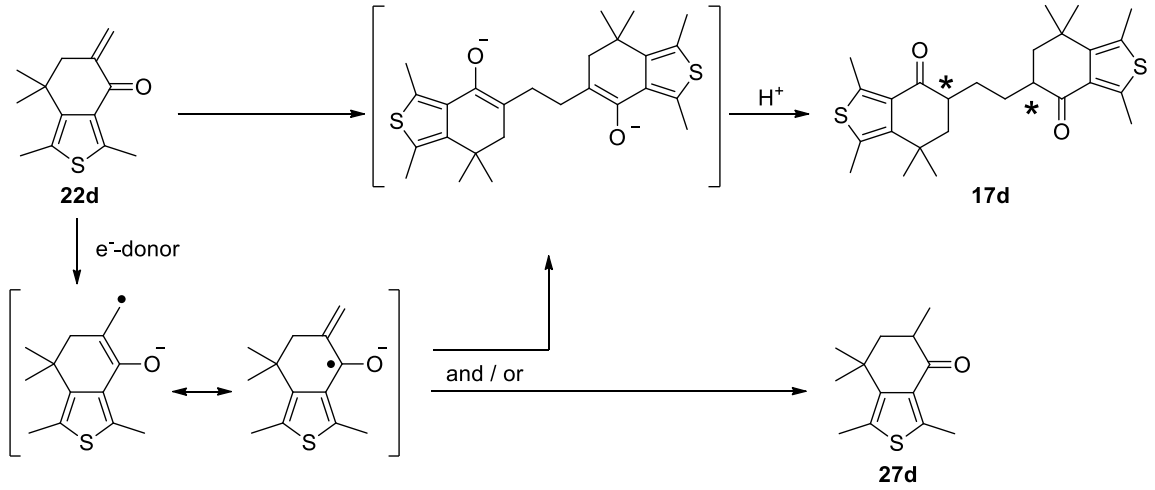

Scheme 3.2-13 Strategy for pcDTE synthesis by radical dimerization of enone **22d**. After 1e⁻-reduction, the radical anion formed from the enone dimerizes to yield the diketone **17d** after protic workup and/or the reduced starting material **27d**, depending on the reaction conditions.

Unfortunately, using the protocol most selective for the formation of the dimer (Table 3.2-2 entry 1), only a pool of products was obtained. These products include the reduced monomer, an oxidized dimer (m/z = $[441]^+$ instead of $[443^+]$), trimer and a compound that probably is the product of a consecutive aldol reaction (*vide infra*). An attempt to capture the reaction products as TMS-enolates (entry 2) failed and yielded mostly the reduced monomer. A procedure proposed for 2-methylenecyclohexanone using magnesium[154] proved to be fast and selective towards two products that by mass and NMR spectrum are assumed to be TMS-adducts derived from monomer and dimer. As desilylation with TBAF or conc. H_2SO_4 was ineffective, this procedure ultimately failed to yield the desired products (entry 3).

Janssen and Lüttke have suggested the use of low-valent titanium to achieve dimerization of a similar system.[155] Though the procedure using lithium aluminum hydride (LAH) to reduce the titanium precursor mainly formed the reduced monomer next to unused starting material (entry 4), using the more familiar Zn/$TiCl_4$ protocol at low temperatures successfully yielded the desired dimer in 36% isolated yield (entry 5). It was found that the titanium species is a vital reagent for this reaction, as no reaction occurred with zinc alone (entry 6). Whether $TiCl_4$ only activates the zinc powder or acts as mediator is beyond the scope of this study. However, older reports[157] suggest that activation of the

zinc is necessary.

Lastly, dimerization by electrolysis was attempted (entry 7). Indeed, the desired product formed, but was accompanied by several unprecedented by-products as well as the known reduced monomer.

Table 3.2-2 Reaction conditions for reductive dimerization of enone **22d**.

Entry	SM	Conditions[a]	Products[b]
1[152]	**22d**	Na (1.5) 4 h, 0 °C to rt (THF)	**27d** + aldol products + dimer/trimer derivatives
2[152]	**22d**	Na/TMS-Cl (1.5 : 10) 4 h, 0 °C (THF)	**22d** + **27d**
3[154]	**22d**	Mg/TMSCl (5 : 10) 3 h, 0 °C to rt (DMF)	TMS-adducts
4[155]	**22d**	LAH/$TiCl_4$ (2.2 : 4.25) 3 d, -78 °C to reflux (THF)	**22d** + **27d** + aldol products
5	**22d**	Zn/$TiCl_4$/pyridine (3 : 1.5 : 1) 1 h, 0 °C (THF)	36% **17d** + **27d** + aldol products
6	**22d**	Zn (THF)	no reaction
7[152]	**22d**	Electrolysis (Pt net, 1 eq e^-, THF)	**17d** + **27d** + others
8	**17d**	Zn/$TiCl_4$/pyridine (6 : 3 : 2) 2 d 70 °C (THF)	**17d** + aldol products
9	**22d**	Zn/$TiCl_4$/pyridine (6 : 3 : 2) 2 h rt, 2 d 70 °C (THF)	5% **pcDTE$_{666}$(Me$_2$)-Me**
10	**22d**	Zn/$TiCl_4$ (6 : 1.5) 45 min rt, 14 h 75 °C (THF)	11% **pcDTE$_{666}$(Me$_2$)-Me**
11	**22d**	Zn/$TiCl_4$/pyridine (6 : 1.5 : 1.5) 13 h 70 °C (THF)[c]	18% **pcDTE$_{666}$(Me$_2$)-Me**

[a] equivalents relative to ketone [b] numbers are isolated yields [c] addition at 70 °C

The obtained dimer **17d** was analyzed extensively by NMR using 2D-techniques such as HH-COSY, HSQC, and HMBC. Though beyond the resolution capabilities of the UPLC system, the NMR analysis showed that two diastereomers are formed during the reaction. The mechanistic study of Bowers *et al.* suggested that due to steric repulsion of the substituents at the β-position, the racemic dimer should be favored.[152] However, for the present unsubstituted terminal alkene almost identical ratios of about 2:3 for the zinc-mediated reaction and about 1:1 for the products of the electrolysis were found.

As separation of the isomers was improbable, reductive dimerization of the diastereomeric mixture was attempted (entry 8). Unexpectedly, this reaction failed to give the desired product but only formed aldol products. However, the similarity of the dimerization and reductive coupling methods made a tandem reaction attractive: Dimerization at low temperature for some minutes followed by classical McMurry conditions indeed yielded the desired product **pcDTE$_{666}$(Me$_2$)-Me** as a mixture of

diastereomers (Scheme 3.2-14). Crucial for the success of the second reaction step herein was the increased amount of reagent compared to normal McMurry couplings.

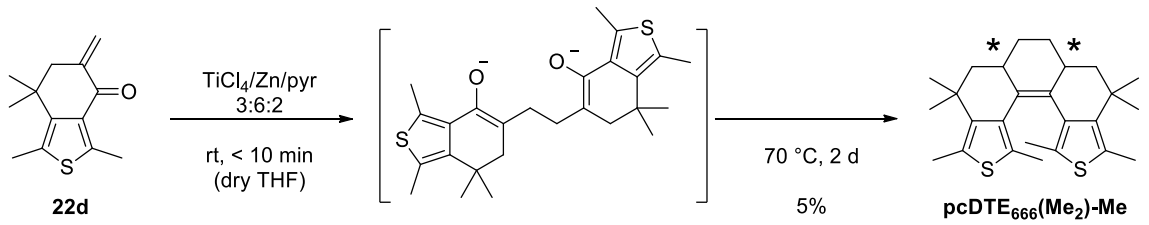

Scheme 3.2-14 Tandem dimerization / reductive coupling of enone **22d**. McMurry coupling conditions achieve the first step very fast even at low temperatures, whereas carbonyl coupling requires heating. In contrast to the large scale reaction using unoptimized conditions (Table 3.2-2, entry 9), the yield could be improved to 18% by addition of **22d** to the low-valent titanium reagent at 70 °C on a semi-preparative scale (entry 11).

Though conversion of the starting material is complete, the tandem reaction only shows low yield of the product.[48] The first reaction step yields the reduced starting material **27d** as a side product. In their study, Bowers *et al.* showed that several factors increase the proportion of this undesired side product (*vide supra*). The most obvious way to reduce its formation is careful drying of the solvent to remove water as the most prominent proton donor. The other proposed mechanism for its formation through disproportionation may only be controlled by the concentration of the reaction. Yet, in the listed and several further assays, no clear dependence could be derived, as also the dimerization is a bimolecular process. Bowers et al reported further that the initially formed radical anion is associated with a counter ion (H^+ or metal) which facilitates dimerization by reduction of the electrostatic repulsion of radical anions and thus favors dimerization. They suggest that dimerization may further be helped by ion pairing of the radical anions and observe a strong effect of Li^+ known for its strong coordination properties. While in the present system this role may be filled by titanium or zinc ions, the effect of lithium salts to the reaction may be worth exploring.

The formation of an aldol follow-up product proved to be fatal to the reaction yield as well and has been reported before.[152-153] Though reversible in theory, reaction conditions seem not to allow for equilibration with the diketone as no further formation of the desired product is observed upon longer heating times. An attempted isolation of the aldol

[48] Separation of the products from by-products however is rather simple. The reduced starting ketone **27d** does not participate in the reductive coupling to form the respective aDTE and thus is more polar than the desired pcDTE. Likewise, aldol products are more polar then the hydrocarbon product.

product(s) was not successful. Yet, the observed *m/z* pattern for the aldol product and a secondary signal as a result of the elimination of water in the UPLC ESI$^+$ trace are in agreement with a product resulting from an intramolecular aldol reaction (Scheme 3.2-15).

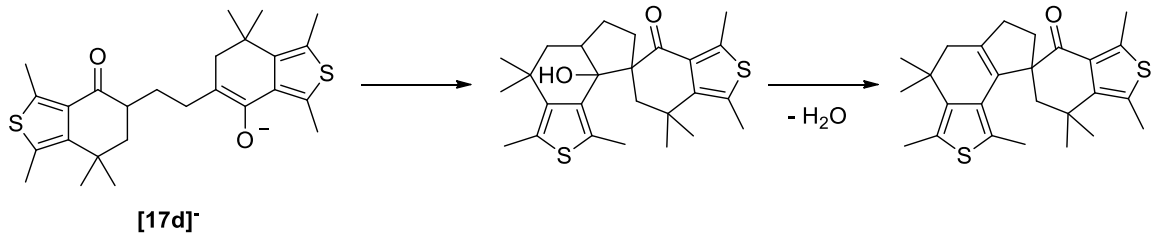

[17d]$^-$

Scheme 3.2-15 Possible structure of the assumed side products in the reductive coupling of diketone **17d**. An attempted isolation of either the aldol or elimination product failed, yet a characteristic *m/z* pattern was regularly observed during UPLC-MS reaction control.

Though only carried out on a smaller scale, it is indicated that the tandem dimerization-coupling protocol can be improved if carried out pyridine-free and if the substrate is added at high temperatures (Table 3.2-2 entry 10 and 11). It is reasoned that the former factor slows down the aldol-reaction pathway whereas the latter speeds up the desired coupling process. Furthermore, as a reductive dimerization using amalgamated zinc in DMF is reported to produce the aldol products selectively,[158] the possible role of zinc in the aldol formation is underlined. As many reagents were investigated[159] prior to the common usage of Zn, an appropriate replacement surely can be found.

From UPLC analysis of the product mixture (Figure 3.3-1 top), three isomeric compounds displaying the right mass to charge ratio were identified. While only having two chiral carbons, it is reasoned that the rigid structure leads to helical chirality (Scheme 3.2-16). These isomers show surprisingly large differences in their absorption spectra (Figure 3.3-1 bottom), yet are almost identical to every separation method available.

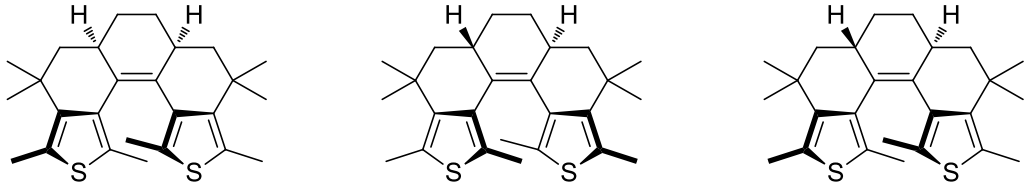

Scheme 3.2-16 The possible diastereomers of **pcDTE$_{666}$(Me$_2$)-Me**. Additionally to the chiral allylic centers, the compounds display helical chirality due to hindered conversion into each other.

Careful elution from a dry-packed normal phase column with pentane was incapable of distinguishing the compounds. Similarly, prep. TLC with cyclohexane or PE could not achieve a satisfying separation.[49] The attempted purification by MPLC on both normal phase and reverse phase columns as well as prep. GPC achieved no separation. Consequently, separation was carried out extensively on reverse phase prep. HPLC, but suffered from low solubility of the substrate in the eluent ACN as well as unsatisfactory peak separation.[50] By changing the stationary phase from C18 to phenyl-hexyl could improve the separation dramatically, yet peak separation on a preparative level was insufficient. Lowering the elution strength by increasing the water content of the eluent reduced the solubility further and additionally caused peak broadening. Finally, any attempt to gain an analyzable amount of isomerically pure product failed.
Also crystallization of the product under various conditions[51] could not separate the isomers completely, but enriched the major isomer in the solution. The obtained enriched mixture was used for both NMR analysis and spectroscopy.

In analogy to **pcDTE$_{666}$(Me$_2$)-Me**, the analogue starting from unsubstituted ketone **3a** was synthesized (Scheme 3.2-17). It was hoped that due to missing steric interference of the benzylic methyl groups, the final step of the sequence would be facilitated. Though the synthesis was already established for the 6-membered ring ketone **3d**, the differences in reactivity caused the appearance of several side products and hence lowered the overall product yield. While synthesis of keto-aldehyde **21a** worked reasonably well, probably due to the elimination step, functionalizations have a higher tendency to lead to bisfunctionalized products. For the transaldolisation of the keto-aldehyde **21a** to enone **22a**, two unprecedented products were observed. Both the α-mono- and α,α-di(hydroxymethyl) ketone showed a complex signal splitting in the ^{1}H-NMR, similar to the spectrum measured for iodoethyl ketone **16d** (Scheme 3.2-6).[52]

[49] The developed plate was fractioned into small stripes and analyzed by UPLC.

[50] On C18 stationary phase, after elution times as high as 3 h, only separation of two of the three isomers was achieved. The injectable amount of product for preparative separations was about 0.5 mg per run.

[51] Ironically, slow evaporation of THF and ACN from the oversaturated solutions prepared for purification by prep. HPLC proved to be most successful in enriching the major diastereomer.

[52] It could be demonstrated that these couplings result both from magnetically unequal geminal protons and from coupling with the exchangeable protons of the alcohol group. The addition of a drop of D_2O to the NMR sample markedly decreased the intensity of one of the signals and lead to a decreased signal splitting.

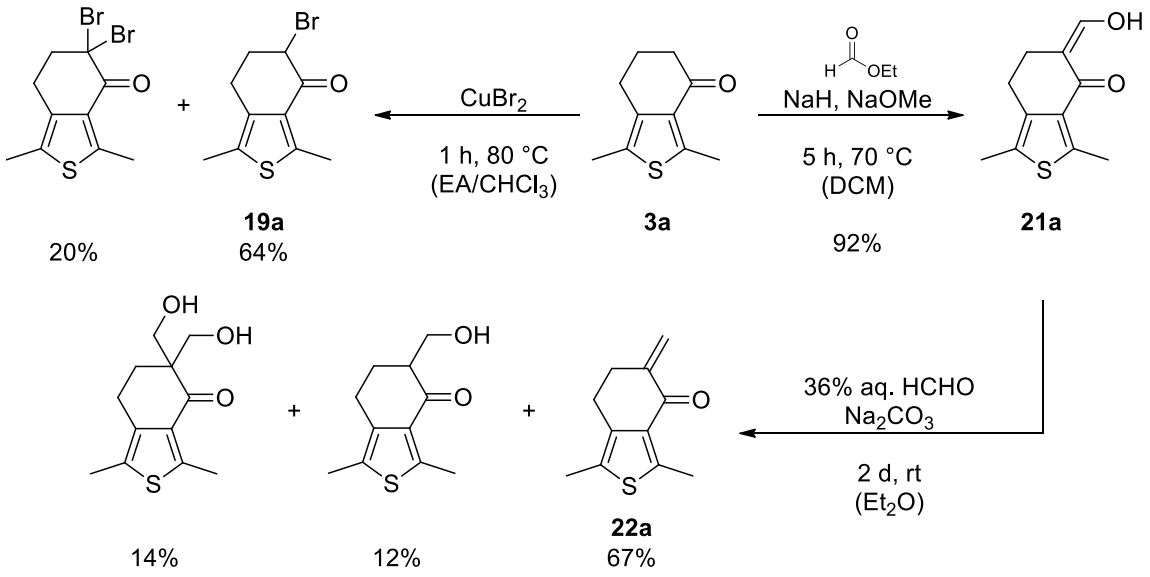

Scheme 3.2-17 Synthesis of precursors for **pcDTE$_{666}$-Me**. In contrast to the methyl-bearing, plain ketone **3d**, functionalization of ketone **3a** is not quantitative and leads to bisfunctionalized products. A similar behavior was already observed for alkylation (Scheme 3.2-5 and Table 3.2-1).

In a final step, the synthesis of both a heterocyclic pcDTE$_{67(S)6}$ and the carbon-bridged **pcDTE$_{666}$-Me** was attempted (Scheme 3.2-18).

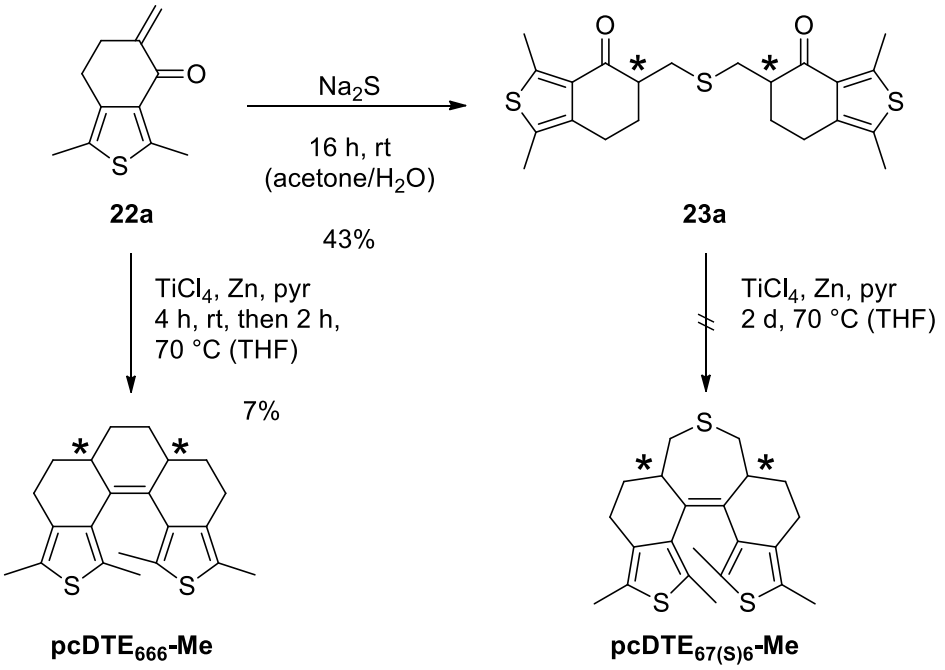

Scheme 3.2-18 Synthesis of **pcDTE$_{666}$-Me** and attempted synthesis of a heterocyclic pcDTE$_{676}$. Using the same protocol as for **pcDTE$_{666}$(Me$_2$)-Me** (Scheme 3.2-12), the yield could not be significantly increased by changing to the less sterically demanding monomer **22a**. However, the reaction time is lowered dramatically from two days to two hours to achieve full conversion.

The 1,7-(4-thia)diketone **23a** was prepared in good yield, though column chromatography only afforded a mediocre amount in good purity. The following McMurry coupling unfortunately suffered from the same drawbacks as the homologue ketone **23d** and afforded, as indicated by UPLC analysis, complex mixtures including a product with the mass of enone **22a**.

Upon applying the protocol for the tandem dimerization-reductive coupling reaction of enone **22d** to the unsubstituted derivative **22a**, the yields of **pcDTE$_{666}$-Me** are equally unsatisfactory. Interestingly, the formation of dimeric enone **22d-dimer** (compare Scheme 3.2-9) was quantitative even upon storage at -20 °C, but seems to be fully reversible after a certain induction time under the reaction conditions for radical dimerization. While the first, radical step was completed after less than 10 min for enone **22d**, after 1 h still only dimer of **22a** was observed. The second reaction step, however, is accelerated drastically from about two days to two hours for the new derivative and again demonstrates the increased reactivity.

Similar to **pcDTE$_{666}$(Me$_2$)-Me**, also for **pcDTE$_{666}$-Me** a mixture of three diastereomers showing shifted absorbance maxima was obtained (Figure 3.3-1). Despite being somewhat less polar, separation of the three isomers could not be achieved and the mixture enriched by crystallization was used to analyze their photochemical behavior in a qualitative fashion.

3.3 Photochemistry of pcDTEs

As for both newly synthesized pcDTEs only diastereomeric mixtures were available, the analysis of the photochemistry can only be carried out on a qualitative level. Though the following spectra cannot be used for quantitative analysis due to solvent effects and spectral overlap of the diastereomers, the UPLC diode array traces of are shown to demonstrate the differences between the three observable open diastereomers of both pcDTEs (Figure 3.3-1).

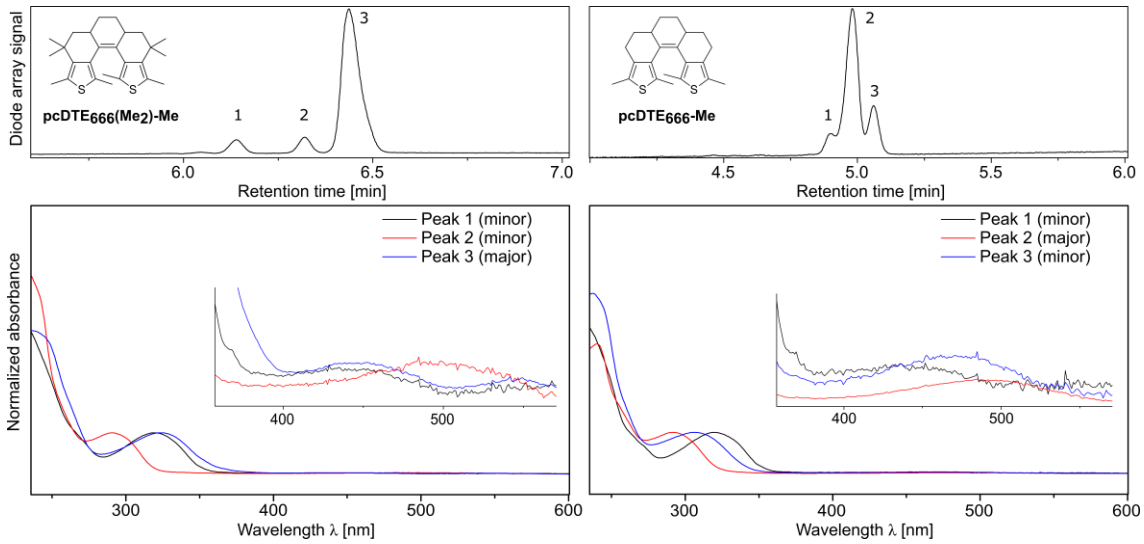

Figure 3.3-1 Absorbance spectra of both pcDTE$_{666}$ synthesized. **Top:** Chromatogram of the isolated diastereomeric mixtures. **Bottom:** UV/vis spectra obtained from the UPLC's diode array trace of such chromatogram, normalized to the absorption band around 300 nm. The inset shows the band of each respective cyclized isomer formed by irradiation with the measurement beam of the diode array.

In general, the observed shifts match the absorption spectra of the *cis*-fused system published by Dinescu and Wang (see Figure 1.2-8).[42] However, most remarkable is the large difference of the absorption maxima for the three isomers of both compounds. Within the open isomers, for **pcDTE$_{666}$(Me$_2$)-Me** this shift is slightly more pronounced ($\Delta\lambda_{max}$ = 33 nm) than for the diastereomers of **pcDTE$_{666}$-Me** ($\Delta\lambda_{max}$ = 30 nm). At the same time, for **pcDTE$_{666}$(Me$_2$)-Me** the most bathochromically absorbing compound is the major diastereomer, whereas the major isomer of **pcDTE$_{666}$-Me** is the most hypsochromically absorbing.

For the closed isomers formed, the trend is reversed: Herein, for both compounds the isomer with the most hypsochromic absorption in the open form displays the most bathochromic absorption maximum in the closed isomer. The maximum difference for the

three isomers of each pcDTE is identical ($\Delta\lambda_{max}$ = 62 nm), as far as these preliminary data allow such interpretation.

A possible explanation for the strong spectral shift is surely to be found in the different geometries of each three diastereomers. For the *cis*-fused pcDTE diastereomers (compare Scheme 3.2-16), a blue-shift seems most probable. A certain contribution of a parallel conformer with disturbed conjugation between the aromatic units and the double bond is conceivable. Yet, at least under UPLC conditions, a slight cyclization is observed for all three diastereomers of both pcDTEs.

For the photochemical analysis of the pcDTEs under irradiation, the same methodology as for the investigation of aDTEs was applied. For both compounds, 10^{-5} M solutions in MeCN were carefully degassed within the cuvette used for irradiation by purging for at least 5 min with a stream of deoxygenated argon to prevent formation of singlet oxygen.

Firstly, the photochemical behavior of the **pcDTE$_{666}$-Me** diastereomeric mixture is explained. Similar to normal DAE, upon irradiation with 313 nm light formation of a bathochromic band typical for the cyclization product is observed (Figure 3.3-2 left). However, only a comparably small increase of the bathochromic band was observed, before unspecific degradation occurred (Figure 3.3-2 right). An estimation of the amount of closed isomers formed failed, as the cyclized isomers supposedly are not stable under the aqueous UPLC conditions.

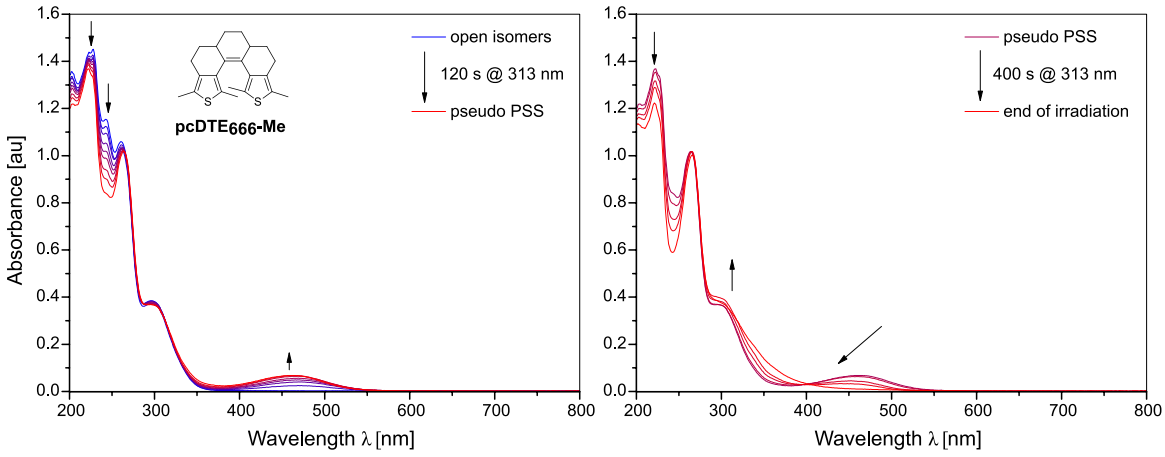

Figure 3.3-2 Spectral evolution during irradiation of **pcDTE$_{666}$-Me** (enriched diastereomeric mixture) upon irradiation with 313 nm light in MeCN. **Left:** A bathochromic band typical for the closed isomer forms. However, already after short irradiation, a maximum absorbance in the bathochromic band is reached (pseudo PSS). **Right:** Upon further irradiation with UV light, unspecific degradation of the closed isomer is observed.

Additionally, the redox potentials and the electrochemical behavior of **pcDTE$_{666}$-Me** were investigated (see Figure 2.4-6 and Table 2.4-1). The oxidation peak potentials E_p^a are virtually identical to **aDTE$_{66}$-Me** except for a little deviation for the second oxidation potential of the closed isomer, which was found to be slightly less negative for **pcDTE$_{666}$-Me**.[53] The amount of closed isomer formed by irradiation within the electrochemical cell was small but finally sufficient to determine its redox potential. Yet, upon irradiation, a second, constant oxidation wave at higher E_p^a was found for the open diastereomers. This observation may be attributed to a diastereomer that is inactive in the photoisomerization.[54] Unfortunately, this possibility could not be explored further due to incompatibility of the cyclized compound towards UPLC analysis.

Secondly, the behavior of the bulkier analogue **pcDTE$_{666}$(Me$_2$)-Me** is discussed. In contrast to the aforementioned derivative, a stable PSS can be reached upon irradiation with 313 nm light and the isomerization can be followed by UPLC (Figure 3.3-3). However, one of the minor open diastereomer (Peak 2 in Figure 3.3-1 left) elutes at the same retention time as the major photoproduct in the UPLC, which renders the two isomers indistinguishable. Nonetheless, the other two diastereomers seem to isomerize in a comparable rate.

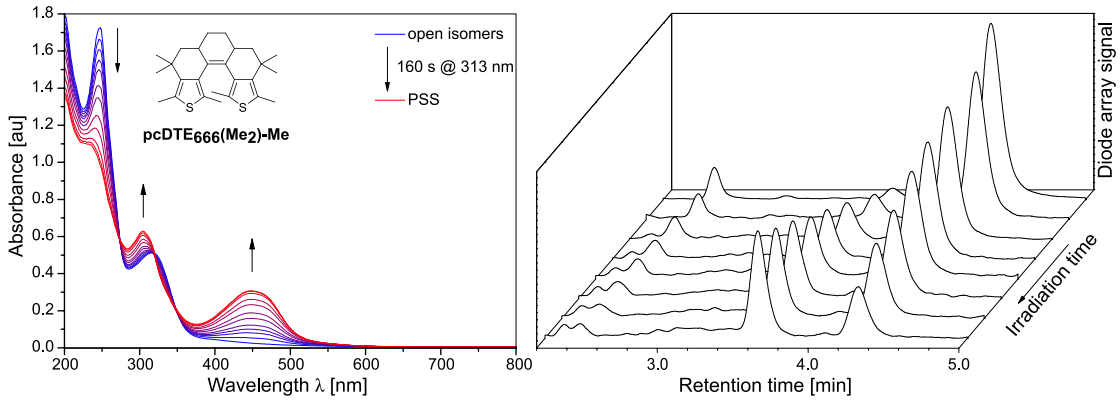

Figure 3.3-3 Spectral evolution during irradiation of **pcDTE$_{666}$(Me$_2$)-Me** (enriched diastereomeric mixture) upon irradiation with 313 nm in MeCN. **Left:** UV/vis spectra during irradiation. The red shifted band typical for the closed isomer builds up. **Right:** UPLC chromatograms after irradiation steps. The major cyclized isomer elutes with the same retention time as one of the minor open isomers.

[53] The oxidation potential of the previously synthesized **pcDTE$_{757}$-Me** were also determined in this study. The E_p^a of the open isomers was found to be higher then for **aDTE$_{77}$-Me**, whereas the oxidation peak potentials for the closed isomer were lower.

[54] Normally, the intensity of the oxidation waves decreases with decreasing amount of the respective species.

The PSS conversion is estimated to consist of about 60% cyclized isomer, though the lack of resolution in the chromatogram prevents exact determination. In contrast to the complete cyclization of aDTEs (PSS ≥ 95%), this value is rather low. Still, it is the largest spectral change observed within the pcDTE synthesized, including the two derivatives reported in an earlier work.[56] As such, the conversion to the closed isomer seems comparable to that reported by Dinescu and Wang.[42]
As for aDTE, cycloreversion is possible by irradiation of the bathochromic band with >350 nm light and leads to almost full restitution of the open isomers spectrum (not shown).

Despite their identical basic structure, distinct differences between both pcDTE systems were found. In general, **pcDTE$_{666}$(Me$_2$)-Me** performed better than the non-methylated analogue **pcDTE$_{666}$-Me** in all aspects investigated (PSS, stability of the isomers, reversibility). The difference of absorption spectra within each group of diastereomers is less pronounced for the unmethylated derivative, indicating that intramolecular interactions play a crucial role in these stiff compounds. Though the pathway of decomposition was not investigated, it seems reasonable that an attack of oxygen on the central diene of the cyclized isomers[47a] is the main degradation path in this electron rich compounds. The shielding effect of the methyl groups thus seems to overcompensate the addition of the inductively donating substituents and increase the stability. Likewise, degradation by intramolecular rearrangement processes (compare Scheme 1.2-6) could be hindered in the “conformationally anchored” **pcDTE$_{666}$(Me$_2$)-Me**.

3.4 Conclusion

The synthesis of pcDTE$_{666}$ was attempted using several methodologies starting from the 6-membered ring ketones **3a** and **3d**. Firstly, direct alkylation using a biselectrophilic C2-unit was attempted (Scheme 3.2-2 path A). However, two-fold alkylation with dihaloethanes failed despite numerous protocols applied and yielded mostly only starting material. In several cases, especially with diiodoethane but also with dibromoethane, a halogenation of the α-position of the ketone was observed.
Using a stepwise alkylation sequence with a masked second reaction side was more successful. For this, THP-protected iodoethanol was employed. Though full deprotonation of ketone **3d** using LiHMDS was verified, only about 50% of the enolate were alkylated. It is assumed that proton transfer from the alkylated species **14d** to the enolate is faster than alkylation. The THP-ether can be deprotected and converted into an iodide in a single step. Yet, only mediocre yields of iodide **16d** were obtained as the product suffers from hydrolysis back to the corresponding alcohol. As observed before, the alkylation of plain ketone **3d** with freshly prepared ethyl iodide **16d** again suffered from intramolecular proton transfer, and instead of 1,6-diketone **17d**, spiropropane **18d** was the main product.

As this intrinsic property of the ketone could not be overcome, a different approach using two C1-functionalized ketones with opposing reactivities was attempted (Scheme 3.2-1 path B). The Michael system **22d** as electrophilic component was synthesized in almost quantitative yield in a two-step sequence of formylation and transaldolisation. However, for the sterically less demanding enone **22a**, two side products reflecting the different reactivity of both systems were obtained. This tendency was also observed for the bromination yielding only monobrominated ketone **19d** but a mixture of mono- and dibrominated ketone **19a**.
Addition of divalent sulfur salts to the bromoketone **19d** yielded the 1,5-(3-thia)diketone **20d** instead of the expected β-thiol. Similarly, the reaction of Michael system **22d** gave the 1,7-(4-thia)diketone **23d** in high yield. The equivalent compound without methyl groups **23a** reacted correspondingly in high conversion. The desired 1,6-(3-thia)diketone **25d** was finally obtained in a tandem deprotection-alkylation sequence using the monoprotected thioacetate **24d** and unsaturated ketone **22d**. Unfortunately, none

of the three thia-diketones reacted to the expected thioether-bridged pcDTE in the subsequent McMurry coupling. Instead, hydrolysis products were obtained.

Finally, synthesis of diketone **17d** succeeded via a radical dimerization of enone **22d**. Interestingly, reductive coupling of the diketone under McMurry conditions did not lead to the expected product, whereas a tandem dimerization-coupling reaction finally afforded the target compound **pcDTE$_{666}$(Me$_2$)-Me**. The overall yield for the reaction was as low as 5%, though the formation of the dimer **17d** was quite effective under optimized conditions. Once formed however, the diketone was prone to aldol-reactions as parallel pathway to the expected reductive carbonyl coupling. It was expected that sterically less demanding enone **22a** would have a higher conversion to the desired pcDTE. Though the reaction times decreased significantly, unfortunately, the product yield remained as low.

Optimization of the reaction (base free conditions, high temperature addition to accelerate the coupling reaction) to avoid this pathway was carried out on the example of enone **22d** on a small scale and indeed lead to higher product yields. Nevertheless, aldol product formation may be reduced more effectively by using other reducing agents than zinc or a slight modification to the diketone structure that prevents enolization of the ketone (Scheme 3.4-1).

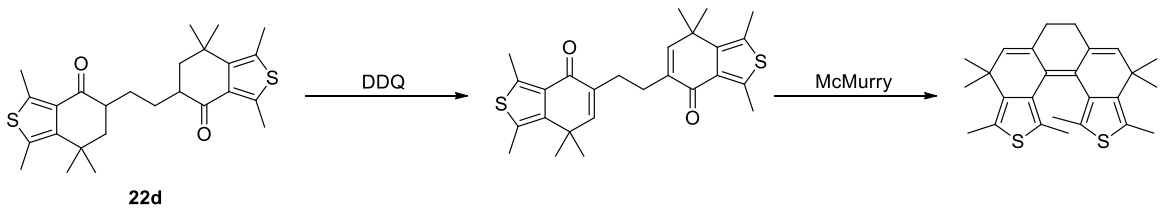

Scheme 3.4-1 Proposed change to the molecular structure inspired by Janssen and Lüttke.[155]

The desired target compounds **pcDTE$_{666}$(Me$_2$)-Me** and **pcDTE$_{666}$-Me** were obtained as mixture of three observable diastereomers with different UV/vis spectra as observed in UPLC analysis. Yet, separation of the isomers could not be achieved by normal phase column chromatography, MPLC, prep. TLC, prep. GPC or reverse phase prep. HPLC, the latter mainly due to poor solubility. Crystallization of the compounds afforded an enriched mixture, but could not afford isomerically pure products.

The photochemical behavior of **pcDTE$_{666}$-Me** was unsatisfying, as amount of closed isomer formed was very low and degradation obviously an important reaction path. The

crowded derivative **pcDTE$_{666}$(Me$_2$)-Me**, however, performed much better. An estimated amount of 60% closed isomer was formed in the PSS, and photochemical cycloreversion could be performed, proving acceptable stability. It can thus be concluded, that the addition of bulky groups in the periphery can greatly increase the resistance towards undesired side reactions.

Though the performance of **pcDTE$_{666}$(Me$_2$)-Me** is still not comparable to optimized modern DAEs, or aDTEs for that matter, it displays similar properties as the first methyl-substituted DAE derivatives reported by Irie and co-workers in 1988.[30a] The aim of future studies thus should be the synthesis of functionalized derivatives, easily accessible using the equivalent chloro-methyl ketone and the synthetic route implemented in this study. In addition to the increased photochemical stability, the functionalization with designated groups as benzonitrile will also facilitate the crystallization of the pure diastereomers and purification by chromatographic methods due to bigger differences in the geometry and higher polarity, respectively (Scheme 3.4-2).

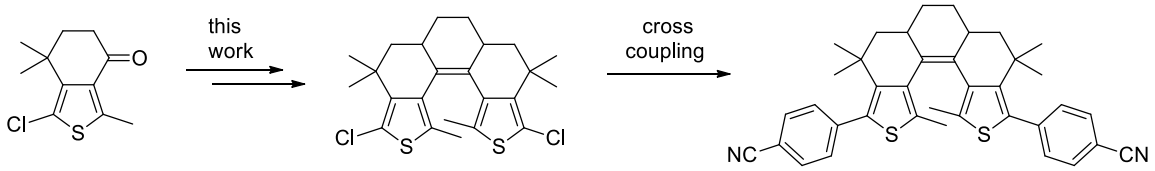

Scheme 3.4-2 Proposed synthetic route to functionalized pcDTEs. The introduction of electron-withdrawing substituents will greatly improve their photochemical stability and facilitate the isolation of pure diastereomers.

Once pure diastereomers are obtained, the determination of photochemical factors as quantum yields, fatigue resistance, and thermal stability of the isomers can be measured to compare the new class of pcDTEs with aDTEs and normal DAEs. Following this path further, the effect of annulation and locking the photochromic system in highly constrained conformation can be understood on a profound level and contribute thus to the development of improved DAE designs.

4. Experimental section

4.1 General methods

If not stated otherwise, all experiments were conducted under normal atmosphere. All reaction flasks were equipped with magnetic stirring bar and reflux condenser if necessary. Reactions under inert atmosphere were carried out in flask dried for at least 5 min under dynamic vacuum (10^{-2} mbar) with a heat gun (~ 500 °C), cooled to room temperature and backfilled with argon.

Reaction control was carried out on TLC plates (60 Å F_{254}-plates, Merck) or by UPLC. TLC plates were eluted in a closed chamber with filter paper stripes on the walls to improve gas phase saturation with the respective solvent and thus reproducibility. For basic elutions, plates were dipped into a Et_3N/PE 1:5 solution and dried on air prior to use. Subsequently, they were used with a usual solvent mixture without further addition of base. Alternatively to detection with UV light, aq. $KMnO_4$ stain or a chamber with iodine on silica was used. Compounds containing ketone or aldehyde groups can be identified and also differentiated staining with Brady's reagent[160] (2,4-Dinitrophenyl-hydrazine and H_2SO_4 in EtOH).

Column chromatography was carried out on silica gel (35–70 µm, 60 Å) using eluents as specified. Alternatively, normal phase chromatography was performed on a Teledyne Isco CombiFlash® Rf+, using a gradient from 0% to 100% polar solvent and halting the gradient upon peak elution, if not stated otherwise.

Light sensitive samples in general were handled under red room light (for emission spectra see Section 6.6). However, preventing exposure to direct daylight proved to be sufficient for most compounds during reactions and workup. Standard room light had no significant overlap with the spectra of the open isomers to cause significant amounts of closed isomer. However, for storage the sample were covered with aluminum foil.

UPLC/MS was performed with a Waters UPLC Acquity equipped with a Waters LCT Premier XE Mass Detector for UPLC-HR-MS, with Waters Alliance systems (consisting of a Waters Separations Module 2695, a Waters Diode Array Detector 996 and a Waters Mass Detector ZQ 2000) on Kinetex® 1.7 µm EVO C18 LC column 50x 2.1 mm, Kinetex® 1.7 µm XB-C18 New column 100x 2.1 mm and ACQUITY UPLC® BEH

Phenyl 1.7 µm 100x 2.1 mm analytical reverse phase columns. The ESI+/- values are obtained from UPLC chromatograms.

Preparative recycling GPC was performed on a LC-9210NEXT preparative recycling GPC (Japan Analytical Industry) with up to three JAIGEL-1H & JAIGEL -2H columns.

Microwave assisted reactions were performed in a CEM Discover 300 W microwave system.

NMR spectra were recorded on a 500 MHz Bruker AV 500, a 400 MHz Bruker AV 400, or a 300 MHz Bruker DPX 300 spectrometer at 25 °C using residual protonated solvent signals as internal standards for ^{1}H and ^{13}C spectra (^{1}H: $\delta(CHCl_3) = 7.26$ ppm, $\delta(CH_2Cl_2) = 5.32$ ppm and ^{13}C: $\delta(CDCl_3) = 77.16$ ppm, $\delta(CD_2Cl_2) = 53.84$ ppm) or $CFCl_3$ as external standard for ^{19}F spectra ($\delta(CFCl_3) = 0$ ppm).

Preparative HPLC was conducted using a Waters 996 Photodiode Array Detector and Waters Fraction Collector III connected to a Waters 600 Controller on C18 (5 µm EVO LC column 250x 21.2 mm) and phenylhexyl (Luna® 5 µm LC column 250x 21.2 mm or Luna® 10 µm 250x 21.2 mm) reverse phase columns with MeCN / H_2O / THF mixtures (20 ml/min flow), degassed by a constant helium purge and subsequently a KNALER degasser. For optimization of the elution conditions, C18 (Kinetex® 5 µm EVO LC column 250x 4.6 mm) and phenylhexyl (Luna® 5 µm LC column 250x 4.6 mm) with a reduced flow (1 ml/min) were used. The runs were carried out isocratically and all samples were injected as saturated solutions in the respective elution solvent mixture.

Dry solvents were obtained from an Innovative Technology Ltd. solvent purification system and either used as such or further dried upon storage on freshly activated 3 Å molecular sieves.

Careful degassing of solvents was achieved by three consecutive freeze-pump-thaw cycles. A Schlenk flask half-filled with the respective solvent is frozen in a liquid nitrogen bath and consequently exposed to high vacuum. For high and low boiling solvents, dynamic or static vacuum is applied during thawing, respectively. Once thawed, the steps are repeated twice. Finally, the gas phase is exchanged by vacuum/argon cycles. Due its expanding nature, aqueous solutions were degassed by applying ultrasound for 10 min and consequent argon purge for 30 min.

4.2 Photochemistry

The irradiation experiments were carried in degassed spectroscopy grade solvents (HPLC-MS grade for MeCN). The analytical UV/vis-spectroscopy was performed on a Cary 50 and Cary 60 UV/vis spectrophotometer equipped with a thermostated cell holder at 25 °C if not stated otherwise. The irradiation was performed in a quartz cuvette using either with a 500 W mercury lamp coupled with a grating monochromator or with a 1000 W high pressure Xenon lamp with optical band pass or cut-off filters.

Actinometry was performed using aq. ferrioxalate[102] at 25 °C for wavelengths until 313 nm, Aberchrome 670[161] in toluene at 21 °C for 436 nm and 1,2-bis(2-methyl-1-benzothiophen-3-yl)perfluorocyclopentene[32b] in ^{n}hexane at 22 °C for 436 nm, 492 nm and 546 nm.

Preparative irradiations were performed using 30 mL quartz tubes placed in a Rayonet RPR 100 photochemical reactor equipped with 250 nm, 300 nm, or 350 nm lamps.

Typical procedure for the determination of the pure closed isomer's spectrum:
A solution of a *Z*-aDTE was irradiated stepwise with UV light until the PSS was reached. During this interconversion to the closed isomer, for at least five irradiation steps samples of 100 µl were taken after a sufficient mixing time, and the corresponding spectrum registered. Isomer ratios are determined by *isocratic* UPLC analysis and integration of the respective peaks in the chromatogram's diode array trace at the most bathochromic isosbestic point.[55] The closed form's spectrum was calculated either by a) linear extrapolation to 100% closed isomer using the "trend" function in Microsoft Excel or b) by averaging of all spectra obtained from subtraction of the *Z*-isomer's spectral contribution for each single spectrum registered and subsequent normalization of the residual spectrum to 100%.

[55] Taking into account that isosbestic points may shift slightly under UPLC conditions (MeCN/water + 0.1% FA or $(NH_4)_2CO_3$) as compared to spectroscopy solutions (pure MeCN), the isosbestic points usually were determined in the respective UPLC mixture.

4.3 (Spectro)electrochemistry

Cyclic voltammetry was performed using a PG310 USB (HEKA Elektronik) potentiostat interfaced to a PC with PotMaster v2x43 (HEKA Elektronik) software for data evaluation. A three-electrode configuration contained in a non-divided cell consisting of a platinum disc (d = 1 mm) as working electrode, a platinum plate as counter-electrode, and a saturated calomel electrode (SCE) with an agar-agar-plug in a Luggin capillary with a diaphragm as reference electrode was used. Measurements were carried out in $1 \cdot 10^{-3}$ M solutions in acetonitrile (HPLC-grade, dried over calcium hydride and distilled) containing 0.1 M Bu_4NPF_6 using a scan rate of dE/dt = 1 V s^{-1}. The data is given in reference to the ferrocene redox couple (Fc/Fc^+), which was used as external standard. Cyclic voltammograms of ring-closed isomers of diarylethenes were obtained by irradiation of the electrochemical cell using a standard laboratory UV-lamp equipped with a 313 nm UV-tube (Vilber Lourmat, 6 W).

Spectro-electrochemistry was performed in a SEC-C Thin Layer Quarz Glass Spectro-electrochemical cell, 0.5 or 1.0 mm optical path length, with platinium mesh electrode as a working electrode, counter electrode: platinum wire, reference electrode: non aqueous reference electrode Ag/Ag^+ (0.01 M $AgNO_3$ in 0.1 M Bu_4NPF_6 acetonitrile), ALS Co., Ltd (Tokyo, Japan) spectrometer: AvaSpec-2048x14 with AvaLigth-DH-S-BAL, and AvaSoft 7.7.2, Avantes (Apeldoorn, Netherlands) Potentiostat: PGSTAT 128N, Deutsche Metrohm GmbH & Co. KG (Filderstadt, Germany) and software: NOVA 1.10.

4.4 Transient absorption spectroscopy

The experimental setup used in the group of Prof. Ernsting (Humboldt Universität zu Berlin) has been described in detail elsewhere.[162]

4.5 Synthetic procedures

Synthesis of ketone **3d** from 2,5-dimethylthiophene and 5,5-dimethylbutyrolactone as well as synthesis of aDTEs **$aDTE_{66}(Me_2)$-Me** and **$aDTE_{77}$-Me** was described earlier.[56] 2-(2-iodoethoxy)tetrahydro-2H-pyran was prepared by protection of freshly distilled

2-bromoethanol with freshly distilled DHP under *p*-toluenesulfonic acid catalysis[163] in 71% yield and subsequent Finkelstein exchange[164] with NaI in boiling acetone in 92% yield.

Eaton's reagent[68] was prepared by mixing $MeSO_3H$ and P_4O_{10} in 10:1 w/w, stirring overnight at room temperature and decanting before use.

4.5.1 Synthesis of the simple building blocks

4-(2,5-Dimethylthiophen-3-yl)-4-oxobutanoic acid (1a)

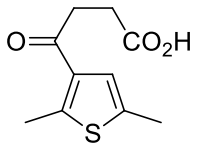

1a

In a 1000 ml three-necked flask, 500 ml dry DCM were cooled to 0 °C and 359.3 g (2.7 mol, 5.5 eq) freshly powdered $AlCl_3$ was added in portions while stirred mechanically. Subsequently, 90.714 g (906.5 mmol, 1.85 eq) succinic anhydride was added to this suspension and stirred for 15 min at low temperature. Then, 54.97 g (490.0 mmol, 1.0 eq) 2,5-dimethylthiophene was added neat to yield an orange suspension. This was stirred at 0 °C for 2 h, then warmed to room temperature and stirred overnight.

The reaction was quenched by pouring on ice, cooled additionally by a cooling bath. After phase separation, the mixture was extracted with 4x 500 ml DCM. The combined organic phases were reduced to about 500 ml under reduced pressure, subsequently extracted with 5x 150 ml 1 M aq. NaOH. The combined aqueous phases were washed with 200 ml DCM, acidified to pH = 1 with 200 ml conc. HCl. The so formed precipitate was collected under suction, washed with 200 ml water and dried under reduced pressure to obtain 72.90 g (343.4 mmol, 70% yield) of the title compound as a light yellow solid that is pure by NMR and used for the next step as such.

^{1}H-NMR (300 MHz, $CDCl_3$): δ [ppm] = 11.28 (bs, 1H), 7.04 – 7.01 (m, 1H), 3.12 (t, *J* = 6.6 Hz, 2H), 2.74 (t, *J* = 6.5 Hz, 2H), 2.66 (s, 3H), 2.42 – 2.39 (m, 3H).
^{13}C-NMR (75 MHz, $CDCl_3$): δ [ppm] = 193.9, 178.6, 148.1, 135.5, 134.9, 125.9, 36.1, 28.1, 16.2, 15.1.
HR-MS (ESI-): *m/z* = 211.046 (calc. 211.043 for $[C_{10}H_{12}O_3S - H]^-$)

Methyl 4-(2,5-dimethylthiophen-3-yl)-4-oxobutanoate (1a-Me)

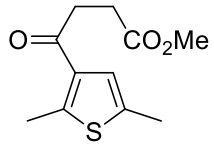

1a-Me

The title compound was obtained by heating 6.580 g (31.0 mmol) ketoacid **1a** with 0.33 ml conc. H_2SO_4 in 35 ml MeOH to reflux for 15 h. Subsequently it was poured on ice, extracted with 3x100 ml EA and the combined organic phases washed with 2x 50 ml 1 M NaOH, dried over $MgSO_4$. After removal of the volatiles, 6.60 g (29.17 mmol, 94% yield) of the title compound were obtained that were pure by TLC and used without further purification.

Methyl 4-(2,5-dimethylthiophen-3-yl)butanoate (2a-Me) and 4-(2,5-dimethyl-thiophen-3-yl)butanoic acid (2a)

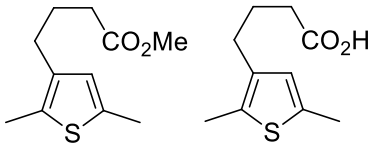

2a-Me **2a**

Reduction of ketoester **1a-Me** with $Et_3SiH/TiCl_4$:

A 500 ml round bottom flask was charged with 5.205 g (23.0 mmol, 1.0 eq) ketoester **1a-Me**, 230 ml dry DCM, 14.7 ml (92.0 mmol, 4.0 eq) Et_3SiH and 10.1 ml (92.0 mmol, 4.0 eq) $TiCl_4$, upon which solution turned red-brown. After stirring at room temperature for 2 h, TLC indicated full conversion to a less polar product. It was poured on ice, and after phase separation extracted with 2x 200 ml DCM. The combined organic phases were washed with water and brine, dried over $MgSO_4$ and concentrated under reduced pressure to yield an oily crude containing silane residues. The crude can used as such for the saponification step or purified by column chromatography (EA/PE 1:5) to afford 4.631 g (21.8 mmol, 94% yield) the reduced ester.

Saponification was carried out in 200 ml 1:1 EtOH/2 M aq. NaOH solution heated to reflux for 6 h. The volatiles were removed under reduced pressure and the mixture washed with 3x 200 ml DCM. After acidification to pH = 1 with conc. HCl it was extracted with 3x 200 ml EA, the combined organic phases dried over $MgSO_4$ and evaporated to obtain the corresponding acid **2a** in quantitative yield.

Clemmensen reduction of ketoacid **1a**:

The procedure was adapted from literature[67]. In a 2000 ml three-necked flask, 28.50 g (105.0 mmol, 0.3 eq) $HgCl_2$ was added to an ice-cold suspension of 297.4 g (4.55 mol, 13.0 eq) zinc in 450 ml water. The fine suspension was treated with 15 ml conc. HCl and shaken for 5 min to yield chunks of amalgamated zinc and a clear solution which was decanted and discarded. The chunks were suspended in 200 ml water, and subsequently treated with 260 ml of AcOH, 470 ml conc. HCl, 350 ml toluene under mechanical stirring at 0 °C. Finally, 74.20 g (350.0 mmol, 1.0 eq) ketoacid **1a** was added neat in small portions to prevent local boiling. After complete addition, the mixture was warmed 120 °C for 20 h with further addition of 100 ml conc. HCl after 8 h of heating. After cooling to room temperature, the phases were separated and further extracted with 3x 500 ml ether. The combined organic phases were concentrated to 1 L, washed with 2x 100 ml water and 100 ml brine and dried over $MgSO_4$. Evaporation of the volatiles under reduced pressure, residual amounts of AcOH were removed on high vacuum overnight to yield 68.40 g (345.0 mmol, 99% yield) of acid **2a** as a grey-beige solid that is pure by NMR and used for the next step without further purification.

Reduced ester **2a-Me**:

^{1}H-NMR (500 MHz, $CDCl_3$): δ [ppm] = 6.44 (s, 1H), 3.66 (s, 3H), 2.50 – 2.43 (m, 2H), 2.37 (s, 3H), 2.31 (t, *J* = 7.5 Hz, 2H), 2.27 (s, 3H), 1.89 – 1.81 (m, 2H).

^{13}C-NMR (126 MHz, $CDCl_3$): δ [ppm] = 174.1, 136.5, 135.3, 130.8, 126.9, 51.6, 33.5, 27.5, 25.7, 15.2, 12.8.

Reduced acid **2a**:

^{1}H-NMR (300 MHz, $CDCl_3$): δ [ppm] = 11.32 (bs, 1H), 6.45 (d, *J* = 0.9 Hz, 1H), 2.50 (t, *J* = 7.5 Hz, 2H), 2.38 (s, 3H), 2.36 (t, *J* = 7.6 Hz, 2H), 2.28 (s, 3H), 1.87 (tt, *J* = 7.5 Hz, 2H).

^{13}C-NMR (75 MHz, $CDCl_3$): δ [ppm] = 179.7, 136.4, 135.4, 130.9, 126.9, 33.4, 27.4, 25.5, 15.3, 12.9.

HR-MS (ESI-): *m*/*z* = 197.066 (calc. 196.065 for $[C_{10}H_{14}O_2S - H]^-$).

1,3-dimethyl-6,7-dihydrobenzo[c]thiophen-4(5H)-one (3a)

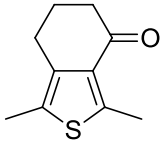

3a

In a 500 ml round bottom flask, 67.42 g (340.0 mmol, 1.0 eq) acid **2a** was dissolved in 150 ml DCM and treated with 150 ml Eaton's reagent[68] under stirring at room

temperature for 24 h. The mixture was poured on ice, diluted with ca 800 ml of water and 150 ml DCM before phase separation. The aqueous phase was further extracted with 2x 300 ml DCM and the combined organic phases were washed with 3x 300 ml 1M NaOH and 100 ml brine and dried over $MgSO_4$. Evaporation of the volatiles under reduced pressure yielded 53.4 g of a brownish solid. This was further purified by sublimation (4x 10^{-1} mbar / 100 °C) to obtain 48.98 g (271.7 mmol, 80% yield) of the title compound as a white solid.

^{1}H-NMR (300 MHz, $CDCl_3$): δ [ppm] = 2.71 (s, 3H), 2.65 (t, *J* = 6.2 Hz, 2H), 2.47 (m, 2H), 2.28 (s, 3H), 2.05 – 1.95 (m, 2H).
^{13}C-NMR (75 MHz, $CDCl_3$): δ [ppm] = 196.2, 147.0, 138.1, 132.3, 127.4, 40.2, 24.8, 23.6, 15.9, 12.6.
HR-MS (ESI+): *m/z* = 181.063 (calc. 181.069 for $[C_{10}H_{12}OS + H]^+$).

Ethyl 5-(2,5-dimethylthiophen-3-yl)-5-oxopentanoate (1b-Et)

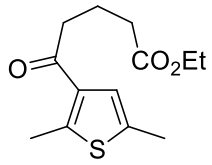

1b-Et

A similar procedure on smaller scale has been published earlier.[56] A 250 ml flask was charged with 160 mL dry DCM, 14.00 g (105.0 mmol, 2.1 eq) freshly powdered $AlCl_3$, cooled to 0° C and treated with 8.931 g (50.00 mmol, 1.0 eq) glutaric acid mono ethyl ester. The mixture was stirred at this temperature for 1 h and subsequently treated with 5.610 g, (50 mmol, 1.0 eq) 2,5-dimethylthiophene in a dropwise manner. The dark red solution was stirred at low temperature for 1 h, then poured on ice. After phase separation, the aqueous phase was extracted with 3x 50 mL DCM, the combined organic phases washed with 30 mL water and brine each, then dried over $MgSO_4$. The solvent was removed under reduced pressure and the crude matter purified by column chromatography (EA/PE 1:9) to yield 11.84 g (46.55 mmol, 93% yield) of the title compound as a light yellow oil.

^{1}H-NMR (300 MHz, $CDCl_3$): δ [ppm] = 6.99 (q, *J* = 1.0 Hz, 1H), 4.12 (q, *J* = 7.1 Hz, 2H), 2.84 (t, *J* = 7.2 Hz, 2H), 2.65 (s, 3H), 2.42 – 2.36 (m, 5H), 2.09 – 1.91 (m, 2H), 1.25 (t, *J* = 7.1 Hz, 3H).
^{13}C-NMR (75 MHz, $CDCl_3$): δ [ppm] = 195.7, 173.5, 147.5, 135.5, 135.2, 126.1, 60.4, 40.6, 33.6, 19.5, 16.2, 15.1, 14.4.
HR-MS (ESI+): *m/z* = 255.105 (calc. 255.077 for $[C_{13}H_{18}O_3S + H]^+$).

5-(2,5-dimethylthiophen-3-yl)-5-oxopentanoic acid (1b)

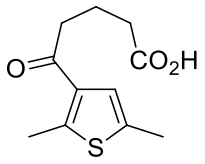

1b

A similar procedure on smaller scale was already published.[165] A 500 ml flask was charged with 25.02 g (219.6 mmol, 1.0 eq) glutaric anhydride and 250 ml dry DCM and subsequently treated with 100.0 g (750.0 mmol, 3.4 eq) freshly powdered $AlCl_3$ at 0 °C. The suspension was warmed to room temperature and 28.05 g (250.0 mmol, 1.14 eq) 2,5-dimethylthiophene added neat. The mixture was stirred for 21 h, poured on ice and after phase separation extracted with 2x 250 ml DCM. The combined organic phases were extracted with 3x 100 ml 2 M NaOH. The combined basic extracts were washed with 100 ml DCM and acidified with conc. HCl to pH = 1, followed by extraction with 3x 250 ml DCM. The combined org. phases were washed with 100 ml water and brine each, dried over $MgSO_4$ and the volatiles evaporated under reduced pressure to yield 27.20 g (120.2 mmol, 55% yield) of the title compound as a light greenish solid that is pure by NMR.

^{1}H-NMR (300 MHz, $CDCl_3$): δ [ppm] = 11.04 (s, 1H), 6.99 (d, *J* = 1.1 Hz, 1H), 2.87 (t, *J* = 7.1 Hz, 2H), 2.65 (s, 3H), 2.47 (t, *J* = 7.2 Hz, 2H), 2.40 (s, 3H), 2.02 (p, *J* = 7.1 Hz, 2H).
^{13}C-NMR (75 MHz, $CDCl_3$): δ [ppm] = 195.6, 179.4, 147.7, 135.4, 135.3, 126.0, 40.5, 33.2, 19.1, 16.2, 15.1.

5-(2,5-Dimethylthiophen-3-yl)pentanoic acid (2b)

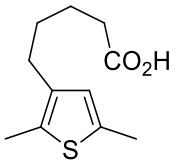

2b

Wolff-Kishner reduction of ketoester **1b-Et**:

The procedure was already published on smaller scale[56] and inspired by a protocol from Thurkauf *et al.*[64a] A 500 ml three-necked flask fitted with reflux condenser was charged with 170 ml triethylene glycole, 6.028 g (23.70 mmol, 1.0 eq) ketoester **1b-Et**, 6.755 g (120.4 mmol, 5.1 eq) KOH and 3.607 g (72.05 mmol, 3.0 eq) hydrazine monohydrate and heated to 160 °C for 1 h. Without distilling off the water and hydrazine, the mixture was

heated to 200 °C for another 7 h until gas evolution ceased. After cooling to room temperature, the yellow solution was treated with 170 ml 1 M HCl and extracted with 5x 100 ml diethyl ether. The combined organic phases were washed with 40 ml water and brine each and dried over $MgSO_4$. The solvent was removed under reduced pressure and the crude product can be used as such for the next step or purified by column chromatography (EA/PE 1:9 + 1 % AcOH) to afford 4.102 g (19.32 mmol, 82 % yield) of the title compound as an greenish oil.

Clemmensen reduction of ketoacid **1b**:

A 500 ml three-necked flask fitted with reflux condenser was charged with 70 ml water and 106.6 g (1.6 mol, 13.8 eq) zinc dust and treated with 10.26 g (37.80 mmol, 0.32 eq) $HgCl_2$ and 5.5 ml conc. HCl under stirring at 0 °C for 5 min before the aq. phase was decanted and discarded. The amalgamated zinc was taken up in 70 ml water, 95 ml AcOH, 170 ml conc. HCl and 125 ml toluene, cooled to 0 °C and 26.73 g (118 mmol, 1.0 eq) ketoacid **1b** added carefully in small portions. Heated to 110 °C for 22 h until TLC indicated full conversion to a less polar product, then poured on ice. After phase separation, the aqueous phase was extracted with 3x 100 ml EA and the combined org. phases washed with 2x 50 ml water and 50 ml brine, dried over $MgSO_4$ and concentrated under reduced pressure. Residual AcOH was azeotropically removed by threefold addition of 20 ml toluene and evaporation under reduced pressure to yield 25.00 g (118 mmol, quant.) of the title compound.

^{1}H-NMR (500 MHz, $CDCl_3$): δ [ppm] = 7.17 (bs, 1H), 6.44 (q, *J* = 1.4 Hz, 1H), 2.45 (t, *J* = 7.5 Hz, 2H), 2.39 – 2.34 (m, 5H), 2.27 (s, 3H), 1.70 – 1.54 (m, 4H).
^{13}C-NMR (126 MHz, $CDCl_3$): δ [ppm] = 179.8, 137.2, 135.2, 130.3, 126.9, 34.0, 30.0, 27.9, 24.5, 15.35, 12.9.
HR-MS (ESI-): *m*/*z* = 211.086 (calc. 211.080 for $[C_{11}H_{16}O_2S\ -H]^-$).

1,3-Dimethyl-5,6,7,8-tetrahydro-cyclohepta[c]thiophen-4-one (3b)

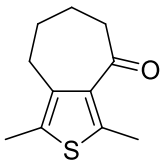

3b

The procedure was already published on smaller scale.[56] A 100 mL flask was charged, 53 mL of Eaton's reagent[68] and 11.25 g (53.0 mmol, 1.0 eq) acid **2b** and stirred at room

temperature for 19 h until TLC indicated full conversion to a less polar product. Water was added and the resulting green suspension extracted with 3x 50 ml EA. The combined organic phases were washed with 50 mL water and brine each and dried over $MgSO_4$. The crude compound was purified by column chromatography (EA/PE 1:10) to afford 8.110 g (41.74 mmol, 79 % yield) of the title compound as a greenish solid. Further purification by sublimation is possible.

^{1}H-NMR (500 MHz, $CDCl_3$): δ [ppm] = 2.73 – 2.67 (m, 2H), 2.66 – 2.61 (m, 2H), 2.55 (s, 3H), 2.28 (s, 3H), 1.84 – 1.73 (m, 4H).
^{13}C-NMR (126 MHz, $CDCl_3$): δ [ppm] = 200.8, 143.8, 138.1, 136.8, 128.4, 41.4, 25.1, 25.0, 21.9, 15.4, 12.8.
HR-MS (ESI+): *m/z* = 195.068 (calc.195.084 for $[C_{11}H_{14}OS+H]^+$).

Methyl 3-(2,5-dimethylthiophen-3-yl)-3-oxopropanoate (1c-Me)

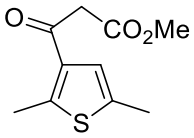

1c-Me

The procedure was adapted from literature.[81,88] A 250 ml three-necked flask equipped with reflux condenser was charged with 5.206 g (130.2 mmol, 2.8 eq) 60% NaH dispersion, 40 ml dry toluene and 8.14 ml (8.377 g, 93.0 mmol, 2.0 eq) dimethyl carbonate. The mixture was heated to 120 °C and 7.172 g (46.5 mmol, 1.0 eq) commercial 3-Acyl 2,5-dimethylthiophene in 30 ml toluene were added in small portions so that gas evolution was kept moderate. After full addition, stirred at this temperature for 1 h until TLC shows full conversion to more polar product. The mixture was slowly poured on ice, acidified to pH = 1 with conc. HCl. After phase separation it was extracted with 2x 100 ml EA, the combined organic phases dried over $MgSO_4$ and the volatiles evaporated. The crude compound was purified by MPLC (EA/CyHex 0-10%) to yield 8.834 g (41.6 mmol, 90% yield) of the title compound as a light brown oil containing about 6% enol tautomer.

Ketoester **1c-Me**:
^{1}H-NMR (500 MHz, $CDCl_3$): δ [ppm] = 6.92 (d, *J* = 1.0 Hz, 1H), 3.81 (s, 2H), 3.74 (s, 3H), 2.65 (s, 3H), 2.40 – 2.38 (m, 3H).
^{13}C-NMR (126 MHz, $CDCl_3$): δ [ppm] = 187.8, 168.2, 149.6, 135.7, 134.4, 125.9, 52.5, 48.5, 16.2, 15.1.
HR-MS (ESI+): *m/z* = 213.057 (calc. 213.058 for $[C_{10}H_{12}O_3S+H]^+$).

Enolester:

^{1}H-NMR (500 MHz, $CDCl_3$): δ [ppm] = 12.43 (s, 1H), 6.77 (d, *J* = 0.7 Hz, 1H), 5.29 – 5.28 (m, 1H), 3.75 (s, 3H), 2.57 (s, 3H), 2.36 (s, 3H).

^{13}C-NMR (126 MHz, $CDCl_3$): δ [ppm] = 173.8, 169.7, 141.2, 135.9, 130.6, 124.9, 88.0, 53.5, 51.3, 15.6.

3-(2,5-Dimethylthiophen-3-yl)propanoic acid (2c)

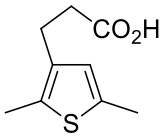

2c

The procedure was adapted from literature.[87] A 250 ml 3-neck flask was charged with 26.35 g (403 mmol, 13.0 eq) Zn and 2.964 g (9.30 mmol, 0.3 eq) $Hg(OAc)_2$, 50 ml water and 2 ml conc. HCl. After stirring at room temperature for 10 min, the aqueous layer was decanted and discarded. The amalgam was treated with 20 ml water, 30 ml AcOH and cooled to 0 C. After addition of 40 ml conc. HCl, 6.580 g (31.0 mmol, 1.0 eq) ketoester **1c-Me** in 50 ml dry toluene was added slowly to prevent strong gas evolution. After full addition, the mixture was heated to 120 °C for 4 h until TLC shows conversion to a major, apolar and a minor, polar product. The mixture was worked up by decanting from the amalgam, phase separation and extraction with 2x 50 ml Et_2O. The volatiles were evaporated and the crude mixture taken up in 120 ml 1:1 EtOH/ 2 M aq. NaOH solution and heated to reflux for 2 h until disappearance of the apolar intermediate. Ethanol was removed under reduced pressure, and the residual brown solution washed with 2x 30 ml DCM. It was acidified with conc. HCl, then extracted with 3x 30 ml DCM. The combined organic phases were dried over $MgSO_4$, and the volatiles removed under reduces pressure. Residues of AcOH were azeotropically removed by threefold addition of 20 ml toluene and evaporation under reduced pressure to yield 5.144 g (27.92 mmol, 90% yield) of the title compound as a beige oil that crystallizes upon cooling to room temperature.

^{1}H-NMR (300 MHz, $CDCl_3$): δ [ppm] = 11.52 (bs, 1H), 6.47 (d, *J* = 0.9 Hz, 1H), 2.78 (t, *J* = 7.7 Hz, 2H), 2.62 – 2.55 (m, 2H), 2.40 – 2.37 (m, 3H), 2.31 (s, 3H).

^{13}C-NMR (75 MHz, $CDCl_3$): δ [ppm] = 179.6, 135.7, 135.2, 131.3, 126.4, 34.9, 23.3, 15.3, 12.6.

HR-MS (ESI-): *m*/*z* = 183.049 (calc. 183.049 for $[C_9H_{12}O_2S\text{ -H}]^-$).

1,3-Dimethyl-5,6-dihydro-4H-cyclopenta[c]thiophen-4-one (3c)

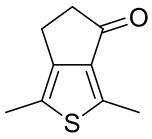

3c

A 100 ml round bottom flask was charged with 5.113 g (27.75 mmol, 1.0 eq) acid **2c**, 30 ml DCM and 30 ml Eaton's reagent[68] and stirred for 8 h at room temperature until TLC shows total consumption of the starting material, the product coloring deep red with Brady's reagent.[160] The resulting red oil was poured on ice and extracted with 3x 50 ml DCM. The combined organic phases were washed with 30 ml 1 M NaOH, dried over $MgSO_4$ and the volatiles evaporated under reduced pressure. MPLC (EA/CyHex 0-20%) yielded 2.591 g (15.58 mmol, 56% yield) of the title compound as a light yellow solid.

^{1}H-NMR (300 MHz, $CDCl_3$): δ [ppm] = 2.95 – 2.88 (m, 2H), 2.78 – 2.70 (m, 2H), 2.60 (s, 3H), 2.29 (d, *J* = 0.6 Hz, 3H).
^{13}C-NMR (75 MHz, $CDCl_3$): δ [ppm] = 199.3, 149.4, 140. 5, 139.8, 126.8, 43.6, 20.4, 13.4, 12.5.
HR-MS (ESI+): *m/z* = 167.054 (calc. 167.053 for $[C_9H_{10}OS+H]^+$).

2,5-Dimethylthiophene-3-carbaldehyde (11)

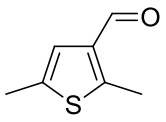

11

The procedure was adapted from literature[95]. In a 250 ml round bottom flask, 4.039 g (36.0 mmol, 1.2 eq) 2,5-dimethylthiophene in 30 ml dry DCM was treated with 4.9 ml (8.535 g, 45.0 mmol, 1.5 eq) $TiCl_4$ at 0 °C. Subsequently, 3.449 g (30.0 mmol, 1.0 eq) dichloro(methoxy)methane was slowly added under strong gas evolution. The mixture was stirred to room temperature for 30 min, when TLC indicated conversion to a more polar major spot that stains red with Brady's reagent[160]. The reaction mix was poured on ice, extracted with 3x 50 ml DCM and the combined organic phases washed with 50 ml water, sat. $NaHCO_3$ and water each, dried over $MgSO_4$, and the volatiles evaporated under reduced pressure to yield a brown oil. MPLC (EA/CyHex) yielded 2.070 g (14.8 mmol, 49% yield) of the title compound as a yellow oil.

^{1}H-NMR (300 MHz, $CDCl_3$): δ [ppm] = 9.93 (s, 1H), 7.00 (d, *J* = 1.1 Hz, 1H), 2.70 (s, 3H), 2.40 (d, *J* = 0.5 Hz, 3H).

^{13}C-NMR (75 MHz, $CDCl_3$): δ [ppm] = 184.5, 150.7, 137.3, 137.0, 124.4, 15.1, 13.5.
HR-MS (ESI+): *m/z* = 141.037 (calc. 141.037 for $[C_7H_8OS + H]^+$).

4.5.2 Synthesis of the functionalizable building blocks

Ethyl 4-(2,5-dichlorothiophen-3-yl)-4-oxobutanoate (4a)

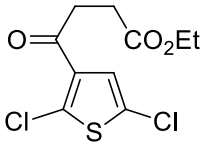

4a

In a 250 ml round bottom flask, 16.46 g (100.0 mmol, 1.0 eq) succinic ethyl ester acid chloride was added over 1 min to a solution of 40.00 g (300.0 mmol, 3.0 eq) $AlCl_3$ granules in 150 ml $MeNO_2$ at 0 °C. The resulting mixture stirred at low temperature for 30 min, and consequently 15.30 g (100.0 mmol, 1.0 eq) 2,5-dichlorothiophene was added neat over 3 min whereupon the solution turned red. It was stirred to room temperature for 2 h when TLC shows complete conversion to a more polar product. The reaction mix was poured on ice, acidified with conc. HCl and after phase separation extracted with 3x 100 ml EA. The combined organic phases were washed with 100 ml 1 M NaOH and 50 ml brine, dried over $MgSO_4$ and evaporated to yield 22.32 g of the title compound as a crude brown oil that was used as such for the next step. The product can be purified by column chromatography (EA/PE 1:10).

^{1}H-NMR (300 MHz, $CDCl_3$): δ [ppm] = 7.20 (s, 1H), 4.14 (q, *J* = 7.1 Hz, 2H), 3.20 (t, *J* = 6.5 Hz, 2H), 2.69 (t, *J* = 6.5 Hz, 2H), 1.25 (t, *J* = 7.1 Hz, 3H).
^{13}C-NMR (75 MHz, $CDCl_3$): δ [ppm] = 191.4, 172.6, 136.5, 132.6, 127.0, 126.9, 60.8, 36.9, 28.1, 14.3.
HR-MS (ESI+): *m/z* = 280.982 (calc. 280.981 for $[C_{10}H_{10}Cl_2O_3S + H]^+$).

Ethyl 4-(2,5-dichlorothiophen-3-yl)-4-oxobutanoate (5a-Et)

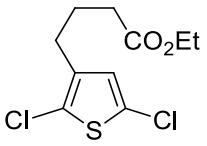

5a-Et

In a 1000 ml round bottom flask, the crude ketoester **4a** was taken up in 600 ml dry DCM. At 0 °C, the solution was treated with 35.14 ml (25.58 g, 220.0 mmol, 2.2 eq) Et_3SiH and subsequently, 23.03 ml (39.83 g, 210 mmol, 2.1 eq) $TiCl_4$ were added over 5 min. It was stirred at 0 °C for 30 min, then warmed to room temperature. After 2 h

total, TLC indicates full conversion to a less polar product that stained only slightly with Brady's reagent.[160] The mixture was poured on ice and after phase separation extracted with 3x 100 ml DCM. The combined organic phases were washed with 100 ml brine, dried over $MgSO_4$ and evaporated to yield the title compound as a crude brown oil containing residual silane and its reaction products. It can be was used as such for the next step or purified by MPLC (EA/CyHex).

^{1}H-NMR (300 MHz, $CDCl_3$): δ [ppm] = 6.64 (s, 1H), 4.12 (q, *J* = 7.1 Hz, 2H), 2.61 – 2.50 (m, 2H), 2.30 (t, *J* = 7.4 Hz, 2H), 1.94 – 1.80 (m, 2H), 1.25 (t, *J* = 7.1 Hz, 3H).
^{13}C-NMR (75 MHz, $CDCl_3$): δ [ppm] = 173.2, 138.0, 126.9, 126.1, 122.3, 60.5, 33.5, 27.6, 24.7, 14.4.

4-(2,5-dichlorothiophen-3-yl)butanoic acid (5a)

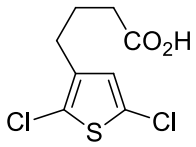

5a

In a 500 ml round bottom flask, the crude ester **5a-Et** was taken up in 320 ml 2 M NaOH/EtOH (1:1) and heated to reflux for 3 h when TLC showed complete conversion to a polar product. All volatiles were evaporated under reduced pressure at 60 °C. The mixture was diluted with 200 ml 2 M NaOH and washed threefold with ether to remove silicon residues. The aqueous phase was acidified to pH = 1 with conc. HCl, extracted with 3x 150 ml EA and the combined EA phases dried over $MgSO_4$. Evaporation under reduced pressure yielded 15.67 g (65.4 mmol, 65% yield over three steps) of the title compound as a light brown oil that solidifies at room temperature and is pure by NMR.

^{1}H-NMR (300 MHz, $CDCl_3$): δ [ppm] = 11.20 (bs, 1H), 6.65 (s, 1H), 2.59 (t, *J* = 7.4 Hz, 2H), 2.39 (t, *J* = 7.4 Hz, 2H), 1.98 – 1.83 (m, 2H).
^{13}C-NMR (75 MHz, $CDCl_3$): δ [ppm] = 179.8, 137.8, 126.9, 126.3, 122.4, 33.2, 27.3, 24.4.

1,3-dichloro-6,7-dihydrobenzo[c]thiophen-4(5H)-one (6a)

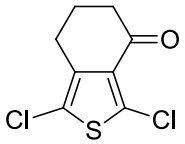

6a

In a 250 ml round bottom flask, the crude acid **5a** was treated with 150 ml conc. H_2SO_4 and stirred at room temperature for 1 h when TLC showed complete conversion to a less polar product. The mixture was poured on ice, extracted with 3x 250 ml EA and the combined organic phases washed with 2x 100 ml 1 M NaOH and 100 ml brine, dried over $MgSO_4$ and evaporated to yield 10.64 g (48.14 mmol, 48% yield over four steps) of the title compound as a light brown oil that readily crystalizes upon cooling to a give white solid that is pure by NMR.

^{1}H-NMR (500 MHz, $CDCl_3$): δ [ppm] = 2.78 – 2.73 (m, 2H), 2.57 – 2.51 (m, 2H), 2.10 – 2.01 (m, 2H).
^{13}C-NMR (126 MHz, $CDCl_3$): δ [ppm] = 192.5, 138.8, 133.6, 131.0, 120.3, 110.1, 39.8, 24.8, 22.6.
HR-MS (ESI+): *m/z* = 220.959 (calc. 220.959 for $[C_8H_6Cl_2OS + H]^+$).

1-chloro-3-methyl-6,7-dihydrobenzo[c]thiophen-4(5H)-one (7a)

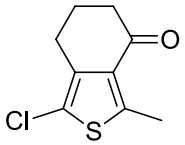

7a

Under inert conditions in a three-necked round bottom flask fitted with reflux condenser, 9.950 g (45.0 mmol, 1.0 eq) ketone **7a**, 4.121 g (4.50 mmol, 0.1 eq) $Pd_2(dba)_3$ and 5.512 g (18.0 mmol, 0.4 eq) $AsPh_3$ were degassed with three vacuum/argon cycles and subsequently suspended in 200 ml degassed, dry DMF. Addition of Me_4Sn, then heated to 60 °C for 5 h after which TLC indicates full conversion to a less polar product. The reaction mix is treated with 200 ml 1 M aq. KF solution and stirred at room temperature overnight. Worked up by addition of 1.5 l of water and consequent extraction with 3x 400 ml of DCM to yield a reddish organic phase and a clear aqueous phase. The combined organic phases were washed with 400 ml of water and 200 ml brine, dried over $MgSO_4$ and evaporated under reduced pressure to yield a black oil that was purified by column chromatography (EA/PE 1:15) to afford 6.07 g (30.28 mmol, 67% yield) of the title compound as a yellow oil that crystalized upon storage.

^{1}H-NMR (300 MHz, $CDCl_3$): δ [ppm] = 2.75 – 2.70 (m, 2H), 2.72 (s, 3H), 2.53 – 2.47 (m, 2H), 2.07 – 1.97 (m, 2H).
^{13}C-NMR (75 MHz, $CDCl_3$): δ [ppm] = 195.2, 147.7, 139.2, 131.4, 118.8, 40.0, 24.7, 23.0, 16.0.
HR-MS (ESI+): *m/z* = 201.015 (calc. 201.014 for $[C_9H_9ClOS + H]^+$).

Methyl 5-(2,5-dichlorothiophen-3-yl)-5-oxopentanoate (4b)

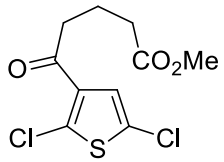

4b

In a 250 ml round bottom flask, a 1 M solution of 9.999 g (60.75 mmol, 1.0 eq) glutaric acid monomethyl ester chloride in $MeNO_2$ was treated with 24.30 g (182.3 mmol, 3.0 eq) $AlCl_3$ granules at 0 °C. The mixture was warmed to room temperature and stirred for 15 min, then cooled again to 0 °C and 9.296 g (60.75 mmol, 1.0 eq) 2,5-dichlorothiophene added in one portion. The mixture was warmed to room temperature and stirred for 2 h, when TLC indicated full conversion to one more polar product. The solution was poured on ice, extracted with 3x 100 ml DCM, the combined organic phases washed with 3x 50 ml 1 M NaOH, 50 ml water and brine, dried over $MgSO_4$ and the volatiles removed under reduced pressure to yield 15.00 g (53.35 mmol, 88% yield) of the title compound as an off-white solid, which was used as such for the next step.

^{1}H-NMR (500 MHz, $CDCl_3$): δ [ppm] = 7.18 (s, 1H), 3.67 (s, 3H), 2.95 (t, *J* = 7.1 Hz, 2H), 2.41 (t, *J* = 7.2 Hz, 2H), 2.01 (psq, *J* = 7.2 Hz, 2H).
^{13}C-NMR (126 MHz, $CDCl_3$): δ [ppm] = 192.6, 173.7, 136.7, 132.3, 127.1, 126.9, 51.7, 41.0, 33.0, 19.0.
HR-MS (ESI+): *m/z* = 280.974 (calc. 280.981 for $[C_{10}H_{10}Cl_2O_3S + H]^+$).

Methyl 5-(2,5-dichlorothiophen-3-yl)pentanoate (5b-Me)

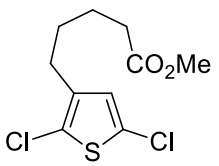

5b-Me

A 1000 ml round bottom flask was charged with 15.00 g (53.35 mmol, 1.0 eq) crude ketoester **4b**, 530 ml dry DCM, 34.1 ml (24.81 g, 213.4 mmol, 4.0 eq) $HSiEt_3$ and 23.4 ml (40.48 g, 213.4 mmol, 4.0 eq) $TiCl_4$ and consequently stirred at room temperature for 17 h, when TLC indicated full conversion to one less polar product. The reaction mixture

was poured on ice, the phases separated, and the aqueous phase extracted further with 2x 100 ml DCM. The combined organic phases were washed with 100 ml water and brine each, dried over $MgSO_4$ and the volatiles removed under reduced pressure to yield a crude oil brown that contains residual silane. It can be was used as such for the next step or purified by MPLC (EA/CyHex).

^{1}H-NMR (500 MHz, $CDCl_3$): δ [ppm] = 6.63 (s, 1H), 3.67 (s, 3H), 2.52 (t, *J* = 7.4 Hz, 2H), 2.34 (t, *J* = 7.3 Hz, 2H), 1.69 – 1.54 (m, 4H).
^{13}C-NMR (126 MHz, $CDCl_3$): δ [ppm] = 174.0, 138.6, 126.9, 126.0, 121.9, 51.7, 33.9, 29.0, 27.8, 24.5.
HR-MS (ESI+): *m*/*z* = 266.976 (calc. 267.001 for $[C_{10}H_{12}Cl_2O_2S + H]^+$).

5-(2,5-dichlorothiophen-3-yl)pentanoic acid (5b)

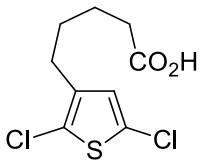

5b

In a 500 ml round bottom flask, the crude ester **5b-Me** was taken up in 500 ml 2 M NaOH/EtOH (1:1) and heated to reflux for 2.5 h, when TLC showed complete conversion to a polar product. All volatiles were evaporated under reduced pressure at 60 C. The remaining aqueous phase was washed with 3x 100 ml DCM remove silicon residues and subsequently acidified to pH = 1 with conc. HCl and extracted with 3x 150 ml DCM. The combined organic phases were dried over $MgSO_4$. Evaporation under reduced pressure yielded 6.750 g (26.66 mmol, 50% yield over two steps) as a yellow oil that solidifies in the fridge and is sufficiently pure as determined by NMR.

^{1}H-NMR (500 MHz, $CDCl_3$): δ [ppm] = 11.48 (bs, 1H), 6.63 (s, 1H), 2.53 (t, *J* = 7.3 Hz, 2H), 2.38 (t, *J* = 7.2 Hz, 2H), 1.70 – 1.56 (m, 4H).
^{13}C-NMR (126 MHz, $CDCl_3$): δ [ppm] = 180.3, 138.5, 126.9, 126.0, 121.9, 33.9, 28.9, 27.7, 24.1.
HR-MS (ESI-): *m*/*z* = 250.975 (calc. 250.971 for $[C_9H_{10}Cl_2O_2S - H]^-$).

1,3-dichloro-5,6,7,8-tetrahydro-4H-cyclohepta[c]thiophen-4-one (6b)

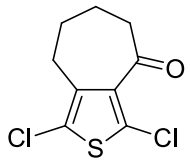

6b

In a 100 ml round bottom flask, 5.316 g (21.00 mmol, 1.0 eq) acid **5b** in 21 ml dry DCM was treated carefully with 2.0 ml (2.932 g, 23.10 mmol, 1.1 eq) oxalyl chloride at room temperature. After the strong gas evolution ceased, three drops of DMF were added. After reaction control by TLC (aliquot quenched with dry MeOH) indicated full conversion, the solvent was removed under reduced pressure without heating to yield a dark brown oil. The crude acid chloride was taken up in 23 ml dry DCM and treated with 7.000 g (52.50 mmol, 2.5 eq) freshly powdered $AlCl_3$ at 0 °C. It was warmed to room temperature and stirred for 18 h. The reaction mixture was poured on ice, the phases separated, and the aqueous phase extracted further with 2x 50 ml DCM. The combined organic phases were washed with 20 ml water and brine each, dried over $MgSO_4$ and the volatiles removed under reduced pressure to yield dark brown oil that was purified by MPLC (EA/CyHex) to yield 4.185 g (17.80 mmol, 85% yield) of the title compound as an off-white solid. Further purification is possible by sublimation.

^{1}H-NMR (500 MHz, $CDCl_3$): δ [ppm] = 2.84 – 2.77 (m, 2H), 2.71 – 2.64 (m, 2H), 1.89 – 1.77 (m, 4H).
^{13}C-NMR (126 MHz, $CDCl_3$): δ [ppm] = 197.2, 137.3, 130.3, 121.5, 41.7, 25.8, 24.7, 22.4.
HR-MS (ESI+): *m/z* = 234.975 (calc. 234.974 for $[C_9H_8Cl_2OS + H]^+$).

1-chloro-3-methyl-5,6,7,8-tetrahydro-4H-cyclohepta[c]thiophen-4-one (7b), 3,3'-dichloro-6,6',7,7'-tetrahydro-4H,4'H-[1,1'-bi(cyclohepta[c]thiophene)]-8,8'(5H,5'H)-dione (8) and 1-chloro-3-phenyl-5,6,7,8-tetrahydro-4H-cyclohepta[c]thiophen-4-one (9)

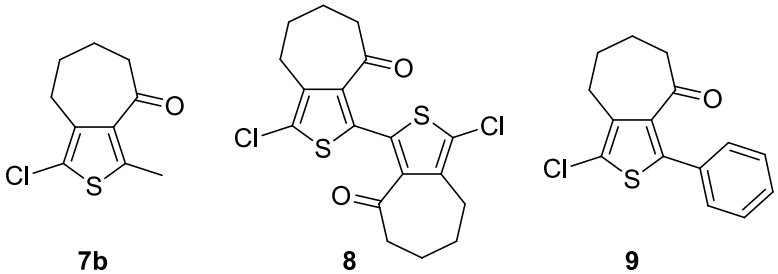

7b **8** **9**

Under inert conditions in a 250 ml two-necked flask with reflux condenser, 0.801 g (0.875 mmol, 0.05 eq) $Pd_2(dba)_3$ and 1.072 g (3.50 mmol, 0.2 eq) $AsPh_3$ were suspended

in 70 ml dry degassed DMF and 4.115 g (17.5 mmol, 1.0 eq) ketone **6b** in 10 ml DMF and 7.28 ml (52.5 mmol, 3.0 eq) $SnMe_4$ added. The green suspension was heated to 60 °C for 24 h until UPLC showed full conversion, then treated with 100 ml 1 M aq. KF solution and stirred at room temperature overnight. The mixture was extracted with 3x 100 ml DCM, the combined organic phases washed with 3x 100 ml water and 100 ml brine, dried over $MgSO_4$ and volatiles removed under reduced pressure. MPLC (EA/CyHex) yielded 0.950 g (2.378 mmol, 27% yield) dimer **8** and methyl-substituted ketone **7b** as a mixture with the phenyl-substituted ketone **9**. Separation of the two compounds could be achieved by bulb-to-bulb distillation, or better by careful manual column chromatography (EA/PE 1:19) which yielded 0.302 g (1.090 mmol, 6% yield) phenyl ketone **9** and 1.885 g (8.779 mmol, 50% yield) of the methylated ketone **7b** as a white solid. Dimer **8** was recrystallized from hot CyHex to yield yellow crystals. Crystals of phenylated ketone **9** suitable for single crystal x-ray analysis were obtained by two-fold recrystallization from hot CyHex with a little amount of EA.

Methylated ketone **7b**:

^{1}H-NMR (500 MHz, $CDCl_3$): δ [ppm] = 2.83 – 2.77 (m, 2H), 2.67 – 2.62 (m, 2H), 2.54 (s, 3H), 1.86 – 1.76 (m, 4H).

^{13}C-NMR (126 MHz, $CDCl_3$): δ [ppm] = 199.4, 144.6, 137.9, 137.0, 120.4, 41.5, 25.3, 24.5, 22.0, 15.5.

HR-MS (ESI+): *m*/*z* = 215.030 (calc. 215.030 for $[C_{10}H_{11}ClOS+H]^+$).

Dimer **8**:

^{1}H-NMR (300 MHz, $CDCl_3$): δ [ppm] = 2.90 – 2.78 (m, 4H), 2.70 – 2.59 (m, 4H), 1.96 – 1.77 (m, 8H).

HR-MS (ESI+): *m*/*z* = 399.007 (calc. 399.005 for $[C_{18}H_{16}Cl_2O_2S_2+H]^+$).

Phenylated ketone **9**:

^{1}H-NMR (500 MHz, $CDCl_3$): δ [ppm] = 7.44 – 7.39 (m, 2H), 7.38 – 7.34 (m, 3H), 2.88 – 2.83 (m, 2H), 2.73 – 2.68 (m, 2H), 1.95 – 1.83 (m, 4H).

^{13}C-NMR (126 MHz, $CDCl_3$): δ [ppm] = 200.4, 144.2, 137.9, 137.6, 132.5, 129.6, 128.8, 128.5, 124.1, 42.3, 25.9, 25.1, 23.2.

HR-MS (ESI+): *m*/*z* = 277.046 (calc. 277.045 for $[C_{15}H_{13}ClOS+H]^+$).

1-(3,5-bis(trifluoromethyl)phenyl)-3-methyl-6,7-dihydrobenzo[c]thiophen-4(5H)-one (10)

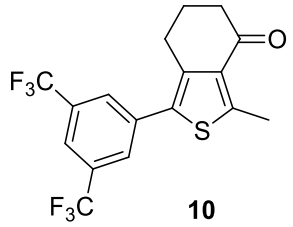

10

The synthesis was adapted from literature.[166] Under inert conditions, a 100 ml Schlenk flask was charged with 0.602 g (3.00 mmol, 1.0 eq) ketone **7a**, 0.067 g (0.30 mmol, 0.1 eq) $Pd(OAc)_2$, 0.172 g (0.36 mmol, 0.12 eq) XPhos and 1.161 g (4.50 mmol, 1.5 eq) 3,5-Bis(trifluoromethyl)phenylboronic acid and degassed by vacuum/argon cycles. Subsequently, 50 ml of degassed ^{n}BuOH was added and stirred for 15 min at room temperature. Then, 0.856 g (5.10 mmol, 1.7 eq) CsOH-hydrate as a 1.2 M degassed, aqueous solution was added at once and stirred at 80 °C overnight. Though the starting material and product are indistinguishable by TLC, UPLC indicates full conversion. The mixture was diluted with water and extracted with 3x 100 ml EA. The combined organic phases were dried over $MgSO_4$ and the volatiles evaporated. Column chromatography (EA/PE 1:50) afforded 0.960 g (2.54 mmol, 85% yield) of the title compound.

^{1}H-NMR (500 MHz, $CDCl_3$): δ [ppm] = 7.84 (s, 2H), 7.82 (s, 1H), 2.93 – 2.87 (m, 2H), 2.84 (s, 3H), 2.62 – 2.55 (m, 2H), 2.09 – 2.01 (m, 2H).
^{13}C-NMR (126 MHz, $CDCl_3$): δ [ppm] = 195.6, 151.2, 140.34, 135.9, 133.2, 132.2 (q, J = 33.4 Hz), 129.1, 128.4 (q, J = 4.2 Hz), 123.1 (q, J = 272.8 Hz), 121.0 – 120.8 (m), 39.9, 26.4, 23.6, 16.2.
^{19}F NMR (471 MHz, $CDCl_3$) δ [ppm] = -63.18.
HR-MS (ESI+): m/z = 379.061 (calc. 379.059 for $[C_{17}H_{12}F_6OS + H]^+$).

4.5.3 Reductive couplings of the building blocks

General procedure for an intermolecular McMurry coupling

The procedure is inspired by a protocol from T. Mukaiyama and co-workers[70] and the "instant method" from A. Fürstner and co-workers[69]. Under inert conditions in a two-necked round bottom flask equipped with a reflux condenser 1.5 eq $TiCl_4$ were slowly dissolved in the given amount of dry THF at 0 °C (0.4 M solution of substrate). After short stirring, 3.0 eq Zn dust were added to the yellow solution, followed by 1.0 eq of substrate and 1.0 eq of dry pyridine. The resulting greenish to brown suspension was

stirred at 80 °C until TLC showed full conversion to one to two apolar products. Consequently, the reaction mixture was treated with half the volume of 1 M HCl, and the mixture extracted with dichloromethane. The combined organic phases were washed with water and brine, dried over $MgSO_4$ and the solvent removed under reduced pressure. The crude product was purified by column chromatography to afford the respective alkene.

1,2-Bis(2,5-dimethylthiophen-3-yl)ethene (12)

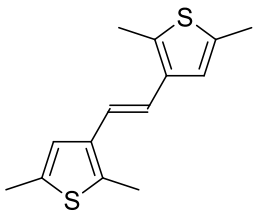

12

Synthesized according to the general procedure for intermolecular McMurry couplings. 0.701 g (5.0 mmol, 1.0 eq) aldehyde **11**, 0.83 ml (1.423 g, 7.50 mmol, 1.5 eq) $TiCl_4$, 0.981 g (15.0 mmol, 3.0 eq) Zn dust and 0.40 ml (0.396 g, 5.00 mmol, 1.0 eq) pyridine were heated for 3 h in 30 ml dry THF. Column chromatography (CyHex) afforded 0.349 g (1.41 mmol, 56% yield) of the title compound with an excess of the *E*-isomer (about 95:5 by NMR of crude). The *Z*-isomer was obtained by preparative irradiation of $2 \cdot 10^{-3}$ M solution of the *E*-isomer in MeCN with 16x 300 nm bulbs for 13 min (PSS determined 16:84 by UPLC) and subsequent purification by column chromatography (CyHex). The *E*-isomer was obtained as a white powder, the *Z*-isomer as clear oil.

<u>*E*-isomer:</u>

^{1}H-NMR (500 MHz, $CDCl_3$): δ [ppm] = 6.89 (d, *J* = 0.9 Hz, 2H), 6.72 (s, 2H), 2.44 – 2.42 (m, 6H), 2.42 (s, 6H).

^{13}C-NMR (126 MHz, $CDCl_3$): δ [ppm] = 136.0, 135.4, 132.9, 123.0, 120.7, 15.4, 13.1.

HR-MS (ESI+): *m*/*z* = 249.076 (calc. 249.077 for $[C_{14}H_{17}S_2 + H]^+$).

<u>*Z*-isomer:</u>

^{1}H-NMR (300 MHz, $CDCl_3$): δ [ppm] = 6.41 (s, 2H), 6.32 (s, 2H), 2.34 (s, 6H), 2.25 (s, 6H).

^{13}C-NMR (75 MHz, $CDCl_3$): δ [ppm] = 135.0, 134.7, 134.2, 126.2, 122.9, 15.3, 13.6.

HR-MS (ESI+): *m*/*z* = 249.075 (calc. 249.077 for $[C_{14}H_{17}S_2 + H]^+$).

3,3'-(But-2-ene-2,3-diyl)bis(2,5-dimethylthiophene) (13)

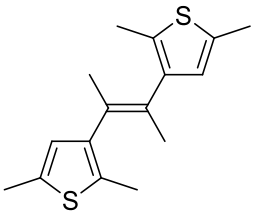

13

Synthesized according to the general procedure for intermolecular McMurry couplings. 0.771 g (5.0 mmol, 1.0 eq) 1-(2,5-dimethylthiophen-3-yl)ethanone, 0.83 ml (1.423 g, 7.50 mmol, 1.5 eq) $TiCl_4$, 0.981 g (15.0 mmol, 3.0 eq) Zn dust and 0.40 ml (0.396 g, 5.00 mmol, 1.0 eq) pyridine were heated for 3 h in 25 ml dry THF. Column chromatography (CyHex) afforded 0.577 g (2.09 mmol, 83% yield) of the title compound with an excess of the *E*-isomer (about 80:20 by NMR and UPLC of mixture). The isomers can be separated by preparative HPLC (PhHex, MeCN/H_2O/THF) or recycling GPC.

E-isomer:

^{1}H-NMR (300 MHz, $CDCl_3$): δ [ppm] = 6.48 (d, *J* = 1.0 Hz, 2H), 2.49 – 2.40 (m, 6H), 2.29 (s, 6H), 1.71 (s, 6H).

^{13}C-NMR (75 MHz, $CDCl_3$): δ [ppm] = 140.4, 135.6, 130.8, 129.5, 126.3, 21.4, 15.4, 13.8.

HR-MS (ESI+): *m/z* = 249.075 (calc. 249.077 for $[C_{14}H_{17}S_2 + H]^+$).

Z-isomer:

^{1}H-NMR (500 MHz, $CDCl_3$): δ [ppm] = 6.25 (d, *J* = 1.0 Hz, 2H), 2.32 – 2.29 (m, 6H), 2.00 (s, 6H), 1.92 (s, 6H).

^{13}C-NMR (126 MHz, $CDCl_3$): δ [ppm] = 140.9, 134.2, 131.0, 129.2, 126.9, 20.8, 15.3, 14.1.

HR-MS (ESI+): *m/z* = 249.076 (calc. 249.077 for $[C_{14}H_{17}S_2 + H]^+$).

1,1',3,3'-Tetramethyl-6,6',7,7'-tetrahydro-5H,5'H-4,4'-bibenzo[c]thiophene-ylidene (aDTE$_{66}$-Me)

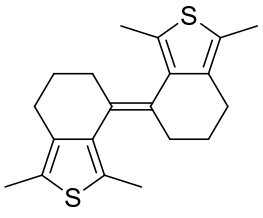

aDTE$_{66}$-Me

Synthesized according to the general procedure for intermolecular McMurry couplings. 1.803 g (10.0 mmol, 1.0 eq) ketone **3a**, 1.65 ml (2.846 g, 15.0 mmol, 1.5 eq) $TiCl_4$,

1.962 g (30.0 mmol, 3.0 eq) Zn dust and 0.81 ml (0.791 g, 10.0 mmol, 1.0 eq) pyridine were heated for 2 h in 35 ml dry THF. Column chromatography (PE) afforded 1.097 g (3.34 mmol, 67% yield) of an isomeric 1:2 mixture, in favor of the *Z*-isomer. The isomers can be separated by slow elution from a long dry-packed column or recycling GPC.

E-isomer:

^{1}H-NMR (500 MHz, $CDCl_3$): δ [ppm] = 2.69 – 2.60 (m, 2H), 2.59 – 2.50 (m, 4H), 2.28 (s, 6H), 2.25 (s, 6H), 2.09 – 2.00 (m, 2H), 1.99 – 1.88 (m, 2H), 1.71 – 1.59 (m, 2H).

^{13}C-NMR (126 MHz, $CDCl_3$): δ [ppm] = 137.4, 134.7, 129.6, 129.5, 127.6, 31.7, 25.5, 24.5, 15.4, 12.9.

HR-MS (ESI+): *m/z* = 328.131 (calc. 328.132 for $[C_{20}H_{24}S_2]^+$).[56]

Z-isomer:

^{1}H-NMR (500 MHz, $CDCl_3$): δ [ppm] = 2.80 – 2.73 (m, 2H), 2.69 – 2.62 (m, 2H), 2.45 – 2.37 (m, 2H), 2.26 (s, 6H), 2.23 – 2.16 (m, 2H), 1.97 – 1.88 (m, 2H), 1.81 – 1.72 (m, 2H), 1.50 (s, 6H).

^{13}C-NMR (126 MHz, $CDCl_3$): δ [ppm] = 137.3, 136.0, 129.4, 129.1, 126.2, 29.2, 24.7, 24.4, 14.4, 12.8.

HR-MS (ESI+): *m/z* = 328.131 (calc. 328.132 for $[C_{20}H_{24}S_2]^+$).[56]

1,1',3,3'-tetramethyl-5,5',6,6',7,7',8,8'-octahydro-4,4'-bi(cyclohepta[c]thiophene-ylidene) (aDTE$_{77}$-Me)

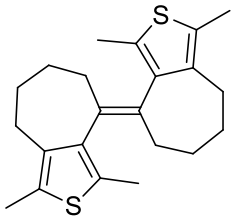

aDTE$_{77}$-Me

The procedure was already published.[56] Under inert conditions in a two-necked round bottom flask equipped with a reflux condenser, 1.10 ml (1.897 g, 10.0 mmol, 2.0 eq) $TiCl_4$ were dissolved in 10 ml dry THF at 0 °C and treated with 1.308 g (20.0 mmol, 4.0 eq) Zn dust. After heating the mixture to 70 °C for 1 h, 0.40 ml (0.396 g, 5.0 mmol, 1.0 eq) pyridine and 0.971 g (5.00 mmol, 1.0 eq) ketone **3b** were added neat and heated to 70 °C for 4 h. Quenched by addition of 10% K_2CO_3 solution and worked up according to the general procedure for intermolecular McMurry couplings. Column chromatography (PE) afforded 0.637 g (1.88 mmol, 75% yield) of an isomeric 1:5.7 mixture, in favor of the *Z*-isomer. The pure *Z*-isomer was obtained by slow elution from a

[56] For several aDTE, instead of the $[M+H]^+$-adduct, the molecular peak $[M]^+$ is the most prominent *m/z* signal. Also, the signal $[M-H]^+$ is observed in the ESI+ ionization mode.

long dry-packed column, for the *E*-isomer further purification by crystallization through slow evaporation out of chloroform in the cold was necessary. Separation of the isomers is possible via prep. GPC.

E-isomer:

^{1}H-NMR (500 MHz, $CDCl_3$): δ [ppm] = 2.82 – 2.75 (m, 2H), 2.52 (ddd, *J* = 12.3, 5.1, 2.3 Hz, 2H), 2.41 – 2.33 (m, 2H), 2.32 (s, 6H), 2.28 (s, 6H), 1.91 – 1.84 (m, 2H), 1.76 – 1.69 (m, 2H), 1.67 – 1.60 (m, 2H), 1.34 – 1.21 (m, 4H).

^{13}C-NMR (126 MHz, $CDCl_3$): δ [ppm] = 141.8, 137.9, 135.1, 127.6, 127.0, 33.5, 31.7, 28.7, 28.5, 13.9, 13.1.

HR-MS (ESI+): *m/z* = 357.175 (calc. 357.171 for $[C_{22}H_{28}S_2 + H]^+$).

Z-isomer:

^{1}H-NMR (500 MHz, $CDCl_3$): δ [ppm] = 2.91 – 2.84 (m, 2H), 2.84 – 2.78 (m, 2H), 2.40 – 2.32 (m, 2H), 2.24 (s, 6H), 1.97 – 1.85 (m, 6H), 1.71 – 1.58 (m, 2H), 1.63 – 1.61 (m, 6H), 1.50 – 1.38 (m, 2H).

^{13}C-NMR (126 MHz, $CDCl_3$): δ [ppm] = 141.2, 136.9, 135.4, 128.2, 127.0, 32.8, 29.7, 28.5, 28.2, 13.6, 13.0.

HR-MS (ESI+): *m/z* = 357.172 (calc. 357.171 for $[C_{22}H_{28}S_2 + H]^+$).

1,1',3,3'-Tetramethyl-5,5',6,6'-tetrahydro-4,4'-bi(cyclopenta[c]thiophene-ylidene) (aDTE$_{55}$-Me)

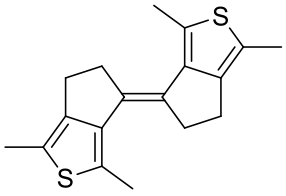

aDTE$_{55}$-Me

Synthesized according to the general procedure for intermolecular McMurry couplings. 0.499 g (3.00 mmol, 1.0 eq) ketone **3c**, 0.50 ml (4.50 mmol, 1.5 eq) $TiCl_4$, 0.589 g (9.00 mmol, 3.0 eq) Zn dust and 0.81 ml (3.00 mmol, 1.0 eq) pyridine were heated overnight in 15 ml dry THF. Column chromatography (PE) afforded 0.453 g (1.50 mmol, quant.) of an isomeric 4:1 mixture, in favor of the *E*-isomer. The isomers can be separated by recycling GPC, though only the *E*-isomer was obtained purely.

E-isomer:

^{1}H-NMR (500 MHz, $CDCl_3$): δ [ppm] = 3.09 (t, *J* = 6.8 Hz, 4H), 2.58 (t, *J* = 6.3 Hz, 4H), 2.45 (s, 6H), 2.31 (s, 6H).

^{13}C-NMR (126 MHz, $CDCl_3$): δ [ppm] = 146.3, 144.0, 129.9, 126.3, 124.8, 40.9, 25.9, 16.0, 13.1.
HR-MS (ESI+): *m*/*z* = 301.108 (calc. 301.108 for $[C_{18}H_{20}S_2 + H]^+$).

<u>*Z*-isomer:</u>[57]

^{1}H-NMR (500 MHz, $CDCl_3$): δ [ppm] = 3.10 – 2.99 (m, 2H), 2.86 (dd, *J* = 14.1, 7.4 Hz, 2H), 2.64 – 2.56 (m, 4H), 2.28 (s, 6H), 2.04 (s, 6H).
^{13}C-NMR (126 MHz, $CDCl_3$): δ [ppm] = 147.0, 144.4, 129.4, 127.9, 124.5, 40.1, 25.8, 15.6, 13.3.
HR-MS (ESI+): *m*/*z* = 301.108 (calc. 301.108 for $[C_{18}H_{20}S_2 + H]^+$).

1,1'-Dichloro-3,3'-dimethyl-6,6',7,7'-tetrahydro-5H,5'H-4,4'-bibenzo[c]thiophene-ylidene (aDTE$_{66}$-Cl)

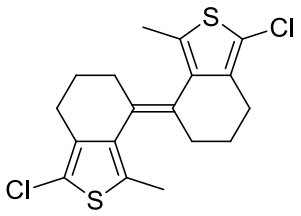

aDTE$_{66}$-Cl

Synthesized according to the general procedure for intermolecular McMurry couplings. 2.007 g (10.0 mmol, 1.0 eq) ketone **7a**, 1.65 ml (2.846 g, 15.0 mmol, 1.5 eq) $TiCl_4$, 1.962 g (30.0 mmol, 3.0 eq) Zn dust and 0.81 ml (0.791 g, 10.0 mmol, 1.0 eq) pyridine were heated for 1.5 h in 25 ml dry THF. Column chromatography (PE) afforded 1.664 g (4.51 mmol, 90% yield) of an isomeric 1:3 mixture, in favor of the *Z*-isomer. The isomers can be separated by slow elution from a long dry-packed column or preparative TLC in pure CyHex, but were used as such for the functionalization step.

<u>*E*-isomer:</u>

^{1}H-NMR (500 MHz, $CDCl_3$): δ [ppm] = 2.72 – 2.64 (m, *J* = 4.3 Hz, 2H), 2.62 – 2.55 (m, *J* = 6.5 Hz, 2H), 2.54 – 2.48 (m, *J* = 12.3 Hz, 2H), 2.22 (s, 6H), 2.06 – 1.91 (m, *J* = 12.9 Hz, 4H), 1.67 – 1.57 (m, 2H).
^{13}C-NMR (126 MHz, $CDCl_3$): δ [ppm] = 136.4, 135.8, 131.0, 129.6, 119.5, 31.7, 24.8, 24.3, 15.5.
HR-MS (ESI+): *m*/*z* = 368.024 (calc. 368.023 for $[C_{18}H_{18}Cl_2S_2]^+$).[56]

<u>*Z*-isomer:</u>

^{1}H-NMR (500 MHz, $CDCl_3$): δ [ppm] = 2.76 – 2.64 (m, 4H), 2.42 – 2.34 (m, 2H), 2.15 – 2.07 (m, 2H), 1.90 – 1.79 (m, 2H), 1.79 – 1.69 (m, 2H), 1.47 (s, 6H).
^{13}C-NMR (126 MHz, $CDCl_3$): δ [ppm] = 136.9, 136.5, 131.0, 129.6, 118.2, 29.2, 24.3, 24.1, 14.6.
HR-MS (ESI+): *m*/*z* = 368.025 (calc. 368.023 for $[C_{18}H_{18}Cl_2S_2]^+$).[56]

[57] Data obained from mixture of both isomers.

1,1'-Dichloro-3,3'-dimethyl-5,5',6,6',7,7',8,8'-octahydro-4,4'-bi(cyclohepta[c]-thiopheneylidene) (aDTE$_{77}$-Cl)

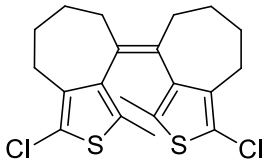

aDTE$_{77}$-Cl

Synthesized according to the general procedure for intermolecular McMurry couplings. 1.074 g (5.00 mmol, 1.0 eq) ketone **7b**, 0.83 ml (1.423 g, 7.50 mmol, 1.5 eq) $TiCl_4$, 0.981 g (15.0 mmol, 3.0 eq) Zn dust and 0.40 ml (0.396 g, 5.0 mmol, 1.0 eq) pyridine were heated for 6 h in 30 ml dry THF. MPLC (CyHex) afforded 0.785 g (1.98 mmol, 79% yield) of the title compound as a 10:1 isomeric mixture in favor of the *Z*-isomer.

<u>*Z*-isomer:</u>

^{1}H-NMR (500 MHz, $CDCl_3$): δ [ppm] = 3.08 – 3.01 (m, 2H), 2.89 (dd, *J* = 13.9, 5.0 Hz, 2H), 2.36 – 2.28 (m, 2H), 1.95 (dd, *J* = 16.5, 10.8 Hz, 4H), 1.89 – 1.81 (m, 2H), 1.66 (s, 6H), 1.71 – 1.59 (m, 2H), 1.51 – 1.41 (m, 2H).

^{13}C-NMR (126 MHz, $CDCl_3$): δ [ppm] = 140.1, 137.7, 135.5, 129.7, 119.1, 32.8, 29.9 (br), 28.3, 27.9, 13.9.

1-(3,5-bis(trifluoromethyl)phenyl)-4-(1-(2,5-dimethylthiophen-3-yl)ethylidene)-3-methyl-4,5,6,7-tetrahydrobenzo[c]thiophene ((F$_3$C)$_2$Ph-aDTE$_{6Me}$-Me)

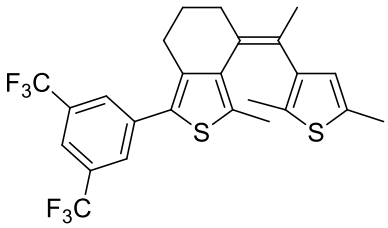

(F$_3$C)$_2$Ph-aDTE$_{6Me}$-Me

Synthesized according to the general procedure for intermolecular McMurry couplings, but using a 1:3 ratio of the coupling partners. 0.189 g (0.50 mmol, 1.0 eq) ketone **10**, 0.231 g (1.50 mmol, 3.0 eq) comm. 1-(2,5-dimethylthiophen-3-yl)ethanone, 0.33 ml (3.00 mmol, 6.0 eq) $TiCl_4$, 0.392 g (6.00 mmol, 12.0 eq) Zn dust and 0.16 ml (2.00 mmol, 4.0 eq) pyridine were heated for 2 h in 15 ml dry THF. Careful column chromatography (PE) afforded a mixture of **(F$_3$C)$_2$Ph-aDTE$_{6Me}$-Me** and **13**. Separation of the two is possible by prep. GPC. Yet, 0.092 g (0.18 mmol, 37% yield) of the title compound was obtained as a 1:9 mixture of both isomers in favor of the *Z*-isomer.

Z-isomer:[57]

^{1}H-NMR (500 MHz, $CDCl_3$): δ [ppm] = 7.85 (s, 2H), 7.76 (s, 1H), 6.44 (s, 1H), 2.73 (s, 2H), 2.59 (s, 2H), 2.38 (s, 3H), 2.08 (s, 3H), 1.87 – 1.69 (m, 5H), 1.68 (s, 3H).

^{13}C-NMR (126 MHz, $CDCl_3$): δ [ppm] = 141.1, 139.4, 138.0, 137.2, 135.3 (d, J_{CF} = 4.4 Hz), 132.0 (q, J_{CF} = 33.2 Hz), 131.4, 130.0, 128.5, 128.5 – 128.3 (m), 128.2, 126.9 – 126.8 (m), 123.5 (q, J_{CF} = 272.8 Hz), 120.1 – 119.9 (m), 29.2, 26.2, 24.1, 21.3, 15.3, 15.1, 13.9.

^{19}F NMR (471 MHz, $CDCl_3$) δ [ppm] = -63.11.

HR-MS (ESI+): *m*/*z* = 500.109 (calc. 500.107 for $[C_{25}H_{22}F_6S_2]^+$).[56]

4.5.4 Functionalization of aDTEs

General Procedure for aDTE Functionalization via Suzuki Coupling

In a typical functionalization of aDTE was achieved on a 1 mmol scale according to the following procedure: In a dry Schlenk finger under inert atmosphere, a 0.2 M solution of the substrate (1.0 eq) in dry THF was treated with 3.0 eq (1.1 eq for monofunctionalization) 2.3 M ^{n}BuLi solution under stirring, added over 1 min at room temperature. The initially colorless solution turned black after some drops and shortly after complete addition, a brown/red suspension formed. It was stirred at room temperature for 30-60 min and quenched by addition of 4.0 eq (1.2 eq for monofunctionalization) $B(O^{i}Pr)_3$ at room temperature at once, whereupon the orange suspension cleared up. Subsequently, it was stirred at room temperature for 30 min.

Meanwhile, in a second, two-necked round bottom flask fitted with a reflux condenser, 0.05 eq $Pd(PPh_3)_4$ and 4.8 eq (1.8 eq for monofunctionalization) of the respective bromobenzene derivative were dissolved in dry THF to give a 0.5 M solution in respect to the coupling partner. Some drops of glycol were added and the mixture consequently degassed by 10 short vacuum/argon cycles. Afterwards, 10 eq degassed 2 M aq. Na_2CO_3 solution were added and heated to 60 °C for 30 min before the generated boronic ester solution was transferred from the first flask via syringe. The mixture was heated until TLC shows full conversion to one to two more polar products, one of them to change color under UV irradiation on the TLC plate. It was worked up by addition of water and threefold extraction with EA, dried over $MgSO_4$ and evaporation of the solvent under reduced pressure. Separation of the two isomers was normally achieved by slow elution from a long dry-packed column (simple aDTEs) or HPLC of the isomeric mixture (functionalized aDTEs).

1,1'-bis(3,5-bis(trifluoromethyl)phenyl)-3,3'-dimethyl-6,6',7,7'-tetrahydro-5H,5'H-4,4'-bibenzo[c]thiophenylidene (aDTE$_{66}$-Ph(CF$_3$)$_2$)

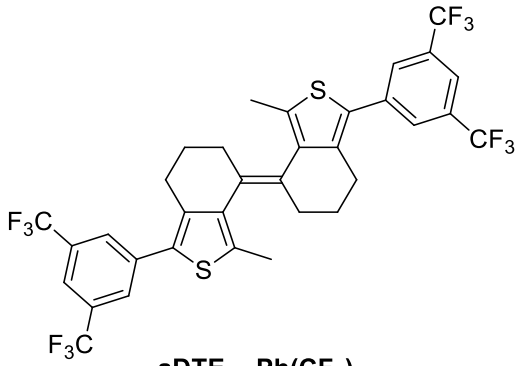

aDTE$_{66}$-Ph(CF$_3$)$_2$

Synthesized according to the general procedure for two-fold aDTE functionalization via Suzuki coupling. 0.074 g (0.20 mmol, 1.0 eq) aDTE **aDTE$_{66}$-Cl**, 0.27 ml (0.60 mmol, 3.0 eq) 2.3 M ^{n}BuLi solution, 0.14 ml (0.113 g, 0.60 mmol, 3.0 eq) B(O^{i}Pr)$_3$, and 0.281 g (0.96 mmol, 4.8 eq) 1-bromo-3,5-bis(trifluoromethyl)benzene, 0.012 g (0.01 mmol, 0.05 eq) Pd(PPh$_3$)$_4$, 10 drops of ethylene glycol and 1.00 ml (2.00 mmol, 10 eq) 2 M Na$_2$CO$_3$. Heated for 24 h. Extraction afforded a yellow oil that was purified by column chromatography (PE) to yield 0.099 g (0.14 mmol, 68% yield) of an isomeric mixture of the title compound. The isomers were separated using preparative HPLC (PhHex, MeCN/H$_2$O/THF 40:20:40).

Z-isomer:

^{1}H-NMR (500 MHz, $CDCl_3$): δ [ppm] = 7.86 (s, 4H), 7.77 (s, 2H), 2.94 (dt, *J* = 14.9, 4.7 Hz, 2H), 2.79 (ddd, *J* = 15.7, 9.0, 7.0 Hz, 2H), 2.60 (ddd, *J* = 15.1, 10.7, 4.7 Hz, 2H), 2.48 – 2.39 (m, 2H), 2.07 (tdd, *J* = 11.5, 5.6, 3.4 Hz, 2H), 1.68 (s, 6H), 1.66 – 1.57 (m, 2H).

^{13}C-NMR (126 MHz, $CDCl_3$): δ [ppm] = 139.3, 138.7, 136.9, 134.8, 132.1 (q, J_{CF} = 33.3 Hz), 129.4, 129.0, 128.6 – 128.2 (m), 123.5 (q, J_{CF} = 272.8 Hz), 120.4 – 120.1 (m), 28.8, 26.1, 23.9, 14.8.

^{19}F NMR (471 MHz, $CDCl_3$) δ [ppm] = -63.11 (s).

HR-MS (ESI+): *m*/*z* = 724.113 (calc. 724.113 for $[C_{34}H_{24}F_{12}S_2]^{+}$).[56]

4,4'-(3,3'-dimethyl-6,6',7,7'-tetrahydro-5H,5'H-[4,4'-bibenzo[c]thiophenylidene]-1,1'-diyl)dibenzonitrile (aDTE$_{66}$-PhCN)

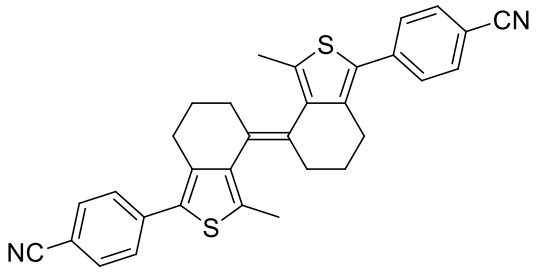

aDTE$_{66}$-PhCN

Synthesized according to the general procedure for two-fold aDTE functionalization via Suzuki coupling. 0.369 g (1.00 mmol, 1.0 eq) aDTE **aDTE$_{66}$-Cl**, 1.30 ml (3.00 mmol, 3.0 eq) 2.3 M ^{n}BuLi solution, 0.92 ml (0.752 g, 4.00 mmol, 4.0 eq) B(O^{i}Pr)$_3$, and 0.874 g (4.80 mmol, 4.8 eq) 4-bromobenzonitrile, 0.058 g (0.05 mmol, 0.05 eq) Pd(PPh$_3$)$_4$, 10 drops of ethylene glycol and 5.00 ml (10.0 mmol, 10 eq) 2 M Na_2CO_3. Heated for 24 h. Extraction afforded a yellow oil that was purified by MPLC (40 g silica, EA/CyHex 0-40%) to yield 0.282 g (0.56 mmol, 56% yield) of an isomeric mixture of the title compound. The isomers were separated using preparative HPLC (PhHex, MeCN/H_2O/THF 40:30:30).

Z-isomer:

^{1}H-NMR (500 MHz, CD_2Cl_2): δ [ppm] = 7.69 – 7.66 (m, 4H), 7.58 – 7.54 (m, 4H), 2.99 (dt, *J* = 14.9, 4.7 Hz, 2H), 2.82 – 2.72 (m, 2H), 2.58 (ddd, *J* = 15.2, 10.8, 4.7 Hz, 2H), 2.45 – 2.36 (m, 2H), 2.09 – 1.99 (m, 2H), 1.64 (s, 6H), 1.59 – 1.51 (m, 2H).

^{13}C-NMR (126 MHz, CD_2Cl_2): δ [ppm] = 139.9, 139.9, 139.4, 135.2, 132.9, 130.7, 129.8, 129.2, 119.5, 110.3, 29.1, 26.7, 24.3, 14.8.

HR-MS (ESI+): *m*/*z* = 502.154 (calc. 502.154 for $[C_{32}H_{26}N_2S_2]^+$).[56]

1,1'-bis(4-bromophenyl)-3,3'-dimethyl-6,6',7,7'-tetrahydro-5H,5'H-4,4'-bibenzo[c]thiophenylidene (aDTE$_{66}$-PhBr)

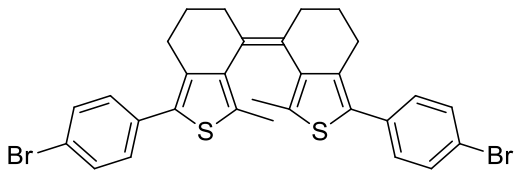

aDTE$_{66}$-PhBr

Synthesized according to the general procedure for two-fold aDTE functionalization via Suzuki coupling. 0.369 g (1.00 mmol, 1.0 eq) aDTE **aDTE$_{66}$-Cl**, 1.30 ml (3.00 mmol,

3.0 eq) 2.3 M ^{n}BuLi solution, 0.92 ml (0.752 g, 4.00 mmol, 4.0 eq) B(O^{i}Pr)$_3$, and 1.353 g (4.80 mmol, 4.8 eq) 4-bromo-iodobenzene, 0.058 g (0.05 mmol, 0.05 eq) Pd(PPh$_3$)$_4$, 10 drops of ethylene glycol and 5.00 ml (10.0 mmol, 10 eq) 2 M Na_2CO_3. Stirred at room temperature for 42 h. Extraction afforded a yellow oil that was purified by MPLC (EA/CyHex) to yield 0.139 g (0.23 mmol, 23% yield) of the *Z*-isomer of the title compound.

Z-isomer:

^{1}H-NMR (500 MHz, $CDCl_3$): δ [ppm] = 7.53 – 7.48 (m, 4H), 7.34 – 7.30 (m, 4H), 2.94 (dt, *J* = 14.8, 4.7 Hz, 2H), 2.79 – 2.68 (m, 2H), 2.51 (ddd, *J* = 14.9, 10.9, 4.7 Hz, 2H), 2.40 (dtd, *J* = 9.3, 6.8, 2.6 Hz, 2H), 2.05 – 1.96 (m, 2H), 1.62 (s, 6H), 1.60 – 1.54 (m, 2H).

^{13}C-NMR (126 MHz, $CDCl_3$): δ [ppm] = 138.4, 137.6, 133.9, 133.1, 131.8, 130.8, 130.2, 129.3, 120.8, 28.8, 26.0, 24.0, 14.5.

HR-MS (ESI+): *m*/*z* = 607.983 (calc. 607.984 for $[C_{30}H_{26}Br_2S_2]^{+}$).[56]

1,1'-bis(4-methoxyphenyl)-3,3'-dimethyl-6,6',7,7'-tetrahydro-5H,5'H-4,4'-bibenzo[c]thiophenylidene (aDTE$_{66}$-PhOMe)

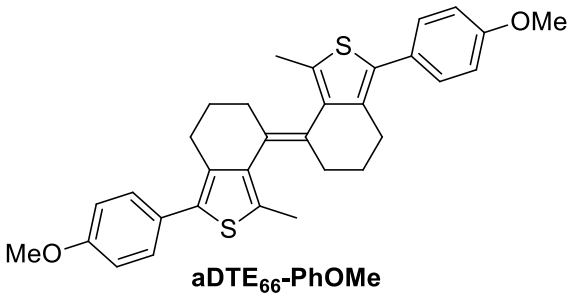

aDTE$_{66}$-PhOMe

Synthesized according to the general procedure for two-fold aDTE functionalization via Suzuki coupling. 0.074 g (0.20 mmol, 1 eq) aDTE **aDTE$_{66}$-Cl**, 0.27 ml (0.60 mmol, 3.0 eq) 2.3 M ^{n}BuLi solution, 0.19 ml (0.150 g, 0.80 mmol, 4.0 eq) B(O^{i}Pr)$_3$, and 0.12 ml (0.180 g, 0.96 mmol, 4.8 eq) 4-bromoanisole, 0.012 g (0.01 mmol, 0.05 eq) Pd(PPh$_3$)$_4$, 10 drops of ethylene glycol and 1.00 ml (2.00 mmol, 10 eq) 2 M Na_2CO_3. Heated for 24 h. Extraction afforded a yellow oil that was purified by column chromatography (PE) to yield 0.062 g (0.12 mmol, 61% yield) of an isomeric mixture of the title compound. The isomers were separated using preparative HPLC (PhHex, MeCN/H_2O/THF 40:24:36).

E-isomer:

^{1}H-NMR (500 MHz, $CDCl_3$): δ [ppm] = 7.45 – 7.40 (m, 4H), 6.95 – 6.92 (m, 4H), 3.84 (s, 6H), 2.84 – 2.71 (m, 4H), 2.63 – 2.55 (m, 2H), 2.34 (s, 6H), 2.19 (d, *J* = 17.5 Hz, 2H), 1.91 – 1.81 (m, 2H), 1.78 – 1.69 (m, 2H).

^{13}C-NMR (126 MHz, $CDCl_3$): δ [ppm] = 158.7, 138.5, 134.9, 132.2, 131.9, 129.9, 129.8, 127.7, 114.1, 55.5, 31.0, 25.6, 25.2, 15.6.

HR-MS (ESI+): *m*/*z* = 512.183 (calc. 512.184 for $[C_{32}H_{32}O_2S_2]^+$).[56]

Z-isomer:

^{1}H-NMR (500 MHz, $CDCl_3$): δ [ppm] = 7.40 – 7.35 (m, 4H), 6.96 – 6.91 (m, 4H), 3.84 (s, 6H), 2.94 (dt, *J* = 14.7, 4.7 Hz, 2H), 2.78 – 2.69 (m, 2H), 2.54 – 2.46 (m, 2H), 2.44 – 2.35 (m, 2H), 2.04 – 1.96 (m, 2H), 1.63 (s, 6H), 1.61 – 1.54 (m, 2H).

^{13}C-NMR (126 MHz, $CDCl_3$): δ [ppm] = 158.7, 138.1, 136.3, 131.8, 131.7, 130.0, 129.3, 127.7, 114.1, 55.5, 28.8, 25.9, 24.1, 14.4.

HR-MS (ESI+): *m*/*z* = 512.183 (calc. 512.184 for $[C_{32}H_{32}O_2S_2]^+$).[56]

4-(1'-chloro-3,3'-dimethyl-6,6',7,7'-tetrahydro-5H,5'H-[4,4'-bibenzo[c]thiophenylidene]-1-yl)-N,N-dimethylaniline (Me_2NPh-$aDTE_{66}$-Cl)

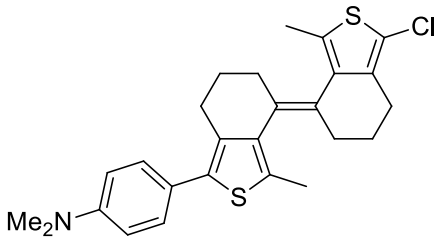

Me_2NPh-$aDTE_{66}$-Cl

Synthesized according to the general procedure for simple aDTE functionalization via Suzuki coupling. 0.682 g (1.70 mmol, 1.0 eq) **$aDTE_{66}$-Cl**, 0.81 ml (1.87 mmol, 1.1 eq) 2.3 M ^{n}BuLi solution, 0.471 ml (0.384 g, 2.04 mmol, 1.2 eq) $B(O^iPr)_3$, and 0.612 g, 3.06 mmol, 1.8 eq) 4-bromo-*N*,*N*-dimethylaniline, 0.098 g (0.085 mmol, 0.05 eq) $Pd(PPh_3)_4$, 10 drops of ethylene glycol and 8.5 ml (2.00 mmol, 10 eq) 2 M Na_2CO_3. Heated for 12 h. Extraction afforded a brown oil that was purified by MPLC (DCM/CyHex +1% Et_3N) to yield 0.348 g (0.77 mmol, 45% yield) of an isomeric mixture of the title compound. The isomers were not separated and used as such for the step.

E/*Z* 1:1 mixture:

^{1}H-NMR (500 MHz, $CDCl_3$): δ [ppm] = 7.42 – 7.38 (m, 2H), 7.37 – 7.33 (m, 2H), 6.79 – 6.75 (m, 4H), 3.00 (s, 6H), 2.99 (s, 6H), 2.97 – 2.94 (m, 1H), 2.85 – 2.58 (m, 8H), 2.56 – 2.44 (m, 3H), 2.43 – 2.33 (m, 2H), 2.32 (s, 3H), 2.27 (d, *J* = 5.3 Hz, 3H), 2.25 – 2.18 (m, 1H), 2.14 (d, *J* = 7.2 Hz, 1H), 2.06 (dd, *J* = 15.8, 9.4 Hz, 1H), 1.99 – 1.94 (m, 2H), 1.93 – 1.85 (m, 1H), 1.85 – 1.77 (m, 1H), 1.76 – 1.66 (m, 2H), 1.65 (s, 3H), 1.63 – 1.57 (m, 1H), 1.56 (s, 3H).

^{13}C-NMR (126 MHz, $CDCl_3$): δ [ppm] = 149.6, 149.5, 138.0, 137.8, 137.0, 136.8, 136.7, 135.9, 135.3, 133.7, 133.3, 132.7, 131.8, 131.3, 131.0, 130.9, 130.6, 129.5, 129.4, 128.9, 128.8, 123.2, 119.2, 117.8, 114.2, 112.6, 112.5, 53.6, 40.7, 40.6, 31.5, 31.4, 29.0, 28.9, 25.8, 25.6, 25.3, 24.8, 24.4, 24.3, 24.2, 24.0,

15.6, 15.5, 14.6, 14.4.

HR-MS (ESI+): *m/z* = 454.142 (calc. 454.143 for $[C_{26}H_{28}ClNS_2 + H]^+$).

4-(1'-(4-(dimethylamino)phenyl)-3,3'-dimethyl-6,6',7,7'-tetrahydro-5H,5'H-[4,4'-bibenzo[c]thiophenylidene]-1-yl)benzonitrile (Me_2NPh-aDTE$_{66}$-PhCN)

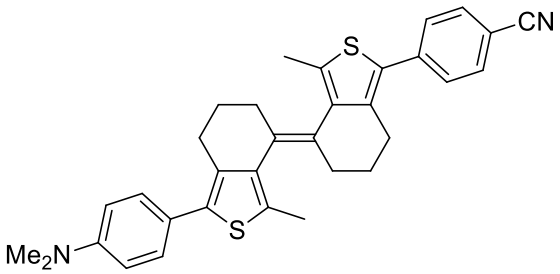

Me_2NPh-aDTE$_{66}$-PhCN

Synthesized according to the general procedure for simple aDTE functionalization via Suzuki coupling. 0.184 g (0.405 mmol, 1.0 eq) **Me_2NPh-aDTE$_{66}$-Cl** (*E/Z* 1:1), 0.53 ml (1.22 mmol, 3.0 eq) 2.3 M ^{n}BuLi solution, 0.37 ml (1.62 mmol, 4.0 eq) $B(O^{i}Pr)_3$, and 0.147 g (0.81 mmol, 2.0 eq) 1-cyano-4-bromobenzene, 0.023 g (0.020 mmol, 0.05 eq) $Pd(PPh_3)_4$, 10 drops of ethylene glycol and 2.0 ml (4.05 mmol, 10 eq) 2 M Na_2CO_3. Heated for overnight. Extraction afforded a brown oil that was purified by column chromatography (DCM/PE 1:1 + 1% Et_3N) to yield 0.169 g (0.33 mmol, 80% yield) of an isomeric 1:1 mixture of the title compound. The *Z*-isomer was obtained pure by HPLC separation.

<u>*E/Z* 1:1 mixture:</u>

^{1}H-NMR (500 MHz, $CDCl_3$): δ [ppm] = 7.69 – 7.63 (m, 4H), 7.62 – 7.58 (m, 2H), 7.57 – 7.52 (m, 2H), 7.38 (dd, *J* = 9.2, 7.2 Hz, 2H), 7.35 (d, *J* = 8.8 Hz, 2H), 6.78 (d, *J* = 7.5 Hz, 4H), 2.99 (s, 6H), 2.99 (s, 6H), 2.98 – 2.94 (m, 2H), 2.91 – 2.45 (m, 12H), 2.44 – 2.38 (m, 2H), 2.37 (s, 3H), 2.34 (s, 3H), 2.23 – 2.13 (m, 2H), 2.08 – 1.95 (m, 2H), 1.92 – 1.82 (m, 2H), 1.82 – 1.68 (m, 2H), 1.66 (s, 3H), 1.61 (s, 3H).

^{13}C-NMR (126 MHz, $CDCl_3$): δ [ppm] = 140.0, 139.7, 139.4, 139.1, 138.1, 137.9, 137.8, 135.4, 135.1, 134.7, 133.9, 133.3, 132.5, 131.4, 131.0, 130.3, 129.9, 129.6, 129.5, 128.8, 128.7, 128.6, 128.2, 119.2, 119.2, 112.6, 109.8, 109.7, 40.7, 31.1, 30.8, 28.9, 28.7, 26.4, 26.1, 26.0, 25.6, 25.2, 24.9, 24.1, 24.0, 15.7, 15.6, 14.6, 14.5.

HR-MS (ESI+): *m/z* = 521.208 (calc. 521.209 for $[C_{33}H_{32}N_2S_2 + H]^+$).

1,1'-bis(3,5-bis(trifluoromethyl)phenyl)-3,3'-dimethyl-5,5',6,6',7,7',8,8'-octahydro-4,4'-bi(cyclohepta[c]thiophenylidene) (aDTE$_{77}$-Ph(CF$_3$)$_2$)

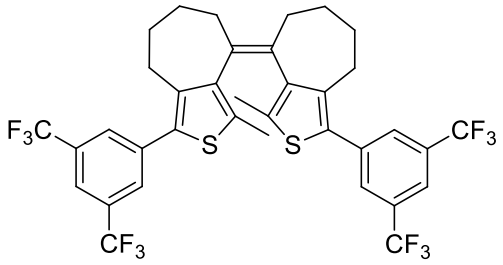

aDTE$_{77}$-Ph(CF$_3$)$_2$

Synthesized according to the general procedure for two-fold aDTE functionalization via Suzuki coupling. 0.099 g (0.25 mmol, 1.0 eq) **aDTE$_{77}$-Cl**, 0.33 ml (0.75 mmol, 3.0 eq) 2.3 M ^{n}BuLi solution, 0.17 ml (0.75 mmol, 3.0 eq) B(O^{i}Pr)$_3$, and 0.381 g (1.30 mmol, 5.2 eq) 1-bromo-3,5-bis(trifluoromethyl)benzene, 0.014 g (0.013 mmol, 0.05 eq) Pd(PPh$_3$)$_4$, 10 drops of ethylene glycol and 1.25 ml (2.50 mmol, 10 eq) 2 M Na_2CO_3. Heated for 12 h. Extraction afforded a yellow oil that was purified by column chromatography (PE) to yield 0.143 g (0.19 mmol, 76% yield) of an isomeric 1:30 *E/Z*-mixture of the title compound.

Z-isomer:

^{1}H-NMR (500 MHz, $CDCl_3$): δ [ppm] = 7.79 (s, 2H), 7.75 (s, 4H), 2.99 – 2.87 (m, 4H), 2.56 (ddd, J = 14.6, 12.3, 2.6 Hz, 2H), 2.09 (t, J = 12.4 Hz, 2H), 2.03 – 1.94 (m, 4H), 1.77 (s, 6H), 1.81 – 1.71 (m, 2H), 1.67 – 1.57 (m, 2H).

^{13}C-NMR (126 MHz, $CDCl_3$): δ [ppm] = 142.1, 139.3, 137.4, 136.0, 134.2, 132.0 (q, J_{CF} = 33.3 Hz), 130.3, 129.2 (s (br)), 123.4 (q, J_{CF} = 272.8 Hz), 120.7 – 120.4 (m), 32.6, 29.2 – 28.6 (m), 28.5, 28.2, 14.1.

HR-MS (ESI+): m/z = 752.140 (calc. 752.144 for $[C_{36}H_{28}F_{12}S_2]^{+}$).[56]

4.5.5 Synthesis of pcDTE

1,3-dimethyl-5-(2-((tetrahydro-2H-pyran-2-yl)oxy)ethyl)-6,7-dihydrobenzo[c]-thiophen-4(5H)-one (14a) and 1,3-dimethyl-5,5-bis(2-((tetrahydro-2H-pyran-2-yl)oxy)-ethyl)-6,7-dihydrobenzo[c]thiophen-4(5H)-one (15a)

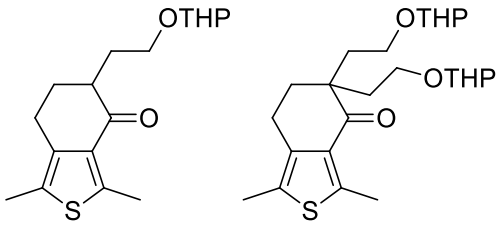

14a **15a**

Under inert conditions, in a three-necked 250 ml round bottom flask, 4.370 g (21.0 mmol, 1.0 eq) ketone **3a** was dissolved in 20 ml dry THF. Then, 21 ml (21.0 mmol, 1.05 eq) commercial LiHMDS (1 M in THF) was added at once and stirred at room temperature overnight. Deprotonation was complete as tested by UPLC analysis of an aliquot quenched with excess *p*-nitro-benzaldehyde. Subsequently, the solution was diluted to 80 ml and cooled to 0 °C and 5.378 g (20.0 mmol, 1.0 eq) 2-(2-iodoethoxy)tetrahydro-2H-pyran was added at once. Kept in an isolated cooling bath, the reaction mixture was warmed to room temperature over a period of 24 h, when UPLC indicates no further conversion. It was diluted with water and extracted with 3x 150 ml diethyl ether. The combined organic phases were dried over $MgSO_4$ and the volatiles evaporated under reduced pressure. Column chromatography (EA/PE 1:10) yielded 2.619 g (8.49 mmol, 40% yield) monoalkylated **14a**, 0.907 g (2.08 mmol, 10% yield) dialkylated **15a** and recovered 1.784 g (8.58 mmol, 40% yield) of ketone **3a**.

Monoalkylated **14a** (only major diastereomer given):

^{1}H-NMR (500 MHz, $CDCl_3$): δ [ppm] = 4.62 – 4.57 (m, 1H), 3.91 – 3.83 (m, 2H), 3.59 – 3.47 (m, 2H), 2.82 – 2.74 (m, 1H), 2.70 (s, 3H), 2.62 – 2.45 (m, 2H), 2.32 – 2.22 (m, 1H), 2.27 (s, 3H), 2.21 – 2.14 (m, 1H), 1.86 – 1.61 (m, 4H), 1.60 – 1.46 (m, 4H).

HR-MS (ESI+): *m*/*z* = 331.104 (calc. 331.134 for $[C_{17}H_{24}O_3S + Na]^+$).

Dialkylated **15a**:

^{1}H-NMR (300 MHz, $CDCl_3$): δ [ppm] = 4.58 – 4.49 (m, 2H), 3.92 – 3.73 (m, 4H), 3.54 – 3.37 (m, 4H), 2.70 (d, *J* = 8.7 Hz, 5H), 2.26 (s, 3H), 2.13 – 1.45 (m, 18H).

HR-MS (ESI+): *m*/*z* = 459.210 (calc. 459.218 for $[C_{24}H_{36}O_5S + Na]^+$).

1,3,7,7-tetramethyl-5-(2-((tetrahydro-2H-pyran-2-yl)oxy)ethyl)-6,7-dihydrobenzo[c]-thiophen-4(5H)-one (14d)

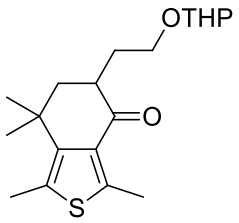

14d

In a 100 ml Schlenk flask, 3.121 g (15.0 mmol, 1.0 eq) ketone **3d** was dissolved in 30 ml dry THF and treated with 16.5 ml (16.5 mmol, 1.1 eq) commercial LiHMDS solution (1 M in THF) at room temperature. After 4 h, deprotonation was complete as tested by UPLC analysis of an aliquot quenched with excess *p*-nitro-benzaldehyde. Consequently, 4.033 g (15.75 mmol, 1.05 eq) 2-(2-iodoethoxy)tetrahydro-2H-pyran was added neat at once and the reaction stirred at room temperature for 16 h. Subsequently, the reaction mixture was treated with aq. NH_4Cl solution and extracted with 3x 100 ml diethyl ether. The combined organic phases were washed with 10% aq. thiosulfate solution, dried over $MgSO_4$, and the volatiles evaporated to yield a brown oil. Column chromatography (EA/PE 1:15 to 1:10) yielded 1.984 g (5.90 mmol, 39% yield) of the title compound as a yellowish solid. The starting ketone was collected together with unreacted alkylating agent.

Two diastereomers:

^{1}H-NMR (300 MHz, $CDCl_3$): δ [ppm] = 4.62 (dd, *J* = 11.7, 7.8 Hz, 1H), 3.96 – 3.78 (m, 2H), 3.63 – 3.45 (m, 2H), 2.82 – 2.69 (m, 1H), 2.65 (s, 3H), 2.42 (s, 3H), 2.40 – 2.30 (m, 1H), 1.92 – 1.47 (m, 9H), 1.45 (s, 3H), 1.34 (s, 3H).

^{13}C-NMR (75 MHz, $CDCl_3$): δ [ppm] = 197.6, 145.6, 144.5, 132.6, 127.9, 98.9, 98.8, 65.9, 65.5, 62.3, 46.4, 46.2, 42.1, 41.8, 34.7, 30.9, 29.9, 29.0, 29.0, 26.3, 25.7, 19.7, 16.1, 15.0.

HR-MS (ESI+): *m*/*z* = 359.167 (calc. 359.165 for $[C_{19}H_{28}O_3S + Na]^+$).

5-(2-iodoethyl)-1,3,7,7-tetramethyl-6,7-dihydrobenzo[c]thiophen-4(5H)-one (16d)

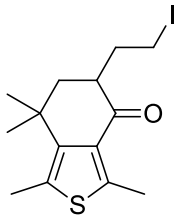

16d

The protocol was inspired by Muller *et al.*[142b] In a round bottom flask, 0.364 g (1.06 mmol) THP-ether **14d** was dissolved in 3 ml degassed toluene and treated with 0.42 ml 57% aq. HI solution. The mixture was stirred for 24 h at room temperature, while another portion of aq. HI was added. The mixture was diluted with and extracted with 3x 20 ml diethyl ether. The combined organic phases were washed with 10% aq. $Na_2S_2O_3$-solution and dried over $MgSO_4$. After removal of the volatiles, column chromatography (EA/PE 1:19 to 1:1) yielded 0.224 g (6.18 mmol, 58%) of the title compound. Furthermore, an important amount of the corresponding alcohol was observed but could not be isolated purely.

^{1}H-NMR (500 MHz, $CDCl_3$): δ [ppm] = 3.45 (ddd, *J* = 9.6, 7.2, 6.2 Hz, 1H), 3.35 (ddd, *J* = 9.6, 7.8, 7.0 Hz, 1H), 2.75 (dtd, *J* = 13.9, 6.1, 4.3 Hz, 1H), 2.65 (s, 3H), 2.54 (dtd, *J* = 13.4, 7.5, 5.9 Hz, 1H), 2.43 (s, 3H), 1.81 (t, *J* = 13.6 Hz, 1H), 1.77 (ddd, *J* = 14.5, 13.2, 6.3 Hz, 1H), 1.67 (dd, *J* = 13.3, 4.3 Hz, 1H), 1.46 (s, 3H), 1.39 (s, 3H).

^{13}C-NMR (126 MHz, $CDCl_3$): δ [ppm] = 196.7, 146.0, 144.3, 132.4, 128.2, 45.8, 45.5, 34.8, 33.2, 29.8, 26.4, 16.1, 15.0, 6.2.

HR-MS (ESI+): *m/z* = 363.005 (calc. 363.028 for $[C_{14}H_{19}IOS+H]^+$).

5,5'-(ethane-1,2-diyl)bis(1,3,7,7-tetramethyl-6,7-dihydrobenzo[c]thiophen-4(5H)-one) (17d) and 1,3,7,7-tetramethyl-6,7-dihydro-4H-spiro[benzo[c]thiophene-5,1'-cyclopropan]-4-one (18d)

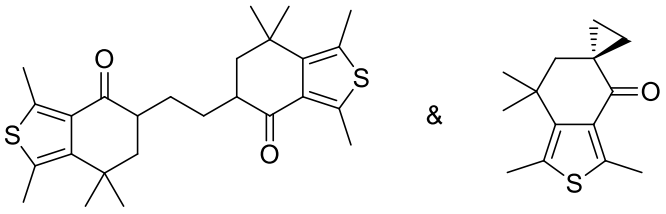

17d & **18d**

Under inert conditions in a 10 ml Schlenk finger, 0.115 g (0.55 mmol, 1.0 eq) ketone **3d** was dissolved in 2 ml dry THF and 0.6 ml (1.1 eq) LiHMDS (1 M in THF) was added at room temperature. After 3 h, 0.199 g (0.55 mmol, 1.0 eq) freshly prepared

iodoketone **16d** in 1.5 ml dry THF was added and stirred for further 28 h at room temperature. It was diluted with 10 ml sat. NH_4Cl solution, extracted with 3x 20 ml diethyl ether and the resulting organic phases washed with 20 ml 10% aq. thiosulfate. Column chromatography (EA/PE 1:20 to 1:1) afforded 0.008 g (0.02 mmol, 3% yield) of diketone **17d** next to 0.080 g (0.34 mmol, 62% yield) of spiroketon **18d**.

Diketone **17d**: *vide infra.*

Spiroketon **18d**:

^{1}H-NMR (300 MHz, $CDCl_3$): δ [ppm] = 2.66 (s, 3H), 2.43 (s, 3H), 1.80 (s, 2H), 1.44 – 1.34 (m, 8H), 0.73 (s, 2H).

^{13}C-NMR (75 MHz, $CDCl_3$): δ [ppm] = 197.1, 145.9, 145.2, 132.7, 1267.0, 48.6, 36.3, 28.6, 26.0, 18.2, 16.1, 15.2.

HR-MS (ESI+): *m/z* = 235.055 (calc. 235.116 for $[C_{14}H_{18}OS+H]^+$).

5-bromo-1,3-dimethyl-6,7-dihydrobenzo[c]thiophen-4(5H)-one (19a) and 5,5-dibromo-1,3-dimethyl-6,7-dihydrobenzo[c]thiophen-4(5H)-one

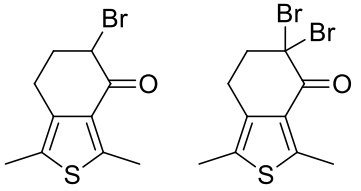

19a

In a 50 ml round bottom two-necked flask, 11.17 g (50.0 mmol, 2.0 eq) $CuBr_2$ was suspended in 13 ml EA to give a pale dark green suspension that was heated to 80 °C. To this, 4.507 g (25.0 mmol, 1.0 eq) ketone **3a** in 10 ml chloroform was added with immediate formation of a fine salt. After 1 h, sat. NH_4Cl was added to prevent further formation of dibromoketone. It was filtered with suction to remove solids and the filtrate extracted with 3x 50 ml EA, dried over $MgSO_4$ and the volatiles evaporated. Column chromatography (EA/PE 1:50) yielded 4.159 g (16.1 mmol, 64% yield) of the title compound as a grey solid. Furthermore, 1.350 g (4.00 mmol, 20% yield) of the dibromide. Single crystals suitable for x-ray analysis were obtained by slow evaporation of EA/PE solution of the monobromide.

Monobromide **19a**:

^{1}H-NMR (300 MHz, $CDCl_3$): δ [ppm] = 4.58 (dd, *J* = 4.3, 3.8 Hz, 1H), 2.97 – 2.82 (m, 1H), 2.74 (s, 3H), 2.78 – 2.66 (m, 1H), 2.41 – 2.33 (m, 2H), 2.31 (s, 3H).

^{13}C-NMR (75 MHz, $CDCl_3$): δ [ppm] = 187.9, 150.2, 135.9, 129.2, 128.7, 51.9, 32.0, 21.3, 16.1, 12.7.

HR-MS (ESI+): *m/z* = 258.971 (calc. 258.979 for $[C_{10}H_{11}BrOS+H]^+$).

Dibromide:

^{1}H-NMR (300 MHz, $CDCl_3$): δ [ppm] = 3.03 – 2.94 (m, 2H), 2.84 – 2.77 (m, 2H), 2.76 (s, 3H), 2.30 (s, 3H).

^{13}C-NMR (75 MHz, $CDCl_3$): δ [ppm] = 181.1, 152.3, 134.9, 128.5, 127.2, 126.1, 69.5, 46.1, 24.3, 16.5, 12.7.

HR-MS (ESI+): *m*/*z* = 336.888 (calc. 336.890 for $[C_{10}H_{10}Br_2OS + H]^+$).

5-bromo-1,3,7,7-tetramethyl-6,7-dihydrobenzo[c]thiophen-4(5H)-one (19d)

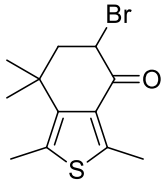

19d

The procedure was adapted from Fitzgerald *et al.*[167] In a 50 ml Schlenk tube, 4.467 g (20.0 mmol, 2.0 eq) $CuBr_2$ was suspended 10 ml EA and heated to 80 °C to give a green solution with substantial amount of insoluble solid. 2.083 g (10.0 mmol, 1.0 eq) ketone **3d** in 10 ml chloroform were added at once and the heating continued for 5.5 h until TLC shows full conversion to a less polar product. The grey precipitate was filtered off and washed with EA until the washing solution was colorless. To this deep green solution charcoal was added until the solution was colorless after some minutes of stirring. The coal was filtered off, washed with DCM and EA, and the volatiles of the collected phases evaporated under reduced pressure to afford 2.633 g (9.27 mmol, 93% yield) of the pure title compound as a grey solid with marked smell. Single crystals suitable for x-ray analysis were obtained by slow evaporation of DCM solutions.

^{1}H-NMR (300 MHz, $CDCl_3$): δ [ppm] = 4.93 (dd, *J* = 13.6, 4.9 Hz, 1H), 2.67 (s, 3H), 2.50 (dd, *J* = 23.9, 10.5 Hz, 1H), 2.43 (s, 3H), 2.32 (dd, *J* = 13.4, 4.9 Hz, 1H), 1.49 (s, 3H), 1.38 (s, 3H).

^{13}C-NMR (75 MHz, $CDCl_3$): δ [ppm] = 187.6, 148.6, 143.4, 130.1, 128.7, 52.5, 51.2, 36.7, 29.4, 26.7, 16.3, 15.0.

HR-MS (ESI+): *m*/*z* = 286.971 (calc. 287.011 for $[C_{12}H_{15}BrOS + H]^+$).

5,5'-thiobis(1,3,7,7-tetramethyl-6,7-dihydrobenzo[c]thiophen-4(5H)-one) (20d)

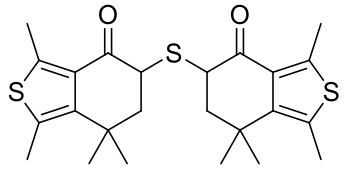

20d

A bigger amount of deep yellow 60% Na_2S (hydrate) was crushed and heated to 140 °C under high vacuum for 1 d to give faint yellow, hard solid that can be stored for longer time. Before usage, it was heated again for 10 min with a heat gun under high vacuum.

The procedure was adapted from literature.[144,168] To a suspension of 0.059 g (0.76 mmol, 0.76 eq) dried Na_2S in 1 ml dry DMF, 0.287 g (1.00 mmol, 1.0 eq) **19d** was added as a solid. The mixture clouded quickly and was stirred at room temperature and the reaction found to be complete after 1.5 h. The reaction mixture was treated with 40 ml water and the voluminous white precipitate was collected by filtration. Subsequently, it was washed with water and a little amount of methanol and dried under reduced pressure. As such, 0.202 g (0.452 mmol, 90% yield) of the title compound were obtained as a white solid that is pure by UPLC, but consists of two diastereomers in a 61:39 ratio according to NMR.

Two diastereomers:

^{1}H-NMR (300 MHz, $CDCl_3$): δ [ppm] = 4.32 (dd, *J* = 10.4, 6.0 Hz, 1H), 4.13 (dd, *J* = 11.1, 5.1 Hz, 1H), 2.67 (s, 3H), 2.67 (s, 3H), 2.43 (s, 6H), 2.25 – 2.06 (m, 4H), 1.51 (s, 3H), 1.48 (s, 3H), 1.42 (s, 3H), 1.40 (s, 3H).

HR-MS (ESI+): *m*/*z* = 447.137 (calc. 447.149 for $[C_{24}H_{30}O_2S_3 + H]^+$).

5-(hydroxymethylene)-1,3-dimethyl-6,7-dihydrobenzo[c]thiophen-4(5H)-one (21a)

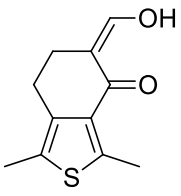

21a

The protocol was inspired by Malkov *et al.*[146c] Workup according to Buchta and Zöllner.[169] In a 500 ml 3-neck round bottom flask with reflux condenser with balloon attached as volumeter, 6.039 g (33.5 mmol, 1.0 eq) ketone **3a** was dissolve in 200 ml dry DCM cooled to 0 °C and treated with 4.020 g (100.5 mmol, 3.0 eq) 60% NaH suspension

and 5.429 g (100.5 mmol, 3.0 eq) NaOMe added at once. It was stirred at low temperature for 15 min, then heated to 70 °C at a rate so that gas evolution was moderate. The viscous mixture was stirred for 5 h at this temperature and subsequently carefully treated with 100 ml water. After phase separation, the organic phase was extracted with 2x 100 ml 1 M NaOH and the unified basic phases acidified to pH = 1 with conc. HCl and extracted with 3x 100 ml DCM. The combined organic phases were dried over $MgSO_4$ and the volatiles evaporated to obtain 6.400 g (30.7 mmol, 92% yield) of the title compound as a light brown solid that was pure by NMR. Only the enol-tautomer was observed.

^{1}H-NMR (300 MHz, $CDCl_3$): δ [ppm] = 14.75 (s, 1H), 7.94 (s, 1H), 2.73 (s, 3H), 2.65 – 2.57 (m, 2H), 2.50 – 2.43 (m, 2H), 2.28 (s, 3H).
^{13}C-NMR (75 MHz, $CDCl_3$): δ [ppm] = 184.3, 172.8, 145.7, 136.3, 130.9, 127.7, 109.3, 24.8, 23.8, 15.5, 12.5.
HR-MS (ESI-): *m/z* = 207.048 (calc. 207.049 for $[C_{11}H_{12}O_2S - H]^-$).

5-(hydroxymethylene)-1,3,7,7-tetramethyl-6,7-dihydrobenzo[c]thiophen-4(5H)-one (21d)

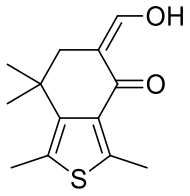

21d

The protocol was inspired by Malkov *et al.*[146c] Workup according to Buchta and Zöllner.[169] Under inert conditions in a 500 ml flask fitted with reflux condenser capped with a balloon, 3.168 g (79.2 mmol, 2.2 eq) NaH suspension (unwashed) and 1.945 g (36.0 mmol, 1.0 eq) NaOMe were suspended in 200 ml toluene at 0 °C. Then, 7.500 g (36.0 mmol, 1.0 eq) ketone **3d** was added at once without visible reaction, followed by addition of 11.6 ml (10.67 g, 144.0 mmol, 4.0 eq) ethyl formate at low temperature. After the first gas evolution ceased, it was warmed to room temperature. After 2 h, a rose-white suspension had formed. TLC control after acidic workup showed full conversion to a less polar product. The mixture was treated with 100 ml 1 M NaOH to yield a brown suspension. After phase separation, the organic phase was further extracted with 2x 100 ml 1 M NaOH. The combined aqueous phases were washed with 100 ml toluene and acidified to pH = 1 with conc. HCl. The formed suspension was extracted with

3x 200 ml Et_2O, the united organic phases dried over $MgSO_4$ and the volatiles evaporated to yield 8.472 g (35.8 mmol, > 99% yield) of the title compound as a brown solid that was pure by NMR and was used as such. Recrystallization is possible from pentane to yield a white fluffy solid. Only the enol-tautomer was observed.

^{1}H-NMR (300 MHz, $CDCl_3$): δ [ppm] = 14.66 (d, *J* = 7.8 Hz, 1H), 7.85 (d, *J* = 7.7 Hz, 1H), 2.70 (s, 3H), 2.41 (s, 3H), 2.30 (s, 2H), 1.32 (s, 6H).
^{13}C-NMR (75 MHz, $CDCl_3$): δ [ppm] = 184.2, 172.5, 145.5, 143.1, 131.1, 127.5, 108.4, 41.3, 35.8, 15.7, 15.2.
HR-MS (ESI+): *m/z* = 237.095 (calc. 237.095 for $[C_{13}H_{16}O_2S + H]^+$).

1,3-dimethyl-5-methylene-6,7-dihydrobenzo[c]thiophen-4(5H)-one (22a), 5-(hydroxylmethyl)-1,3-dimethyl-6,7-dihydrobenzo[c]thiophen-4(5H)-one and 5,5-bis(hydroxymethyl)-1,3-dimethyl-6,7-dihydrobenzo[c]thiophen-4(5H)-one

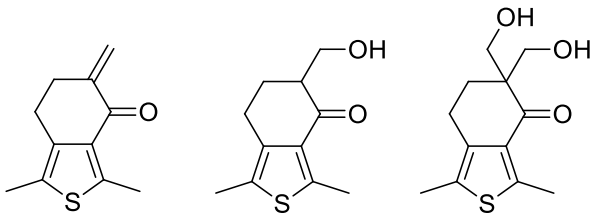

22a

The protocol was inspired by Malkov *et al.*[146c] A 500 ml round bottom flask was charged with 6.248 g (30.0 mmol, 1.0 eq) keto-aldehyde **21a,** 120 ml dry ether, 15.90 g (150 mmol, 5.0 eq) Na_2CO_3 and 30.0 ml (1.0 ml per mmol substrate) 36% formaline solution. The mixture was stirred vigorously at room temperature for 2 d and subsequently treated with 100 ml 1 M NaOH. After phase separation, it was extracted with 2x 100 ml 1 M NaOH and the combined basic phases acidified to pH = 1 with conc. HCl. Subsequent extraction with 3x 150 ml ether and washing with 2x 100 ml water afforded a yellow organic phase that was dried over $MgSO_4$ and the volatiles evaporated to give an yellow-orange oily suspension. As crystallization from 250 ml CyHex was not successful, purification was carried out by MPLC (EA/CyHex) to afford 3.686 g (20.1 mmol, 67% yield) of the enone as a yellow solid as well as 0.728 g (3.46 mmol, 12% yield) *α*-(hydroxymethyl)ketone and 1.004 g (4.18 mmol, 14% yield) *α,α*-di(hydroxymethyl)ketone[58]. Attempted acidic elimination to afford the title compound from the monoalkohol using 1 M HCl in CyHex/EA was very slow and not followed

[58] The presence of exchangeable protons in the diol was tested in NMR by addition of one drop D_2O, which led to a strong decrease of the respective signal and a reduced splitting of the residual signals.

further. The enone partially converted into a dimeric form upon storage even in the freezer.

Enone **22a**:

^{1}H-NMR (300 MHz, $CDCl_3$): δ [ppm] = 6.13 (d, *J* = 1.9 Hz, 1H), 5.41 (dd, *J* = 2.9, 1.2 Hz, 1H), 2.76 (s, 3H), 2.74 – 2.69 (m, 4H), 2.29 (s, 3H).

^{13}C-NMR (75 MHz, $CDCl_3$): δ [ppm] = 185.4, 148.4, 144.8, 137.8, 132.7, 127.2, 121.4, 32.1, 24.5, 16.1, 12.5.

HR-MS (ESI+): *m*/*z* = 193.069 (calc. 193.069 for $[C_{11}H_{12}OS + H]^+$).

α-(hydroxymethyl)ketone:

^{1}H-NMR (300 MHz, $CDCl_3$): δ [ppm] = 3.96 – 3.84 (m, 1H), 3.83 – 3.71 (m, 1H), 3.26 (bs, 1H), 2.85 (ddd, *J* = 16.0, 4.4, 3.3 Hz, 1H), 2.71 (s, 3H), 2.67 – 2.48 (m, 2H), 2.28 (s, 3H), 2.09 – 1.96 (m, 1H), 1.80 (qd, *J* = 12.9, 4.6 Hz, 1H).

^{13}C-NMR (75 MHz, $CDCl_3$): δ [ppm] = 199.2, 147.7, 137.9, 132.2, 127.7, 63.9, 50.1, 26.6, 24.1, 16.0, 12.5.

HR-MS (ESI+): *m*/*z* = 211.082 (calc. 211.079 for $[C_{11}H_{14}O_2S + H]^+$).

α,α-di(hydroxymethyl)ketone:

^{1}H-NMR (300 MHz, $CDCl_3$): δ [ppm] = 3.96 (dd, *J* = 11.3, 4.7 Hz, 2H), 3.73 (dd, *J* = 11.3, 8.1 Hz, 2H), 3.21 (dd, *J* = 8.1, 4.7 Hz, 2H, 2x OH), 2.74 (dd, *J* = 1.9, 1.2 Hz, 2H), 2.71 (s, 3H), 2.28 (s, 3H), 1.87 (t, *J* = 6.6 Hz, 2H).

^{13}C-NMR (75 MHz, $CDCl_3$): δ [ppm] = 200.6, 148.9, 137.0, 131.4, 127.7, 65.3, 51.6, 27.2, 20.2, 16.2, 12.5.

HR-MS (ESI+): *m*/*z* = 241.088 (calc. 241.090 for $[C_{12}H_{16}O_3S + H]^+$).

1,3,7,7-tetramethyl-5-methylene-6,7-dihydrobenzo[c]thiophen-4(5H)-one (22d)

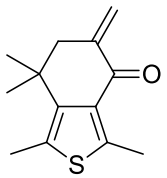

22d

The protocol was inspired by Malkov *et al.*[146c] In a 500 ml flask, 7.799 g (33.00 mmol, 1.0 eq) ketoaldehyde **21d** was dissolved in 150 ml dry diethyl ether and 17.49 g (165 mmol, 5.0 eq) Na_2CO_3 and 16.0 ml (0.5 ml per mmol substrate) 36% formaline solution were added. The mixture was stirred strongly at room temperature overnight, with further addition of 6.995 g (66.0 mmol, 2.0 eq) Na_2CO_3 after 1 h and 16 h, respectively, to obtain a stirrable suspension. Basic TLC indicates full conversion after

20 h.[59] The mixture was treated with 100 ml 1 M NaOH and filtered over celite to remove solids. The plug was washed with EA, and the combined filtrates, after phase separation, extracted with 2x 100 ml EA. The combined organic phases are washed with 100 ml 1 M NaOH and brine, the resulting yellow organic phase dried over $MgSO_4$ and the volatiles evaporated. The title compound was obtained as 7.72 g of an off-white solid that has only minor impurities and can be used as such. Purification is possible via column chromatography (EA/PE 1:10 + 1% Et_3N) to yield 7.198 g (32.7 mmol, 99% yield) of the title compound. Upon storage in the freezer, minor amounts of a dimer formed, but the process seems to be reversible.

^{1}H-NMR (300 MHz, $CDCl_3$): δ [ppm] = 6.14 (dt, *J* = 2.1, 1.1 Hz, 1H), 5.35 (dd, *J* = 3.5, 1.6 Hz, 1H), 2.72 (s, 3H), 2.57 (t, *J* = 1.3 Hz, 2H), 2.43 (s, 3H), 1.35 (s, 6H).
^{13}C-NMR (75 MHz, $CDCl_3$): δ [ppm] = 185.6, 148.2, 144.7, 143.5, 132.5, 127.2, 122.0, 48.6, 35.9, 28.5, 16.4, 15.2.
HR-MS (ESI+): *m/z* = 221.099 (calc. 221.100 for $[C_{13}H_{16}OS+H]^+$).

5,5'-(thiobis(methylene))bis(1,3-dimethyl-6,7-dihydrobenzo[c]thiophen-4(5H)-one) (23a)

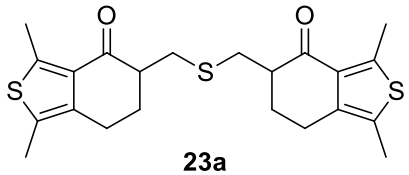

23a

A 25 ml round bottom flask was charged with 0.442 g (2.30 mmol, 1.0 eq) enone **22a**, 0.184 g (1.38 mmol, 0.6 eq) Na_2S hydride in 11 ml water and 22 ml acetone and stirred overnight. From the brownish solution, the volatiles were removed under reduced pressure, the mixture diluted with 20 ml water, and filtered under suction. The precipitate was washed with a little water and then dissolved in a EA/acetone/DCM mixture. The solution was dried over $MgSO_4$, filtered and the volatiles evaporated. Though high conversion was achieved, column chromatography (EA/PE 1:10 to 1:5) only afforded 0.194 g (0.50 mmol, 43% yield) of the title compound purely as a yellowish solid. The possible diastereomers are not resolved by UPLC.

[59] Neutral TLC cannot differentiate between the starting material and the product. Contrary, on basic TLC the starting material has a lowered R_f, whereas the product retains the R_f under these conditions. In contrast to the product, the starting enol stains red with Brady's reagent.

^{1}H-NMR (300 MHz, $CDCl_3$): δ [ppm] = 3.26 – 3.15 (m, 2H), 2.82 (dt, *J* = 16.1, 4.5 Hz, 2H), 2.70 (s, 6H), 2.68 – 2.52 (m, 6H), 2.42 – 2.31 (m, 2H), 2.28 (s, 6H), 1.99 – 1.80 (m, 2H).
^{13}C-NMR (75 MHz, $CDCl_3$): δ [ppm] = 196.0, 195.9, 147.3, 147.3, 137.9, 137.8, 132.0, 132.0, 127.4, 49.0, 48.5, 33.4, 32.8, 28.3, 28.2, 23.7, 23.6, 16.0, 12.5.
HR-MS (ESI+): *m/z* = (calc. 419.117 for $[C_{22}H_{26}O_2S_3 + H]^+$).

5,5'-(thiobis(methylene))bis(1,3,7,7-tetramethyl-6,7-dihydrobenzo[c]thiophen-4(5H)-one) (23d)

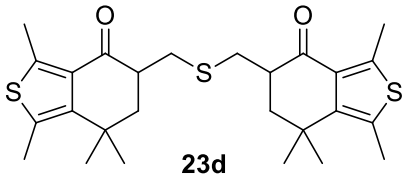

23d

In a 25 ml flask, 0.441 g (2.0 mmol, 1.0 eq) **22d** was dissolved in 10 mL acetone and cooled to 0 °C. Then, 0.156 g (1.20 mmol, 0.6 eq) 60-63% Na_2S hydrate in 10 ml water was added over 2 min. The immediate yellow solution changed into a red/orange suspension. Stirred for 20 h at room temperature when TLC indicated conversion to a single product. The thick suspension was diluted with 100 ml water and DCM. Phase separation was achieved by addition of brine and chloroform. The combined organic phases were dried over $MgSO_4$ and the volatiles evaporated to yield a yellow solid. Column chromatography (EA/PE 1:15) afforded 0.361 g (0.76 mmol, 76% yield) of the title compound as an off-white powder. The possible diastereomers are not resolved by UPLC.

^{1}H-NMR (300 MHz, $CDCl_3$): δ [ppm] = 3.27 (ddd, *J* = 12.9, 3.9, 2.5 Hz, 2H), 2.82 (dddd, *J* = 9.6, 8.6, 4.6, 1.4 Hz, 2H), 2.65 (s, 6H), 2.63 – 2.52 (m, 2H), 2.43 (s, 6H), 2.07 – 1.82 (m, 4H), 1.47 (s, 6H), 1.36 (s, 3H), 1.35 (s, 3H).
^{13}C-NMR (75 MHz, $CDCl_3$): δ [ppm] = 196.0, 146.3, 144.6, 132.2, 128.1, 45.5, 45.4, 45.3, 44.9, 34.7, 33.5, 32.8, 29.8, 26.4, 26.4, 16.1, 15.0.
HR-MS (ESI+): *m/z* = 475.182 (calc. 475.180 for $[C_{26}H_{34}O_2S_3 + H]^+$).

_S_-(1,3,7,7-tetramethyl-4-oxo-4,5,6,7-tetrahydrobenzo[c]thiophen-5-yl) ethanethioate (24d)

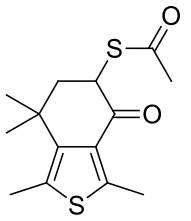

24d

A 25 ml round bottom flask was charged with 0.414 g (4.50 mmol, 1.5 eq) potassium thioacetate and 0.862 g (3.00 mmol, 1.0 eq) bromoketone **19d** and suspended in 15 ml dry THF. After short time, a yellow/orange suspension with a fine white precipitate had formed that changed to red within 16 h of stirring at room temperature. After TLC shows full conversion, the solvent was evaporated and the residue taken up in 30 ml water. It was extracted with 3x 30 ml DCM, dried over $MgSO_4$ and the volatiles evaporated to yield a brown oil. Column chromatography (EA/PE 1:15) afforded 0.740 g (2.62 mmol, 87% yield) of the title compound as a yellow oil that crystallized in the fridge.

^{1}H-NMR (300 MHz, $CDCl_3$): δ [ppm] = 4.64 (dd, *J* = 14.1, 4.6 Hz, 1H), 2.65 (s, 3H), 2.43 (s, 3H), 2.40 (s, 3H), 2.21 (t, *J* = 13.6 Hz, 1H), 1.97 (dd, *J* = 13.2, 4.6 Hz, 1H), 1.46 (s, 6H).
^{13}C-NMR (75 MHz, $CDCl_3$): δ [ppm] = 194.9, 190.4, 147.9, 143.8, 131.4, 128.4, 49.5, 47.3, 35.7, 30.7, 29.5, 26.3, 16.2, 15.0.
HR-MS (ESI+): *m*/*z* =283.084 (calc. 283.083 for $[C_{14}H_{18}O_2S_2 + H]^+$).

1,3,7,7-tetramethyl-5-(((1,3,7,7-tetramethyl-4-oxo-4,5,6,7-tetrahydrobenzo[c]-thiophen-5-yl)methyl)thio)-6,7-dihydrobenzo[c]thiophen-4(5H)-one (25d)

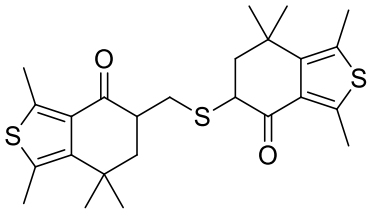

25d

The protocol was adapted from literature.[149] In a 10 ml Schlenk tube, 0.565 g (2.00 mmol, 1.0 eq) thioacetate **24d** was dissolved in 3 ml dry MeOH (dried over molsieves and filtered with Teflon syringe filter) and heated for 10 min to 60 °C. To the resulting yellow solution, 0.25 ml (3.00 mmol, 1.5 eq) 37% aq. HCl was added and stirring continued for 5 h until UPLC indicated full conversion of the starting material.

Upon cooling to room temperature, a voluminous white precipitate formed from the yellow solution. A second flask was charged with 0.441 g (2.00 mmol, 1.0 eq) enone **22d**, 3 ml EA and 0.55 ml (4.00 mmol, 2.0 eq) Et_3N. To this, the reaction mix was added over 3 min at room temperature under stirring. Within 5 min after addition, a fine white solid precipitated from the dark brown solution. It was stirred at room temperature overnight and the resulting green suspension diluted with water and extracted with 3x 50 ml DCM. The combined organic phases were washed with sat. NH_4Cl solution, dried over $MgSO_4$ and the volatiles evaporated to yield a white solid with a green oily impurity. Column chromatography (EA/PE 1:20 to 1:15) afforded some unreacted ketone **22d** and 0.459 g (1.00 mmol, 50% yield) of the title compound as a white solid. NMR revealed a 1:1 diastereomeric mixture.

Diastereomeric 1:1 mixture:

^{1}H-NMR (500 MHz, $CDCl_3$): δ [ppm] = 3.91 – 3.79 (m, 1H), 3.36 (dt, *J* = 12.5, 3.9 Hz, 1H), 2.96 – 2.81 (m, 1H), 2.80 – 2.68 (m, 1H), 2.67 – 2.63 (m, 6H), 2.43 (s, 6H), 2.20 – 2.09 (m, 2H), 2.03 (ddd, *J* = 17.8, 9.4, 4.3 Hz, 1H), 1.93 (td, *J* = 13.6, 8.5 Hz, 1H), 1.49 – 1.46 (m, 6H), 1.39 – 1.35 (m, 6H).

HR-MS (ESI+): *m/z* =461.160 (calc. 461.164 for $[C_{25}H_{32}O_2S_3 + H]^+$).

5,5'-(ethane-1,2-diyl)bis(1,3,7,7-tetramethyl-6,7-dihydrobenzo[c]thiophen-4(5H)-one) (17d)

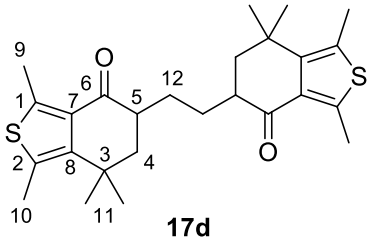

17d

Synthesis under McMurry conditions:

The protocol was inspired by the procedure of Janssen and Lüttke,[155] but uses Zn instead of $LiAlH_3$. Under inert conditions, a 10 ml Schlenk tube was charged with 2 ml dry THF and 0.83 ml (0.75 mmol, 1.5 eq) $TiCl_4$ at 0 °C to give a yellow suspension. Addition of 0.098 g (1.50 mmol, 3.0 eq) Zn at once gave a grey-blue suspension that turned brown upon treatment with 0.04 ml (0.50 mmol, 1.0 eq) dry pyridine. After short stirring, 0.110 g (0.50 mmol, 1.0 eq) **22d** was added in 0.5 ml THF, which rapidly caused a coloration to black. After 1 h TLC indicated full conversion. The mixture was treated with 10 ml 1 M HCl and extracted with 3x 20 ml DCM, the combined organic phases dried over $MgSO_4$ and the volatiles evaporated under reduced pressure. The crude product was

purified by column chromatography (EA/PE 1:20 to 1:10) to yield 0.020 g (0.045 mmol, 36% yield) of the title compound as a white solid. Due to very similar R_f values, the single fractions were identified by UPLC.

Synthesis under electrolysis conditions:

The protocol was inspired by the procedure of Bowers *et al.*[152] The reduction potential of enone **22d** in MeCN was determined to be E_p^c = -2.334 V (against SCE). In a double H cell equipped with a platinum net, 0.101 mg (0.46 mmol) were treated with one equivalent electrons at a working potential of E_p^a = -2.100 V (against SCE) using 0.1 M Et_4NPF_6 as electrolyte. After electrolysis, the dark red reaction mixture was treated with 1 ml 0.1 M $HClO_4$ solution in AcOH, whereupon the solution turned yellow immediately. After evaporation of the volatiles, the resulting solid was purified by column chromatography as above to yield 0.020 mg (0.09 mmol, 20% yield) of the title compound. NMR indicates a higher preference for one diastereomer than in the wet chemical approach.

^{1}H-NMR (500 MHz, $CDCl_3$): δ [ppm] = 2.65 (s, 6H, 2x C9H_3), 2.62 – 2.50 (m, 2H, 2x C5H), 2.43 (s, 6H, 2x C10H_3), 2.21 – 2.14 (m, 1H, 1x C12H), 2.10 – 2.01 (m, 1H, 1x C12H), 1.91 – 1.79 (m, 4H, 2x C4H_2), 1.53 – 1.47 (m, 1H, 1x C12H), 1.46 (2x s, 6H, 2x C11H_3), 1.39 – 1.35 (m, 1H, 1x C12H), 1.34 (2x s, 6H, 2x C11H_3).

^{13}C-NMR (126 MHz, $CDCl_3$): δ [ppm] = 197.8 (2x C6), 145.8 (2x C1), 144.7 (2x C2), 132.6 (2x C7), 127.9 (2x C8), 46.0 (1x C4), 45.7 (1x C4), 45.2 (1x C5), 44.8 (1x C5), 34.69 (2x C3), 29.9 (2x C11), 26.5 (1x C12), 26.3 (2x C11), 26.0 (1x C12), 16.1 (2x C9), 15.0 (2x C10).

HR-MS (ESI+): *m/z* = 443.208 (calc. 443.207 for $[C_{26}H_{34}O_2S_2 + H]^+$).

1,3,10,12-tetramethyl-4,5,5a,6,7,7a,8,9-octahydrophenanthro[3,4-c:5,6-c']dithiophene (pcDTE$_{666}$-Me)

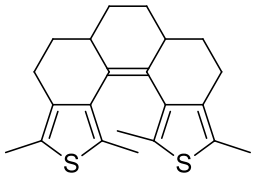

pcDTE$_{666}$-Me

A 20 ml Schlenk tube was charged with 4 ml dry THF and cooled to 0 °C. To this, 0.13 ml (1.20 mmol, 1.5 eq) $TiCl_4$ was added, followed by 0.157 g (2.40 mmol, 3.0 eq) Zn and 65 µl (0.80 mmol, 1.0 eq) dry pyridine. In a second 50 ml round bottom flask, the same reagent was prepared in 16 ml THF. To the first flask, 0.154 g (0.80 mmol,

1.0 eq) enone **22a** in 2 ml THF was added at low temperature and stirred for 4 h to room temperature when UPLC indicates full conversion of the starting material. The reaction mixture was transferred to the second flask and heated to 70 °C for 2 h. Subsequently, it was diluted with 10% Na_2CO_3 and brine and extracted with 3x 20 ml EA. The combined organic phases were dried over $MgSO_4$ and the volatiles evaporated. Subsequent column chromatography (DCM/PE 1:9) afforded 0.010 g (0.028 mmol, 7% yield) of the title compound as white powder. UPLC indicates formation of three diastereomers with different absorption spectra.

Due to the complex isomeric mixture, the NMR spectra could not be interpreted and are instead attached as measured (Figure 4.6-1).
HR-MS (ESI+): *m/z* = 354.146 (calc. 354.148 for $[C_{22}H_{26}S_2]^+$).[56]

1,3,4,4,9,9,10,12-octamethyl-4,5,5a,6,7,7a,8,9-octahydrophenanthro[3,4-c:5,6-c']dithiophene (pcDTE$_{666}$(Me$_2$)-Me)

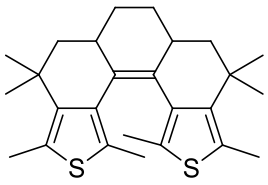

pcDTE$_{666}$(Me$_2$)-Me

In a 20 ml Schlenk tube under inert conditions at 0 °C, 0.70 ml (6.38 mmol, 1.5 eq) $TiCl_4$ was slowly added to 20 ml dry THF. To the yellow suspension, 0.834 g (12.75 mmol, 3.0 eq) Zn were added at once to form a grey-blue suspension that turned brown upon treatment with 0.34 ml (4.25 mmol, 1.0 eq) dry pyridine. After short stirring, 0.936 g (4.25 mmol, 1.0 eq) **22d** were added in 5 ml THF followed by immediate coloration to black. UPLC control after 2 h indicates full conversion of the starting matter to dimer **17d** and a minor amount of reduced ketone **27d**. Consequently, the reaction mixture was transferred to second flask containing the same amount of reagent in 60 ml dry THF and was heated to 70 °C for 2 d until TLC indicated total disappearance of the dimer. The mixture is treated with 50 ml brine and 1 M HCl and extracted with 3x 100 ml DCM, the combined organic phases washed again with brine, dried over $MgSO_4$ and the volatiles evaporated under reduced pressure. The crude product was purified by column chromatography (100% PE to EA/DCM 1:10) to yield 0.046 g (0.12 mmol, 5% yield) of a diastereomeric mixture as a white solid.

Separation of the diastereomers by careful normal phase column chromatography (pentane) was unsuccessful. Also prep. TLC (pentane) could not achieve full separation. From the developed plate the stationary phase was fractioned in small stripes, suspended in DCM and filtered after extensive ultrasound treatment. The batches were analyzed by UPLC. Prep. GPC yielded no separation. Separation by prep. HPLC on a C18-capped stationary phase was impractical to long retention times needed for separation and consequent peak broadening. On a phenyl-hexyl stationary phase, separation of one isomer could be achieved, yet, low solubility of the material prevented further use of the method. Accumulation of the major isomer was achieved by slow evaporation of THF and ACN from the oversaturated solutions prepared for purification by prep. HPLC.

Due to the complex isomeric mixture, the NMR spectra could not be interpreted and are instead attached as measured (Figure 4.6-2).

HR-MS (ESI+): m/z = 410.210 (calc. 410.210 for $[C_{26}H_{34}S_2]^+$).[56]

4.6 Selected ^{1}H and ^{13}C-NMR spectra

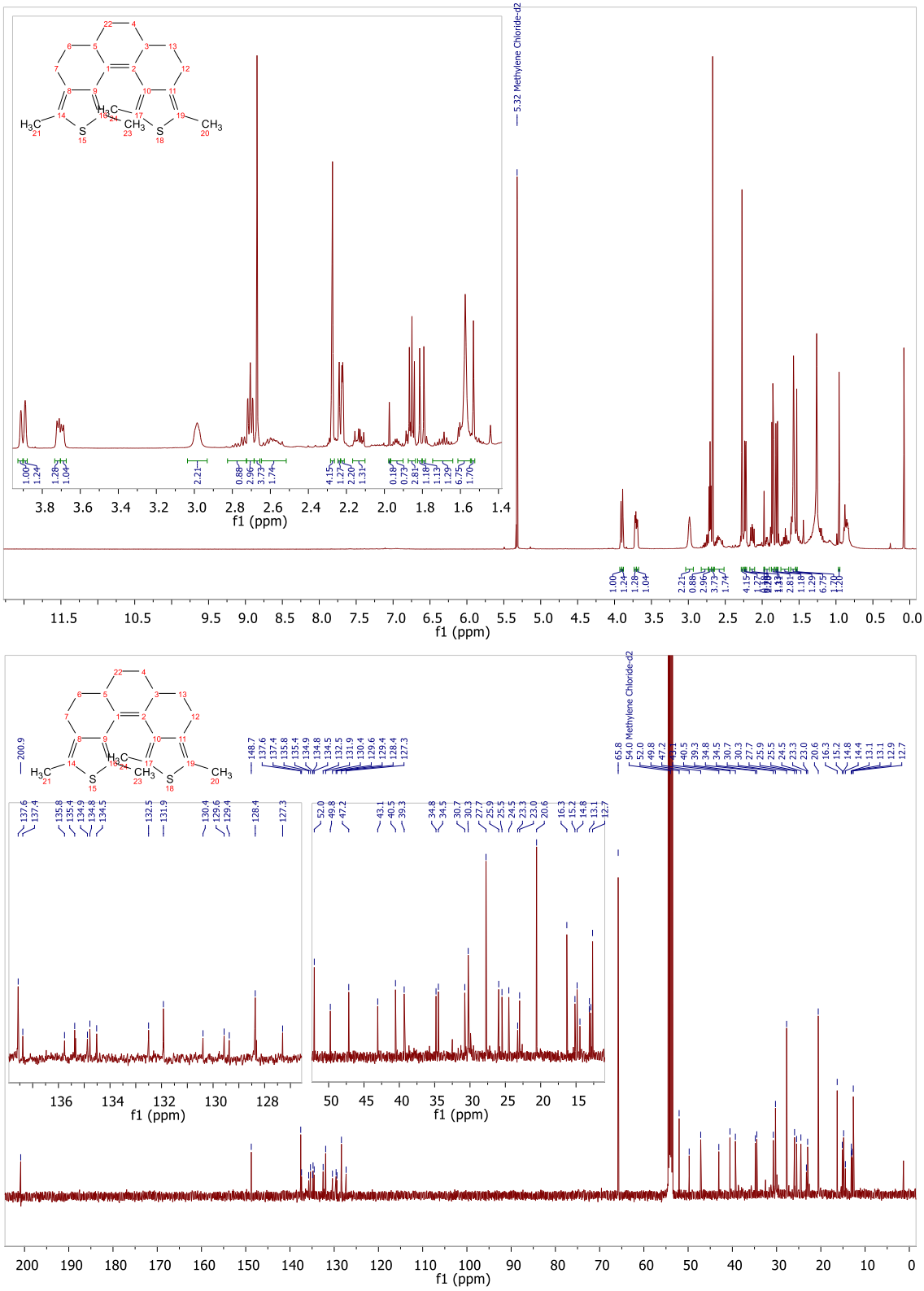

Figure 4.6-1 NMR spectra of **pcDTE$_{666}$-Me**. **Top:** ^{1}H-NMR (500 MHz, CD_2Cl_2). **Bottom:** ^{13}C-NMR (126 MHz, CD_2Cl_2).

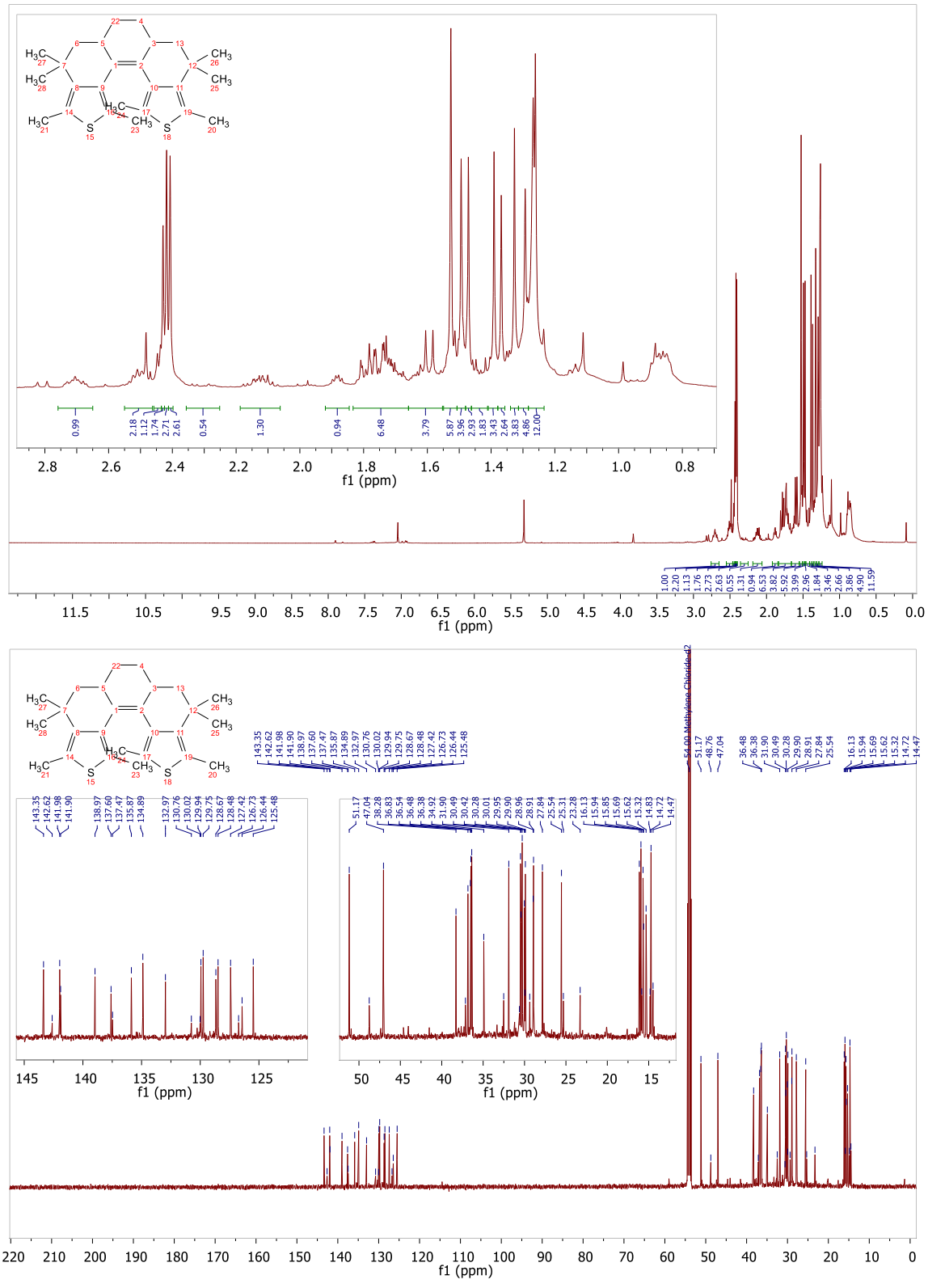

Figure 4.6-2 NMR spectra of **pcDTE$_{666}$(Me$_2$)-Me**. **Top:** ^{1}H-NMR (500 MHz, CD_2Cl_2). **Bottom:** ^{13}C-NMR (126 MHz, CD_2Cl_2).

4.7 Crystal structures

The prepared single-crystals were mounted using a microfabricated polymer film crystal-mounting tool (dual-thickness MicroMount, MiTeGen) using low viscosity oil (perfluoropolyalkylether; viscosity 1800 cSt, ABCR) to reduce the X-ray absorption and scattering. A Bruker D8 Venture single-crystal X-ray diffractometer with area detector using Mo-K_α ($\lambda = 0.71073$ Å) radiation was used for data collection the given temperature. Multiscan absorption corrections implemented in SADABS [170] were applied to the data. The structures were solved by intrinsic phasing (SHELXT-2013)[171] and refined by full-matrix least-squares methods on F^2 (SHELXL-2014).[172] The hydrogen atoms were placed at calculated positions and refined by using a riding model.

The asymmetric units are shown in the following. All disordered atoms and solvent molecules are shown if not stated otherwise. For aDTE, the length of the central double as well as the distances between both inner α-carbons and both outer α-carbons of the two thiophenes are given. Where applicable, the torsion of the phenyl units is given, defined as S-C_{quat}-C_{quat}-C_H.

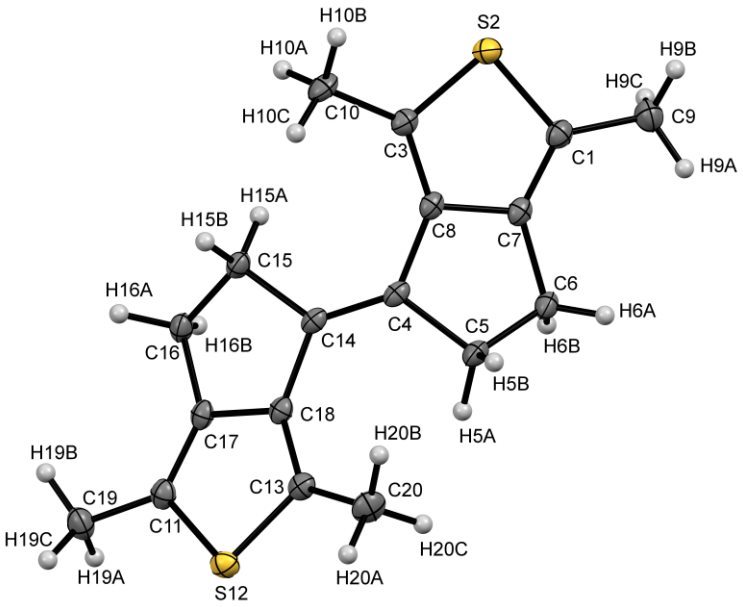

Figure 4.7-1 Asymmetric unit of *E*-**aDTE$_{55}$-Me**. Bond length central double bond [Å]: 1.343(2). Selected distances through space [Å]: C3-C13 5.841(2); C1-C11 8.233(2).

Crystallographic details:

Name	***E*-aDTE$_{55}$-Me**
Chemical formula	$C_{18}H_{20}S_2$
M_r	300.46
Crystal system	Orthorhombic
Space group	Pbca
***a* [Å]**	15.547 (3)
***b* [Å]**	7.905 (2)
***c* [Å]**	24.936 (5)
α [°]	90
β [°]	90
γ [°]	90
***V* [Å^3]**	3064.6 (12)
Temperature [K]	103
Z	8
No. of reflections measured	113793
No. of independent reflections	3402
R_{int}	0.043
$(\sin \theta/\lambda)_{max}$ (Å^{-1})	0.643
R[F2 > 2σ(F2)]	0.029
wR(F2)	0.082
S	1.05

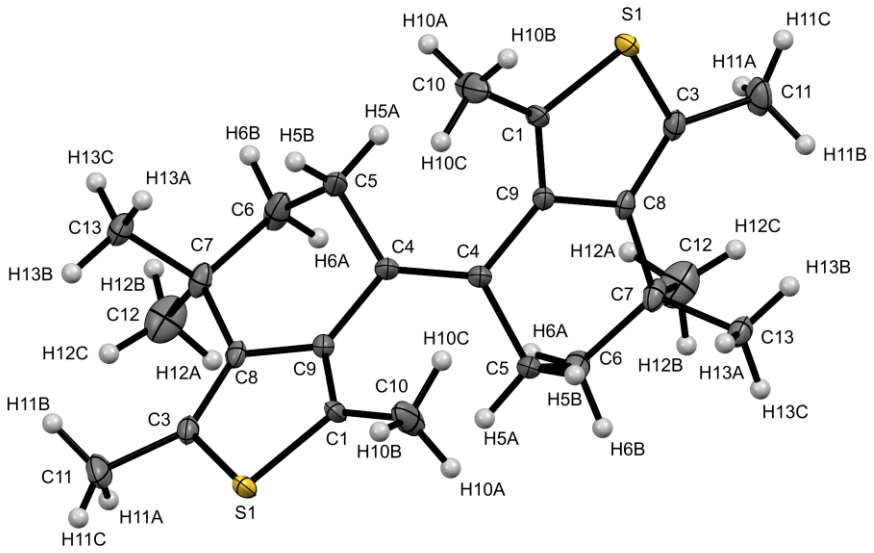

Figure 4.7-2 Asymmetric unit of *E*-**aDTE$_{66}$(Me$_2$)-Me**. A second molecule in the unit cell with inversed ring conformation at both C5 and C6 was omitted for clarity. Bond length central double bond [Å]: 1.359(4). Selected distances through space [Å]: C1-C1 5.279(4); C3-C3 8.438(5).

Crystallographic details:

Name	***E*-aDTE$_{66}$(Me$_2$)-Me**
Chemical formula	$C_{24}H_{32}S_2$
M_r	384.62
Crystal system	Monoclinic
Space group	P2/c
***a* [Å]**	14.310 (3)
***b* [Å]**	5.993 (2)
***c* [Å]**	24.651 (5)
α [°]	90
β [°]	95.81 (3)
γ [°]	90
***V* [Å^3]**	2103.3 (9)
Temperature [K]	100
Z	4
No. of reflections measured	55149
No. of independent reflections	4378
R_{int}	0.043
(sin θ/λ)$_{max}$ (Å^{-1})	0.626
R[F2 > 2σ(F2)]	0.056
wR(F2)	0.183
S	1.16

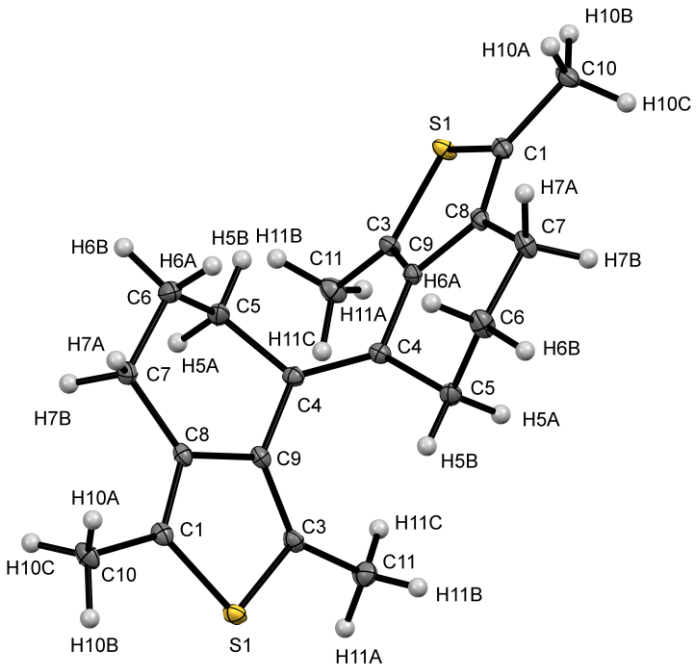

Figure 4.7-3 Asymmetric unit of *E*-**aDTE$_{66}$-Me**. Bond length central double bond [Å]: 1.358(2). Selected distances through space [Å]: C3-C3 5.358(3); C1-C1 8.350(3).

Crystallographic details:

Name	***E*-aDTE$_{66}$-Me**
Chemical formula	$C_{20}H_{24}S_2$
M_r	328.51
Crystal system	Monoclinic
Space group	C2/c
***a* [Å]**	21.062 (4)
***b* [Å]**	11.550 (2)
***c* [Å]**	7.186 (2)
α [°]	90
β [°]	106.14 (3)
γ [°]	90
***V* [Å^3]**	1679.1 (7)
Temperature [K]	100
Z	4
No. of reflections measured	14897
No. of independent reflections	1719
R_{int}	0.030
(sin θ/λ)$_{max}$ (Å^{-1})	0.626
R[F2 > 2σ(F2)]	0.031
wR(F2)	0.085
S	1.07

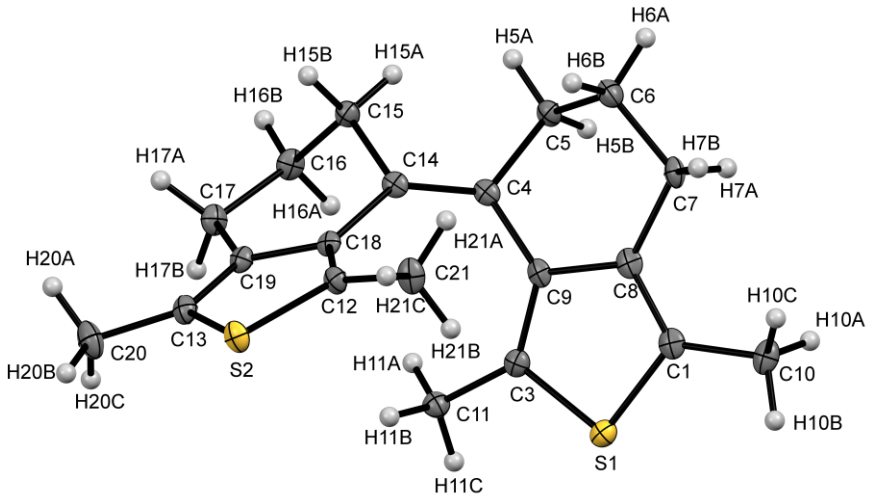

Figure 4.7-4 Asymmetric unit of *Z*-**aDTE$_{66}$-Me**. Bond length central double bond [Å]: 1.360(4). Selected distances through space [Å]: C3-C12 3.414(4); C1-C13 7.229(5).

Crystallographic details:

Name	***Z*-aDTE$_{66}$-Me**
Chemical formula	$C_{20}H_{24}S_2$
M_r	328.51
Crystal system	Triclinic
Space group	P
***a* [Å]**	7.224 (5)
***b* [Å]**	10.135 (7)
***c* [Å]**	12.423 (7)
α [°]	109.66 (3)
β [°]	91.89 (2)
γ [°]	100.24 (3)
***V* [Å^3]**	838.7 (9)
Temperature [K]	100
Z	2
No. of reflections measured	17353
No. of independent reflections	3426
R_{int}	0.054
(sin θ/λ)$_{max}$ (Å^{-1})	0.627
R[F2 > 2σ(F2)]	0.054
wR(F2)	0.152
S	1.09

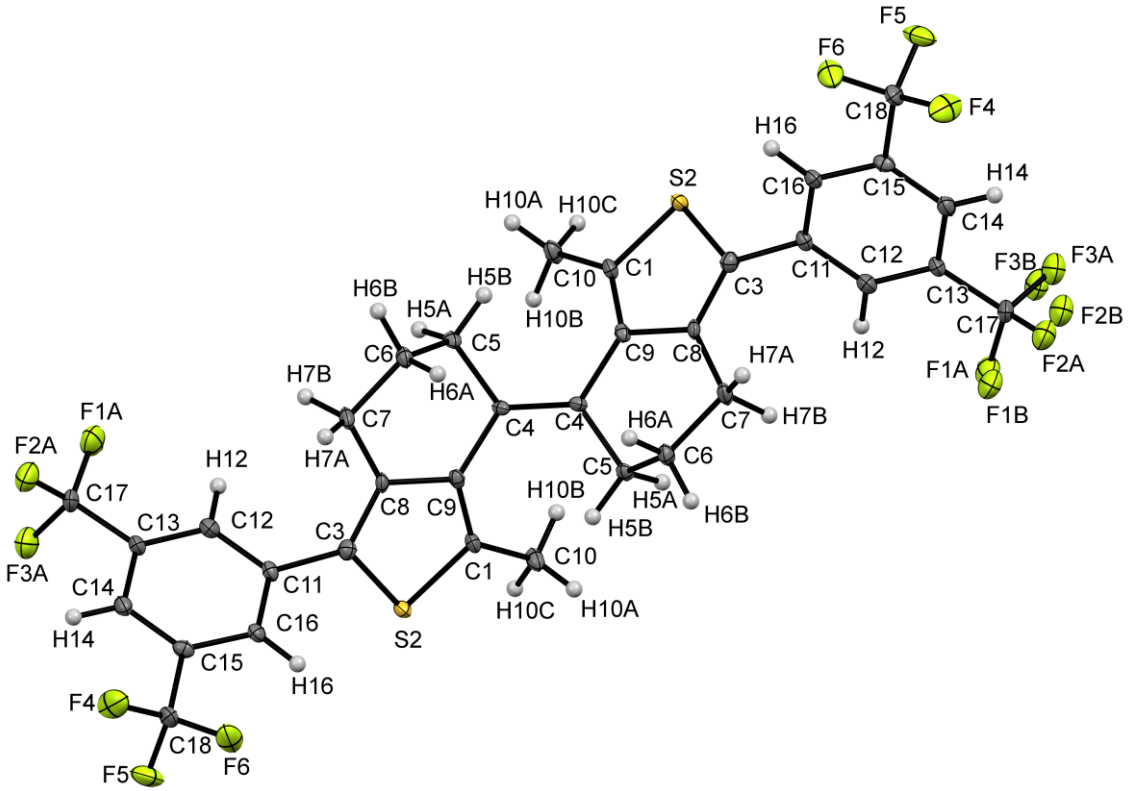

Figure 4.7-5 Asymmetric unit of *E*-**aDTE$_{66}$-Ph(CF$_3$)$_2$**. Bond length central double bond [Å]: 1.376(5). Selected distances through space [Å]: C1-C1 5.448(6); C3-C3 8.520(6). Torsion of phenyl units [°]: 63.2(6).

Crystallographic details:

Name	***E*-aDTE$_{66}$-Ph(CF$_3$)$_2$**
Chemical formula	$C_{34}H_{24}F_{12}S_2$
***M*$_r$**	724.65
Crystal system	Monoclinic
Space group	C2
***a* [Å]**	21.680 (4)
***b* [Å]**	4.927 (2)
***c* [Å]**	15.248 (3)
α [°]	90
β [°]	114.73 (3)
γ [°]	90
***V* [Å^3]**	1479.2 (8)
Temperature [K]	100
Z	2
No. of reflections measured	17474
No. of independent reflections	3264
***R*$_{int}$**	0.030
(sin θ/λ)$_{max}$ (Å^{-1})	0.641
R[F2 > 2σ(F2)]	0.051
wR(F2)	0.136
S	1.36

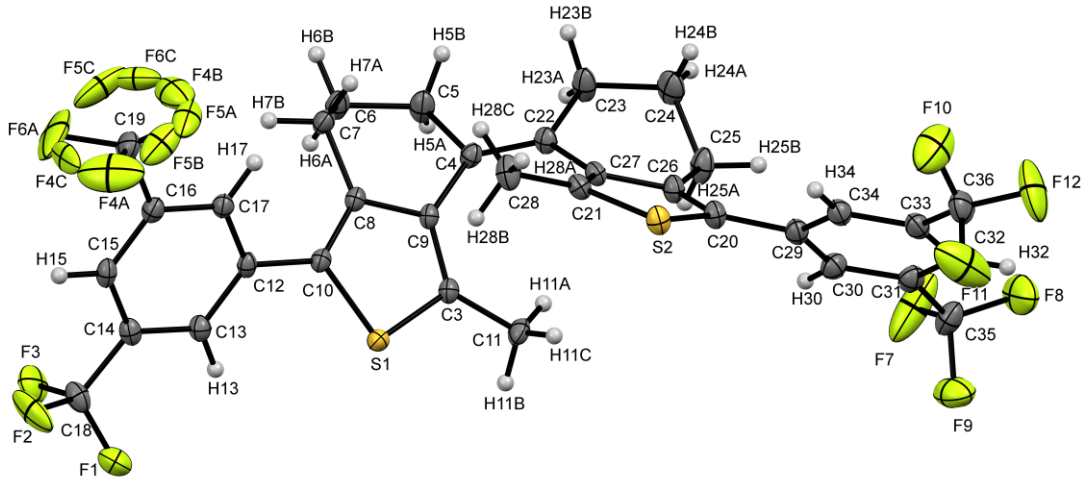

Figure 4.7-6 Asymmetric unit of *Z*-**aDTE$_{66}$-Ph(CF$_3$)$_2$**. One molecule of MeCN in the asymmetric unit was omitted for clarity. Bond length central double bond [Å]: 1.349(3). Selected distances through space [Å]: C3-C21 3.379(3); C10-C20 6.983(4). Torsion of phenyl units [°]: -39.0(2) and -35.6(3).

Crystallographic details:

Name	***Z*-aDTE$_{66}$-Ph(CF$_3$)$_2$**
Chemical formula	$C_{35.16}H_{24}F_{12.03}N_{0.58}S_2$
***M*$_r$**	747.37
Crystal system	Triclinic
Space group	P
***a* [Å]**	8.2539 (18)
***b* [Å]**	12.270 (3)
***c* [Å]**	16.654 (7)
α [°]	84.77 (3)
β [°]	88.748 (18)
γ [°]	73.908 (18)
***V* [Å^3]**	1613.9 (9)
Temperature [K]	100
Z	2
No. of reflections measured	59479
No. of independent reflections	7185
***R*$_{int}$**	0.062
(sin θ/λ)$_{max}$ (Å^{-1})	0.644
R[F2 > 2σ(F2)]	0.048
wR(F2)	0.126
S	1.04

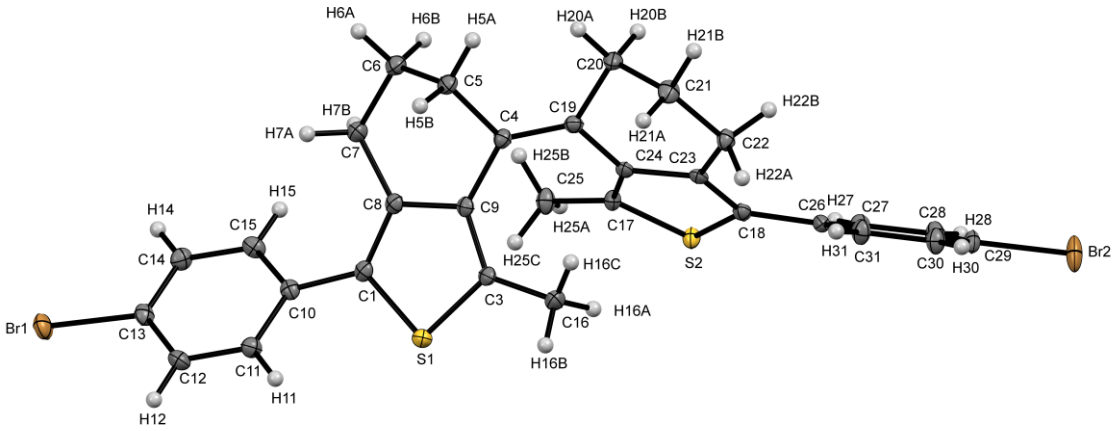

Figure 4.7-7 Asymmetric unit of *Z*-**aDTE$_{66}$-PhBr**. Bond length central double bond [Å]: 1.350(3). Selected distances through space [Å]: C3-C17 3.442(3); C1-C18 7.061(3). Torsion of phenyl units [°]: 30.9(3) and 27.0(3).

Crystallographic details:

Name	***Z*-aDTE$_{66}$-PhBr**
Chemical formula	$C_{30}H_{26}Br_2S_2$
M_r	610.43
Crystal system	Monoclinic
Space group	P21/c
***a* [Å]**	12.881 (3)
***b* [Å]**	7.595 (2)
***c* [Å]**	25.565 (5)
α [°]	90
β [°]	91.25 (3)
γ [°]	90
***V* [Å^3]**	2500.5 (10)
Temperature [K]	100
Z	4
No. of reflections measured	31410
No. of independent reflections	5538
R_{int}	0.055
$(\sin \theta/\lambda)_{max}$ (Å^{-1})	0.643
R[F2 > 2σ(F2)]	0.030
wR(F2)	0.077
S	1.01

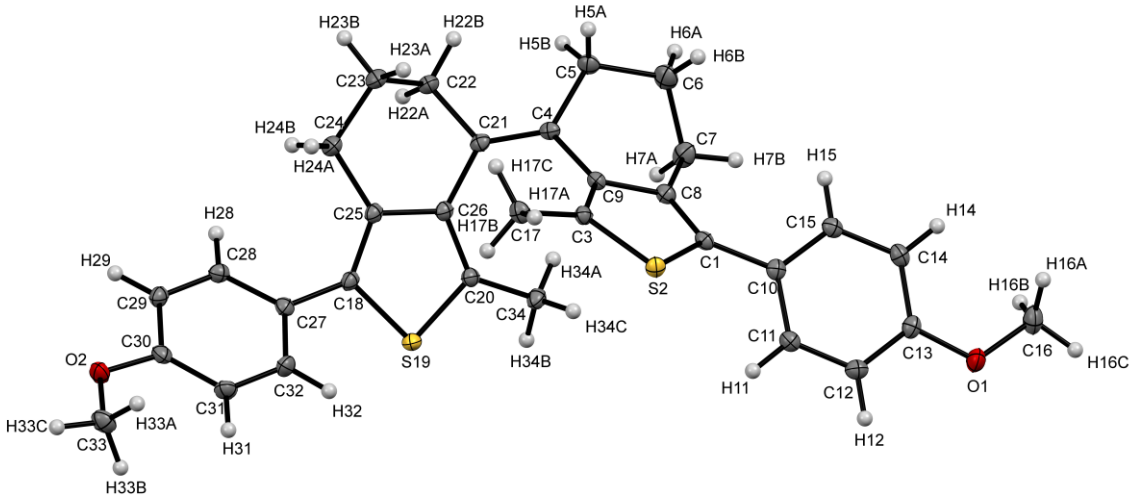

Figure 4.7-8 Asymmetric unit of *Z*-**aDTE$_{66}$-PhOMe**. Bond length central double bond [Å]: 1.351(2). Selected distances through space [Å]: C3-C20 3.257(3); C1-C18 6.735(4). Torsion of phenyl units [°]: 41.1(2) and 36.9(2).

Crystallographic details:

Name	***Z*-aDTE$_{66}$-PhOMe**
Chemical formula	$C_{32}H_{32}O_2S_2$
M_r	512.69
Crystal system	Triclinic
Space group	P
***a* [Å]**	7.999 (4)
***b* [Å]**	9.899 (6)
***c* [Å]**	16.193 (9)
α [°]	86.85 (3)
β [°]	87.02 (3)
γ [°]	81.55 (2)
***V* [Å^3]**	1265.0 (12)
Temperature [K]	100
Z	2
No. of reflections measured	46307
No. of independent reflections	5619
R_{int}	0.053
(sin θ/λ)$_{max}$ (Å^{-1})	0.644
R[F2 > 2σ(F2)]	0.037
wR(F2)	0.089
S	1.05

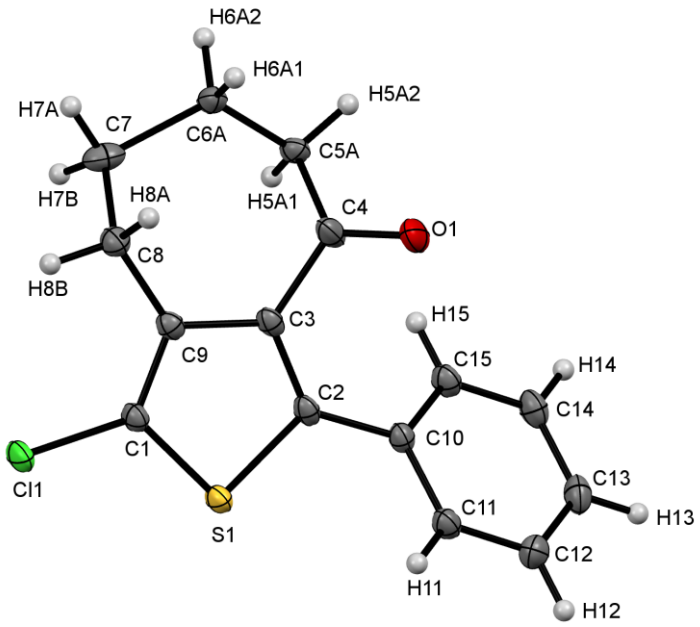

Figure 4.7-9 Asymmetric unit of ketone **9**. Disordered carbons C5B and C6B as well as corresponding protons originating from a different conformation of the 7-membered ring removed for clarity. Torsion of phenyl unit [°]: -44.5(1).

Crystallographic details:

Name	**9**
Chemical formula	$C_{15}H_{13}ClOS$
M_r	276.76
Crystal system	Monoclinic
Space group	P21/c
***a* [Å]**	13.9212 (10)
***b* [Å]**	8.3735 (6)
***c* [Å]**	12.0544 (10)
α [°]	90
β [°]	113.739 (2)
γ [°]	90
***V* [Å^3]**	1286.28 (17)
Temperature [K]	100
Z	4
No. of reflections measured	29762
No. of independent reflections	3157
R_{int}	0.025
$(\sin \theta/\lambda)_{max}$ (Å^{-1})	0.669
R[F2 > 2σ(F2)]	0.028
wR(F2)	0.075
S	0.97

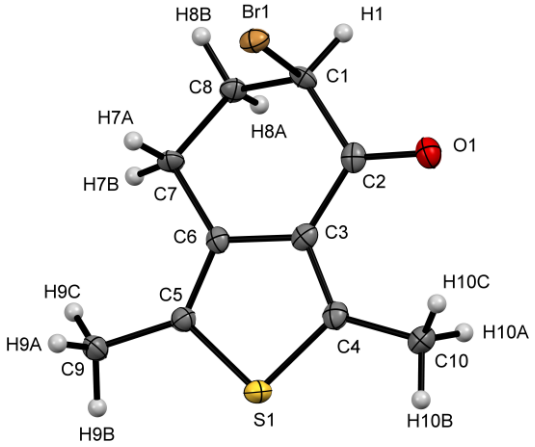

Figure 4.7-10 Asymmetric unit of ketone **19a**.

Crystallographic details:

Name	**19a**
Chemical formula	$C_{10}H_{11}BrOS$
M_r	259.16
Crystal system	Orthorhombic
Space group	P212121
***a* [Å]**	6.0118 (6)
***b* [Å]**	10.2136 (10)
***c* [Å]**	16.2330 (15)
α [°]	90
β [°]	90
γ [°]	90
***V* [Å^3]**	996.74 (17)
Temperature [K]	100
Z	4
No. of reflections measured	7825
No. of independent reflections	1754
R_{int}	0.093
$(\sin \theta/\lambda)_{max}$ (Å^{-1})	0.596
R[F2 > 2σ(F2)]	0.048
wR(F2)	0.119
S	1.03

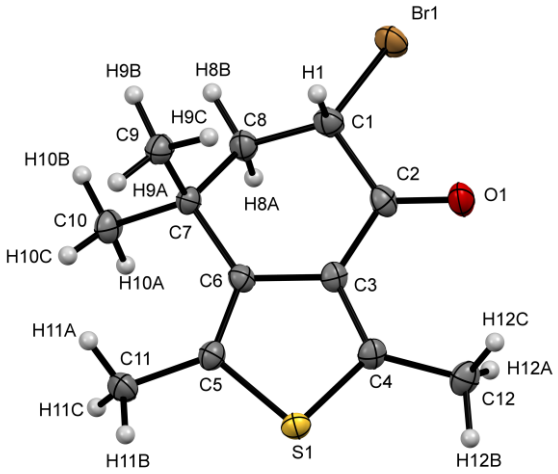

Figure 4.7-11 Asymmetric unit of ketone **19d**.

Crystallographic details:

Name	**19d**
Chemical formula	$C_{12}H_{15}BrOS$
M_r	287.21
Crystal system	Monoclinic
Space group	P21/n
***a* [Å]**	10.4747 (4)
***b* [Å]**	16.5717 (7)
***c* [Å]**	14.0127 (7)
α [°]	90
β [°]	95.424 (2)
γ [°]	90
***V* [Å^3]**	2421.48 (18)
Temperature [K]	100
Z	8
No. of reflections measured	19815
No. of independent reflections	4472
R_{int}	0.113
$(\sin \theta/\lambda)_{max}$ (Å^{-1})	0.606
R[F2 > 2σ(F2)]	0.046
wR(F2)	0.128
S	1.06

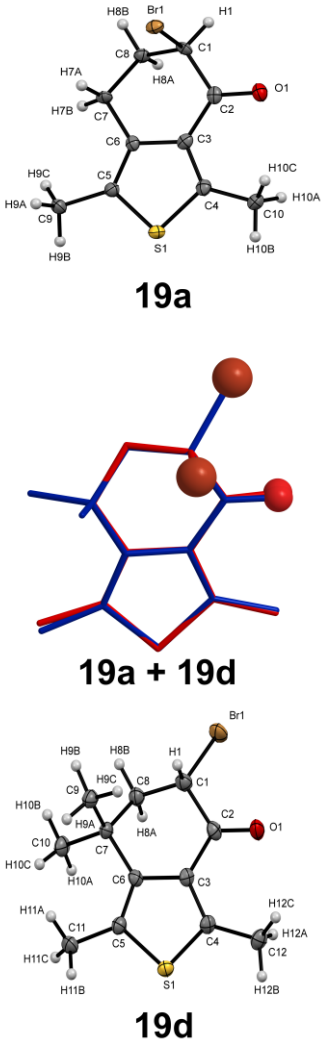

Figure 4.7-12 Comparison of the two employed 6-membered ring ketones employed for synthesis. Ketone **19a** and **19d** are brominated in the axial and equatorial position, respectively. The overlay (middle) shows the bromine and oxygen atoms as balls. It was created in ChemBio3D (CambridgeSoft).

5. References

[1] a) H. Bouas-Laurent, H. Dürr, in *Pure Applied Chemistry, Vol. 73*, **2001**, p. 639; b) H. Dürr, *Angewandte Chemie* **2004**, *116*, 3404-3418.

[2] K. Xiao, H.-J. Zhang, L.-J. Xuan, J. Zhang, Y.-M. Xu, D.-L. Bai, in *Studies in Natural Products Chemistry, Vol. 34* (Ed.: R. Atta ur), Elsevier, **2008**, 453-646.

[3] a) G. M. Wyman, *Chemical Reviews* **1955**, *55*, 625-657; b) G. S. Hammond, J. Saltiel, J. S. Bradshaw, N. J. Turro, A. A. Lamola, V. Vogt, R. C. Counsell, D. O. Cowan, C. Dalton, *Journal of the American Chemical Society* **1964**, *86*, 3197.

[4] D. H. Waldeck, *Chemical Reviews* **1991**, *91*, 415-436.

[5] H. Meier, *Angewandte Chemie International Edition in English* **1992**, *31*, 1399-1420.

[6] D. L. Beveridge, H. H. Jaffé, *Journal of the American Chemical Society* **1965**, *87*, 5340-5346.

[7] A. V. El'tsov, *Organic Photochromes, Vol. 1*, Springer US, **1990**.

[8] G. B. Kistiakowsky, W. R. Smith, *Journal of the American Chemical Society* **1934**, *56*, 638-642.

[9] E. Maccarone, A. Mamo, G. Perrini, M. Torre, *Journal of the Chemical Society, Perkin Transactions 2* **1981**, 324-326.

[10] a) J. Yu, M. J. Gaunt, J. B. Spencer, *The Journal of Organic Chemistry* **2002**, *67*, 4627-4629; b) S. M. Abdur Rahman, M. Sonoda, M. Ono, K. Miki, Y. Tobe, *Organic Letters* **2006**, *8*, 1197-1200.

[11] a) J. D. Fitzpatrick, M. Orchin, *The Journal of Organic Chemistry* **1957**, *22*, 1177-1179; b) G. Scarlata, M. Torre, *Journal of Heterocyclic Chemistry* **1976**, *13*, 1193-1196.

[12] a) J. Saltiel, S. Ganapathy, C. Werking, *The Journal of Physical Chemistry* **1987**, *91*, 2755-2758; b) S. Yamashita, *Bulletin of the Chemical Society of Japan* **1961**, *34*, 487-489.

[13] W. M. Moore, D. D. Morgan, F. R. Stermitz, *Journal of the American Chemical Society* **1963**, *85*, 829-830.

[14] a) K. B. Jørgensen, *Molecules* **2010**, *15*, 4334; b) C. S. Wood, F. B. Mallory, *The Journal of Organic Chemistry* **1964**, *29*, 3373-3377; c) F. B. Mallory, C. S. Wood, J. T. Gordon, *Journal of the American Chemical Society* **1964**, *86*, 3094-3102.

[15] a) R. M. Kellogg, M. B. Groen, H. Wynberg, *The Journal of Organic Chemistry* **1967**, *32*, 3093-3100; b) E. Fischer, J. Larsen, J. B. Christensen, M. Fourmigué, H.

G. Madsen, N. Harrit, *The Journal of Organic Chemistry* **1996**, *61*, 6997-7005; c) F. B. Mallory, C. W. Mallory, in *Organic Reactions*, John Wiley & Sons, Inc., **2004**.

[16] L.-Y. Yang, M. Harigai, Y. Imamoto, M. Kataoka, T.-I. Ho, E. Andrioukhina, O. Federova, S. Shevyakov, R. S. H. Liu, *Photochemical & Photobiological Sciences* **2006**, *5*, 874-882.

[17] a) J. Saltiel, A. S. Waller, D. F. Sears, *Journal of Photochemistry and Photobiology A: Chemistry* **1992**, *65*, 29-40; b) D. Sampedro Ruiz, A. Cembran, M. Garavelli, M. Olivucci, W. Fuß, *Photochemistry and Photobiology* **2002**, *76*, 622-633.

[18] T. Wismonski-Knittel, G. Fischer, E. Fischer, *Journal of the Chemical Society, Perkin Transactions 2* **1974**, 1930-1940.

[19] D. Gegiou, K. A. Muszkat, E. Fischer, *Journal of the American Chemical Society* **1968**, *90*, 3907-3918.

[20] D. Lenoir, J. E. Gano, J. McTague, *Tetrahedron Letters* **1986**, *27*, 5339-5342.

[21] J. E. Gano, B. S. Park, A. A. Pinkerton, D. Lenoir, *The Journal of Organic Chemistry* **1990**, *55*, 2688-2693.

[22] M. Oelgemöller, R. Frank, P. Lemmen, D. Lenoir, J. Lex, Y. Inoue, *Tetrahedron* **2012**, *68*, 4048-4056.

[23] a) J. E. Gano, B.-S. Park, A. A. Pinkerton, D. Lenoir, *Acta Crystallographica Section C* **1991**, *47*, 162-164; b) J. E. Gano, B. S. Park, G. Subramaniam, D. Lenoir, R. Gleiter, *The Journal of Organic Chemistry* **1991**, *56*, 4806-4808; c) J. E. Gano, C. Kluwe, K. Kirschbaum, A. A. Pinkerton, P. Sekher, E. Skrzypczak-Jankun, G. Subramaniam, D. Lenoir, *Acta Crystallographica Section C* **1997**, *53*, 1723-1725.

[24] M. Oelgemoller, B. Brem, R. Frank, S. Schneider, D. Lenoir, N. Hertkorn, Y. Origane, P. Lemmen, J. Lex, Y. Inoue, *Journal of the Chemical Society, Perkin Transactions 2* **2002**, 1760-1771.

[25] a) K. A. Muszkat, D. Gegiou, E. Fischer, *Chemical Communications (London)* **1965**, 447-448; b) K. A. Muszkat, E. Fischer, *Journal of the Chemical Society B: Physical Organic* **1967**, 662-678.

[26] M. M. Krayushkin, *Chemistry of Heterocyclic Compounds* **2001**, *37*, 15-36.

[27] a) M. Irie, *Chemical Reviews* **2000**, *100*, 1685-1716; b) M. Irie, T. Fukaminato, K. Matsuda, S. Kobatake, *Chemical Reviews* **2014**, *114*, 12174-12277.

[28] a) R. Naef, E. Fischer, *Helvetica Chimica Acta* **1974**, *57*, 2224-2233; b) M. V. Sargent, C. J. Timmons, *Journal of the American Chemical Society* **1963**, *85*,

2186-2187; c) M. V. Sargent, C. J. Timmons, *Journal of the Chemical Society (Resumed)* **1964**, 2222-2225.

[29] C. E. Ramey, V. Boekelheide, *Journal of the American Chemical Society* **1970**, *92*, 3681-3684.

[30] a) M. Irie, M. Mohri, *The Journal of Organic Chemistry* **1988**, *53*, 803-808; b) S. Nakamura, M. Irie, *The Journal of Organic Chemistry* **1988**, *53*, 6136-6138.

[31] a) A. Perrier, S. Aloise, M. Olivucci, D. Jacquemin, *The Journal of Physical Chemistry Letters* **2013**, *4*, 2190-2196; b) T. Kudernac, T. Kobayashi, A. Uyama, K. Uchida, S. Nakamura, B. L. Feringa, *The Journal of Physical Chemistry A* **2013**, *117*, 8222-8229.

[32] a) M. Irie, K. Sakemura, M. Okinaka, K. Uchida, *The Journal of Organic Chemistry* **1995**, *60*, 8305-8309; b) T. Sumi, Y. Takagi, A. Yagi, M. Morimoto, M. Irie, *Chemical Communications* **2014**, *50*, 3928-3930.

[33] R. B. Woodward, R. Hoffmann, *Journal of the American Chemical Society* **1965**, *87*, 395-397.

[34] K. Uchida, E. Tsuchida, Y. Aoi, S. Nakamura, M. Irie, *Chemistry Letters* **1999**, *28*, 63-64.

[35] R. Göstl, B. Kobin, L. Grubert, M. Pätzel, S. Hecht, *Chemistry – A European Journal* **2012**, *18*, 14282-14285.

[36] W. Li, C. Jiao, X. Li, Y. Xie, K. Nakatani, H. Tian, W. Zhu, *Angewandte Chemie-International Edition* **2014**, *53*, 4603-4607.

[37] M. Walko, B. L. Feringa, *Chemical Communications* **2007**, 1745-1747.

[38] a) K. Morinaka, T. Ubukata, Y. Yokoyama, *Organic Letters* **2009**, *11*, 3890-3893; b) S. Fukumoto, T. Nakashima, T. Kawai, *Angewandte Chemie International Edition* **2011**, *50*, 1565-1568.

[39] T. Nakashima, R. Fujii, T. Kawai, *Chemistry – A European Journal* **2011**, *17*, 10951-10957.

[40] S. Fukumoto, T. Nakashima, T. Kawai, *European Journal of Organic Chemistry* **2011**, 5047-5053.

[41] a) M. Takeshita, M. Nagai, T. Yamato, *Chemical Communications* **2003**, 1496-1497; b) M. K. Hossain, M. Takeshita, T. Yamato, *Tetrahedron Letters* **2005**, *46*, 431-433; c) M. K. Hossain, M. Takeshita, T. Yamato, *European Journal of Organic Chemistry* **2005**, 2771-2776.

[42] L. Dinescu, Z. Yuan Wang, *Chemical Communications* **1999**, 2497-2498.

[43] M. M. Krayushkin, S. N. Ivanov, B. V. Lichitskii, A. A. Dubinov, L. G. Vorontsova, Z. A. Starikov, A. Y. Martynkin, *Russian Journal of Organic Chemistry* **2004**, *40*, 79-84.

[44] K. Ichimura, S. Watanabe, *Tetrahedron Letters* **1972**, *13*, 821-824.

[45] S. Kobatake, K. Uchida, E. Tsuchida, M. Irie, *Chemical Communications* **2002**, 2804-2805.

[46] M. Hanazawa, R. Sumiya, Y. Horikawa, M. Irie, *Journal of the Chemical Society, Chemical Communications* **1992**, 206-207.

[47] a) K. Higashiguchi, K. Matsuda, S. Kobatake, T. Yamada, T. Kawai, M. Irie, *Bulletin of the Chemical Society of Japan* **2000**, *73*, 2389-2394; b) M. Irie, T. Lifka, K. Uchida, S. Kobatake, Y. Shindo, *Chemical Communications* **1999**, 747-750.

[48] M. Herder, B. M. Schmidt, L. Grubert, M. Pätzel, J. Schwarz, S. Hecht, *Journal of the American Chemical Society* **2015**, *137*, 2738-2747.

[49] Y. Yokoyama, *Chemical Reviews* **2000**, *100*, 1717-1740.

[50] F. G. Erko, J. Berthet, A. Patra, R. Guillot, K. Nakatani, R. Métivier, S. Delbaere, *European Journal of Organic Chemistry* **2013**, 7809-7814.

[51] Q. Luo, Y. Liu, X. Li, H. Tian, *Photochemical & Photobiological Sciences* **2010**, *9*, 234-238.

[52] T. Sumi, T. Kaburagi, M. Morimoto, K. Une, H. Sotome, S. Ito, H. Miyasaka, M. Irie, *Organic Letters* **2015**, *17*, 4802-4805.

[53] a) X. Guo, J. Zhou, M. A. Siegler, A. E. Bragg, H. E. Katz, *Angewandte Chemie International Edition* **2015**, *54*, 4782-4786; b) X. Guo, J. Zhou, M. A. Siegler, A. E. Bragg, H. E. Katz, *Angewandte Chemie* **2015**, *127*, 4864-4868.

[54] M. Takeshita, T. Hirowatari, A. Takedomi, *Tetrahedron Letters* **2016**, *57*, 3565-3567.

[55] M. Herder, Doktorarbeit, Humboldt-Universität zu Berlin (Berlin), **2015**.

[56] M. Kleinwächter, Diplomarbeit, Humboldt-Universität zu Berlin (Berlin), **2012**.

[57] M. Calvin, H. W. Alter, *The Journal of Chemical Physics* **1951**, *19*, 768-770.

[58] a) K. Shibata, S. Kobatake, M. Irie, *Chemistry Letters* **2001**, *30*, 618-619; b) S. Takami, T. Kawai, M. Irie, *European Journal of Organic Chemistry* **2002**, 3796-3800.

[59] a) S. Kobatake, K. Uchida, E. Tsuchida, M. Irie, *Chemistry Letters* **2000**, *29*, 1340-1341; b) K. Morimitsu, K. Shibata, S. Kobatake, M. Irie, *The Journal of*

Organic Chemistry **2002**, *67*, 4574-4578; c) H. Shoji, D. Kitagawa, S. Kobatake, *Research on Chemical Intermediates* **2013**, *39*, 279-289.

[60] K. Morimitsu, S. Kobatake, M. Irie, *Tetrahedron Letters* **2004**, *45*, 1155-1158.

[61] K. Fukuzumi, Y. Unoh, Y. Nishii, T. Satoh, K. Hirano, M. Miura, *The Journal of Organic Chemistry* **2016**, *81*, 2474-2481.

[62] D. Prim, G. Kirsch, *Synthetic Communications* **1995**, *25*, 2449-2455.

[63] I. Cauquil-Caubère, J.-M. Kamenka, *European Journal of Medicinal Chemistry* **1998**, *33*, 867-877.

[64] a) A. Thurkauf, X. Chen, S. Zhang, Y. Gao, A. Kieltyka, J. W. F. Wasley, R. Brodbeck, W. Greenlee, A. Ganguly, H. Zhao, *Bioorganic & Medicinal Chemistry Letters* **2003**, *13*, 2921-2924; b) N. Rackelmann, L. Bialy, H. Englert, K. Wirth, P. Arndt, U. Heinelt, J. Weston, M. Follmann, *Patent* **2010**, WO 2010/025856 A025851.

[65] a) L. N. Lucas, J. van Esch, R. M. Kellogg, B. L. Feringa, *Chemical Communications* **1998**, 2313-2314; b) Linda N. Lucas, Jaap J. D. d. Jong, Jan H. v. Esch, Richard M. Kellogg, Ben L. Feringa, *European Journal of Organic Chemistry* **2003**, 155-166.

[66] F. M. Piller, P. Knochel, *Organic Letters* **2009**, *11*, 445-448.

[67] E. L. Martin, *Journal of the American Chemical Society* **1936**, *58*, 1438-1442.

[68] P. E. Eaton, G. R. Carlson, J. T. Lee, *The Journal of Organic Chemistry* **1973**, *38*, 4071-4073.

[69] A. Fuerstner, A. Hupperts, A. Ptock, E. Janssen, *The Journal of Organic Chemistry* **1994**, *59*, 5215-5229.

[70] M. Teruaki, S. Toshio, H. Junichi, *Chemistry Letters* **1973**, *2*, 1041-1044.

[71] D. Y. Curtin, H. Gruen, B. A. Shoulders, *Chemistry and Industry* **1958**, 1205-1206.

[72] a) H. Güsten, M. Salzwedel, *Tetrahedron* **1967**, *23*, 187-191; b) H. Güsten, M. Salzwedel, *Tetrahedron* **1967**, *23*, 173-185; c) Á. Kvaran, Á. E. Konráðsson, C. Evans, J. K. F. Geirsson, *Journal of Molecular Structure* **2000**, *553*, 79-90.

[73] a) M. Bukowska-Strzyżewska, J. Skoweranda, *Journal of Crystallographic and Spectroscopic Research* **1987**, *17*, 625-631; b) M. Bukowska-Strzyżewska, J. Skoweranda, W. Maniukiewicz, W. Strzyżewski, *Journal of Crystallographic and Spectroscopic Research* **1988**, *18*, 713-720.

[74] M. Traetteberg, E. B. Frantsen, F. C. Mijlhoff, A. Hoekstra, *Journal of Molecular Structure* **1975**, *26*, 57-68.

[75] M. Traetteberg, E. B. Frantsen, *Journal of Molecular Structure* **1975**, *26*, 69-76.

[76] J. Harada, K. Ogawa, S. Tomoda, *Acta Crystallographica Section C* **1995**, *51*, 2125-2127.

[77] J. Wissler, A. Mulder, R. Tampe, M. Bolte, *Acta Crystallographica Section E* **2006**, *62*, 5649-5650.

[78] J. Leimner, P. Weyerstahl, *Chemische Berichte* **1982**, *115*, 3697-3705.

[79] A. N. Lowell, M. W. Fennie, M. C. Kozlowski, *The Journal of Organic Chemistry* **2008**, *73*, 1911-1918.

[80] P. Dallemagne, L. P. Khanh, A. Alsaïdi, O. Renault, I. Varlet, V. Collot, R. Bureau, S. Rault, *Bioorganic & Medicinal Chemistry* **2002**, *10*, 2185-2191.

[81] Y. Jiang, X. Chen, Y. Zheng, Z. Xue, C. Shu, W. Yuan, X. Zhang, *Angewandte Chemie International Edition* **2011**, *50*, 7304-7307.

[82] M. M. El-Abadelah, M. R. Kamal, W. M. Tokan, S. a. O. Jarrar, *Journal für Praktische Chemie/Chemiker-Zeitung* **1997**, *339*, 284-287.

[83] A. Zivkovic, H. Stark, *Tetrahedron Letters* **2010**, *51*, 3769-3771.

[84] T.-A. Tran, Y.-J. Shin, B. Kramer, J. Choi, N. Zou, P. Vallar, P. Martens, P. Douglas Boatman, J. W. Adams, J. Ramirez, Y. Shi, M. Morgan, D. J. Unett, S. Chang, H.-H. Shu, S.-F. Tung, G. Semple, *Bioorganic & Medicinal Chemistry Letters* **2015**, *25*, 1030-1035.

[85] A. E. Gould, R. Adams, S. Adhikari, K. Aertgeerts, R. Afroze, C. Blackburn, E. F. Calderwood, R. Chau, J. Chouitar, M. O. Duffey, D. B. England, C. Farrer, N. Forsyth, K. Garcia, J. Gaulin, P. D. Greenspan, R. Guo, S. J. Harrison, S.-C. Huang, N. Iartchouk, D. Janowick, M.-S. Kim, B. Kulkarni, S. P. Langston, J. X. Liu, L.-T. Ma, S. Menon, H. Mizutani, E. Paske, C. C. Renou, M. Rezaei, R. S. Rowland, M. D. Sintchak, M. D. Smith, S. G. Stroud, M. Tregay, Y. Tian, O. P. Veiby, T. J. Vos, S. Vyskocil, J. Williams, T. Xu, J. J. Yang, J. Yano, H. Zeng, D. M. Zhang, Q. Zhang, K. M. Galvin, *Journal of Medicinal Chemistry* **2011**, *54*, 1836-1846.

[86] J. Koo, *Journal of the American Chemical Society* **1953**, *75*, 1889-1891.

[87] D. Plażuk, A. Vessières, E. A. Hillard, O. Buriez, E. Labbé, P. Pigeon, M.-A. Plamont, C. Amatore, J. Zakrzewski, G. Jaouen, *Journal of Medicinal Chemistry* **2009**, *52*, 4964-4967.

[88] K. L. Rinehart, R. J. Curby, D. H. Gustafson, K. G. Harrison, R. E. Bozak, D. E. Bublitz, *Journal of the American Chemical Society* **1962**, *84*, 3263-3269.

[89] J. Jovanovic, M. Schurmann, H. Preut, M. Spiteller, *Acta Crystallographica Section E* **2001**, *57*, 1100-1101.

[90] K. Ogawa, J. Harada, S. Tomoda, *Acta Crystallographica Section B* **1995**, *51*, 240-248.

[91] P. Espinet, A. M. Echavarren, *Angewandte Chemie International Edition* **2004**, *43*, 4704-4734.

[92] V. Farina, B. Krishnan, *Journal of the American Chemical Society* **1991**, *113*, 9585-9595.

[93] D. K. Morita, J. K. Stille, J. R. Norton, *Journal of the American Chemical Society* **1995**, *117*, 8576-8581.

[94] B. E. Segelstein, T. W. Butler, B. L. Chenard, *The Journal of Organic Chemistry* **1995**, *60*, 12-13.

[95] A. Rieche, H. Gross, E. Höft, *Chemische Berichte* **1960**, *93*, 88-94.

[96] a) K. Morimitsu, S. Kobatake, S. Nakamura, M. Irie, *Chemistry Letters* **2003**, *32*, 858-859; b) K. Morimitsu, S. Kobatake, M. Irie, *Molecular Crystals and Liquid Crystals* **2005**, *431*, 451-454.

[97] M. Herder, M. Utecht, N. Manicke, L. Grubert, M. Patzel, P. Saalfrank, S. Hecht, *Chemical Science* **2013**, *4*, 1028-1040.

[98] a) R. N. Beale, E. M. F. Roe, *Journal of the Chemical Society (Resumed)* **1953**, 2755-2763; b) J. Saltiel, J. T. D'Agostino, *Journal of the American Chemical Society* **1972**, *94*, 6445-6456.

[99] a) H. Suzuki, *Bulletin of the Chemical Society of Japan* **1960**, *33*, 396-405; b) H. Suzuki, *Bulletin of the Chemical Society of Japan* **1960**, *33*, 406-410; c) S. Hiroshi, *Bulletin of the Chemical Society of Japan* **1960**, *33*, 379-388; d) S. Hiroshi, *Bulletin of the Chemical Society of Japan* **1962**, *35*, 1715-1723.

[100] a) H. Mauser, in *Zeitschrift für Naturforschung B, Vol. 23*, **1968**, 1021; b) H. Mauser, in *Zeitschrift für Naturforschung B, Vol. 23*, **1968**, 1025.

[101] T. Benincori, E. Brenna, F. Sannicolò, L. Trimarco, G. Schiavon, S. Zecchin, G. Zotti, *Macromolecular Chemistry and Physics* **1996**, *197*, 517-528.

[102] C. G. Hatchard, C. A. Parker, *Proc. R. Soc. London, Ser. A* **1956**, *235*, 518-536.

[103] G. Gauglitz, *GIT Fachz. Lab. 29* **1985**, 186-197.

[104] S. Pu, W. Liu, W. Miao, *Journal of Physical Organic Chemistry* **2009**, *22*, 954-963.

[105] S. Lee, Y. You, K. Ohkubo, S. Fukuzumi, W. Nam, *Chemical Science* **2014**, *5*, 1463-1474.

[106] a) M. Irie, T. Eriguchi, T. Takada, K. Uchida, *Tetrahedron* **1997**, *53*, 12263-12271; b) A. T. Bens, J. Ern, K. Kuldova, H. P. Trommsdorff, C. Kryschi, *Journal of Luminescence* **2001**, *94/95*, 51-54.

[107] T. W. J. Taylor, A. R. Murray, *Journal of the Chemical Society (Resumed)* **1938**, 2078-2086.

[108] E. H. P. Tan, G. C. Lloyd-Jones, J. N. Harvey, A. J. J. Lennox, B. M. Mills, *Angewandte Chemie International Edition* **2011**, *50*, 9602-9606.

[109] a) S. Yamashita, *Bulletin of the Chemical Society of Japan* **1961**, *34*, 972-976; b) W. J. Muizebelt, R. J. F. Nivard, *Chemical Communications (London)* **1965**, 148-149; c) W. J. Muizebelt, R. J. F. Nivard, *Journal of the Chemical Society B: Physical Organic* **1968**, 913-920; d) W. J. Muizebelt, R. J. F. Nivard, *Journal of the Chemical Society B: Physical Organic* **1968**, 921-922.

[110] a) M. S. Kharasch, J. V. Mansfield, F. R. Mayo, *Journal of the American Chemical Society* **1937**, *59*, 1155-1155; b) F. R. Mayo, C. Walling, *Chemical Reviews* **1940**, *27*, 351-412.

[111] L. Zechmeister, W. H. McNeely, *Journal of the American Chemical Society* **1942**, *64*, 1919-1921.

[112] a) G. S. Hammond, J. Saltiel, *Journal of the American Chemical Society* **1963**, *85*, 2516-2517; b) J. Saltiel, G. S. Hammond, *Journal of the American Chemical Society* **1963**, *85*, 2515-2516.

[113] S. Fredrich, R. Göstl, M. Herder, L. Grubert, S. Hecht, *Angewandte Chemie International Edition* **2016**, *55*, 1208-1212.

[114] M. Montalti, A. Credi, L. Prodi, M. Gandolfi, *Handbook of Photochemistry,, Vol. Third Edition*, CRC Press, Boca Raton, **2006**.

[115] a) Y. Moriyama, K. Matsuda, N. Tanifuji, S. Irie, M. Irie, *Organic Letters* **2005**, *7*, 3315-3318; b) H. Logtenberg, W. R. Browne, *Organic & Biomolecular Chemistry* **2013**, *11*, 233-243.

[116] Y.-C. Chen, W.-T. Sun, H.-F. Lu, I. Chao, G.-J. Huang, Y.-C. Lin, S.-L. Huang, H.-H. Huang, Y.-D. Lin, J.-S. Yang, *Chemistry – A European Journal* **2011**, *17*, 1193-1200.

[117] a) W. R. Browne, J. J. D. de Jong, T. Kudernac, M. Walko, L. N. Lucas, K. Uchida, J. H. van Esch, B. L. Feringa, *Chemistry – A European Journal* **2005**, *11*, 6414-6429; b) W. R. Browne, J. J. D. de Jong, T. Kudernac, M. Walko, L. N. Lucas, K. Uchida, J. H. van Esch, B. L. Feringa, *Chemistry – A European Journal* **2005**, *11*, 6430-6441.

[118] B. Gorodetsky, N. R. Branda, *Advanced Functional Materials* **2007**, *17*, 786-796.

[119] a) G. F. Wright, *Journal of the American Chemical Society* **1939**, *61*, 2106-2110; b) M. A. Doran, R. Waack, *Journal of Organometallic Chemistry* **1965**, *3*, 94-96; c) T. A. Ward, G. Levin, M. Szwarc, *Journal of the American Chemical Society* **1975**, *97*, 258-261; d) S. Sorensen, G. Levin, M. Szwarc, *Journal of the American Chemical Society* **1975**, *97*, 2341-2345.

[120] O. Abdul-Rahim, A. N. Simonov, J. F. Boas, T. Rüther, D. J. Collins, P. Perlmutter, A. M. Bond, *The Journal of Physical Chemistry B* **2014**, *118*, 3183-3191.

[121] T. Koshido, T. Kawai, K. Yoshino, *The Journal of Physical Chemistry* **1995**, *99*, 6110-6114.

[122] a) M. Bragadin, P. Cescon, A. Berlin, G. A. Pagani, F. Sannicolo, *Synthetic Metals* **1987**, *18*, 241-246; b) M. Onoda, T. Iwasa, T. Kawai, K. Yoshino, *Journal of the Physical Society of Japan* **1991**, *60*, 3768-3776.

[123] M. Bragadin, P. Cescon, A. Berlin, F. Sannicolò, *Die Makromolekulare Chemie* **1987**, *188*, 1425-1430.

[124] a) K. Matsuda, S. Yokojima, Y. Moriyama, S. Nakamura, M. Irie, *Chemistry Letters* **2006**, *35*, 900-901; b) G. Guirado, C. Coudret, M. Hliwa, J.-P. Launay, *The Journal of Physical Chemistry B* **2005**, *109*, 17445-17459.

[125] S. Andreades, E. W. Zahnow, *Journal of the American Chemical Society* **1969**, *91*, 4181-4190.

[126] B. Gorodetsky, H. D. Samachetty, R. L. Donkers, M. S. Workentin, N. R. Branda, *Angewandte Chemie* **2004**, *116*, 2872-2875.

[127] Y. Kuriyama, T. Arai, H. Sakuragi, K. Tokumaru, *Chemical Physics Letters* **1990**, *173*, 253-256.

[128] M. Quick, F. Berndt, A. L. Dobryakov, I. N. Ioffe, A. A. Granovsky, C. Knie, R. Mahrwald, D. Lenoir, N. P. Ernsting, S. A. Kovalenko, *The Journal of Physical Chemistry B* **2014**, *118*, 1389-1402.

[129] a) H. Miyasaka, S. Araki, A. Tabata, T. Nobuto, N. Malaga, M. Irie, *Chemical Physics Letters* **1994**, *230*, 249-254; b) J. C. Owrutsky, H. H. Nelson, A. P. Baronavski, O. K. Kim, G. M. Tsivgoulis, S. L. Gilat, J. M. Lehn, *Chemical Physics Letters* **1998**, *293*, 555-563; c) J. Ern, A. T. Bens, A. Bock, H. D. Martin, C. Kryschi, *Journal of Luminescence* **1998**, *76/77*, 90-94; d) J. Ern, A. T. Bens, H. D. Martin, S. Mukamel, D. Schmid, S. Tretiak, E. Tsiper, C. Kryschi, *Chemical Physics* **1999**, *246*, 115-125; e) J. Ern, A. Bens, H. D. Martin, S. Mukamel, D. Schmid, S. Tretiak, E. Tsiper, C. Kryschi, *Journal of Luminescence* **2000**, *87/89*, 742-744; f) J. Ern, A. T. Bens, H. D. Martin, S. Mukamel, S. Tretiak, K. Tsyganenko, K. Kuldova, H. P. Trommsdorff, C. Kryschi, *The Journal of Physical Chemistry A* **2001**, *105*, 1741-1749; g) H. Miyasaka, M. Murakami, A. Itaya, D. Guillaumont, S. Nakamura, M. Irie, *Journal of the American Chemical Society* **2001**, *123*, 753-754; h) Y. Ishibashi, M. Fujiwara, T. Umesato, H. Saito, S. Kobatake, M. Irie, H. Miyasaka, *The Journal of Physical Chemistry C* **2011**, *115*,

4265-4272; i) Y. Ishibashi, T. Umesato, S. Kobatake, M. Irie, H. Miyasaka, *The Journal of Physical Chemistry C* **2012**, *116*, 4862-4869.

[130] a) P. Gajdek, R. S. Becker, F. Elisei, U. Mazzucato, A. Spalletti, *Journal of Photochemistry and Photobiology A: Chemistry* **1996**, *100*, 57-64; b) G. Bartocci, G. Galiazzo, G. Ginocchietti, U. Mazzucato, A. Spalletti, *Photochemical & Photobiological Sciences* **2004**, *3*, 870-877.

[131] F. Berndt, A. L. Dobryakov, M. Quick, R. Mahrwald, N. P. Ernsting, D. Lenoir, S. A. Kovalenko, *Chemical Physics Letters* **2012**, *544*, 39-42.

[132] I. N. Ioffe, M. Quick, M. T. Quick, A. L. Dobryakov, C. Richter, A. A. Granovsky, F. Berndt, R. Mahrwald, N. P. Ernsting, S. A. Kovalenko, *Journal of the American Chemical Society* **2017**, *139*, 15265-15274.

[133] P. R. Hania, R. Telesca, L. N. Lucas, A. Pugzlys, J. van Esch, B. L. Feringa, J. G. Snijders, K. Duppen, *The Journal of Physical Chemistry A* **2002**, *106*, 8498-8507.

[134] a) D. Dulić, T. Kudernac, A. Pužys, B. L. Feringa, B. J. van Wees, *Advanced Materials* **2007**, *19*, 2898-2902; b) E. Griese, Masterarbeit, Humboldt-Universität zu Berlin (Berlin), **2017**.

[135] A. Majumder, A. Sarkar, A. Mandal, P. Ghosh, *Journal of Chemical and Pharmaceutical Research* **2012**, *4*, 2599-2602.

[136] J. Kitzing, *Berichte der deutschen chemischen Gesellschaft* **1894**, *27*, 1578-1580.

[137] J. lbarzo, R. M. Ortuño, *Tetrahedron* **1994**, *50*, 9825-9830.

[138] W. G. Kofron, C. R. Hauser, *The Journal of Organic Chemistry* **1970**, *35*, 2085-2086.

[139] F. W. Lewis, L. M. Harwood, M. J. Hudson, M. G. B. Drew, J. F. Desreux, G. Vidick, N. Bouslimani, G. Modolo, A. Wilden, M. Sypula, T.-H. Vu, J.-P. Simonin, *Journal of the American Chemical Society* **2011**, *133*, 13093-13102.

[140] D. A. Evans, R. P. Polniaszek, K. M. DeVries, D. E. Guinn, D. J. Mathre, *Journal of the American Chemical Society* **1991**, *113*, 7613-7630.

[141] a) C. R. Noe, M. Knollmüller, P. Gärtner, K. Mereiter, G. Steinbauer, *Liebigs Annalen* **1996**, *1996*, 1015-1021; b) N. Uludag, S. Patir, T. Höukelek, *Journal of Heterocyclic Chemistry* **2006**, *43*, 585-591; c) M. J. Spallek, S. Stockinger, R. Goddard, F. Rominger, O. Trapp, *European Journal of Inorganic Chemistry* **2011**, *2011*, 5014-5024.

[142] a) P. E. Sonnet, *Synthetic Communications* **1976**, *6*, 21-26; b) T. Muller, D. Coowar, M. Hanbali, P. Heuschling, B. Luu, *Tetrahedron* **2006**, *62*, 12025-12040; c) S. P. Schmidt, D. W. Brooks, *Tetrahedron Letters* **1987**, *28*, 767-768; d) A. Wagner, M. P. Heitz, C. Mioskowski, *Tetrahedron Letters* **1989**, *30*, 557-558.

[143] a) Z.-N. Huang, B.-A. Xu, S. Jin, M.-G. Fan, *Synthesis* **1998**, *1998*, 1092-1094; b) Y. Chen, D. X. Zeng, M. G. Fan, *Organic Letters* **2003**, *5*, 1435-1437.

[144] S. F. Hornbuckle, P. Livant, T. R. Webb, *The Journal of Organic Chemistry* **1995**, *60*, 4153-4159.

[145] J.-L. Gras, *Tetrahedron Letters* **1978**, *19*, 2111-2114.

[146] a) G. M. Ksander, J. E. McMurry, M. Johnson, *The Journal of Organic Chemistry* **1977**, *42*, 1180-1185; b) E. Mernyák, E. Kozma, A. Hetényi, L. Márk, G. Schneider, J. Wölfling, *Steroids* **2009**, *74*, 520-525; c) A. V. Malkov, D. Pernazza, M. Bell, M. Bella, A. Massa, F. Teplý, P. Meghani, P. Kočovský, *The Journal of Organic Chemistry* **2003**, *68*, 4727-4742.

[147] R. Karmakar, D. Mal, *Tetrahedron Letters* **2011**, *52*, 6098-6102.

[148] a) E. Vedejs, T. H. Eberlein, D. J. Mazur, C. K. McClure, D. A. Perry, R. Ruggeri, E. Schwartz, J. S. Stults, D. L. Varie, *The Journal of Organic Chemistry* **1986**, *51*, 1556-1562; b) J. Li, J. A. Wisner, M. C. Jennings, *Organic Letters* **2007**, *9*, 3267-3269.

[149] K. Yanagihara, S. Umezawa, K. Miyaji, Patent, (Ed.: L. Nissan Chemical Industries), US, **2011**.

[150] T. Miyakoshi, S. Saito, J. Kumanotani, *Chemistry Letters* **1982**, *11*, 83-84.

[151] T. Miyakoshi, S. Saito, J. Kumanotani, *Chemistry Letters* **1981**, *10*, 1677-1678.

[152] K. W. Bowers, R. W. Giese, J. Grimshaw, H. O. House, N. H. Kolodny, K. Kronberger, D. K. Roe, *Journal of the American Chemical Society* **1970**, *92*, 2783-2799.

[153] H. O. House, R. W. Giese, K. Kronberger, J. P. Kaplan, J. F. Simeone, *Journal of the American Chemical Society* **1970**, *92*, 2800-2810.

[154] H. Maekawa, M. Sakai, T. Uchida, Y. Kita, I. Nishiguchi, *Tetrahedron Letters* **2004**, *45*, 607-609.

[155] J. Janssen, W. Lüttke, *Chemische Berichte* **1982**, *115*, 1234-1243.

[156] J. P. Zimmer, J. A. Richards, J. C. Turner, D. H. Evans, *Anal. Chem.* **1971**, *43*, 1000.

[157] Wiemann, Gardan, Patent (Ed.: C. N. d. l. R. Scientifique), France, **1959**.

[158] K. K. Kapoor, S. Kumar, B. A. Ganai, *Tetrahedron Letters* **2005**, *46*, 6253-6255.

[159] J. E. McMurry, *Chemical Reviews* **1989**, *89*, 1513-1524.

[160] O. L. Brady, G. V. Elsmie, *Analyst* **1926**, *51*, 77-78.

[161] A. P. Glaze, H. G. Heller, J. Whittall, *Journal of the Chemical Society, Perkin Transactions 2* **1992**, 591-594.

[162] A. L. Dobryakov, S. A. Kovalenko, A. Weigel, J. L. Pérez-Lustres, J. Lange, A. Müller, N. P. Ernsting, *Review of Scientific Instruments* **2010**, *81*, 113106.

[163] G. R. Newkome, C. R. Marston, *The Journal of Organic Chemistry* **1985**, *50*, 4238-4245.

[164] Y. Li, S. Xu, X. Li, K. Chen, H. Tian, *Chemistry Letters* **2007**, *36*, 664-665.

[165] E. Griese, Bachelorarbeit, Humboldt-Universität zu Berlin (Berlin), **2014**.

[166] J. Yang, S. Liu, J.-F. Zheng, J. Zhou, *European Journal of Organic Chemistry* **2012**, 6248-6259.

[167] D. H. Fitzgerald, K. M. Muirhead, N. P. Botting, *Bioorganic & Medicinal Chemistry* **2001**, *9*, 983-989.

[168] E. Cuthbertson, A. D. U. Hardy, D. D. MacNicol, *Journal of the Chemical Society, Perkin Transactions 1* **1975**, 254-262.

[169] E. Buchta, R. Zöllner, *Justus Liebigs Annalen der Chemie* **1968**, *716*, 102-105.

[170] G. M. Sheldrick, University of Göttingen, Göttingen, **1996**, Program for Empirical Absorption Correction of Area Detector Data.

[171] G. M. Sheldrick, University of Göttingen, Göttingen, **2013**, Program for Crystal Structure Solution.

[172] G. M. Sheldrick, University of Göttingen, Göttingen, **2014**, Program for Crystal Structure Refinement.

6. Appendix

6.1 Abbreviations

Abs	absorbance
au	arbitrary unit
AcOH	acetic acid
bp	boiling point
cyHex	cyclohexane
CV	cyclic voltammetry
dba	dibenzylideneacetone
DAE	diarylethene
DCM	dichloromethane
DDQ	2,3-Dichloro-5,6-dicyano-1,4-benzoquinone
DHP	dihydropyran
DME	dimethoxyethane
DMF	dimethylformamide
DMSO	dimethylsulfoxide
DSC	differential scanning calorimetry
DTE	dithienylethene
EA	ethyl acetate
ESA	excited-state absorption
FC	Franck-Condon
Fc/Fc+	ferrocene/ferrocenium
GPC	gel permeation chromatography
Hex	^{n}hexane
HMBC	heteronuclear multiple-bond correlation spectroscopy
HPLC	high performance chromatography
HSQC	heteronuclear single-quantum correlation spectroscopy
MeCN	acetonitrile
$MeNO_2$	nitromethane
MS	mass spectrometry
n.a.	not available
n.d.	not determined
NMP	*N*-methyl-2-pyrrolidon
NMR	nuclear magnetic resonance
Pd(C)	palladium (10%) on charcoal
PE	petrol ether
PPA	polyphosphoric acid
prep.	preparative
PSS	photostationary state
pyr	pyridine
rt	room temperature
sat.	saturated
SCE	standard calomel electrode
SEC	spectro-electrochemistry
SE	stimulated emission
THP	tetrahydropyran
TFA	trifluoroacetic acid
TEG	triethylene glycol
TLC	thin layer chromatography
TMS	trimethylsilyl-
UPLC	ultra-high performance chromatography

Reagents:

Brady's reagent

2,4-Dinitrophenyl-hydrazine and H_2SO_4 in EtOH[160]

Eaton's reagent

$MeSO_3H$ and P_4O_{10} in 10:1 w/w ratio[68]

Abbreviations for NMR spectra:

d	doublet
m	multiplet
p	pentet
q	quartet
s	singlet
t	triplet
bs	broad singlet
psq	pseudo quintet

6.2 Index of compounds

Simple aDTE$_{66}$

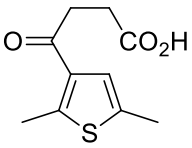

1a

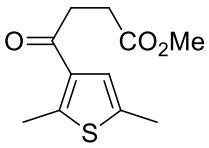

1a-Me

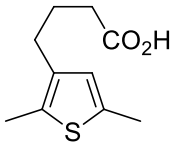

2a

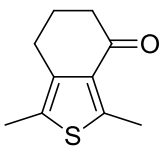

3a

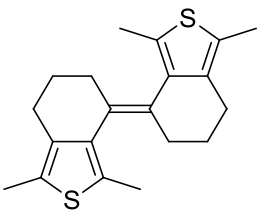

aDTE$_{66}$-Me

Simple aDTE$_{77}$

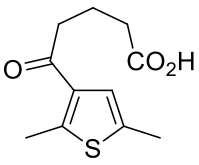

1b

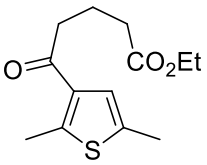

1b-Et

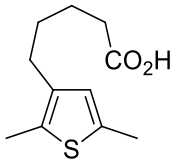

2b

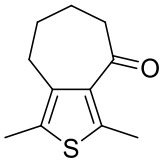

3b

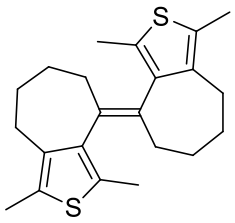

aDTE$_{77}$-Me

Simple aDTE$_{55}$

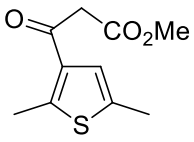

1c-Me

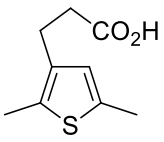

2c

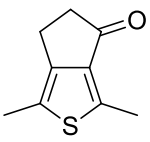

3c

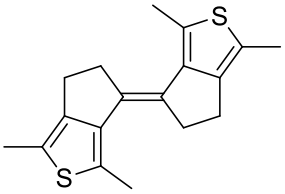

aDTE$_{55}$-Me

Functionalized aDTE$_{66}$

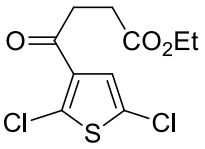

4a

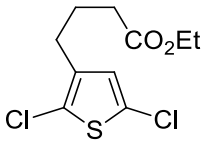

5a-Et

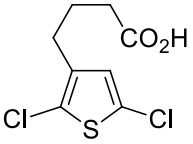

5a

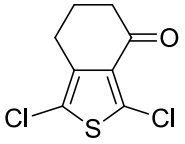

6a

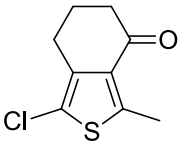

7a

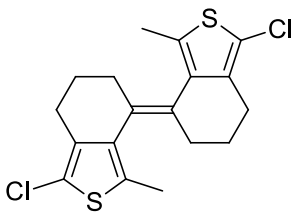

aDTE$_{66}$-Cl

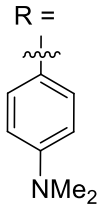

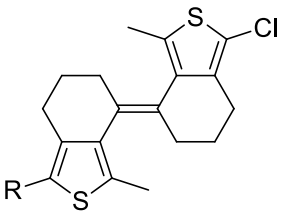

Me$_2$NPh-aDTE$_{66}$-Cl

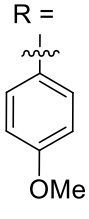

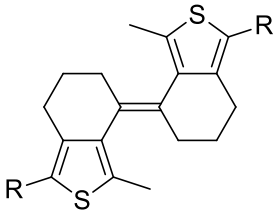

aDTE$_{66}$-PhOMe

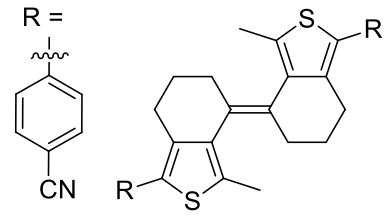

aDTE$_{66}$-PhCN

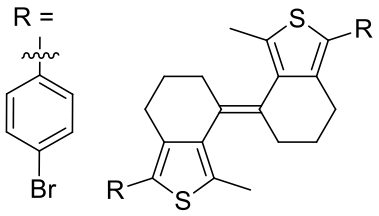

aDTE$_{66}$-PhBr

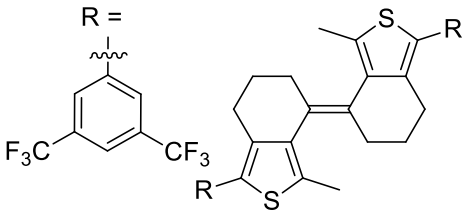

aDTE$_{66}$-Ph(CF$_3$)$_2$

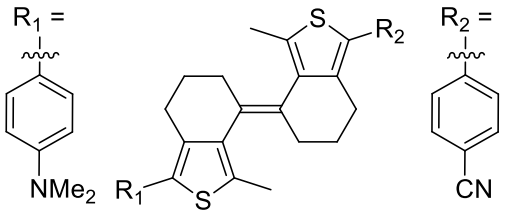

Me$_2$NPh-aDTE$_{66}$-PhCN

Functionalized aDTE$_{77}$

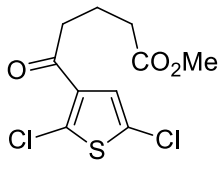

4b

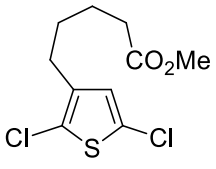

5b-Me

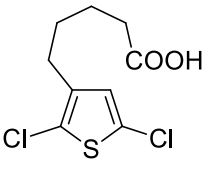

5b

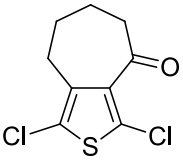

6b

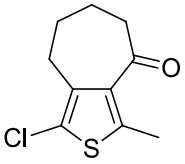

7b

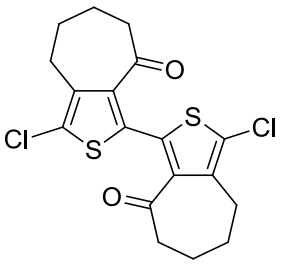

8

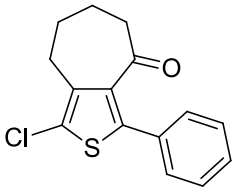

9

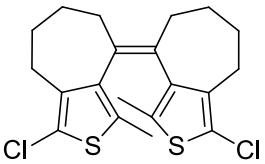

aDTE$_{77}$-Cl

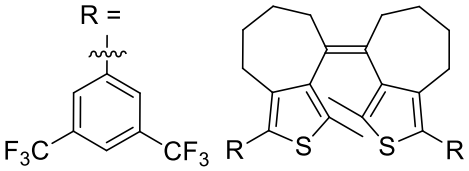

aDTE$_{77}$-Ph(CF$_3$)$_2$

Hybrid aDTE and unconstrained DTE

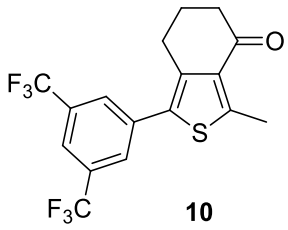

10

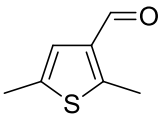

11

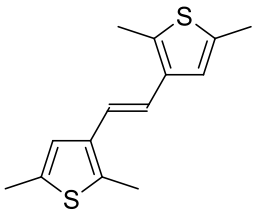

12

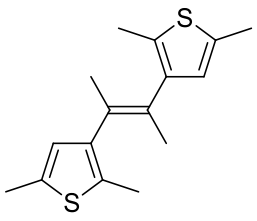

13

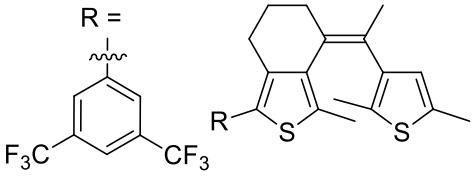

$(F_3C)_2$Ph-aDTE$_{6Me}$-Me

pcDTE from **3a**

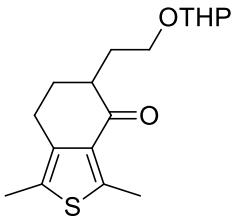

14a

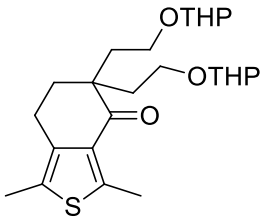

15a

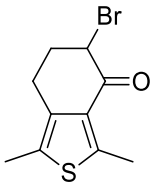

19a

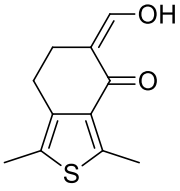

21a

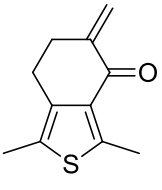

22a

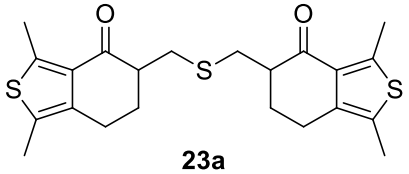

23a

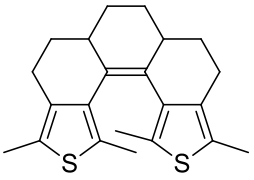

pcDTE$_{666}$-Me

pcDTE from **3d**

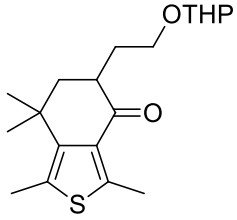

14d

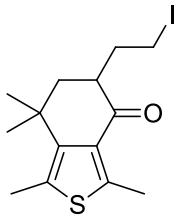

16d

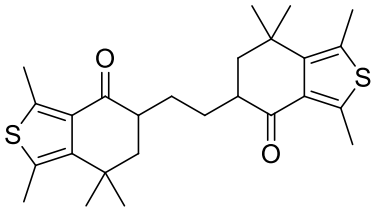

17d

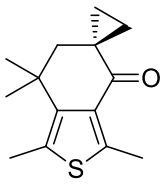

18d

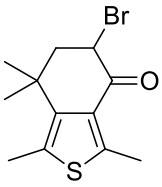

19d

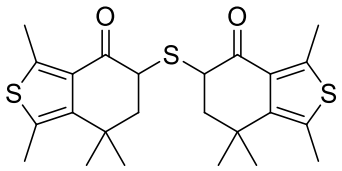

20d

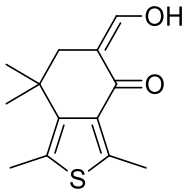

21d

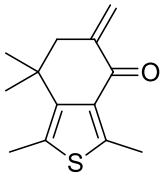

22d

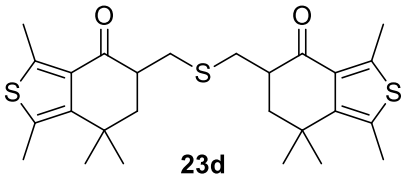

23d

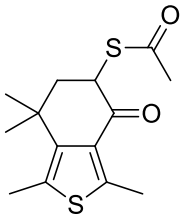

24d

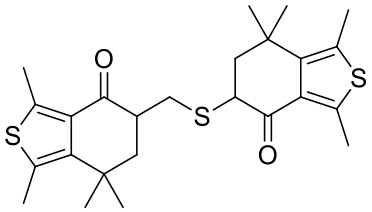

25d

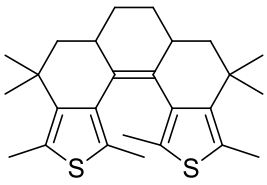

pcDTE$_{666}$(Me$_2$) Me

6.3 Index of figures

Figure 1.2-1 Double bond isomerization of stilbene.[5] 7

Figure 1.2-2 Potential energy curves for twisting about the central double bond of stilbene.[17a] 7

Figure 1.2-3 Interconversion of the three switching states for stilbene. 8

Figure 1.2-4 Stilbenes locked in the *Z*-configuration. [25,28] 10

Figure 1.2-5 Exemplary structure of normal and inverse DAE. 11

Figure 1.2-6 Biasing the population of the photoactive *ap*-conformer by steric bulk. 12

Figure 1.2-7 Biasing the population of the photoactive *ap*-conformer by intramolecular interactions. 13

Figure 1.2-8 Fixating the conformation of DAE by covalent bonds. 14

Figure 1.2-9 Bis-heteroaromatic DAE with an isomarizable double bond. 16

Figure 2.1-1 Structure of the two annulated dithienylethenes (aDTE) synthesized in an earlier study.[56] 20

Figure 2.2-1 Configurational assignment of *E*- and *Z*-isomer by ^{1}H-NMR spectroscopy. 28

Figure 2.2-2 ORTEP plot (50% probability thermal ellipsoids) of the crystal structures of $aDTE_{66}$-Me. 29

Figure 2.2-3 ORTEP plot (50% probability thermal ellipsoids) of the crystal structure of *E*-$aDTE_{55}$-Me. 35

Figure 2.2-4 Attempted structural assignment of monosubstituted ketone 7a by HMBC. 39

Figure 2.2-5 Structural assignment of monosubstituted ketone 7a by comparison with dimethyl-derivative 3a. 40

Figure 2.3-1 Extinction coefficients for *E*- and *Z*-aDTE in MeCN. 51

Figure 2.3-2 Extinction coefficients of the pure cyclized aDTEs isomers in MeCN. 52

Figure 2.3-3 Comparison of UV/vis spectra of aDTEs and normal DAEs[48,55] bearing the same substituent. 54

Figure 2.3-4 Spectral development during irradiation of $aDTE_{66}$-$Ph(CF_3)_2$ in MeCN ($c = 10^{-5}$ M) with 302 nm light.....55

Figure 2.3-5 ΔAbs-diagram according to Mauser[100b] for $aDTE_{66}$-$Ph(CF_3)_2$. 55

Figure 2.3-6 UPLC analysis of $aDTE_{66}$-$Ph(CF_3)_2$ in MeCN ($c = 10^{-5}$ M) after distinct irradiation times with UV-light. 56

Figure 2.3-7 Cycloreversion of *C*-$aDTE_{66}$-$Ph(CF_3)_2$ in MeCN ($c = 10^{-5}$ M) with white light, starting from PSS mixture. 57

Figure 2.3-8 Irradiation of *Z*-$aDTE_{77}$-$Ph(CF_3)_2$ in MeCN ($c = 10^{-5}$ M) with 313 nm light. 59

Figure 2.3-9 Photochemistry of $aDTE_{55}$-Me in MeCN ($c = 10^{-5}$ M) upon irradiation with 313 nm light. 60

Figure 2.3-10 Comparison of normalized absorption of half-stiff $(F_3C)_2$Ph-$aDTE_{6Me}$-Me and its symmetrical parent compound $aDTE_{66}$-$Ph(CF_3)_2$. 61

Figure 2.3-11 Photochemistry of $(F_3C)_2$Ph-$aDTE_{6Me}$-Me in MeCN (1:9 *E/Z* isomer mixture, $c = 10^{-5}$ M). 62

Figure 2.3-12 Molar absorptivities of unconstrained reference compounds in MeCN. 62

Figure 2.3-13 Spectral evolution of $aDTE_{66}$-$Ph(CF_3)_2$ over multiple cyclization / cycloreversion cycles in MeCN ($c = 10^{-5}$ M).....68

Figure 2.3-14 Switching of $aDTE_{66}$-$Ph(CF_3)_2$ in the solid state. 69

Figure 2.3-15 Conversion of $Z \rightarrow E$ of $aDTE_{66}$-$Ph(CF_3)_2$, mediated by eosin Y in MeCN ($c = 10^{-5}$ M). 73

Figure 2.4-1 Cyclic voltammogram of aDTE$_{66}$-Me. 78

Figure 2.4-2 SEC of the open isomers of aDTE$_{66}$-Me. 79

Figure 2.4-3 SEC of the closed isomer of aDTE$_{66}$-Me. 80

Figure 2.4-4 Comparison of the UV/vis spectra of the species observed in the SEC of aDTE$_{66}$-Me. 81

Figure 2.4-5 Cyclic voltammogram of unconstrained DTEs and simple aDTEs. 82

Figure 2.4-6 Graphical illustration of the peak potentials of aDTEs, pcDTEs and reference compounds in MeCN. 84

Figure 2.4-7 SEC of *C*-aDTE$_{66}$-PhOMe. 86

Figure 2.5-1 Transient absorption experiment of DTE 12 in ^{n}hexane. 91

Figure 2.5-2 Modelling of population of the excited state. 92

Figure 2.5-3 Transient absorption experiment of stiff aDTE$_{66}$-Me in ^{n}hexane. 96

Figure 2.5-4 Transient absorption experiment of open isomers of stiff aDTE$_{66}$-PhCN in n-hexane. 98

Figure 2.5-5 Transient absorption experiment of *C*-aDTE$_{66}$-PhCN in MeCN after excitation with 560 nm laser pulses. 99

Figure 3.2-1 Qualitative deprotonation test using *p*-NO_2-benzaldehyde as trapping reagent. 108

Figure 3.3-1 Absorbance spectra of both pcDTE$_{666}$ synthesized. 123

Figure 3.3-2 Spectral evolution during irradiation of pcDTE$_{666}$-Me (enriched diastereomeric mixture) upon irradiation with 313 nm light in MeCN. 124

Figure 3.3-3 Spectral evolution during irradiation of pcDTE$_{666}$(Me_2)-Me (enriched diastereomeric mixture) upon irradiation with 313 nm in MeCN. 125

Figure 4.6-1 NMR spectra of pcDTE$_{666}$-Me. 182

Figure 4.6-2 NMR spectra of pcDTE$_{666}$(Me$_2$)-Me. 183

Figure 4.7-1 Asymmetric unit of *E*-aDTE$_{55}$-Me. 185

Figure 4.7-2 Asymmetric unit of *E*-aDTE$_{66}$(Me$_2$)-Me. 186

Figure 4.7-3 Asymmetric unit of *E*-aDTE$_{66}$-Me. 187

Figure 4.7-4 Asymmetric unit of *Z*-aDTE$_{66}$-Me. 188

Figure 4.7-5 Asymmetric unit of *E*-aDTE$_{66}$-Ph(CF$_3$)$_2$. 189

Figure 4.7-6 Asymmetric unit of *Z*-aDTE$_{66}$-Ph(CF$_3$)$_2$. 190

Figure 4.7-7 Asymmetric unit of *Z*-aDTE$_{66}$-PhBr. 191

Figure 4.7-8 Asymmetric unit of *Z*-aDTE$_{66}$-PhOMe. 192

Figure 4.7-9 Asymmetric unit of ketone 9. 193

Figure 4.7-10 Asymmetric unit of ketone 19a. 194

Figure 4.7-11 Asymmetric unit of ketone 19d. 195

Figure 4.7-12 Comparison of the two employed 6-membered ring ketones employed for synthesis. 196

Figure 6.6-1 Emission spectrum of a red light fluorescent tube. 225

Figure 6.6-2 Emission spectrum of a white light fluorescent tube. 225

Figure 6.6-3 Emission spectrum of a white light compact fluorescent tube. 225

Figure 6.6-4 Emission spectrum of a white light LED (cell phone camera light). 226

Figure 6.6-5 Emission spectrum of a portable 254 nm fluorescent tube as used for TLC plate control. 226

Figure 6.6-6 Emission spectrum of a portable 366 nm fluorescent tube as used for TLC plate control. 226

6.4 Index of schemes

Scheme 1.2-1 Exemplary photochemical equilibrium between two chemical species A and B. 3

Scheme 1.2-2 Examples for photochromic systems with different photochemical reaction types. 4

Scheme 1.2-3 Photochromism of stilbene. 6

Scheme 1.2-4 Influencing the thermal equilibrium of stilbene by introduction of bulky groups. 9

Scheme 1.2-5 Photochemistry of DAE. 11

Scheme 1.2-6 Formation of the by-product results from further irradiation of the cyclized isomer with UV light. 14

Scheme 1.2-7 Example of a bis-heteroaromatic DAE that only operates in the double bond isomerization regime.[53] 16

Scheme 2.1-1 Characteristics of functionalizable sides in the three aDTE isomers. 20

Scheme 2.2-1 General structure of aDTEs. 23

Scheme 2.2-2 Retrosynthesis of simple and functionalized aDTEs. 24

Scheme 2.2-3 Synthesis of $aDTE_{66}$-Me. 26

Scheme 2.2-4 Definition of key characteristics of stilbenoid compounds. 29

Scheme 2.2-5 Synthesis of $aDTE_{77}$-Me. 31

Scheme 2.2-6 Alternative routes to acid 2c. 33

Scheme 2.2-7 Synthesis of aDTE$_{55}$-Me. 34

Scheme 2.2-8 Synthesis of functionalizable aDTE$_{66}$. 37

Scheme 2.2-9 Overlay of single crystal x-ray structures of simple and functionalized aDTE$_{66}$. 41

Scheme 2.2-10 Synthesis of functionalizable aDTE$_{77}$. 43

Scheme 2.2-11 Side products of Stille methylation of ketone 6b. 43

Scheme 2.2-12 Synthesis of the hybrid half-stiff $(F_3C)_2$Ph-aDTE$_{6Me}$-Me. 44

Scheme 2.2-13 Synthesis of unconstrained 12 in a two-step sequence. 45

Scheme 2.2-14 Synthesis of unconstrained 13 from commercial starting material. 46

Scheme 2.2-15 General synthesis of simple and functionalized aDTE. 47

Scheme 2.2-16 Synthesized example of a half-stiff hybrid aDTE and two unconstrained reference compounds 12 and 13. 48

Scheme 2.3-1 Switching behavior of aDTE$_{66}$(Me_2)-Me as observed earlier.[56] 49

Scheme 2.3-2 General switching behavior for the aDTE photosystem upon irradiation with UV-light. 50

Scheme 2.3-3 General photochemical behavior of aDTE$_{66}$ upon direct excitation. 58

Scheme 2.3-4 Reaction scheme for the photoreaction of *E*-aDTE$_{55}$-Me upon irradiation with UV-light. 60

Scheme 2.3-5 Switching modes of 3-state photochrome aDTE$_{66}$. 75

Scheme 2.4-1 Electrochemical behavior of aDTE$_{66}$. 81

Scheme 2.4-2 Proposed modification to aDTE structures to enable a second electrochemical switching pathway. 88

Scheme 2.5-1 Summary of the transient absorption behavior of *E*- and *Z*-12 in n-hexane upon excitation with 324 nm. 94

Scheme 2.5-2 Summary of the transient absorption behavior of *E*- and *Z*-aDTE$_{66}$-Me in ^{n}hexane upon excitation with 324 nm. 97

Scheme 2.5-3 Summary of the transient absorption behavior of *E*-, *Z*- and *C*-aDTE$_{66}$-PhCN after excitation with 350 nm and 560 nm laser pulses, respectively. 100

Scheme 3.1-1 Two derivatives of pcDTE have been reported earlier.[56] In analogy to the nomenclature of aDTE systems (compare Scheme 2.2-1), the digits in subscript signify the ring sizes of both peripheral and the central ring moiety. 103

Scheme 3.1-2 Target structure for the current pcDTE studies. 104

Scheme 3.2-1 Precursors used for the synthesis of pcDTEs. 105

Scheme 3.2-2 Retrosynthetic considerations for the synthesis of pcDTE$_{666}$. 106

Scheme 3.2-3 Overview of attempted concerted C2-bridging starting materials, reagents and identified products. 107

Scheme 3.2-4 Attempted C2-bridging of ketone 3d using diethyl oxalate. 108

Scheme 3.2-5 Alkylation of ketones 3a and 3d with THP-iodoethanol. 109

Scheme 3.2-6 Conversion of the THP protection group into a leaving group. 110

Scheme 3.2-7 Attempted bridging by nucleophilic attack of enolate 3d on C2-iodide 16d. 111

Scheme 3.2-8 Formation of 1,5-(3-thia)diketone 20d from bromide 19d. 112

Scheme 3.2-9 Formation of the Michael-system 22d as C1-synthon. 112

Scheme 3.2-10 Synthesis of the protected α-thiol 24d and tandem deprotection-coupling sequence with α,β-unsaturated ketone 22d to yield the desired 1,6-(3-thia)diketone 25d. 113

Scheme 3.2-11 Attempted McMurry coupling of the sulfur bridged diketones 20d, 25d and 23d. 113

Scheme 3.2-12 Attempted dimerization of unsaturated ketone 22d using $NaNO_2$. 114

Scheme 3.2-13 Strategy for pcDTE synthesis by radical dimerization of enone 22d. 115

Scheme 3.2-14 Tandem dimerization / reductive coupling of enone 22d. 117

Scheme 3.2-15 Possible structure of the assumed side products in the reductive coupling of diketone 17d. 118

Scheme 3.2-16 The possible diastereomers of $pcDTE_{666}(Me_2)$-Me. 118

Scheme 3.2-17 Synthesis of precursors for $pcDTE_{666}$-Me. 120

Scheme 3.2-18 Synthesis of $pcDTE_{666}$-Me and attempted synthesis of a heterocyclic $pcDTE_{676}$. 120

Scheme 3.4-1 Proposed change to the molecular structure inspired by Janssen and Lüttke.[155] 128

Scheme 3.4-2 Proposed synthetic route to functionalized pcDTEs. 129

6.5 Index of tables

Table 2.2-1 Structural parameters of $aDTE_{66}$-Me and reference compounds in the single crystal. 30

Table 2.2-2 Structural parameters of $aDTE_{55}$-Me and reference compounds in the single crystal. 36

Table 2.2-3 Structural parameters of functionalized $aDTE_{66}$ in the single crystal. 41

Table 2.3-1 Photochemical efficiency and PSS composition of aDTEs in MeCN at 25 °C. 65

Table 2.3-2 Thermal isomerization of distinct aDTEs in boiling NMP (bp = 203 °C)..... 70

Table 2.4-1 Anodic and cathodic peak potentials (E_p^a / E_p^c) of aDTEs, pcDTEs and reference compounds. 84

Table 3.2-1 Alkylation of ketones 3a and 3d with THP-iodoethanol and ratio of products. 110

Table 3.2-2 Reaction conditions for reductive dimerization of enone 22d. 116

6.6 Emission spectra of additional light sources[60]

The spectra were measured using a spectrometer[61] connected to an optical fiber, pointed towards the light source. The intensities are arbitrary for this reason.

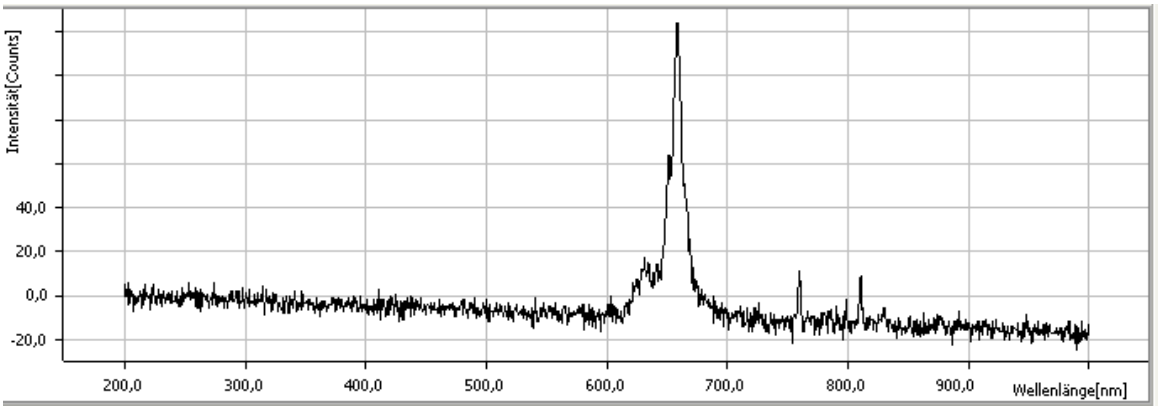

Figure 6.6-1 Emission spectrum of a red light fluorescent tube.

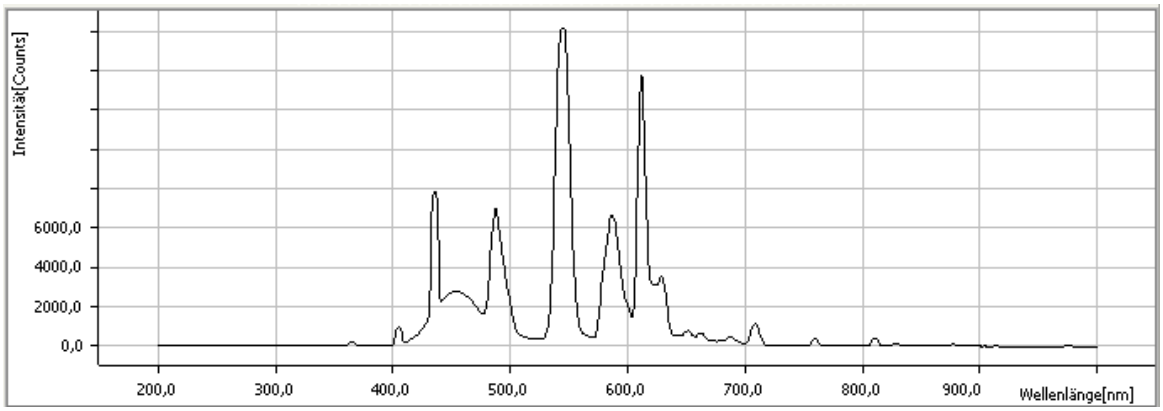

Figure 6.6-2 Emission spectrum of a white light fluorescent tube.

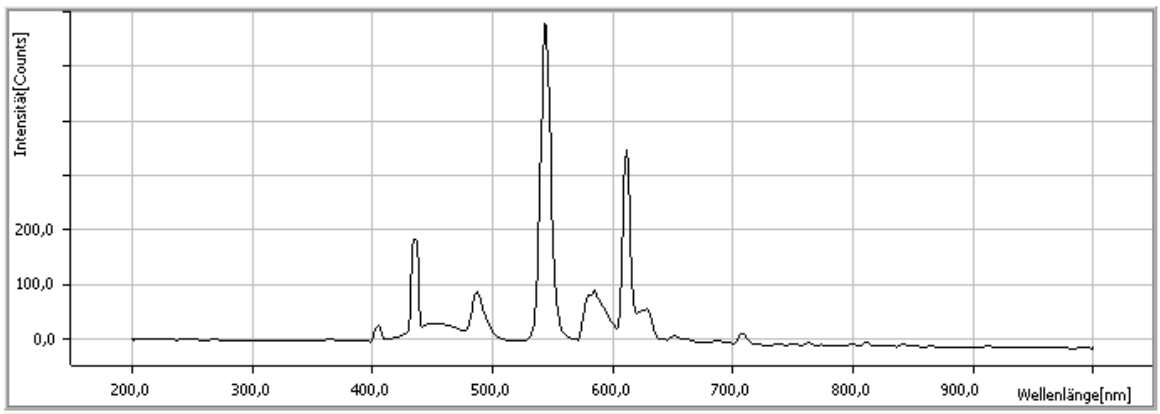

Figure 6.6-3 Emission spectrum of a white light compact fluorescent tube.

[60] The spectra were determined in collaboration with Dipl.-Chem. Johannes Gurke.

[61] Measured using an Avantes AvaSpec-2048x14 spectrometer.

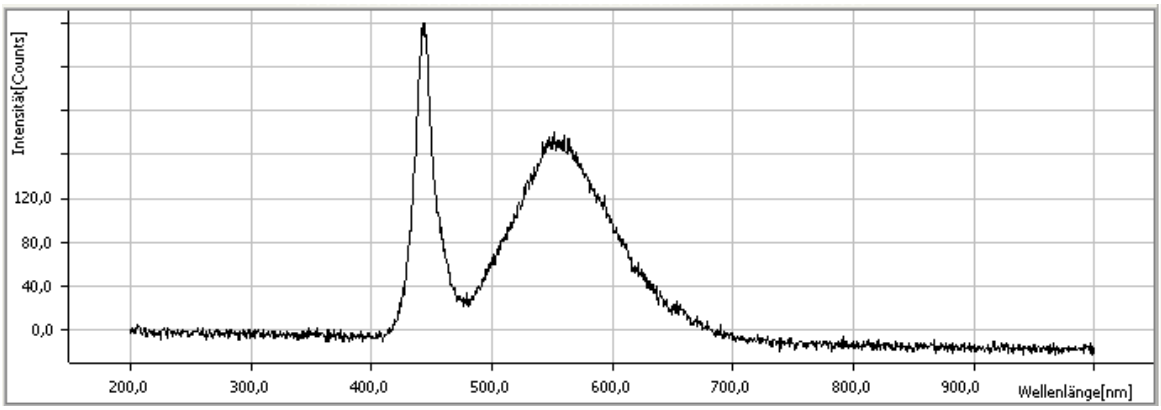

Figure 6.6-4 Emission spectrum of a white light LED (cell phone camera light).

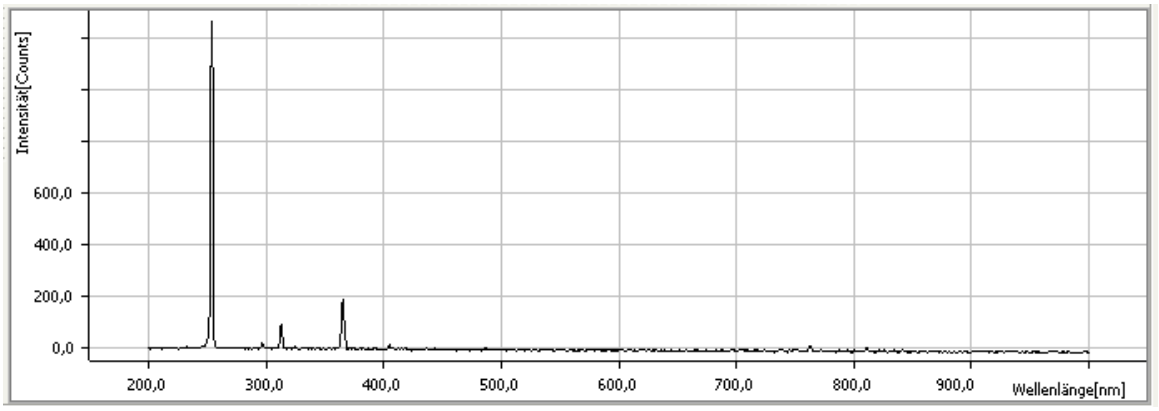

Figure 6.6-5 Emission spectrum of a portable 254 nm fluorescent tube as used for TLC plate control.

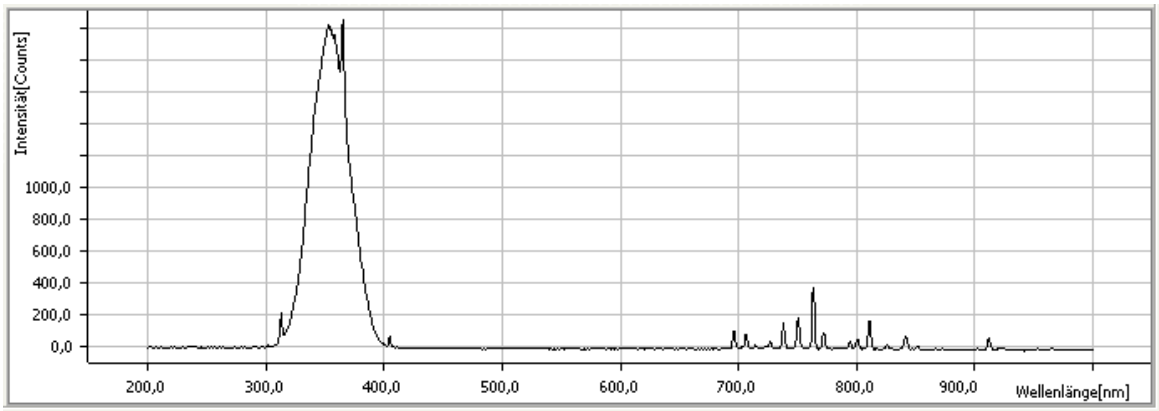

Figure 6.6-6 Emission spectrum of a portable 366 nm fluorescent tube as used for TLC plate control.